UNIVERSITY COLLEGE LONDON

End Point Detection in Reactive Ion Etching

Christopher James Pugh

This thesis has been submitted towards the completion of Doctorate of Engineering with the department of Electrical and Electronic Engineering of UCL.

I, Christopher James Pugh confirm that the work presented in this thesis is my own. Where information has been derived from other sources, I confirm that this has been indicated in the thesis.

Signed:

Abstract

End-point detection for deep reactive ion etch of silicon in the semiconductor industry has been investigated with a focus on statistical treatments on optical emission spectroscopy. The data reduction technique Principal components analysis (PCA) has been briefly reviewed and analysed as an introduction to independent component analysis (ICA). ICA is a computational dimension reduction technique capable of separating multivariate data into single components. In this instance PCA and ICA are used in to combine the spectral channels of optical emission spectroscopy of plasma processes into a reduced number of components. ICA is based on a fixed-point iteration process maximizing non-gaussianity as a measure of statistical independence. ICA has been shown to offer an improvement in signal to noise ratio when compared to principal component analysis, which has been widely used in previous studies into end-pointing. In addition to the end-point investigation, a study was carried out into the fabrication of arrays of free standing silicon nanorods. The fabrication process consisted of an electron beam lithograpy stage to pattern bare silicon, followed by a deep reactive ion etch - using the Bosch process - to create the nanorods. A variety of difference diameter nanorods, with a selection of pitch dimensions were created using this technique.

Acknowledgements

I would like to thank my parents for supporting me throughout the course of my EngDoc studies and assisting enormously by providing a place to live and work whilst I completed the writing of this thesis. My family as a whole has been extremely helpful and encouraging throughout the course of my studies so I offer my thanks to them. I would like to offer thanks to my supervisor Professor Arokia Nathan for enabling my project to take place. I offer thanks to my selection of industry based supervisors; initially Leslie Lea - then of SPTS and now of Oxford Instruments; later Yiping Song took over as Leslie changed employer, I am extremely grateful to him and the technical advice offered as I developed my thesis subject matter. Although Oliver Ansell of SPTS was not technically a supervisor, the help and time offered by him were invaluable to my project. Also I would like to thank David Tossell of SPTS for overseeing my time at the junction 24 site of SPTS. Finally I would like to acknowledge my loving girlfriend Sarah for putting up with me as I relocated not once, but twice in order to get my work completed.

Glossary of Terms

PCA – Principal Component Analysis

ICA – Independent Component Analysis

OES – Optical Emission Spectroscopy

SOI – Silicon on insulator – Silicon has an oxide layer grown on it, with a silicon layer grown on top of the oxide layer.

Matlab – Numerical Computation software from Math Works

ICP – Inductively coupled plasma

SPTS – Surface Process Technology Systems

LCN – London Centre for Nanotechnology

UCL – University College London

Bosch Process – A deep reactive ion etch process

Table of Contents

1. Chapter 1 Introduction 13
1.1. A brief introduction to the project........ 13
1.2. Surface Process Technology Systems – About the company........ 14
1.3. Semiconductor Industry........ 15
1.4. References 17
2. Chapter 2 - Experimental Equipment 18
2.1. Plasma Generation........ 18
2.2. Advanced Silicon Etch tool – London Centre for Nanotechnology........ 21
2.3. SPTS Pegasus - SPTS Newport, Junction 28 Site........ 22
2.4. SPTS Rapier - SPTS Newport, Junction 24 site 24
2.5. Loadlocks – wafer loading system 25
2.6. Alternative Etch Tools 25
2.7. Verity Spectrograph 26
2.8. Electron Beam Lithography – Spin Coater - LCN........ 29
2.9. Raith 150 Two Electron Beam Lithography Tool – LCN clean room 30
2.10. Oxygen Plasma Chamber (ashing)........ 32
2.11. Edwards A500 Electron Beam Evaporator – LCN Clean Room 33
2.12. Hitachi Leo - Scanning Electron Microscope........ 35
2.13. Carl Zeiss Supra - Scanning Electron Microscope 36
2.14. The Bosch Process........ 36
2.15. Silicon Etch via Fluorine 37
2.16. Passivation Step 38
2.17. Bosch Process Passivation Step Polymerisation Mechanism........ 39
2.18. The Bosch Process Steps 40
2.19. References 44
3. Chapter 3 – A review of the plasma etching industry........ 45
3.1. Plasma Etching - an Introduction........ 45
3.2. Plasma Etching – The Technique........ 46
3.3. End Point Detection 48
3.4. Laser Interferometry - Theory........ 55
3.5. Low open area end point detection........ 58
3.6. Optical Emission Spectroscopy 60
3.7. Optical Emission Spectroscopy in III/V Compound Etching 69
3.8. Statistical Treatments of Optical Emission Spectroscopy 71
3.9. Laser Interferometry........ 80
3.10. III/V Compounds 84
3.11. Conclusion........ 90
3.12. References 93
4. Chapter 4 – Optical Emission Spectroscopy........ 96
4.1. Optical Emission Spectroscopy (OES) - Theory 96
4.2. Limitations of Optical Emission Spectroscopy as an End Point Detection System 101
4.3. Noise in Optical Emission Spectra........ 102
4.4. References 104

5. Chapter 5 - Principal Component Analysis 105
5.1. Principal Component Analysis - Theory 105
5.2. Experimental Method 109
5.3. Surface Process Technology Systems (SPTS) Advanced Silicon Etch (ASE) - 100% Resist Coverage 110
5.4. Surface Process Technology Systems (SPTS) Advanced Silicon Etch (ASE) Patterned Silicon - 15% Coverage 110
5.5. SPTS Pegasus Oxide Etch ~ 1% Open Area 111
5.6. Results and Discussion - SPTS Advance Silicon Etch tool 111
5.7. SPTS Patterned Silicon ~ 15% Open Area 119
5.8. SPTS Silicon Oxide Etch Low Open Area ~1% 130
5.9. Conclusion 136
5.10. References 139
6. Chapter 6 - Independent Component Analysis 140
6.1. Introduction 140
6.2. Independent Component Analysis – An Overview 141
6.3. Independent Component Analysis – A Basis 142
6.4. ICA – Mathematical Theory 142
6.5. Independence of Joint and Marginal Distributions 143
6.6. Independent Component Analysis methodology - low open area tests 149
6.7. ICA Methodology – Repeatability Tests 152
6.8. ICA Results 152
6.9. OES – No processing 152
6.10. One wavelength – A selection of single wavelengths over the given time of the etch 154
6.11. Independent Component Analysis 156
6.12. ICA results of wafer 59 - 10 components 158
6.13. A comparison of the effect of different parameters on Independent Component Analysis performance 163
6.14. Comparison of Independent Component Analysis and Principal Component Analysis methods for improving signal to noise ratio 164
6.15. Comparison of ICA results for reduced open area 168
6.16. ICA - Discussion 169
6.17. References 172
7. Chapter 9 – Nanorod Fabrication 174
7.1. Silicon Nanorod Methodology 174
7.2. Mask Patterning – London Centre for Nanotechnology (LCN). 175
7.3. Electron Beam Resist Spin-coating 175
7.4. Electron Beam Lithography 176
7.5. Ashing – Oxygen Plasma Etch 179
7.6. Electron Beam Evaporation 179
7.7. Liftoff 180
7.8. Plasma Etching 181
7.9. Pillar Etch Results 182
7.10. Silicon Nanorod Fabrication – Discussion and Further Work 228
7.11. References 232

8. Conclusion 233
9. Appendix 1 - Reaction Mechanisms 236
10. Appendix 2 - ICA Theory of operation 241

Table of Figures

Figure 2.1.1 A sketch of a parallel plate reactor 18
Figure 2.1.2 Sketch of a helical ICP coil chamber........ 19
Figure 2.1.3 Example of a plasma chamber including a funnel to focus the diffusing plasma on to the substrate 21
Figure 2.2.1 - An example of an SPTS ICP chamber similar to that found in LCN clean room. 22
Figure 2.3.1 An example of SPTS Pegasus silicon etch tool. Similar to the tools used in the SPTS locations. 23
Figure 2.4.1 SPTS Rapier system - as used in SPTS junction 24 site. Here there are two tools attached to a single robotic delivery system. 24
Figure 2.7.1 Verity SD1024 Spectrograph 26
Figure 2.8.1 Electron Beam Resist Spin Coater 29
Figure 2.9.1 Raith 150 Two Direct Write - Electron Beam Lithography Tool 30
Figure 2.10.1 Oxygen Plasma Chamber (Ashing chamber) 32
Figure 2.11.1 Edwards A500 Electron Beam Evaporator 33
Figure 2.12.1 Hitachi Leo - Scanning Electron Microscope 35
2.13.1 Carl Zeiss Supra - Scanning Electron Microscope 36
Figure 2.15.1 The mechanism of silicon etching by fluorine. A two channel concerted reaction between F atoms and the fluorinated layer. Gaseous SiF2 and surface bound fluorosilicon radicals are formed. The radicals are further fluorinated to form higher SiFx species. 37
Figure 2.16.1 Scallop formation 39
Figure 2.18.1 Step One of Bosch Process – Application of passivation layer 40
Figure 2.18.2 Step Two of Bosch Process – Anisotropic removal of passivation layer 41
Figure 2.18.3 Step Three of Bosch Process – Isotropic etch of exposed Silicon layer 42
Figure 3.2.1 A typical parallel plate plasma reactor. 47
Figure 3.3.1 Different stages in the etch process. Under etch is defined as when the film is not entirely removed. The ideal etch is when the film is removed completely and over etch is when the next layer of material starts to be removed. The image is not to scale and the measurements are purely illustrative. 48
Figure 3.3.2a) The ideal end point is a step change with no noise in the signal. b) In a real end point trace there is noise and drift. The end point also occurs over a finite period of time. Here the intensity is given in arbitrary units but is often shown as counts. These examples are illustrative to demonstrate the complexity of end point determination. 50
Figure 3.4.1 Interference, the basis for laser end point detection[21] 56
Figure 3.5.1Open area fraction used in various etching processes 59
Figure 3.6.1 Results obtained by Hirobe *et al..* for the determination of end point using 674nm optical emission line (N_2 as the emission species) 60
Figure 3.6.2 Results obtained by Hirobe *et al*. detailing the sample areas for which an end point was achievable 61
Figure 3.6.3 Plasma emission spectrum, oxide parallel plate etcher [40] 63
Figure 3.6.4 a) Optical emission signals from ~1% exposed area SiO_2 contact etch, parallel plate etcher. b) Same data, displayed as ratio of end point to background signals. End point detected (ratio has been digitally filtered)[40] 64
Figure 3.6.5 Approximately 1% exposed area SiO_2 contact etch, parallel plate[40] 65

Figure 3.6.6 Open-loop *(*circles) and closed-loop (CL1: line with triangles; CL2: 66
Figure 3.6.7 Representative spectra from semiconductor oxide etch process showing three of the many process steps that can be distinguished using OES[43]. The details of the steps are not provided in the article. 68
Figure 3.7.1 Trace of Ga peak intensity (417 nm) and its slope during AlGaAs/GaAs etching in BCl_3/N_2 ICP etching[7] 69
Figure 3.7.2 Trace of Gallium peak intensity (417 nm) and its slope during InGaP/GaAs etching in BCl_3 /N_2 ICP etching[44]. 70
Figure 3.8.1 Summary of results of chamber state models found by Chen *et al. [45].* Here PCA is principal component analysis; PLS is partial least squares; R^2 is the degree of correlation; ER is the etch rate and ARDE is aspect ratio dependent etch. 73
Figure 3.8.2 Optical Emission Spectroscopy Principal Component Analysis from a typical etch (solid line) and the one-step-ahead prediction output from the jump-linear filter (dashed line). The Principal component labels have been added to the image for clarity. 75
Figure 3.8.3 OES trace for decreasing open area etches. The left shows the untreated data. The right shows the treated system using T^2 analysis[47]... 76
Figure 3.8.4 Principal components of Optical Emission Spectroscopy data[38] 78
Figure 3.8.5 Loading plot of the second and third PCs. A circle criterion is used to select important wavelengths[38].. 79
Figure 3.9.1 Double beam laser interferometer with typical response curve[49]. 80
Figure 3.9.2 Single beam interferometer with typical response curve[49]. 81
Figure 3.9.3 Calculated reflectance when etching a later of optically absorbent silicide over polysilicon[50] 82
Figure 3.9.4 Optical emission interferometry to determine end point of a) bare poly-silicon and b) patterned silicon[15].. 84
Figure 3.10.1 Etch rate monitoring using lasers with wavelengths of 1.15µm and 0.6328µm[37]. Here the quantum well structures are identified as Q1-Q3 85
Figure 3.10.2 Laser interferometry signal as a function of etching time, for a Graded Index Separate Confinement structure 4 quantum well (GIS-SC-4QWs) laser structure. The arrows denote heterointerfaces and A, B, C, D, E, and F are regions of the laser structure as described in the table alongside[51].. 87
Figure 3.10.3 Part of an interference signal measured using near IR LIR to follow the process[21] ... 89
Figure 3.10.4 A trace for a complete etch through a 400µm silicon wafer[21]................................... 90
Figure 4.1.1 Spherical coordinate system[1] 96
Figure 4.1.2 Energy levels and transitions of Hydrogen atom 97
Figure 5.1.1 Multivariate optical emission data often contains vast numbers of readings. For the purpose of this report up to 1200 wavelengths are recorded in each time interval which is generally set to 0.1s. A 30 minute process would collect 21,600,000 individual measurements..................... 106
Figure 5.4.1 Process of deposition followed by etching to obtain an artificial end point signal........ 111
Figure 5.6.1 PCA loadings for blanket etch of resist 112
Figure 5.6.2 Principal Component Analysis Scores of blanket resist etch. An end point can be resolved between 600 and 750 seconds where the oscillatory nature is replaced by a linear pattern. 113
Figure 5.6.3 First Principal Component Loading 114
Figure 5.6.4 First Principal Component Scores 115

Figure 5.6.5 Second Principal Component 2 Loading 115
Figure 5.6.6 Second Principal Component Score 116
Figure 5.6.7 Third Principal Component 3 Loading 117
Figure 5.6.8 Third Principal Component Score 118
Figure 5.7.1 First 10 principal component loadings from polymer removal step 119
Figure 5.7.2 Principal Component scores for 5 process cycles 120
Figure 5.7.3 Principal Component scores over single polymer removal stepThe first principal component loadings (wavelength contributions) are shown below (Figure 5.7.4). The significant contributions are positive from wavelengths associated with fluorine and from a wavelength associated with CF_2. 121
Figure 5.7.4 1st Principal Component Loading 121
Figure 5.7.5 1st Principal Component score 122
Figure 5.7.6 2nd Principal Component loading 123
Figure 5.7.7 2nd Principal Component score 123
Figure 5.7.8 3rd principal component loading 124
Figure 5.7.9 3rd principal component score 125
Figure 5.7.10 4th principal component loading 126
Figure 5.7.11 4th principal component score 127
Figure 5.7.12 5th principal component loading 128
Figure 5.7.13 5th principal component score 128
Figure 5.7.14 Scanning electron microscope images showing two separate areas on a patterned wafer after etching. The degradation caused by excessive cycle times during Bosch process is shown on both areas. 129
Figure 5.8.1 Untreated spectral data from patterned oxide etch 131
Figure 5.8.2 Table detailing the percentage of variation contained in the first 6 principal components 131
Figure 5.8.3 PC loadings from the treated data of patterned silicon on oxide wafer 133
Figure 5.8.4 1st 4 Principal Component scores of treated oxide etch 134
Figure 5.8.5 Principal Components 2-4 only 135
Figure 6.5.1 A Probability Distribution Function for two high-kurtosis variables such as speech. The joint probability is shown on the horizontal plane (image taken from [4]). 145
Figure 6.5.2 A Probability Distribution Function for two gaussian variables such as signal mixtures is shown in the solid surface. The joint probability is shown on the horizontal plane (image taken from [4]). 145
Figure 6.6.1 Carrier wafer with patterned Silicon On Insulator (SOI) coupons fixed to it 150
Figure 6.9.1 Mid process optical emission spectrum 153
Figure 6.9.2 Post end-point spectrum 154
Figure 6.10.1 Single wavelength time series. Wavelengths of 273nm (Dummy), 440 nm (SiFx) and 706.5nm (F) shown. 155
6.10.2 Single wavelengths showing cyclic nature of Bosch process used. Wavelengths of 273nm (Dummy), 440 nm (SiFx) and 706.5nm (F) shown. 155
Figure 6.12.1 First Independent Component Analysis results - 10 components 159
Figure 6.12.2 Single component from wafer 46 process run showing clear end point. 160
Figure 6.12.3 Graph showing ICA contributions from wavelengths. 161
Figure 6.12.4 Wavelength contributions to ICA - component 3 162

Figure 6.13.1 Independent Component Analysis results for different parameters. 163
Figure 6.13.2 Comparison of different ICA parameters.. 164
Figure 6.14.1 Graph showing example of signal drop and noise area. 165
Figure 6.14.2 Comparison of Independent Component Analysis to Principal Component Analysis across full range of wavelengths... 166
Figure 6.14.3 Comparison of all eight ICA parameter iterations and PCA technique........................ 167
Figure 6.15.1 Low open area Optical Emission Spectroscopy data 168
Figure 7.4.1 Positive and Negative Mask Application.. 177
7.9.1.1 Run 1 - Pillars showing good uniformity across wide area 185
Figure 7.9.1.2 Run 1 - Pillars showing re-entrant features and mask etch. 185
Figure 7.9.1.3 Run 1 - Pillars at edge of sample. 186
Figure 7.9.2.1 Run 2 - majority of pillars have been removed.. 187
Figure 7.9.2.2 Run 2 some pillars remain but highly re-entrant... 187
Figure 7.9.2.3 Run 2 - individual pillar shows extreme re-entrant 188
Figure 7.9.2.4 Run 2 pillars highly re-entrant with mask etching evident at pillar top 188
Figure 7.9.3.1 Run 3 - central area of Titanium mask prior to etching 189
Figure 7.9.3.2 Run 3 - showing taped and un-taped at edge area of sample 190
Figure 7.9.3.3 Run 3 - Shell like pillar etch structure 190
Figure 7.9.3.4 Run 3 - pillars at edge of mask area, not etched correctly further into masked area . 191
Figure 7.9.3.5 Run 3 - Pillar tops showing mask etching 192
Figure 7.9.3.6 Run 3 - pillars at edge of mask clearly defined, further in the mask has issues 192
7.9.3.7 Run 3 - Central area of mask showing no etching having occurred. 193
Figure 7.9.4.1 Run 4 - A shell like structure at top of pillars, pillars etched at edge of mask............ 194
Figure 7.9.4.2 Run 4 - Pillars re-entrant with shell like structure at edge of wafer, mask problem still evident 194
Figure 7.9.5.1 Run 5 - pre-etch mask clearly defined throughout... 195
Figure 7.9.5.2 Run 5 - Low magnification mask showing clear definition throughout 196
Figure 7.9.5.3 Run 5 - Pillar etching throughout sample area 197
Figure 7.9.5.4 Run 5 - Pillars less re-entrant, however shell like structure is still evident. Pillars evident throughout masked area 198
Figure 7.9.6.1 Run 6 - Pre etch mask 199
Figure 7.9.6.2 Run 6 - Pillars showing beginning of mask removal, evidence of double etch step.... 199
Figure 7.9.7.1 Run 7 - Continuation of run 6 showing further result of mask etching 201
Figure 7.9.7.2 Run 7 - Pillars etched with shell like structure shown 202
Figure 7.9.8.1 Run 8 - Well defined pillars, no mask removal, low re-entrant.................................. 203
Figure 7.9.8.2 Run 8 - Clear pillars, clean etch no mask erosion 203
Figure 7.9.9.1 Run 9 - low diameter pillars showing re-entrant with shell like structure 204
Figure 7.9.10.1 Run 10 - Pillars etched cleanly, no re-entrant. Some grass evident at base of pillars. 205
Figure 7.9.10.2 Run 10 - Grass shown with pillars for comparison 206
Figure 7.9.10.3 Run 10 - Pillar tops high magnification, scallops shown. 206
Figure 7.9.11.1 Run 11 - Post etch shows cleanly etched pillars with low re-entrant; grass like structures are highly evident at base of pillars.. 207
Figure 7.9.11.2 Run 11 - Pillar tops showing scallop result of Bosch process. Mask diameter shown. 208

Figure 7.9.12.1 Run 12 - Pillar tops clearly defined 209
Figure 7.9.12.2 Run 12 - Pillars etched cleanly with very low re-entrant and low grass 209
Figure 7.9.13.1 Run 13 - shows some grass evident at base of pillars, re-entrant is low 210
Figure 7.9.13.2 Run 13 - Pillar tops are clean and well defined 210
Figure 7.9.14.1 Run 14 - pillars etched cleanly with good definition. Re-entrant is low but evident. 211
Figure 7.9.14.2 Run 14 - Pillars show good definition with low grass. 212
The SEM image above (Figure 7.9.14.3) clearly shows the re-entrance with the pillar tops significantly wider than their corresponding bases. The lack of grass is also clearly evident. 212
Figure 7.9.15.1 Run 15 - Pillars cleanly etched throughout sample area. There are some un-etched areas outside of sample. 213
Figure 7.9.15.2 Run 15 - Majority of pillars etched cleanly some mask removal on individual pillars evident. 213
Figure 7.9.15.3 Run 15 Pillar height reduced to 4.7um 214
Figure 7.9.15.4 Run 15 - Pillar diameters reduced to 330nm 215
Figure 7.9.16.1 Run 16 - Sample area clearly defined but significant grassing is evident 216
Figure 7.9.16.2 Run 16 - Pillars show clean etch profile, thickening at base. Grassing is highly evident. 216
Figure 7.9.16.3 Run 16 - Pillars thicker at base. Approximately double the diameter as at the top. 217
Figure 7.9.16.4 Run 16 - Mask has been removed leading to pillar cores being etched leaving shell structure........ 217
Figure 7.9.16.5 Run 16 - Significant grassing observed outside of sample area. 218
Figure 7.9.17.1 Run 17 - Pillars etched at 300nm diameter, grass evident outside of sample. 219
Figure 7.9.17.2 Run 17 - Pillars knocked over reveal sample area not suffering from grassing. 219
Figure 7.9.17.3 Run 17 - Outside of sample area grass is highly evident. 220
Figure 7.9.18.1 Run 18 - Mask is patchy in regular areas, potentially due to low diameter of mask 221
Figure 7.9.18.2 Run 18 -Pillars regular and cleanly etched 222
Figure 7.9.18.3 Run 18 - Low grassing found between pillars 222
Figure 7.9.19.1 Run 19 - Pillars well populated, cleanly etched zero grass evident. 223
Figure 7.9.19.2 Run 19 - Zero evidence of grass between pillars or outside sample area. Pillars cleanly etched with low re-entrance. 224
Figure 7.9.19.3 Run 19 - Pillar tops show signs of mask removal. 224
Figure 7.9.20.1 Run 20 - Mask has areas where mask has been removed. 225
Figure 7.9.20.2 Run 20 - Low diameter pillars <100nm with aspect ratio of >30:1. 226
Figure 7.9.21.1 Run 21 - Highly regular pillars grassing outside sample area 227
Figure 7.9.21.2 High quality pillar population slight grassing evident 227
Figure 7.10.1 Silicon Nanorod photovoltaic device 229

1. Chapter 1 Introduction

1.1. A brief introduction to the project

The following work is a report describing a research project into end point detection for reactive ion etching of silicon. The research contained within the report was conducted within the Department of Electronic and Electrical Engineering at University College London (UCL), in conjunction with and supported by Surface Process Technology Systems of Newport (SPTS). Over the course of the research project practical work has been carried out at both the London centre for Nanotechnology (LCN) at UCL and on site at SPTS. The project was split between the two geographical locations with the first two years spent based at the university and the final two years spent operating from the headquarters of SPTS.

The main focus of the research was to start with an investigation into end point detection for reactive ion etching. Over the course of the project the focus narrowed to concentrate on optical emission spectroscopy as an end point diagnostic tool in reactive ion etching. A further narrowing of the work resulted in a particular concentration on the use of statistical techniques to improve signal quality observed when using optical emission spectroscopy.

A second aspect also introduced into the project was the development of a full fabrication technique for the manufacture of Silicon nanorods. This process involved the patterning of Silicon samples using electron beam lithography (EBL), followed by the transfer of a hard titanium mask onto the EBL pattern. This hard mask was then etched using the plasma process equipment of SPTS.

The following report will commence with a list of the equipment used over the course of the work. This is followed by a contemporary literature review covering various end point techniques. The established technique of principal component analysis is then evaluated. Independent component analysis is then evaluated as a novel method of improving the signal to noise ratio. Finally a review of the work conducted into the fabrication of silicon nanorods is presented.

1.2. Surface Process Technology Systems – About the company

Surface Process Technology Systems is a capital equipment manufacturer for the microelectronics fabrication industry. SPTS was first founded almost thirty years ago, which for those in the microelectronics capital processing industry is a considerable history. They are a manufacturer of plasma etch, plasma deposition and thermal processing equipment for the semiconductor industry. The following details the types of tools that are sold by SPTS and the markets they operate in.

ETCH	DEPOSITION	THERMAL
• Inductively Coupled Plasma (ICP) etching of silicon, dielectrics, polymers and metals	• Plasma Enhanced Chemical Vapour Deposition (PECVD)	• Atmospheric Pressure Chemical Vapour Deposition (APCVD)
• Deep Reactive Ion etching (DRIE) of silicon	• Physical Vapour Deposition (PVD)	• Diffusion and LPCVD Furnaces
• Dry release etch using HF or XeF_2	• Metal-Organic Chemical Vapour Deposition (MOCVD)	

SPTS as a company continuously looks to the future in an attempt to preempt the tool and process requirements their customers will need before they know they need it. To this end the company works closely with universities and research groups to develop their tools and processes. This close relationship led to the formation of the Sumitomo Surface Technology Systems Chair of Nanotechnology at University College London. Included in the sponsorship was funding for several research projects including this one. Whilst working on this project, the experience in plasma etching gained over many years of operation by SPTS was beneficial to the progress of the work carried out.

1.3. Semiconductor Industry

The semiconductor industry has been growing at an exponential rate since the invention of the integrated circuit (IC)[1]. First credited to Kilby[2] in 1958 an integrated circuit was a hugely significant invention as it allowed all of the features of an electronic circuit to be included on a single device. ICs have two key benefits: low cost and high performance. They are lower cost as multiple electronic devices can be manufactured simultaneously. In addition less material is required to make an IC than to construct a discrete circuit. Integrated circuits have improved performance by making the transistors smaller. As the transistors are smaller, the switching times are decreased, the time taken to activate the transistor is reduced. In addition, by decreasing the size of transistors, the voltage required to activate the switch can be reduced and the efficiency of the transistor can be increased. Thus the power consumption of the transistor is reduced.

Robert Noyce[3] developed his own integrated circuit design in 1960; where Kilby had used Germanium as the semiconductor, Noyce used Silicon. Silicon rather than Germanium (or alternative semiconductor) is the preferred material for the production of most microelectronics as it has the highest durability under high power and high temperature conditions. In addition Silicon forms a stable oxide, which is not water soluble, whereas Germanium does not. This allows several mass production techniques, furthermore reducing the cost of production.

Mass production techniques have developed rapidly in line with the designs for ICs (microchips). The scalability of transistors on silicon microchips have allowed and encouraged designers to incorporate increasing numbers of transistors onto microchips. The increase in transistor density on microchips was well predicted by the famous Moore’s law[4].

Moore's law describes a long-term trend in the history of computing hardware: the number of transistors that can be placed inexpensively on an integrated circuit doubles approximately every two years. Initially the law was a hypothesis stated by Gordon E. Moore in 1965 to describe the fact that since its invention in 1958 the number of transistors in an IC had doubled every year and that trend would continue

for at least ten years. In fact Moore's law has held true until the present day, more than just accurately predicting the rate of change of the industry, members of the semiconductor industry now use the law to develop roadmaps for their planned technologicical progress[5]. This benchmark for progress has been maintained through a variety of techniques, initially wafer yields were maintained at high levels by removing particle contaminants, and processes could be designed to robustly meet design criteria with relatively high yields. However, it is interesting to note that throughout the last 40 years, the semiconductor industry has been able to achieve this phenomenal growth without substantial implementation of automatic process control, processes could be designed to robustly meet design criteria with relatively high yields. This is now a key area for growth within the semiconductor industry, the ideal processing world consisting of human interaction being reduced to loading wafers at the start of the production line and removing devices at the end. This has lead to a continuous demand for the development of superior diagnostic equipment and techniques.

One of the key technologies which are being widely used in order to develop integrated circuits so as to keep up with Moore's law is wafer stacking. Essentially this is when rather than having a single chip on a wafer; multiple chips are stacked on the same wafer. In order to enable this, a new fabrication technique has been developed known as: Through Silicon Vias (TSVs). A VIA is a vertical interconnect access. A TSV is a connection between separate layers within the wafer. A channel is etched through the entire wafer, at which point a connection is inserted through the wafer connecting all of the various components[6]. TSVs are of particular importance as they cover only a very small surface area of a process wafer, with the rest of the surface masked, often less than a single percent open area is involved in TSV etching[7]. This leads to a very low change in the chemistry of the process plasma when the TSV etch is complete. This change in plasma chemistry is used as a diagnostic tool in optical emission spectroscopy[8].

1.4. References

1. Brattain, J.B., *The Transistor a Semiconductor Triode.* Physical Review, 1948. **74**: p. 230-231.
2. Kilby, J.S., *Miniaturized Electronic Circuits*, U.S.P. Office, Editor. 1959: USA.
3. Noyce, R.N., *Semiconductor device and lead structure*, U.S.P. Office, Editor. 1959: USA.
4. Moore, G., *Cramming more components onto integrated circuits.* Electronics, 1965. **38**(8).
5. Hutcheson, D.G., *Moore's Law: The History and Economics of an Observation thath Changed the World.* The Electrochemical Society Interface, 2005. **14**(1).
6. *Through Silicon Via and 3-D Wafer/ Chip Stacking Technology*. in *VLSI Circuits, 2006*. 2006: IEEE Conference Publications.
7. Geert Van der Plas. *Design Issues and Considerations for Low-Cost 3D TSV IC Technology*. in *IEEE international Solid-State Circuits Conference*. 2010.
8. Hirobe, K. and T. Tsuchimoto, *End Point Detection in Plasma Etching by Optical Emission Spectroscopy.* Journal Electrochemical Society: Solid-State Science and Technology, 1980. **127**(1): p. 234-235.

2. Chapter 2 - Experimental Equipment

2.1. Plasma Generation

Plasma process tools operate by exciting gaseous species at low pressure using electromagnetic energy. The gaseous species are ionized in a vacuum system, with energy transmitted from a high frequency electric field. In a conventional reactive ion etch tool, the energy is provided by a radio frequency (RF) electric field between two parallel plates, the frequency of 13.56 MHz is licensed as the industry standard. A conventional parallel plate reactor is sketched below (Figure 2.1.1):

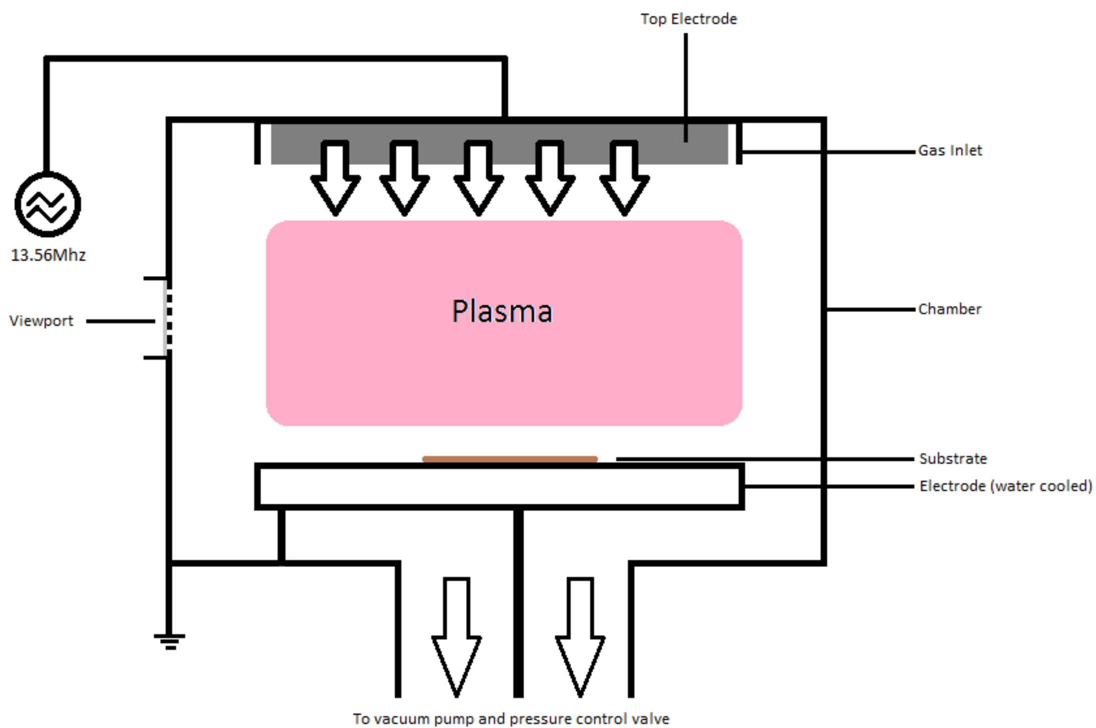

Figure 2.1.1 A sketch of a parallel plate reactor

The RF electric field is generated by a separate RF generator which is connected to the top electrode and the lower electrode. The gas species is introduced into the chamber, typically

via a showerhead unit to disperse the gas evenly across the chamber. The high energy field supplied by the RF generator between the top electrode and the lower transduces energy into the gas molecules, this causes the molecules to dissociate and break apart into ions and electrons. The lighter electrons acquire high speeds from the RF field and tend to leave the plasma by striking the chamber walls where they are fed out to ground. The much more massive ions respond less significantly to the electric field. This leaves a high degree of extremely reactive free radicals in the plasma. It is these free radicals which chemically react with the surface of the substrate.

For an inductively coupled plasma (ICP) system, the energy is provided by the field from a coil surrounding the plasma chamber, as sketched below (Figure 2.1.2). An RF voltage is applied to the coil surrounding the chamber. This generates an RF current which induces a time varying magnetic field in the reactor, which in turn induces an electric current in the gas molecules contained within the chamber. This accelerates the gaseous species and leading to the formation of a plasma within the chamber.

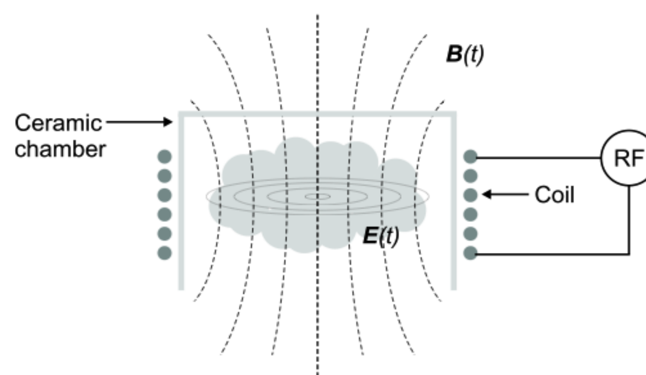

Figure 2.1.2 Sketch of a helical ICP coil chamber

The entire system acts as a transformer, the plasma, surrounded by the coil, will act as the secondary coil, accelerating the electrons and ions. The 'secondary coil' leads to the

production of more ions and electrons. The electrons are much lighter than the ions and they acquire a larger speed for the same energy input. As a result they tend to leave the plasma. The plasma then develops an overall positive electrical potential compared to the surroundings. This causes the ions in the plasma to be accelerated towards the chamber walls. Often an independently biased electrostatic wafer chuck is used. This allows a further element of control over the ion bombardment occurring at the wafer surface. The strength of the bias applied is used as one of several important control mechanisms in the development of etch recipes.

Despite the constant flux of charged particles out of the plasma, the discharge is sustained through ionization of the neutral gases entering the chamber. The ionized gases relax from excited states, this relaxation often is facilitated by the emission of photons causing the plasma to exhibit a characteristic glow. In the regions close to the chamber walls and wafer surface there is a large electric field, resulting in electron depletion and absence of ionization. This causes a non-glowing, easily observable, so-called dark-space or sheath to develop in these regions. Using RF frequencies prevents excessive charging of insulating substrates and enhances the efficiency of the ionization processes.

The electric field is used to supply the energy to the gaseous species within the chamber to create the plasma. Simultaneously a magnetic field can be applied to the chamber to further control the position of the gaseous species, this is known as magnetic confinement[1]. Magnetic confinement results in inductive coupling producing a dense plasma with high ion density and high radical density. The high plasma density gives a 5-10 times higher etch rate than in traditional capacitive coupled RIE systems, as the supply of radicals is the limiting factor in the etch process. The chamber pressure is also kept low to

avoid increased scattering, therefore the directionality of the ion bombardment is maintained.

The ability to form very dense plasmas and at the same time control the ion bombardment of the substrate enables high etch rates with high mask selectivity. In more contemporary tools, the plasma generation chamber has been completely isolated from the process chamber, even further increasing the control of the ion bombardment. This is the case in the SPTS Pegasus tool used and the SPTS Rapier, these tools exhibit higher etch rates whilst maintaining high quality etch profiles for devices structures.

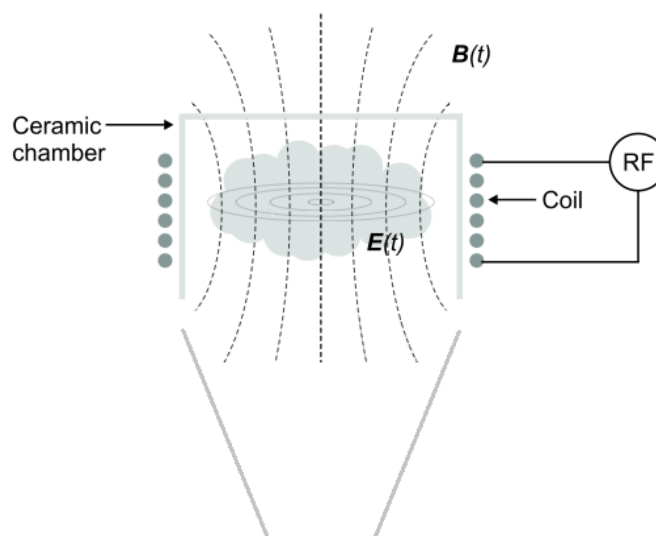

Figure 2.1.3 Example of a plasma chamber including a funnel to focus the diffusing plasma on to the substrate

2.2. Advanced Silicon Etch tool – London Centre for Nanotechnology

The Surface Process Technology Systems Deep Reactive Ion Etching (DRIE) system) is designed to provide high aspect ratio etching of silicon using inductively coupled plasma (ICP) reactive ion etching (RIE). With Advanced Silicon Etch (ASE), licensed Bosch process, microstructures can be obtained up to ~20:1 aspect ratio. Inductively Coupled Plasam

Reactive Ion Etching uses an RF magnetic field to further excite the electron cloud and reactive ions, increasing the density of ions and neutrals and consequently the etch rate. The advanced silicon etch tool uses the Bosch process (described in detail later in the work), which is a technique where the combination of alternate SF_6 etch and C_4F_8 passivation (deposition) process cycles is used to achieve high etch rate and high directionality silicon etch. The Surface Technology Systems Deep Reactive Ion Eth system consists of a process chamber, a load lock carousel assembly, a prime power distribution/ process chamber electronics rack, a gas box, a RF generator stack, as well as a computer control station.

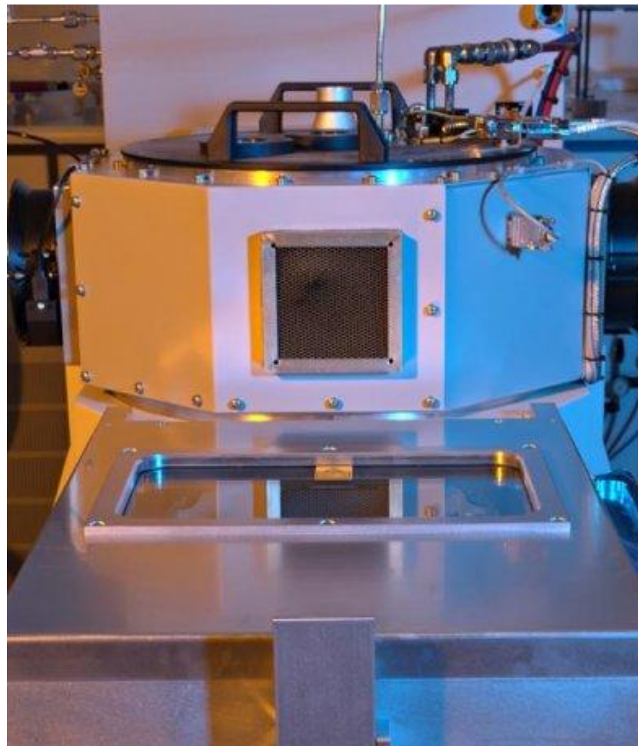

Figure 2.2.1 - An example of an SPTS ICP chamber similar to that found in LCN clean room.

2.3. SPTS Pegasus - SPTS Newport, Junction 28 Site

The SPTS Pegasus tool manufactured by SPTS is an advance on the previous DRIE etch tool (ASE) described above. The plasma is generated in a separate chamber from the etch

chamber. The plasma travels by diffusion to the process chamber, a combination of funnel and baffle is used to direct the plasma onto the surface of the substrate. The formation of the plasma in a separate chamber reduces uncontrolled ion bombardment occurring on the surface of the wafer. The result of this is that there is further control and capability in terms of the etch rate and aspect ratios that can be obtained with the tool. Two versions of this tool were used, both found in the site named above (Junction 28). One tool was used with a 300mm carrier wafer, the second with a 200mm carrier. The tool can be adapted relatively easily to accommodate different wafer sizes, with little or no change in the performance. The platen that the wafer sits on is changed over, whilst the majority of the machine is unchanged. If a significant change in the platen size, say from 150mm to 300mm takes place, it is likely that the process recipe will have to be changed as the amount of material being etched is increased.

Figure 2.3.1 An example of SPTS Pegasus silicon etch tool. Similar to the tools used in the SPTS locations.

2.4. SPTS Rapier - SPTS Newport, Junction 24 site

The SPTS Rapier shares a significant amount of design with the STS tools. The tools that STS and Aviza (prior to being merged into SPTS) built individually were based largely on the same original technology. The two companies share common ancestry as they were both originally part of Electrotech. Although the tool designs branched off once the companies began to operate independently, the fundamentals are still largely similar. As would be expected in terms of two directly competing companies the tool efficiency of the two flagship tools - the Pegasus and the Rapier - have extremely close etch capabilities in terms of rates, uniformities and profile attainability.

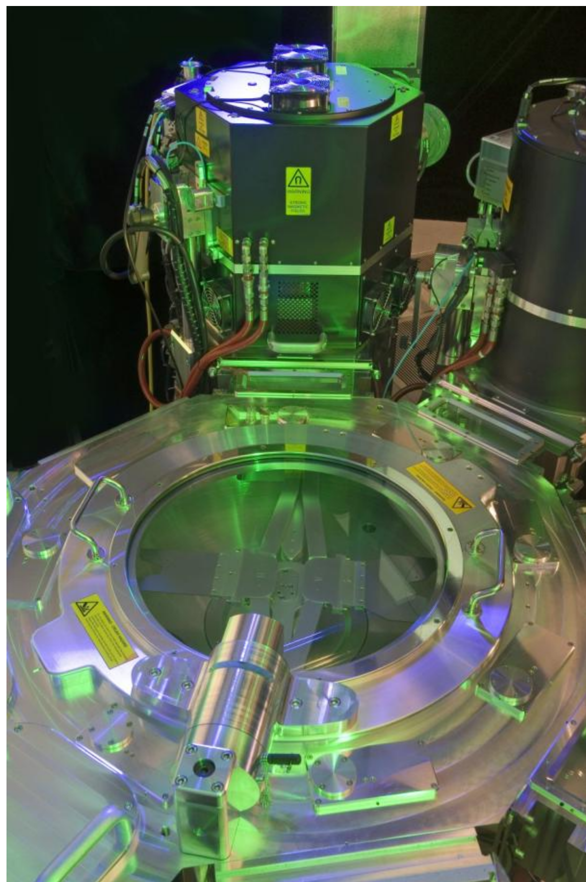

Figure 2.4.1 SPTS Rapier system - as used in SPTS junction 24 site. Here there are two tools attached to a single robotic delivery system.

2.5. Loadlocks – wafer loading system

The tool used in the LCN clean room is manually loaded; a single wafer is loaded, the load lock is manually pumped down and the wafer is loaded into the chamber to be processed. This limits the automation process, as a user is required to remove the finished wafer and replace it with the next. This tool, like most SPTS tools, can easily be adapted to take on a robotic arm in order to automate the loading process. Coupled with the robotic loading arm, a further method to improve automation is to include a cassette loading mechanism. In this instance the wafers are loaded into a cassette, this is then placed into a loadlock. This loadlock is then pumped down to vacuum. This allows for runs of up to 25 wafers to be programmed and run consecutively without any user input. In production level locations it is often the case that this tool, like many other SPTS tools will be fed substrates via a robotic distribution arm. This reduces the need for human involvement and is a step towards the ideal situation of full automation. Tools in this format can be arranged in a 'cluster' formation; whereby several machines are serviced by the same distribution arm. Each tool in the process line is set up for a specific part of the overall manufacturing process. For example, there could be deposition tools and a variety of etch tools, so as to prevent any cross contamination between chambers which would have an adverse effect on tool performance. If a titanium mask were being used for one part of the process, the titanium would be a potential contaminant. In order to reduce the risk of contamination a separate machine would then be used to etch the titanium step.

2.6. Alternative Etch Tools

The etch tools described in the above section are tools which have been used over the course of this project. There are of course alternative etch tools offered by separate

companies. Some of the companies that offer suitable tools for the work are: Oxford Instruments, Plasma Therm or Applied Materials. There are several other companies which offer tools with similar capabilities.

2.7. Verity Spectrograph

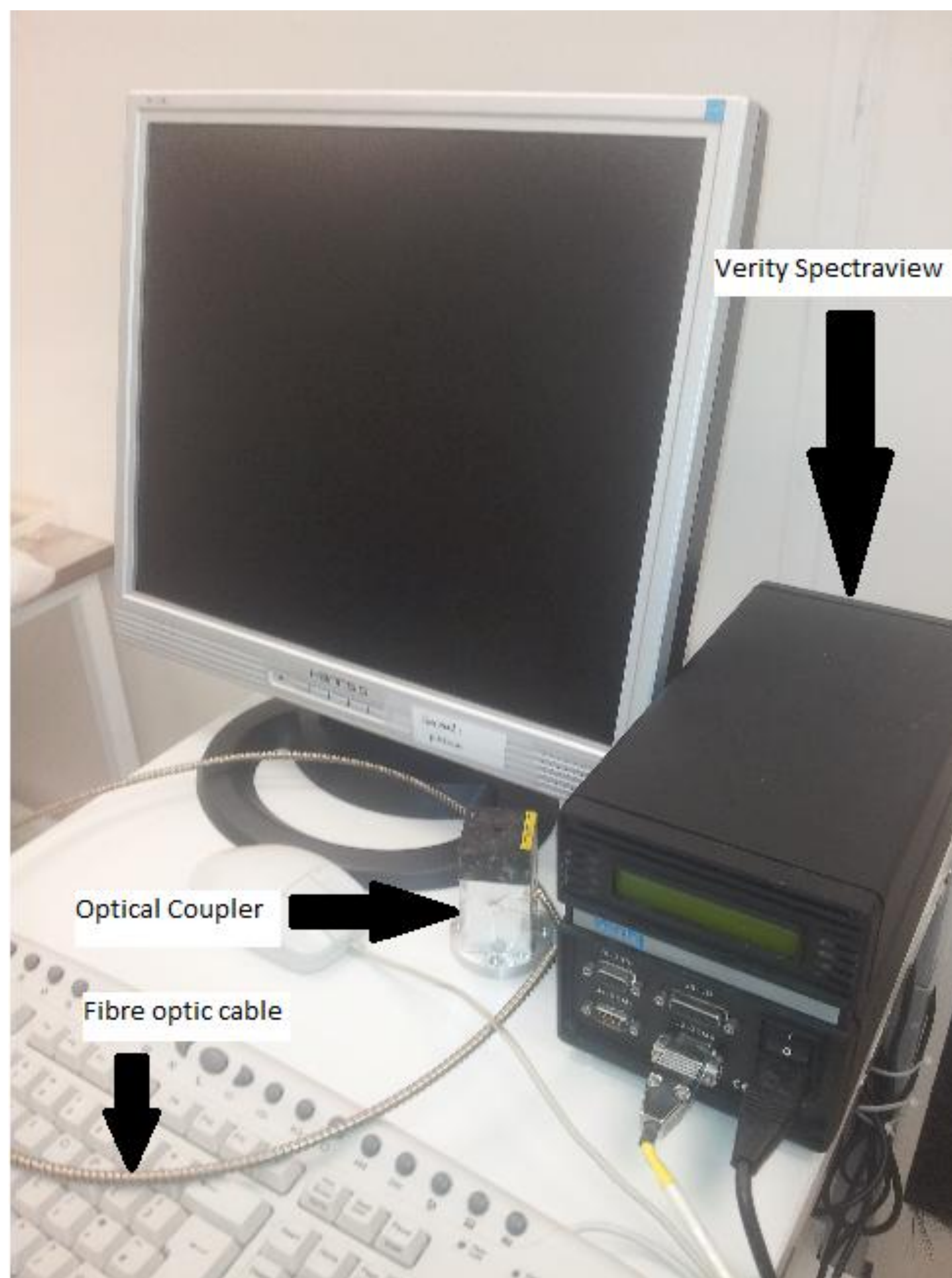

Figure 2.7.1 Verity SD1024 Spectrograph

The Verity Spectrometer is an example of an optical emission spectrometer. There are many other OES systems available such as those supplied by Ocean Optics. For this work the Verity system has been used to collect optical emission spectroscopy (OES) data. The hardware is pictured here, with the software installed onto a nearby computer. The optical cable is shown circling the optical coupler. The optical coupler is used to optically connect the spectrometer hardware to the plasma chamber to enable the contents of the chamber to be diagnosed. In the above photo the spectrometer is not connected to an etch tool. The optical coupler is attached to a viewing port on the plasma tool. There is a lens inside the coupler which focuses the light from the chamber onto the opening of the fibre-optic cable. This cable then transmits the optical signal from the plasma chamber (via the coupler) onto the charge coupled device (CCD) built into the spectrograph. This then changes the optical signal from the plasma into an electronic signal to be analyzed using the verity Spectrograph™ software. Photons fall onto the CCD creating a current, in a given time the number of photons that fall on the CCD will cause a measureable current which is converted by the tool into an intensity measurement. The length of time the photons are summed is known as the integration time. A standard integration time of 0.1 seconds was used for the majority of this work, reducing the integration time increases the noise, whilst increasing the time reduces temporal resolution and can lead to the CCD becoming saturated. For brighter (higher power density) plasmas it is important to maintain a lower integration time as the large number of photons can quickly saturate the CCD. The spectrograph used in this work had a CCD with 1024 elements, capable of monitoring and recording wavelengths down to a resolution of 0.5nm. The spectrometer used in this case is capable of monitoring wavelengths in the range of 200nm to 800nm. This includes wavelengths in the visible range and also in the ultra violet. Due to the harmful nature of

UV electromagnetic radiation a glass window is often placed over the viewing port, this blocks the UV. In some instances a quartz window is used which allows the transmission of the lower wavelength UV radiation. Individual wavelengths or ranges of wavelengths can be monitored and recorded.

The advanced software of the Verity also allows the integration of equations so that one wavelength can be mathematically treated with another, for example a ratio of two wavelengths can be set up to deliver the best results. The software has various end-point algorithms in place which allow for threshold based equations to be used to trigger end-point. The Verity can also be connected directly to the etch tool enabling direct communications between the Verity and the etch tool. With this enabled, the verity can deliver an end-point signal which automatically ends the etch process taking place on the plasma tool. One of the key aspects of the software that made it suitable for the work carried out here was the recording of the total spectrum, rather than single wavelengths (or ranges thereof). This complete spectral data could then be exported to be statistically treated externally.

2.8. Electron Beam Lithography – Spin Coater - LCN

Figure 2.8.1 Electron Beam Resist Spin Coater

In order to use the electron beam lithography tool, the appropriate resist needs to be applied to the surface of the sample in question. The resist used in this work was PMMA (polymethyl methylacrylate) in Anisole 6% solids supplied by MicroChem. This can be applied to either individual pieces or entire wafers. Depending on the size and dimensions of the sample the spin coating recipe has to be adjusted to ensure the correct thickness of film applied. In general there is a ramping step where the spin speed of the chuck is slowly increased. This step disperses the resist across the wafer. Once the final speed is reached it is held for a controlled time. The speed of the final step determines the thickness of the applied layer. Once the sample is coated it is placed on a hot plate to cure the film. At this point the sample is ready to be written on using the electron beam lithography tool.

2.9. Raith 150 Two Electron Beam Lithography Tool – LCN clean room

Figure 2.9.1 Raith 150 Two Direct Write - Electron Beam Lithography Tool

The Raith 150 two Direct Write Electron Beam Lithography tool (EBL) uses a focused beam of electrons to realize nano-scale patterning on sample substrates. As described above the sample is coated with the electron beam resist. It is then placed into the EBL chamber. The inbuilt scanning electron microscope (SEM) is used to calibrate the write aspect of the tool to the sample. The SEM is used to focus the beam accurately onto the surface of the wafer. This is required as different samples have different thicknesses, to ensure the optimum resolution the tool must be calibrated to the exact height of the surface to be patterned. This process involves focusing on an artefact on the sample, a particle of some kind. By focusing on the artefact the tool is calibrated in terms of the height of the sample. This ensures that the focal point of the patterning electron beam is correctly aligned onto the surface to be patterned and the optimum resolution can be achieved. Once focused the electron beam is used to write a dot feature onto the sample, the microscope is then used to refocus on this dot, which is smaller than the original particle. Once focused a second dot

is burnt. This process continues until the size of the dot is approximately 30nm, which is an acceptable resolution for the e-beam lithography. At this point the EBL is ready to begin writing the sample design.

The sample design is loaded into the software. In this case a simple design of a regular repeating unit of discs was used however far more complicated layered structures can be built, using multiple layers of patterning for example. The software breaks the design up into write areas, which are then stitched together; each write area requires the beam to be shifted to a new location. Once the design has been processed the beam begins to write directly onto the surface of the sample. The scanning nature of the tool means that each feature is individually written, this in turn means that process times can be extremely high. For example a sample of $2mm^2$ with patterning with a pitch of less than 1um the process time could be many hours. This is the disadvantage of working with EBL. Optical lithography techniques can deliver much faster results, however they cannot achieve the resolution due to the physical constraints of working with light as the patterning radiation. When optical methods of lithography are used the resolution is limited to ½ the wavelength of the light used. When an electron beam is used for lithography the resolution can be controlled by manipulating the energy of the electron beam and consequently its wavelength.

$$E=hc/\lambda$$

Where E= energy (J), h is Planck's constant (J.s), c is the speed of light (m/s) and λ is the wavelength of the electron beam (m/s).

Once the sample has been patterned with the electron beam, the resist needs to be developed. The sample is placed into developer solution for the appropriate amount of time; the sample is then placed into a stop solution and subsequently dried.

The developer solution used in this project was methyl isobutyl ketone (MIBK) in isopropyl alcohol (IPA) supplied by MicroChem. The ratio of the solution used was 1:3 MIBK to IPA. The stop solution used was pure IPA, again supplied by MicroChem.

2.10. Oxygen Plasma Chamber (ashing)

Figure 2.10.1 Oxygen Plasma Chamber (Ashing chamber)

Once the electron beam resist has been developed and sufficiently dried it is placed into the oxygen plasma chamber for a short period. Approximately 20 seconds is sufficient. This process removes any unwanted polymer which remains after the development. Potentially thin layers (10nm or so) of polymer resist may remain on the surface of the wafer having not been completely removed. Applying the oxygen plasma to the sample will remove these

thin layers. The plasma will also remove a layer of the chosen masked area however, this should be a significantly thicker (300nm) layer and as such the oxygen plasma will not completely remove the mask. If left for too long in the oxygen plasma chamber the entire mask can be removed, making it important to closely monitor. Depending on the plasma chamber used or ashing it is important to evaluate the etch rate of the resist film in the oxygen plasma to ensure that the entire patterned film is not removed.

2.11. Edwards A500 Electron Beam Evaporator – LCN Clean Room

Figure 2.11.1 Edwards A500 Electron Beam Evaporator

The electron beam evaporator has a lengthy pump down time of approximately 4 hours; therefore it is generally the case that several samples are treated simultaneously. The

samples are placed onto the evaporators table, outside of the tool. The samples are placed with the side to be coated facing upwards, held in place using Kapton tape (clearly with the patterned area not covered by the tape). Once the samples are fixed to the table, the table is placed into the top of the evaporator with the samples facing downwards. The table is affixed to a rotating mechanism which spins when the evaporation is taking place; this improves the uniformity of the film being applied.

Once the samples and the table are correctly in place, the chamber is pumped down to a high vacuum level, approximately 10^{-7} Torr. This low pressure is required to avoid impurities and contamination in the applied layer.

When the appropriate pressure is established the electron beam is powered up, this is then directed onto the crucible containing the chosen metal to be coated onto the samples; in this case Titanium was used as the hard mask material. The electron beam quickly heats the metal and evaporation begins. Once the rate of evaporation is stable, the internal shutters are opened exposing the samples to the vaporized metal and the coating begins.

The thickness of the evaporated layer is determined by a quartz crystal which exhibits a change in the frequency of vibration as the layer is deposited onto the samples. The change in frequency occurs according to the following equation.

$$\omega = v_0 \left(1 + \frac{6M}{m_0}\right)^{-1/2}$$

Where ω is new frequency, v_0 is the original frequency M is the new mass and m_0 is the original mass.

In the A500 there are two such thickness indicators. The first is active for the entirety of the evaporation whilst the second is only active whilst the shutters are open and the sample is exposed. The second crystal resonator monitor provides the actual thickness of the coating; the first is useful as a comparison.

Once the desired thickness is achieved the shutter is closed and the electron beam is deactivated. The tool is allowed to cool under vacuum (again to prevent impurities in the film). Once cooled, the tool is brought up to atmosphere and the samples can be removed.

2.12. Hitachi Leo - Scanning Electron Microscope

Figure 2.12.1 Hitachi Leo - Scanning Electron Microscope

The first of two scanning electron microscopes used to obtain images in the project was an Hitachi Leo scanning electron microscope (similar to the one pictured above). This was used at the SPTS junction 24 site to obtain images of the pillars etched in silicon. The microscope was used to identify problems with the etch process and develop a working process recipe. However for resolutions approaching 100nm this SEM was unable to achieve sufficient quality images to be useful.

2.13. Carl Zeiss Supra - Scanning Electron Microscope

2.13.1 Carl Zeiss Supra - Scanning Electron Microscope

As described above when dealing with features smaller than 100nm the Hitachi SEM was not able to realize high enough resolutions to deliver useful images. In these instances a Carl Zeiss Supra SEM similar to the one shown above was used to obtain images of the features. Unfortunately due to the high demand for this tool, it was only available for images which were unobtainable through the use of other lower resolution SEMs.

2.14. The Bosch Process

Although technically the Bosch process is not a piece of equipment, it was a widely used process on the majority of the etch processes over the course of this project. The following is a brief description of the process.

The Bosch process is a widely used switching process, otherwise known as a time based multiplex system. The Bosch process was patented[2] by the Robert Bosch^{GmbH} Company and is licensed out to various companies including SPTS. It is a three stage etch process that allows for the etching of deep structures with high quality profile performance. Etch

profiles can be created with close to vertical side walls approaching 90 degrees to the surface, whilst maintaining high etch rates of upwards of 3um/min. The two significant aspects of the Bosch process are a silicon etch stage and a polymer deposition passivation stage.

2.15. Silicon Etch via Fluorine

When silicon is exposed to fluorine it develops a fluorinated surface layer. This layer penetrates several monolayers into the bulk. Fluorine atoms enter into this layer and attack subsurface Si-Si bonds. At this point Si-F bonds, a free radical SiF_2 and a stable product SiF_4 are formed.

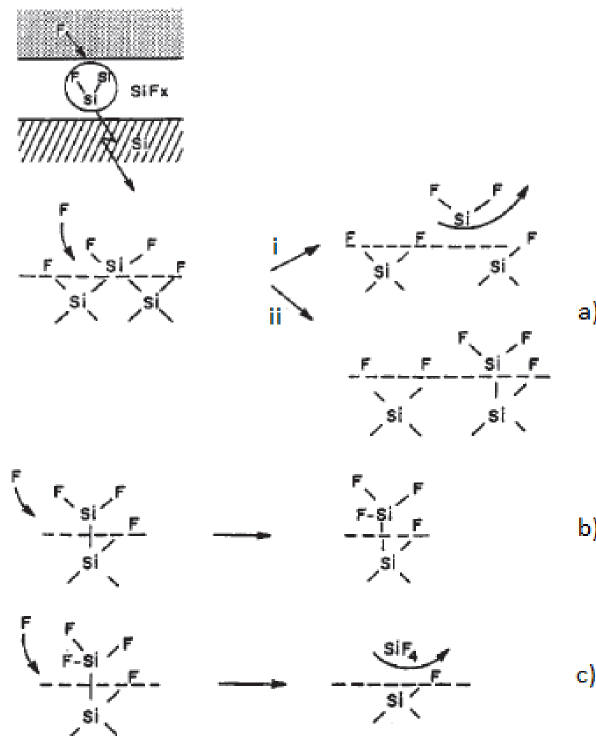

Figure 2.15.1 The mechanism of silicon etching by fluorine. A two channel concerted reaction between F atoms and the fluorinated layer. Gaseous SiF2 and surface bound fluorosilicon radicals are formed. The radicals are further fluorinated to form higher SiFx species.

The radical species in the fluorosilicon crust then combine with more fluorine to form SiF_4. SiF_4 is a volatile and can be extracted from the chamber in gaseous form. The reaction can be observed using optical emission spectroscopy. The SiF_2 radicals which are created react with F to form an excited state of SiF_3. This excited state chemilumineses and can be observed with a broad peak around 500nm. Optical emission spectroscopy within this work has observed a key wavelength for monitoring the etch process based on a wavelength of 440nm[3].

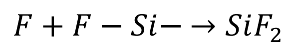

$$F + F - Si- \rightarrow SiF_2$$

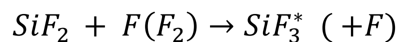

$$SiF_2 + F(F_2) \rightarrow SiF_3^* \ (+F)$$

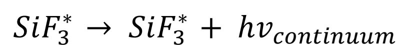

$$SiF_3^* \rightarrow SiF_3^* + hv_{continuum}$$

It has been shown in previous literature that 440nm is a line associated with SiF_x[4] and is often used as a spectral line to follow in optical emission spectroscopy of silicon etching.

2.16. Passivation Step

The second key step in the Bosch process is a deposition step. In this process a polymer layer is deposited isotropically (equally in all directions) on the surface of the substrate. The $(CF_2)_x$ based polymer is highly inert and unreactive in the etch phase. The polymer passivation layer protects the surface from the isotropic etching that takes place in the etch step. Surfaces parallel to the substrate are cleared by the anisotropic nature of the etch step as it is preferentially removed due to the applied bias causing physical removal (sputtering). Perpendicular surfaces are coated with the polymer, but are not subject to the sputtering. The polymer on these perpendicular surfaces (such as trench sidewalls) is slowly removed by the isotropic aspect of the etch stage. Once the etch stage is underway and

material is removed at the bottom of the etched feature, silicon is exposed which is not coated with the passivation layer, as this silicon is etched isotropically it is etched sideways as quickly as it is etched downwards. This leads to the formation of what are known as scallops[5] and are a direct result of the cycling nature of the Bosch process (Figure 2.16.1 Scallop formation). These scallops are a manifestation of surface roughness. The length of time of the stages in the Bosch process are manipulated to reduce the depth of the scallops whilst maximising the etch rate.

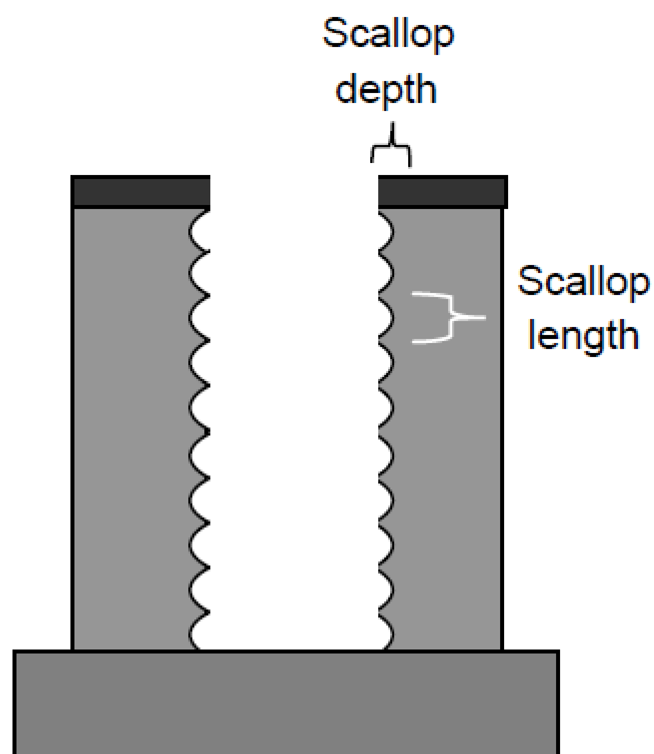

Figure 2.16.1 Scallop formation

2.17. Bosch Process Passivation Step Polymerisation Mechanism

The mechanism of the polymerisation that takes place in the passivation step is a complex one. A range of gases can be used as the source of the reactants for the process step. For the purposes of this work C_4F_8 was used, but CF_4 or C_2F_6 are common alternatives. It has

been shown that the mechanism has several reaction pathways[6]. A full list of these reaction pathways is contained in appendix 1 at the end of this report. A good example of a polymerising chemistry is a situation where the parent gas is already an active. In C_4F_8 plasmas, polymerization by associative detachment can proceed through C_4F_8 : $C_nF_k^-$ + C_4F_8 → $C_{n+4}F_{k+8}$ +e, which allows the growth of a polymer chain to grow four times faster than CF_4, assuming the rates are comparable[7].

2.18. The Bosch Process Steps

Step 1

The first step of the Bosch process is the application of a passifying polymer layer (Figure 2.18.1). This is a deposition process step, often using a C_4F_8 reactant gas. This is an isotropic process, whereby all exposed surfaces are coated equally, both those parallel with the plane of the wafer and those perpendicular.

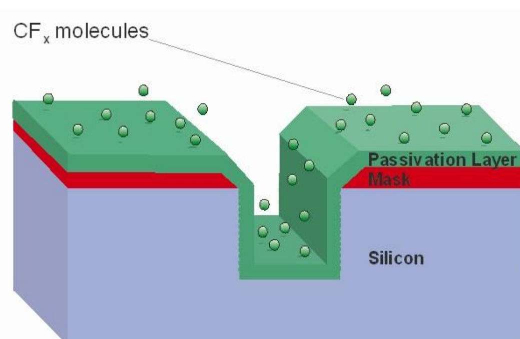

Figure 2.18.1 Step One of Bosch Process – Application of passivation layer

Step 2

The second step is the first of two etch steps. A bias is applied to the wafer which draws ions and radicals towards the wafer. The ions and radicals approach the substrate perpendicularly to the plane of the surface. This bias results in an anisotropic nature to the

etch, so that any surface parallel to the plane of the wafer will be etched whilst perpendicular surfaces such as side walls are relatively undamaged by the process (Figure 2.18.2). This stage of the process removes the passivation layer from the surfaces parallel to the plane of the wafer (such as the base of trenches), which exposes the underlying silicon (or alternative substrate material).

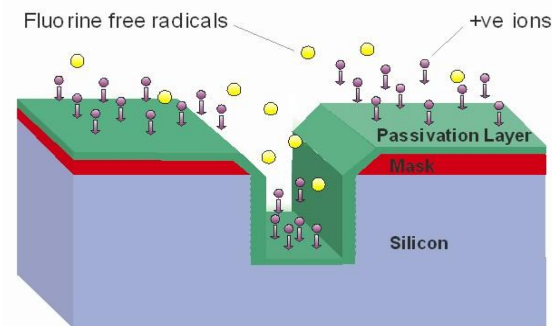

Figure 2.18.2 Step Two of Bosch Process – Anisotropic removal of passivation layer

Step 3

Once the passivation layer is removed from the surfaces parallel to the plane of the wafer in step 2, the underlying substrate material (in most cases Silicon) can be etched by the Fluorine radicals (Figure 2.18.3). The Fluorine radicals bond with the Silicon of the substrate and form volatiles. These volatiles evaporate and are removed from the chamber by the pumping system. The etching parts of the cycle are largely anisotropic, with the sidewalls etching at a relatively low rate. However they do etch, with the passivation layer being removed as a consequence. This is particularly evident in step 3, where as a result of the etch becoming deeper, an area of silicon sidewall is exposed which is not coated in passivation polymer, therefore it is not protected. In order to maintain the anisotropic nature of the entire process (and to prevent mask stripping) once step 3 has run for an allotted time the cycle is repeated with a fresh deposition of the passivation layer to protect

the sidewalls and the mask from damaging levels of etching. This also applies a layer to the most recently uncovered sidewall area, protecting it from further etching.

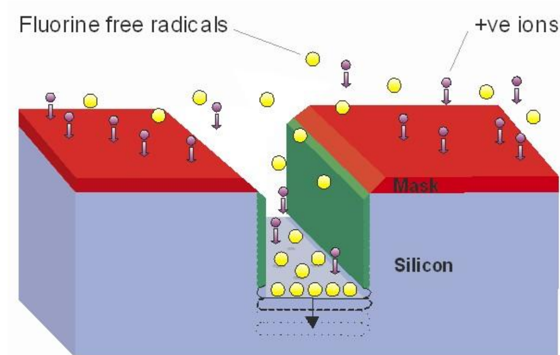

Figure 2.18.3 Step Three of Bosch Process – Isotropic etch of exposed Silicon layer

The length of time that a Bosch process cycle lasts is a controllable factor. It is desirable to have short cycle times as this increases the uniformity of the side walls, leading to an improved etch profile. The limiting factor is the physical capability of the process tools. This is one area where the hardware is constantly being developed, to allow faster switching, cycle times can vary from several seconds to fractions of a second.

One of the unavoidable results of the Bosch process is the formation of scallops. This is caused by the removal of the silicon at the base of a feature, which exposes unprotected silicon on the sidewalls, this silicon is etched isotropically with the base and the walls etched equally. Once the isotropic etch stage is finished the exposed silicon is coated in a layer of the polymer, this prevents any further etching of this area of sidewall and results in a permanent scallop feature. These scallops can be reduced through the manipulation of the relative lengths of the deposition and etch steps within each cycle, by reducing the cycle times the scallop size is reduced. It is often the case that larger scallops will lead to a faster

etch rate, however the larger size scallops are also likely to be detrimental to device performance.

2.19. References

1. V. J. Minkiewicz, *et al*., *Magnetic field control of reactive plasma etching.* Applied Physics Letters, 1979. **35**(5): p. 2.
2. F. Laermer and A. Schilp, *Method of Anistropically Etching Silicon*, R.B. GmbH, Editor. 1996: USA.
3. Herman, I., P. , *Optics Diagnostics for Thin Film Processing*. 1996: Academic Press.
4. Flamm, D.L., *Mechanisms of silicon etching in fluorine and chlorine containing plasmas.* Pure and Applied Chemistry, 1990. **6**(9): p. 1709.
5. Yu-Chen Hsin, *et al*. *Effects of etch rate on scallop of through silicon vias (TSVs) in 200mm and 300mm wafers*. in *Electronic Components and Technlogy Conference (ECTC)*. 2011: IEEE.
6. W.W. Stoffels and E. Stoffels, *Polymerization of fluorocarbons in reactive ion etching plasmas.* Journal Vacuum Science and Technology A, 1997. **16**(1): p. 87.
7. W. W. Stoffels and E. Stoffels, *Polymerization in Fluorocarbon Plasmas.* Japanese Journal of Nuclear Fusion Research, 1999. **75**.

3. Chapter 3 – A review of the plasma etching industry

3.1. Plasma Etching - an Introduction

Since its invention 1947[1, 2] by Bardeen, Brattain and Shockley the transistor has seen an enormous amount of development, it now takes a significant role in many areas of everyday life. One of the key developments has been the reduction in size of transistors, which has followed a pattern famously predicted by Gordan Moore[3]. The prediction essentially stated that the number of transistors in a fixed size of microchip would double every year.

This prediction requires that the size of transistors requires must consistently decrease in order to be able to fit more on the size same chip. In order to maintain pace with the decreasing size of transistors there has been regular developments in the fabrication processes involved. One of the key processes involved in the fabrication of silicon structures for micro-electronics today is lithography. This is essentially the writing of patterns onto silicon. The patterns act as masks in the development of electrical circuits on silicon. Once the pattern has been fixed onto the silicon an etch process is required to remove the uncovered silicon. Initially a “wet” chemical etch[4] was used to remove the unwanted silicon. However this is an isotropic process and as a result there is etching that occurs beneath the mask. This “over-etch” or undercut is not such a problem for large dimension devices as the amount of over-etch is small relative to the device size. As device dimensions reduce this over-etch becomes more significant and can lead to device failure. An alternative to the “wet” etching is “dry” etching which uses plasmas. This was first investigated in the late 1960’s as a method for resist stripping[5], over the next decade plasmas became widely used due to the possibility of anisotropic etching This is done using electric fields to accelerate ions from a plasma towards the silicon. The ions can be made to

strike the surface of the silicon at almost exclusively normal incidence. This dramatically reduces the amount of over-etch that occurs and as a result smaller device sizes can be achieved with reduced failure rate. Since then plasmas have become widely used as the preferred etch tool for processing silicon in manufacturing lines for micro-electronic devices. As the technology developed the plasma processes have also been expanded so as to be able to etch other devices such as III/V devices[6, 7] and MicroElectroMechanical Systems[8-10] (MEMS). Plasma etching is still the chosen technique for the etching of features in both these emerging fields and the established field of silicon etching. However the microelectronics industry is voracious in its requirement for smaller transistors and other features on microchips. This has resulted in an entirely new set of problems in the fabrication process. One major problem is the determination of the finishing point of an etch, this is known as the *end point* of the process.

3.2. Plasma Etching – The Technique

The simplest plasma etching tools are designed as a plasma chamber which can be operated at a low pressure. Contained within the chamber are two opposed parallel plate electrodes. Selected gases are fed into the plasma chamber with a controlled flow rate into and out of the chamber. This flow rate is controlled to maintain a fixed pressure within the chamber. When a high frequency voltage is applied between the electrodes a current flows and a plasma is formed. The plasma will have a characteristic glow; the colour of which varies depending on the gases contained in the plasma. The plasma itself is made up of charged particles[11], it can be thought of as an ionised gas containing equal numbers of free positive and negative charges. Semiconductor wafers or other substrate materials are placed on the electrode surfaces. The reactive chemical species within the plasma react

with the surface atoms of the wafer (or other substrate) and form volatiles. These volatiles can then evaporate and the result is the etching of the surface of the wafer. By controlling the gases contained within the plasma it is possible to control the degree of etching that takes place. Materials which are not susceptible to etching by the reactants in the plasma can be used as masks and as such controlled pattern etching can be achieved[12].

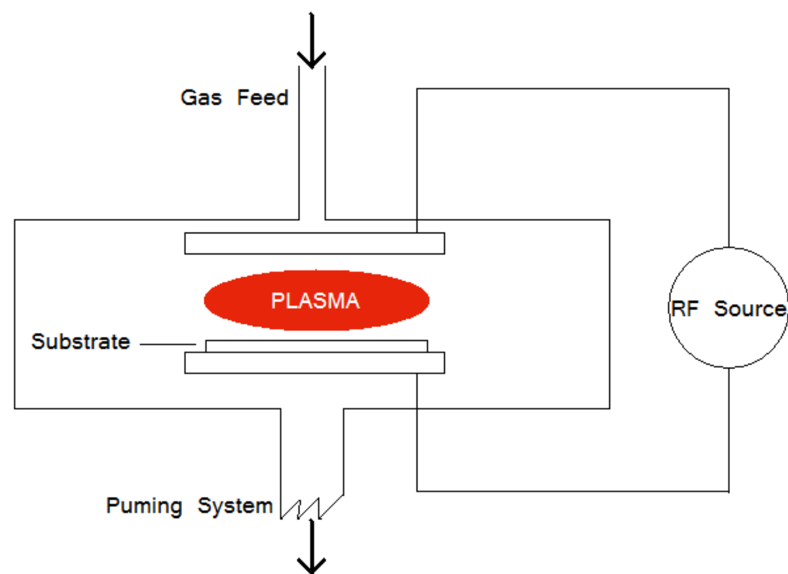

Figure 3.2.1 A typical parallel plate plasma reactor.

3.3. End Point Detection

When a feature is being etched it is vital to be able to determine at what point the etch process should be halted. If the process runs too long then there will be over-etch and if too short under-etch. The point at which the ideal etch has been reached is known as the end point of the etch process (see Figure 3.3.1).

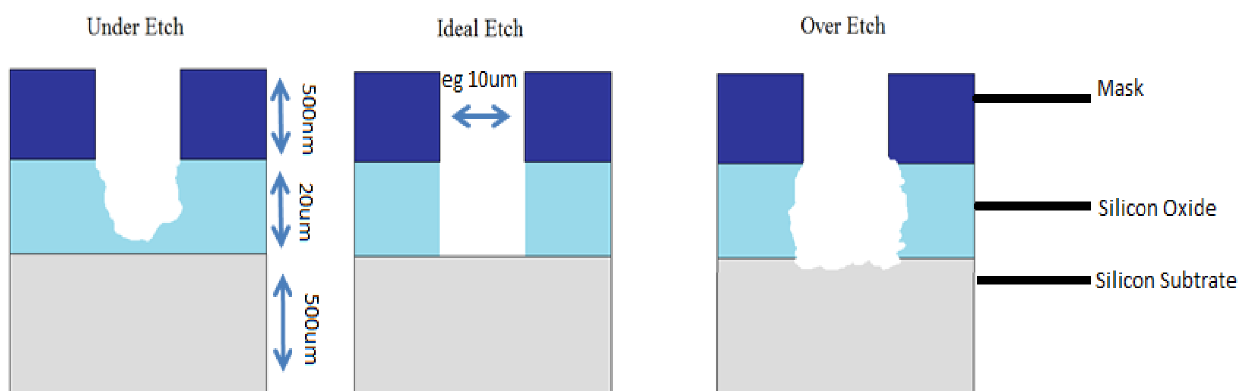

Figure 3.3.1 Different stages in the etch process. Under etch is defined as when the film is not entirely removed. The ideal etch is when the film is removed completely and over etch is when the next layer of material starts to be removed. The image is not to scale and the measurements are purely illustrative.

If any etching takes place beyond the end point then the device will not be as intended and as such there will be an unknown effect upon the device performance. As features and devices become ever smaller even a small degree of over-etching can destroy the functionality of the device.

In the past manipulation of the process parameters of the plasma – etch time, plasma power, gas flow rate etc – has been used to determine suitable recipes for different requirements. The end point was predetermined according to the assumed etch rate and the depth of etching required. However this is not an accurate system. Performance of

plasma etch tools can vary significantly between different machines. The condition of the machine will also have a significant impact upon the performance of an etch tool, as such a process recipe will require calibration on a regular basis to ensure that a chosen recipe is yielding the appropriate results. In an industrial manufacturing line this is not a productive technique and as such is expensive.

There are several parameters of a plasma which vary over the course of an etch process. These will change over time and will often exhibit a significant variation when an end point is achieved. Some of the process parameters are as follows: process pressure[13]; overall impedance of the plasma chamber[14]; concentration of the plasma reactants or products[15]; reflective properties of the surface of the wafer[16]. All of these will exhibit a change at end point which can be used to signal the end of the process. In all cases there will be an end point trace such as in the diagram below (Figure 3.3.2) whereby a step change is observed at the end point fig (a). In reality there will be noise associated with the trace and this makes the end point harder to determine. In addition to this there is a further problem in that the end point will occur over a finite period of time rather than instantaneously. As a result of these factors a real end point trace looks more like the trace shown in fig (b). The finite time period associated with the end point is a result of non-uniform etching. In line with the demands of the industrial sector the size of the wafers being etched is gradually increasing. As a result of this the amount of time over which an end point may occur is also increasing as it is difficult to maintain a uniform etch rate across the entire surface of a larger diameter wafer. As the etching tools are developed and improved it is thought that it will be possible to achieve more uniform etch rates for larger

wafers. This will improve the situation but there will always be a finite time span over which the end point occurs.

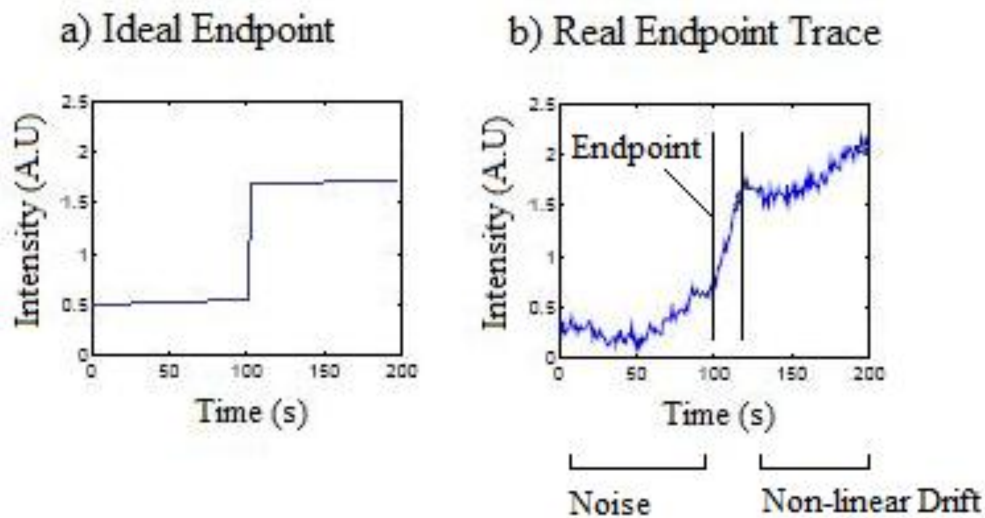

Figure 3.3.2a) The ideal end point is a step change with no noise in the signal. b) In a real end point trace there is noise and drift. The end point also occurs over a finite period of time. Here the intensity is given in arbitrary units but is often shown as counts. These examples are illustrative to demonstrate the complexity of end point determination.

In order to overcome this problem end pointing has been in use since the 1970s[17] Several techniques have been developed in order to overcome the issues described above. The ideal situation is to have a real time system so that the ongoing etch process can be monitored as it takes place and the process can be halted once the desired end point conditions are satisfied (e.g. when the correct depth is reached).

There are several techniques which have been investigated with regards to end point detection including mass spectrometry[18], pressure change[11] and bias change[19]. However two techniques have received significantly more attention due to their

effectiveness, versatility and comparatively low cost. The two most commonly used techniques are:

1. Optical Emission Spectroscopy (OES)
2. Laser Interferometry (LIR)

The first of these techniques measures the frequency of light that is emitted from the plasma as the etch process is underway. In fact a full spectrum is taken and there are peaks in intensity at certain frequencies which are determined by the contents of the gas in the plasma. The main gases that are present are the input gases as required for the etch process (and species derived from the reactant gases). However there is also the by-products of the etch process as well. For example in the case of a silicon etch there will be high intensity spectral lines associated with the reactants from the source gas SF_6 such as Fluorine radicals. There will also be spectral lines associated with the products such as SiF_x, amongst others. Using these characteristic spectral lines it is possible to determine when there is a change in material on the surface that is being etched. For example if the common situation of a silicon layer on top of a silicon oxide layer is taken. The end point required is the point at which the silicon is removed and the silicon oxide layer is exposed. As this occurs there will be an increase in the intensity of the spectral line associated with the reactant Fluorine which is no longer being used to etch the Silicon. There will be a corresponding decrease in the concentration of the by-product of the form SiF_x which are no longer being produced. The spectral lines associated with these products will also show a reduction in intensity. These intensity changes can be observed and an end point signal generated.

Laser interferometry uses another optical technique. A laser beam is directed towards the surface of the material being etched. Upon incidence with the surface there will be a reflection of the beam, there will also be a slight transmission of the beam into the surface. The material is made up of layers and as the transmitted part of the beam reaches the boundary of the next layer there will be a second reflection. This will continue through the material for each of the layers of the material. The separate reflected waves are directed towards a receiver which measures the signal strength. The reflected beams originate from the same source and have the same coherence and as such will exhibit interference characteristics. However there is a variation in phase which will occur due to the magnitude of the separation between the separate layers.   As the surface layer is etched the distance between the first and second layer is changing with time, as a result there is a change in the interference occurring between the different reflected components (reflected from the buried interfaces and the from the surface). This can be seen as a time varying change in the signal strength that is observed at the detector as a sinusoidal signal. By analysing the frequency of the signal it is possible to determine the rate at which each layer is removed and as such a real time etch rate can be calculated using the properties of the material being etched.

Although both of these techniques offer reliable methods for near real time measurements of both etch rate and end point they both have their limitations. In the case of OES the major limitation is that as the features that are being etched become smaller and smaller the change in the signals observed at end point also become smaller and smaller. In the case of extremely small features it is difficult to determine the end point as the signal is difficult to distinguish from the ambient noise exhibited in the spectral information due to

the instability of the plasma. Secondly as the features are being etched one part may be finished before another and begin to exhibit the required signal for end point whereas another part of the wafer may be unfinished. This issue is made more significant as the size of the wafer that is involved is increasing as the industry standard increases. As a result of this the signal that corresponds to the end point is a gradual change rather than an instantaneous one. This leads to issues about how to define the end point, whether it be at the start of the signal change or at the end. This is an important definition to make as choosing the end point at the wrong time could lead to over or under etch issues as discussed earlier. A further complication with the use of OES as the end-pointing system is that it requires a stop layer in the design of the feature that is being etched. This is the required in order for a change to be clear in the trace of the signal; the intensity of the spectral lines associated with the etching process must change. This is caused by a change in the concentration of the plasma reactants or products. In some devices there is no stop layer as the feature is simply a trench such as with the etching of gratings for optical microelectromechanical systems (MEMS)[20]. For these cases there will clearly be no change in the optical properties when end point is achieved. In some instances a stop layer has been introduced in order to allow the use of OES for end point determination[21], however as devices become smaller this becomes unfeasible.

Laser interferometry also has its limitations. The most significant problem is that laser interferometry only acts a diagnostic tool for a small area of a wafer. If there is a variation in etch rate across the surface of a wafer, the area being monitored may show as having etched completely whereas another may not be finished.. As a result when the sample is finished another area may require more etching. This is an increasingly significant problem

as the size of wafers used is increasing. As such it is difficult to maintain a uniform plasma over the surface of the entire wafer. A second limitation of the LIR is that as the size of features becomes smaller the wavelength of the laser used becomes comparable to the size of the features used. This means that a physical limit is approached whereby it is impossible to determine an end point using the LIR method. Although it is possible to use a higher frequency (shorter wavelength) laser, a new problem arises in that the higher energy laser begins to cause changes to the properties of the plasma which in turn can cause problems with the etching. It is also possible that higher energy lasers will have a detrimental effect upon the surface of the material being etched[22, 23]. This can be a problem as the laser can lead to irregularities in the plasma causing variation in the etch rate where the laser is incident on the wafer. Another problem with LIR is that for each etch process being carried out the laser has to be aligned so that it is incident on a suitable area of the wafer in question. This slows the process which in an industrial setting will lead to an increase in costs.

A completely separate system for end point detection is the Hercules plasma diagnostic tool. This is based upon the “Self Excited Electron plasma Resonance Spectroscopy” system (SEERS)[24]. The tool measures plasma characteristics such as electron collision rate, electron density and bulk power and uses them to determine such properties as wafer reactions and tool condition[24-26]. SEERS is based on the nonlinearity of the space charge sheath at the RF electrode, which provides harmonics with the modulated sheath width and high-frequency oscillations in the bulk plasma. The technique uses a passive, non-invasive probe which is insensitive to plasma deposition and negative ions[27, 28]. Although this system is extremely promising in the field of plasma diagnostics including end pointing there

is as yet little published information about the effectiveness of the tool. The pure potential of the technique warranted mentioning but without accepted and published results it is difficult to offer a critique of the technique.

Another aspect of plasma etching which is often incorporated into end point systems is fault detection. By analysing the changes that occur to etch rates and emission spectra (which can both be retrieved from the above end point techniques[29]) it is possible to obtain information about the state of the plasma chamber and the efficiency of the machine [30-34]. This is extremely significant as it potentially allows further automation of the etch process. When problems occur and etch rates deviate from the expected, an automatic signal can be sent to the process engineer notifying that a chamber clean or alternative process recipes are required in order to maintain the necessary etch rate. In fully automated systems the engineer could potentially be bypassed and the cleaning system could be conducted as required without human intervention.

3.4. Laser Interferometry - Theory

Using laser interferometry for end point detection in plasma etch is a widely established practice [21, 35, 36]. It is used *in situ* in dry etching processes in the semiconductor industry in the production of many devices from integrated optical devices[20] through to III-V semiconductors[37]. When a laser is directed onto a substrate surface (in the following example a polysilicon film on silicon oxide, on silicon is used to describe the theory of interferometry), the light is partially reflected and partially refracted (see Figure 3.4.1 Interference, the basis for laser end point detection[21] The refracted light will follow the shortest optical path length according to Fermat's Principle.

For the reflected beam the angle of reflection is equal to the angle of incidence. The refracted beam will follow Snell's law.

$$n_i \sin\theta_i = n_t \sin\theta_t$$

where n_i is the refractive index for light in the film of incidence and n_t is the refractive index for the film of transmission θ_t and θ_i are the angles of incidence and refraction respectively.

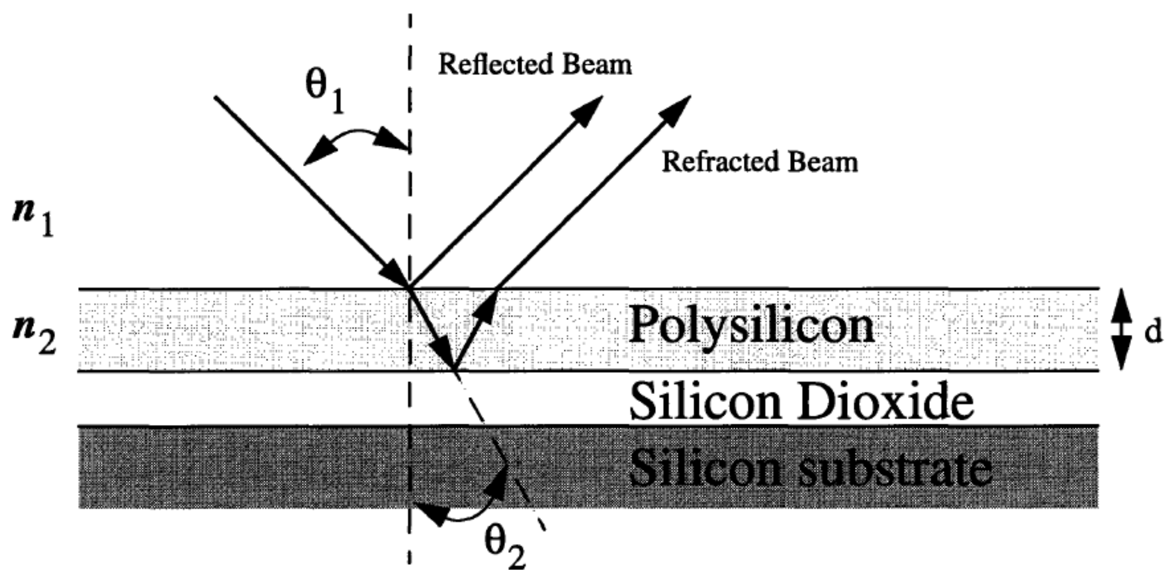

Figure 3.4.1 Interference, the basis for laser end point detection[21]

The optical path difference between the two reflected and refracted beams is:

$$\Delta l_{opt} = 2n_2 d \; cos\theta_2$$

Where d is the thickness of the film (in this example the film is polysilicion). Constructive interference of the laser beam occurs when the optical path length difference between the reflected and refracted beams is equal to an integer number of wavelengths of light in the polysilicon film.

$$\Delta l_{opt} = mn_1\lambda$$

Here m is an integer and λ is the wavelength of the incident laser beam. Destructive interference occurs when the optical path length difference is a half integer of the wavelength. The time period between the maxima and minima corresponding to constructive and destructive interference can be described in terms of the thickness of the polysilicon film:

$$\Delta d_{film} = \frac{\lambda}{2n_2 cos\theta_2}$$

The index of refraction in vacuum n_1 is taken to be unity. During the etch process there is a modulation in the interference of the reflected and refracted beams. This leads to an oscillation in the intensity of the observed signal. By evaluating the time between successive maxima or minima (Δt)it is possible to calculate the etch rate:

$$EtchRate = \frac{\Delta d_{\mathrm{film}}}{\Delta \mathrm{t}}$$

Where Δd_{film} is the thickness of film etched in one period. By including details of the wavelength of the incident light and the distance between the reflecting layers[11] it is possible to deliver real time etch rates. Complex models can be built up to include multiple layers of different materials in complex structures.

When interferometry is used to determine the etch rate a single wavelength is often used (although there are white light interferometry techniques used as well). In order to achieve this, a laser source is generally used. This provides light that is of a specific wavelength and also of a high intensity in a localised area. This provides the etch rate that occurs for a specific area on the wafer i.e. the area where the laser is focused.

3.5. Low open area end point detection

When plasma etching poly-silicon gates and metals, end point detection has been widely used for many years[17]. However the trend described by Moore's law has lead to the development of smaller and smaller features. This is particularly the case in many oxide etching processes where involving contact and via features. In these situations end point detection has proven significantly more difficult and in many cases unsuccessful[38]. The difference between these two scenarios is the surface area that is being etched and the surface area that is covered with photo-resist. The area being etched is known as the open area. In test wafers a "blanket" etch is often used where the surface of an entire wafer is exposed to the plasma and etched, this is a 100% open area etch. In the case of gate etches the majority of poly-silicon exposed to the plasma and consequently is removed leading to an open area etch of approximately 80%. For metal etches the open area may be between 10-80% depending on the size of the inter-connects involved. When contact and via etches are involved the open area is typically much lower. For both cases the open are can be between 0.1-0.5% or less depending on the size of the features involved, this is described below

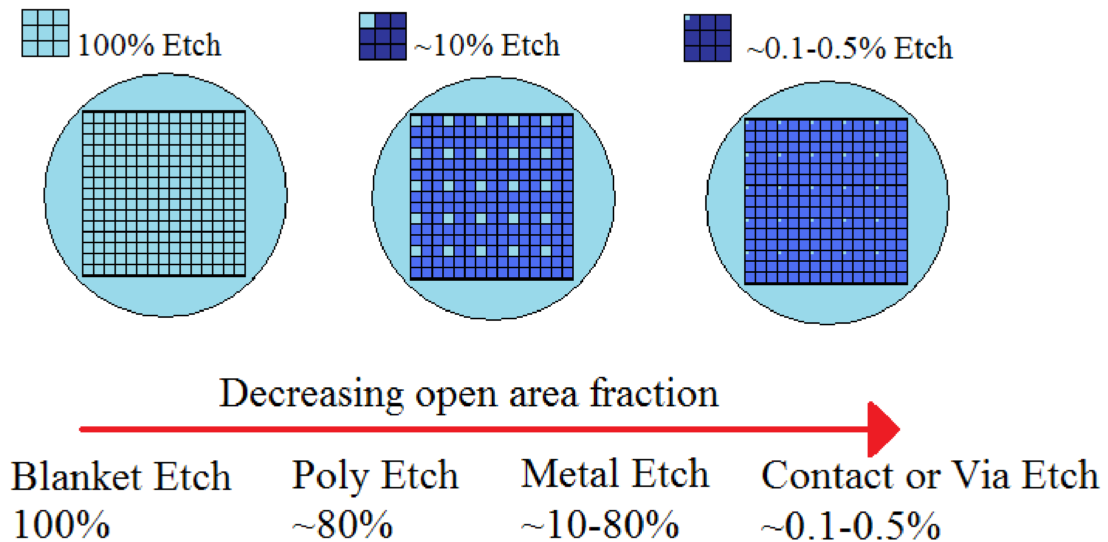

Figure 3.5.1Open area fraction used in various etching processes

The signal that corresponds to an end point changes depending on the amount of open area that is being etched. As there the fraction of open area decreased the amount of signal observed at end point reduces. As the amount of signal that is observed falls the noise that is inherent to the plasma system begins to have a more serious effect upon the ability to determine the end point. This signal to noise ratio is of fundamental importance as for the lower open areas it becomes difficult to determine the difference between a genuine end point and a change in signal corresponding to noise. This is an area that is a significant focus of research for many groups. There have been many efforts made using statistical techniques to improve the signal to noise ratio and these will be discussed later in this review.

3.6. Optical Emission Spectroscopy

One of the earliest uses of OES for end point determination was carried out in 1980 by Hirobe *et al.*[39]. In this work Hirobe demonstrates that by analysing the optical emissions of two specific wavelengths it was possible to determine the end point of a plasma etch. In this instance an etch of silicon nitride (Si_3N_4) on poly-silicon was conducted and the two wavelengths chosen were one relating to N_2 (674nm) and another relating to SiF_x (777nm).

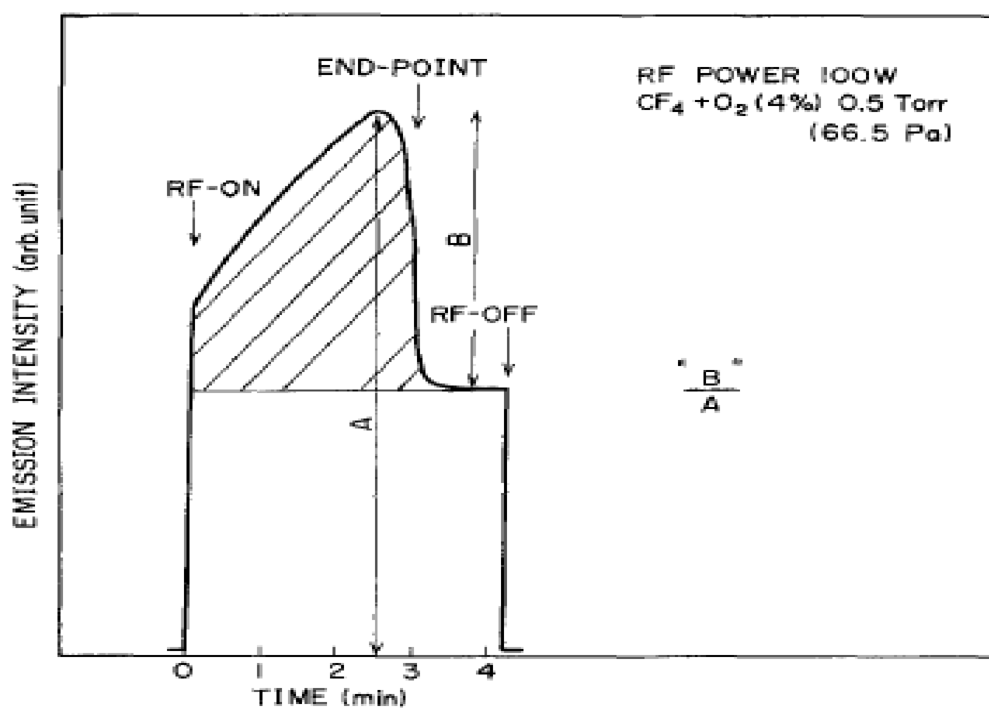

Figure 3.6.1 Results obtained by Hirobe *et al.*. for the determination of end point using 674nm optical emission line (N_2 as the emission species)

It is clear to see from this result that there is a significant change that occurs at the end point of the etch process. However these results are not for individual features but for relatively large surface areas, this is detailed further below where Hirobe uses the ratio of the two intensities B and A as shown in the picture (the minimum and maximum intensity

respectively) to describe the surface area for which it was possible to obtain an end point simply using individual wavelengths to determine the end point.

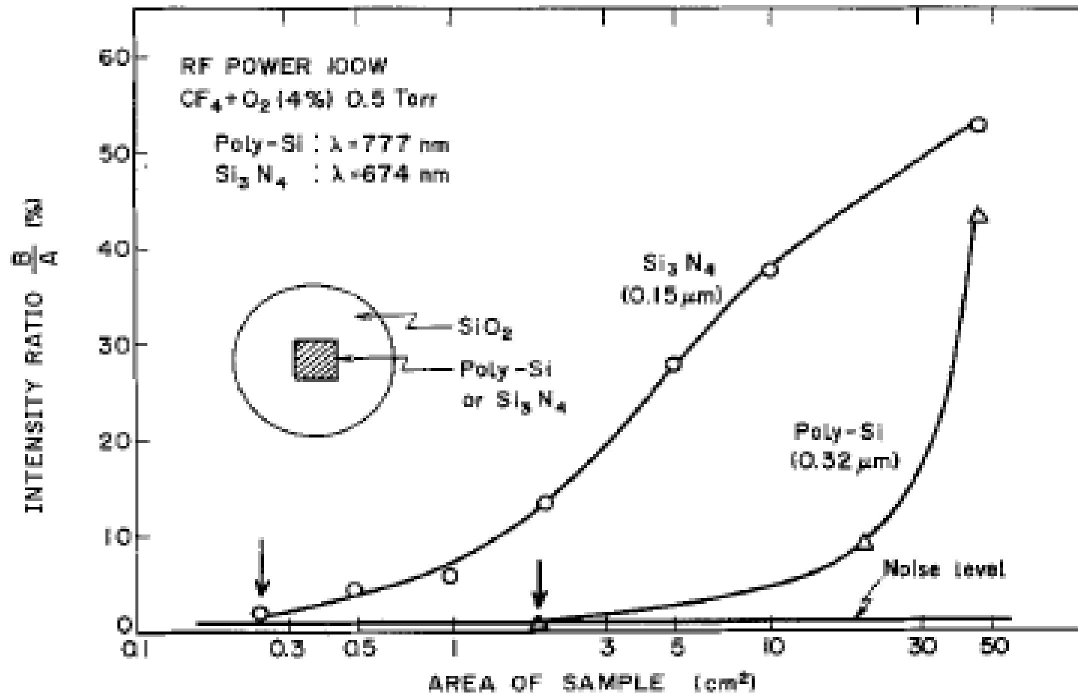

Figure 3.6.2 Results obtained by Hirobe *et al*. detailing the sample areas for which an end point was achievable

Hirobe used sample sizes of $0.3cm^2$ for Si_3N_4 and $2cm^2$ for poly-silicon and was unable to evaluate an end point. These are significant sizes, many orders of magnitude larger than the sizes of features etched in current plasma etch processes. Thus this pioneering work proved the principle but also highlighted some of the issues that remain a problem to this day.

In 1995 Litvak[40] conducted a similar work in this field using a monochromator/photomultiplier approach with signal conditioning and end point algorithms to analyse optical spectra in order to achieve an end point. In this case Litvak was investigating end point determination in SiO_2 contact etch in both parallel plate (diode)

and high density plasma reactors, and high selectivity poly-Si over SiO_2 in a chemical downstream reactor. Of the two the former is of interest here whereas the latter is of less interest as although OES is used to identify the end point there is no plasma in which the excitation energy is provided by chemical ''heat of reaction'', this is known as chemiluminescence. In this article Litvak attempts to overcome the problems of noise found when using a monochromator/photomultiplier system. The two significant types of noise are identified as the following:

Photon noise or ''shot noise''[41] is noise which arises from statistical fluctuations in the creation and detection of photons. In many cases, a small signal change is seen at end point.   This signal change is small compared to background radiation, which is often from the same emitting species; the background radiation drives up the total number of detected photons, and therefore the noise also increases.

Background drift and fluctuations. As described the signal change at end point is often small, when this is the case small changes in plasma stability, or in surface conditions, may interfere with end point detection as they lead to fluctuations in the optical emissions which swamp the end point signal.

In order to resolve the noise issues described above Litvak proposes and shows the effectiveness of using a second channel to act as a background noise channel which can then be used in conjunction with an end point detecting signal (through a simple ratio algorithm) to eliminate the noise. This provides a simple system for determining end point with significantly reduced impact due to noise.

The following figures (Figure 3.6.3 through Figure 3.6.5) are taken directly from the work of Litvak[40]. Figure 3.6.3 shows the complete spectrum for a silion oxide etch. Included are the emission lines that Litvak uses for his end point signal (CO 483nm) and also the line he uses to enable him to eliminate the background radiation (H 486nm / Ar 488nm)

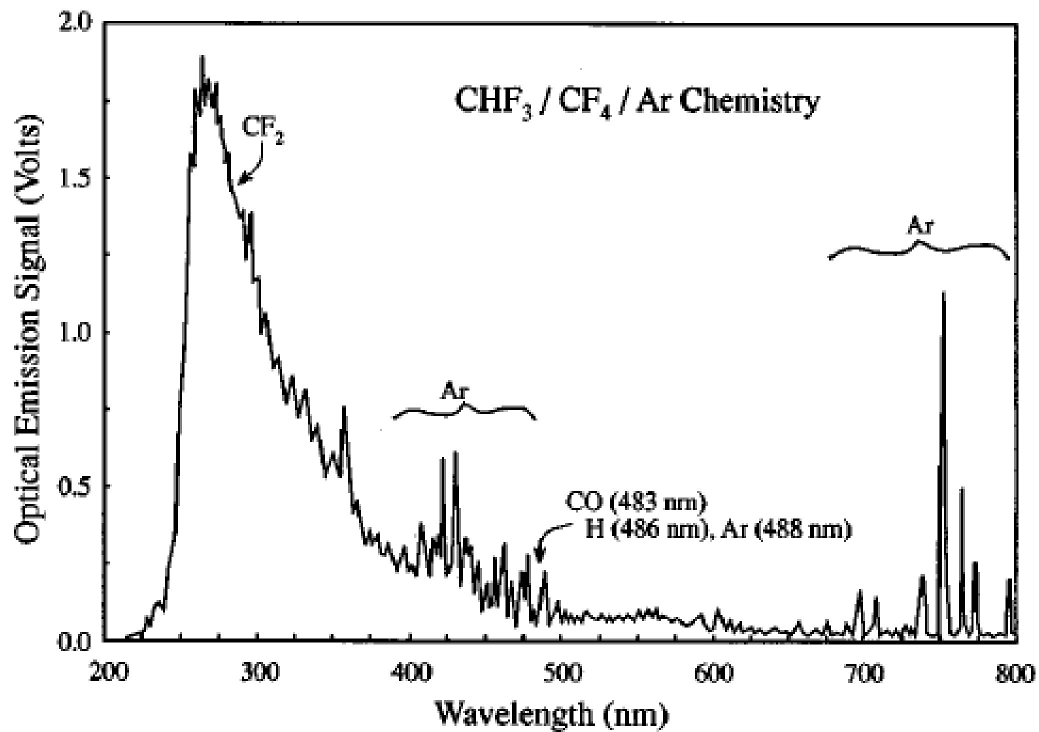

Figure 3.6.3 Plasma emission spectrum, oxide parallel plate etcher [40]

In the following figure (Figure 3.6.4) Litvak has shown the trace achieved for the two emission lines from an SiO_2 plasma etch. In the first trace (a) there is no single unambiguous signal change in which could be considered an end point. However when the two are combined (b) in order to remove the background noise using the simple ration technique there is a clear change in the signal which can be attributed to the end point

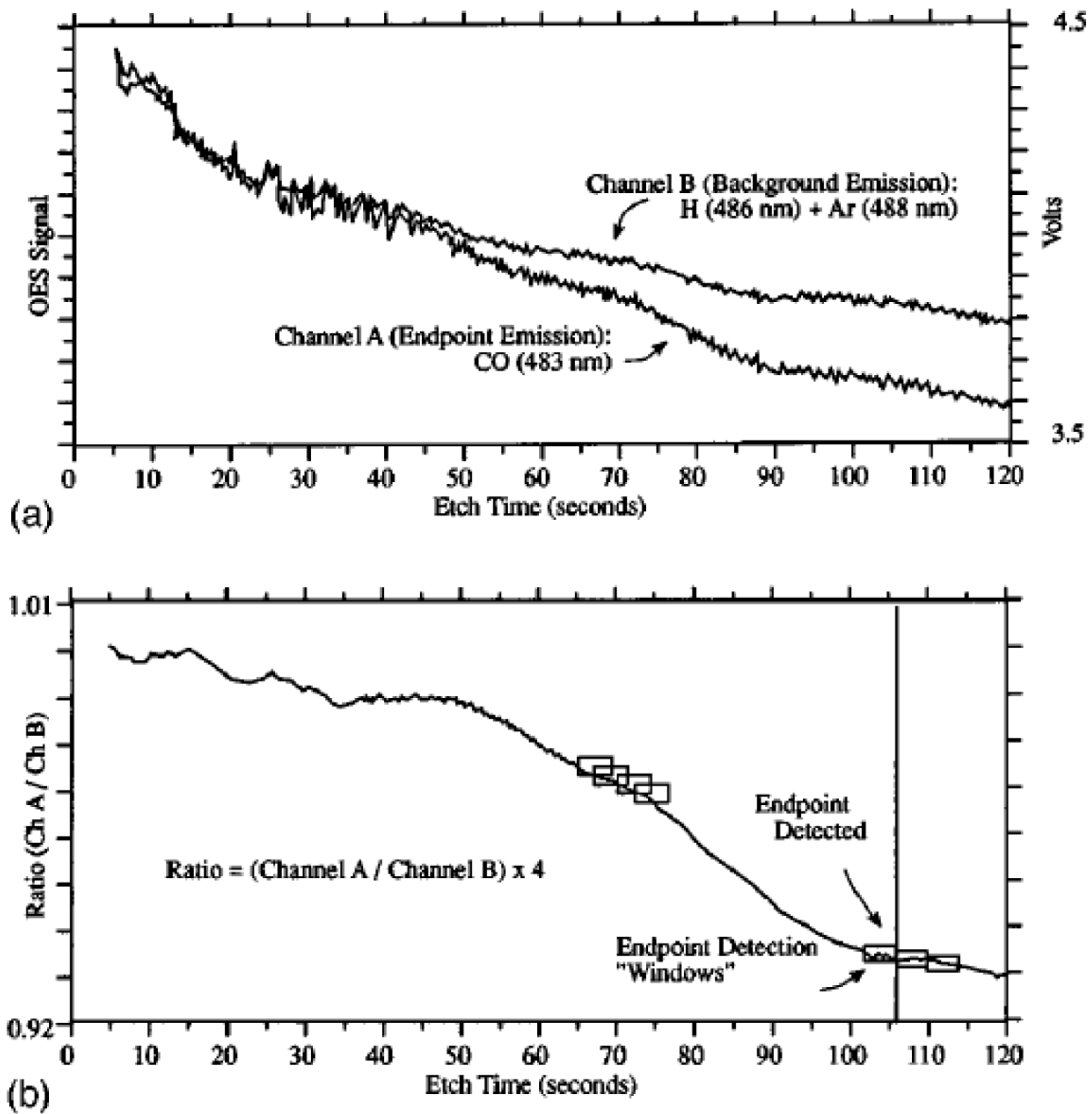

Figure 3.6.4 a) Optical emission signals from ~1% exposed area SiO_2 contact etch, parallel plate etcher. b) Same data, displayed as ratio of end point to background signals. End point detected (ratio has been digitally filtered)[40]

The final trace (Figure 3.6.5) from Litvaks work shows that the technique yields two separate end points for a two stage etch process involving shallow contact etching and a deeper contact etch.

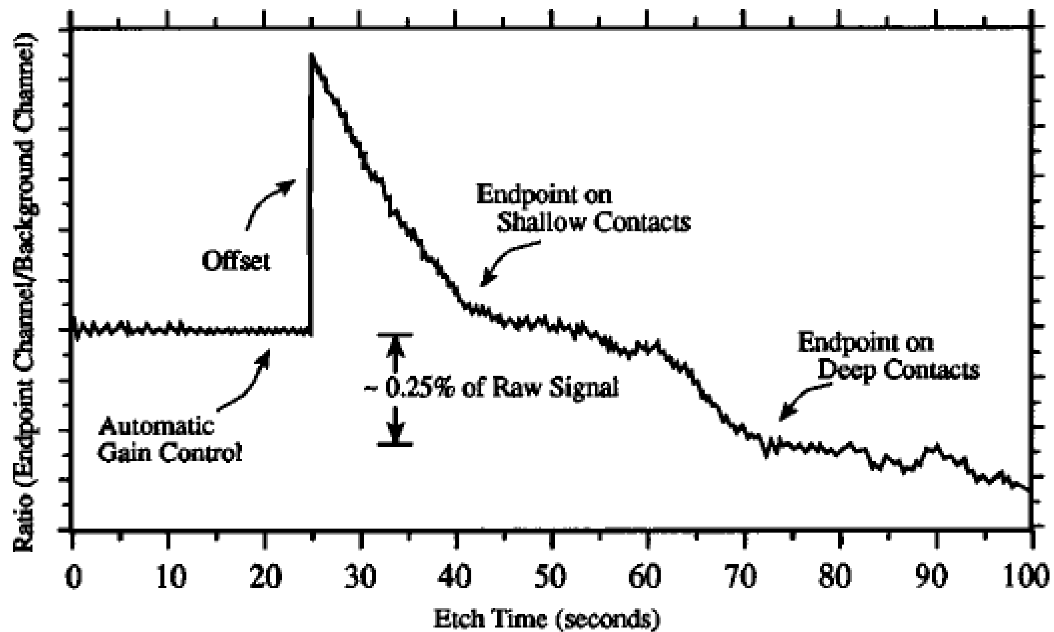

Figure 3.6.5 Approximately 1% exposed area SiO_2 contact etch, parallel plate[40]

Through the introduction of a second channel used to eliminate background noise Litvak has shown that it is possible to determine end points for low exposed (~1%) area etch processes. In order to achieve this, a simple ratio algorithm was used; this has shown that statistical treatments are a possibility for reducing the effect of noise and increasing the signal to noise ratio.

In 1996 Benson *et al.*[29] demonstrated a similar technique which uses actinometry to provide a real time sensor system for monitoring and controlling the etch rate. Actinometry is a technique which takes the ratio of emission intensity of the species of interest to that of an inert species[42]. This technique is the same as that used in the work of Litvak[40]. Benson *et al.*. have used Fluorine as the active and Argon as the inert species. The process is used to maintain a constant etch rate for a polysilicon etch with results shown below (Figure 3.6.6).

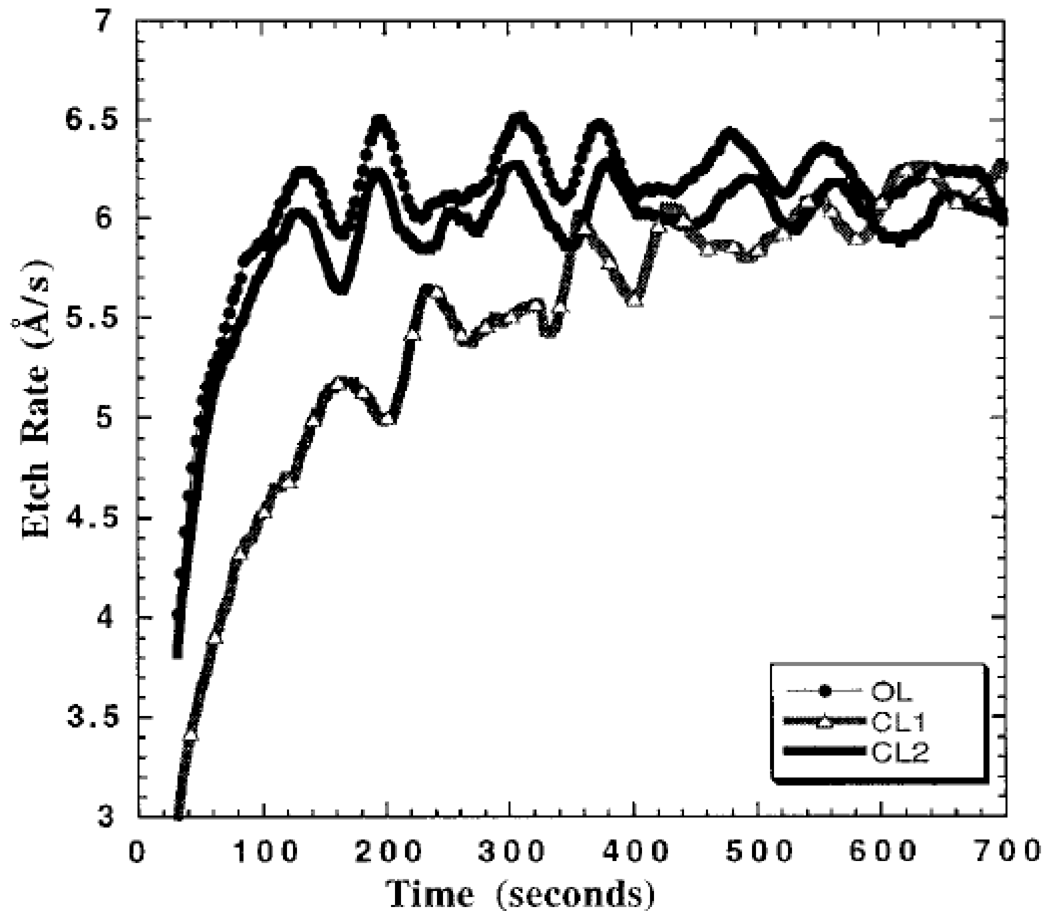

Figure 3.6.6 Open-loop *(*circles) and closed-loop (CL1: line with triangles; CL2: thick solid line*)* etch rate results [29]

In the results there are two different feedback control experiments. In CL1 (closed-loop 1), the controller was designed to keep the fluorine concentration, V_{bias} and pressure constant. The idea being that by keeping those variables fixed, the etch rate could be made to follow a chosen trajectory. For CL2 the loop was designed so that the plasma controller would follow the trajectories of the variables from the open loop case. The results show that for CL2 the etch rate follows that of the open loop case in magnitude and shape. The results for the CL1 case are less clear with a significant variation in the etch rate being observed where it was expected to be more constant. Although these cases show the use of OES to monitor and control etch rate it is clear that the use of OES to control the parameters of a plasma

process in order to achieve a desired etch rate is not straightforward. This is key to the use of OES as an end pointing system as if it can be used to attain a determinable and stable etch rate the traditional method of end pointing using the time of etch becomes more feasible.

In 1998 Stevenson *et al.*[43] reported a complete plasma monitoring system that was able to continuously perform fault detection whilst simultaneously able to respond to end point signals. This system uses OES device to capture the required data for the aforementioned analyses. The system was initially designed for printed wiring board applications where the features involved are clearly much larger than those involved in silicon etching. However the group have adapted the tool to perform similar analyses of integrated circuit production. The initial results given in this report although promising are very limited and show that the system is able to identify the differences between the emission spectra observed in totally difference processes and not the variation in individual processes which is the requirement for accurate end point detection. These results are shown below (Figure 3.6.7) and provide details of the spectra observed in plasma etch processes of integrated circuits.

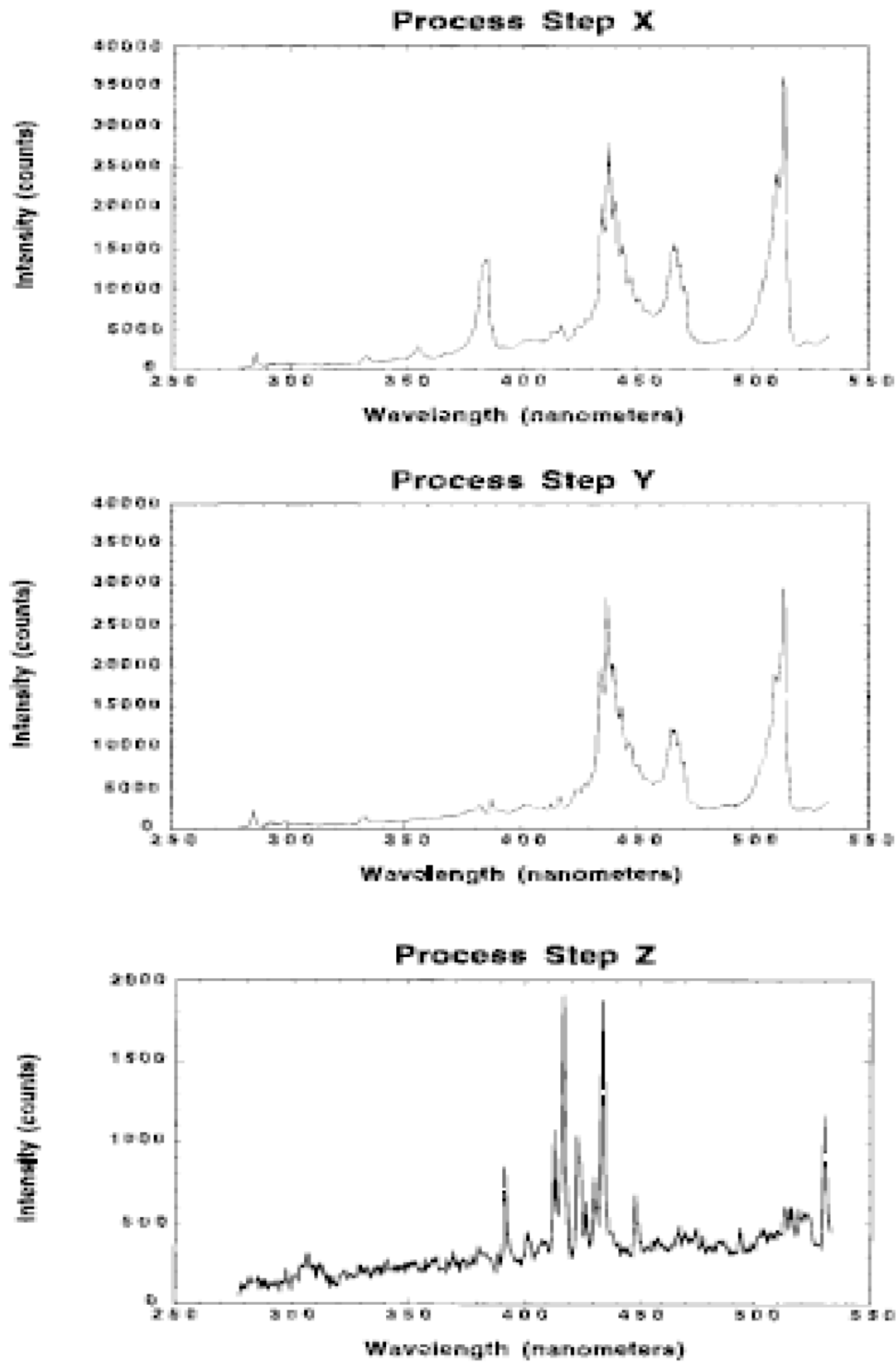

Figure 3.6.7 Representative spectra from semiconductor oxide etch process showing three of the many process steps that can be distinguished using OES[43]. The details of the steps are not provided in the article.

Although it is clear that there are three separate processes being observed here the authors provide no details of the nature of these processes other than that they are all oxide etches. This suggests that this system would have the accuracy to achieve reasonable results for process identification but may require improved sensibility for end point detection.

3.7. Optical Emission Spectroscopy in III/V Compound Etching

The use of OES for silicon etching has been largely discussed but another area where OES has begun to be developed is for the etching of advanced III/V compound devices. This has been demonstrated by Lee *et al.*[7] where bipolar transistors were fabricated using a dry etch plasma process. OES was used to follow the etching of the AlGaAs giving the following trace (Figure 3.7.1).

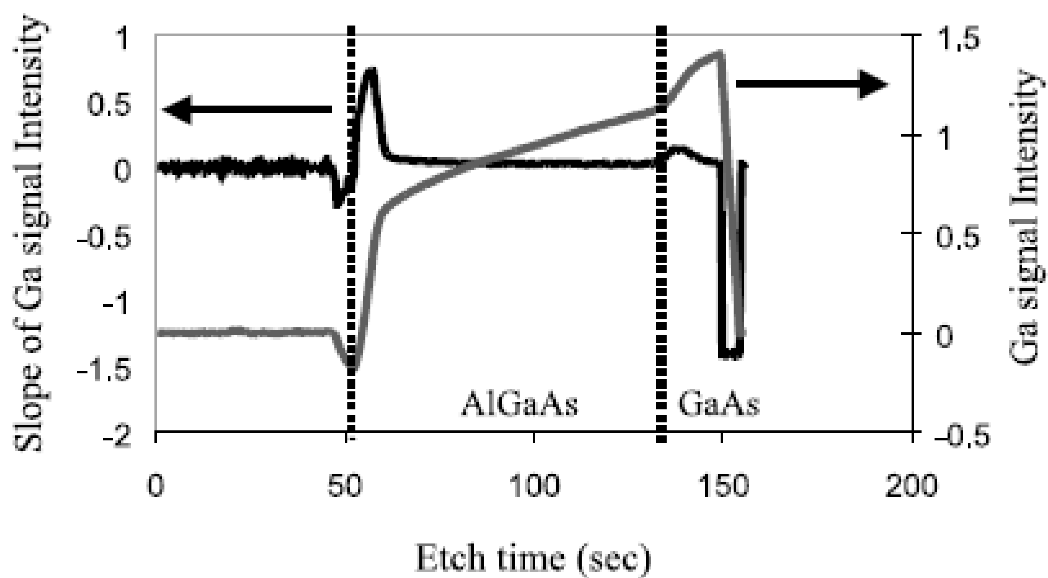

Figure 3.7.1 Trace of Ga peak intensity (417 nm) and its slope during AlGaAs/GaAs etching in BCl_3/N_2 ICP etching[7]

Although this trace shows a clear deviation that occurs at the point where there is a transition between the layer of AlGaAs and GaAs the pattern density (previously referred to in this work as open area) of this etch was approximately 50%. This is significantly larger open area than that seen in contact and via etches (less than 0.5%). However this is an untreated signal and a single emission line is used where in the earlier cases two signals have been combined to increase the signal to noise ratio. However this work does clearly show the potential for OES to be used for end pointing in applications other than silicon and silicon oxide etching. Using a similar technique this group also applied the same technique to determine the end point of an etch process with Indium Gallium Phosphide (InGaP) on Gallium Arsenide (GaAs). Again in this case the pure trace (slope of this trace is also shown) was used to obtain the end point; the same photo-resist pattern was also used. The trace used is shown below (Figure 3.7.2).

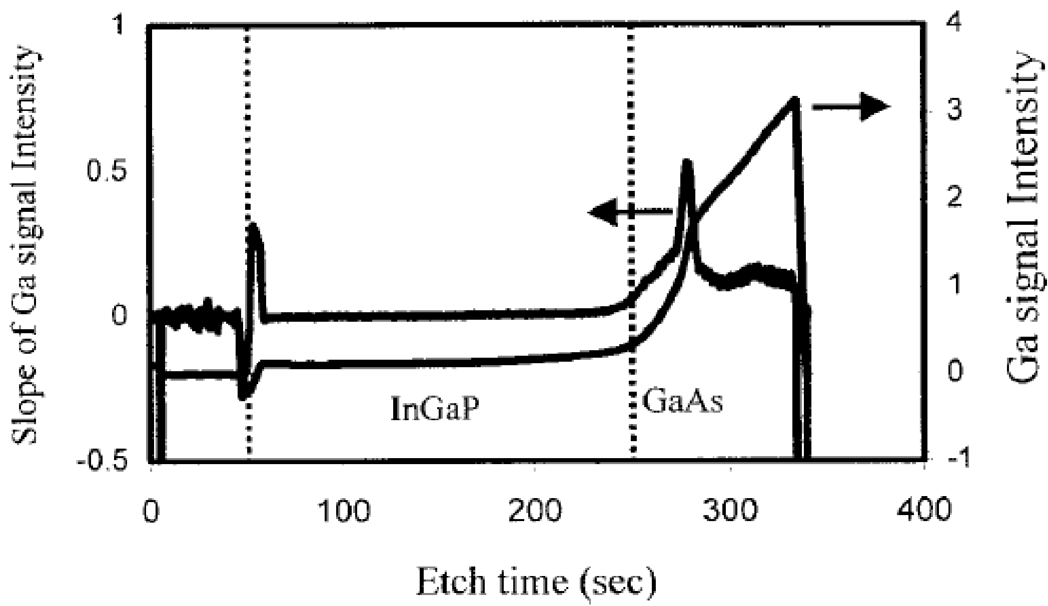

Figure 3.7.2 Trace of Gallium peak intensity (417 nm) and its slope during InGaP/GaAs etching in BCl_3 /N_2 ICP etching[44].

3.8. Statistical Treatments of Optical Emission Spectroscopy

The previous work that has been conducted into using OES as a tool for the determination of end point in plasma etching has predominantly used spectral information without any statistical treatments. Although this has been shown to work for some cases where a relatively large open area involved, when smaller open areas are concerned the signal to noise ratio that is observed becomes very small. The changes in the signal intensities that occur at end point become indistinguishable from the noise at which point the technique becomes unviable. Through the use of mathematical modelling of the system and statistical analysis such as multivariate statistics it is possible to increase the signal to noise ratio and achieve end point detection for low open area etching.

A first example of multivariate analysis has already been discussed wherein the spectral information of an inert gas was used to act as a background feed in order to eliminate noise[29, 40]. In these cases there are only two channels used to reduce noise. The principal behind multivariate analysis is in essence the same, the significant difference being that more than two channels are used. One of the key problems in this approach is the determination of which channels to use to obtain useful information. With modern spectrographs using charge coupled devices to record the spectrum large data sets are obtained for individual plasma processes. During a plasma etch a spectrum may be recorded between 200nm and 800nm with a resolution of 0.5nm leading to 1200 intensity readings for each time interval. Only a select few of these will have significant variations in their intensities due to the changes in the plasma, which in turn are a result of the changes in the conditions at surface of the wafer. Thus the action of determining which wavelengths to use in order to achieve the clearest results is formidable.

This technique of reducing the number of variables in order to improve the simplicity of the statistics was considered by Chen *et al.*[45]. In this instance Principal Component Analysis (PCA) and Partial Least-squares Analysis (PLS) were used in order to determine which spectral lines were associated with particular characteristics of the etch; the etch rate, the Aspect-Ratio Dependent Etching (ARDE) in the centre and at the edge of the wafer and wafer etch uniformity. A third technique was also used which was based upon regression models using the intensities of preselected wavelengths. In this latter case the wavelengths were selected based upon the species associated with them which are active in the etch process. An R^2 technique, which evaluates the degree of correlation between two results was used to evaluate the effectiveness of the techniques by comparing predicted results with the measured results. Using the preselected wavelength techniques provided results which could model greater than 80% of the etch rate and uniformity results but could only model 65% of the variation in ARDE. Despite the high R^2 values obtained irregularities in the plasma caused highly correlated variation in the spectral lines. This induced a multicollinearity problem leading to the possibility of poor predictive ability of the model.

The PCA model used is based on reducing the number of variables by projecting the data onto a lower dimensional space and converting into an uncorrelated data set. PCA transforms the input variables to a set of orthogonal variables known as principal components (PCs), which are linear combinations of the original variables. In this case seven Principal Components were found to be able to explain 99.9% of the process variation. The models based on these seven PCs were able to explain 85% and 95% of the variation in etch rate and uniformity respectively. Also 75% of ARDE could be modelled.

The technique was also used to show that only 10-20 of the spectral peaks had any significant effect upon the PCs.

The final approach adopted in this work was Partial Least Squares Analysis. Like PCA, PLS projects the data onto a low dimensional space defined by a small number of basis vectors known as latent variables. These latent variables contain a summary of the important information contained in the original data set. For PLS both the input variables and the response variables are used to achieve the transformation. One result of this is that less inputs are required to achieve the same information, here it was shown that 2-6 inputs were able to predict the wafer responses as accurately as the PCA approach. The results that were achieved are all summarised in the following table (Figure 3.8.1).

TABLE II. Summary of the results of chamber state models.

Data reduction method	No. of input variables	R^2	Adj. R^2	Data reduction method	No. of input variables	R^2	Adj. R^2
Response: oxide–ER				Response: oxide–uniformity			
Species identification	8	0.88	0.834	Species identification	8	0.94	0.92
PCA	7	0.89	0.851	PCA	7	0.96	0.951
PLS	5	0.9	0.872	PLS	5	0.96	0.955
Response: ARDE at center				Response: ARDE at edge			
Species identification	8	0.56	0.392	Species identification	8	0.64	0.507
PCA	7	0.62	0.5	PCA	7	0.74	0.66
PLS	2	0.42	0.38	PLS	3	0.64	0.6

Figure 3.8.1 Summary of results of chamber state models found by Chen *et al. [45].* Here PCA is principal component analysis; PLS is partial least squares; R^2 is the degree of correlation; ER is the etch rate and ARDE is aspect ratio dependent etch.

Of the three techniques used here to reduce the size of data sets used there was no overwhelmingly superior method with all achieving similar efficiencies. However the PLS achieved the same results using less inputs. This work shows promising results however the results are not based on real time readings but on many wafers and having taken individual spectra for several wafers during the repeated etch processes. An improvement on this work would involve developing the system to be able to provide real time predictions based on the OES output from the models.

PCA has also been used in a separate case that has included the time dependent nature of a plasma etch. Rangan *et al.*[46] describe a method whereby real time varying OES signals are described as a dynamical system. A model of this system is built off-line from empirical data; this model can then have data from future real time models fitted to it. Internal states corresponding to the real time models can then be estimated. Using this method raw OES data is converted to just a few state variables. This achieves a more manageable data set which can be used in feedback control. The model is also shown to be able to identify physical characteristics of the etch such as key spectral lines of the OES data and the end point of the etch. In this work the model is demonstrated on a commercial etch process using an Al/TiN/SiO_2 multilayer wafer. However the results could be applied to other etch processes such as silicon on silicon oxide. The results (Figure 3.8.2) of this work show that using a simple method for modelling and filtering of OES data based on PCA and jump linear filtering it was possible to identify the key spectral lines and also identify transitions between the different layers. The figure below (Figure 3.8.2) shows the variation in the principal components over the duration of the process. The PC variation is essentially the

variation in optical intensity of several wavelengths which have been combined by the principal component technique. The end point of the process is also included in the figure (shown as the clear drop in OES intensity from 20 to -10 in PC 1).

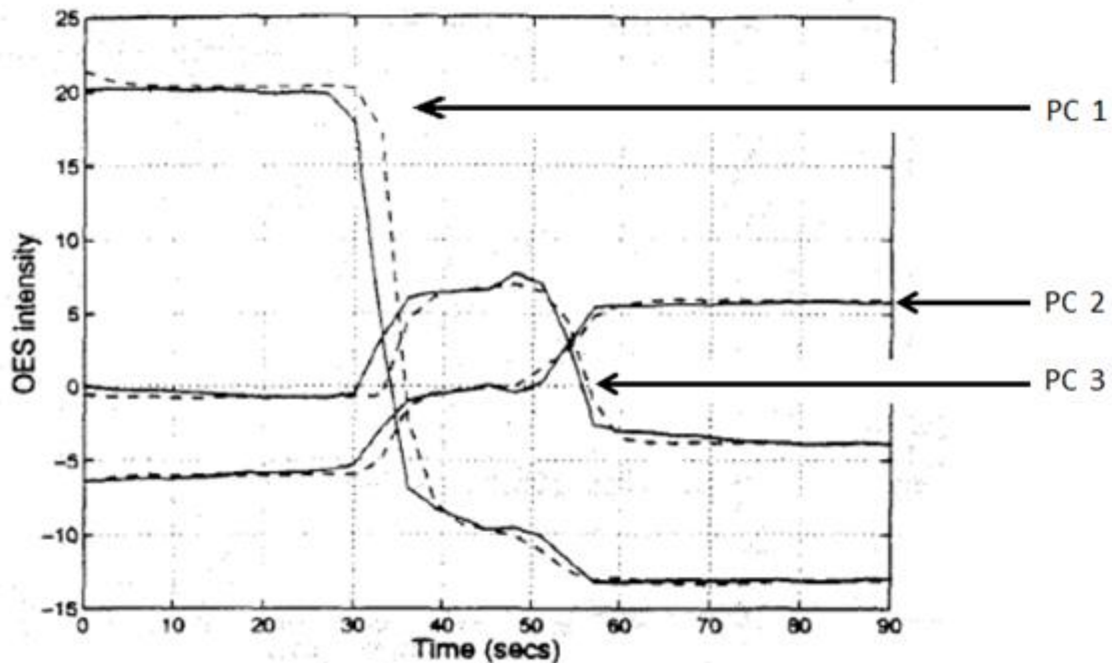

Figure 3.8.2 Optical Emission Spectroscopy Principal Component Analysis from a typical etch (solid line) and the one-step-ahead prediction output from the jump-linear filter (dashed line). The Principal component labels have been added to the image for clarity.

PCA has developed to be a key statistical tool in the field. The aforementioned work has mainly hinted at its possible use as a technique for assisting in the determination of end point. In 2000 White *et al.*[47] carried out an extensive study into the use of PCA with a direct relation to end point detection for low open area plasma etching. In this case PCA is used to determine which spectral channels should be used in the end point detection and the respective weightings. This practice is then added to through the use of T^2 and Q statistics proposed by Le[48] to determine the end point once the appropriate principal

components have been determined. The use and efficiency of the T^2 is demonstrated in the article in the following graphs (Figure 3.8.3). The two techniques produce a single statistic that utilises the correlation between different channels. Essentially the techniques give a single value that shows a significant change when two signals show a correlated change. This can be applied to two separate wavelengths or to two principal components, when the two wavelengths or two components see a correlated change the T^2 value will change significantly.

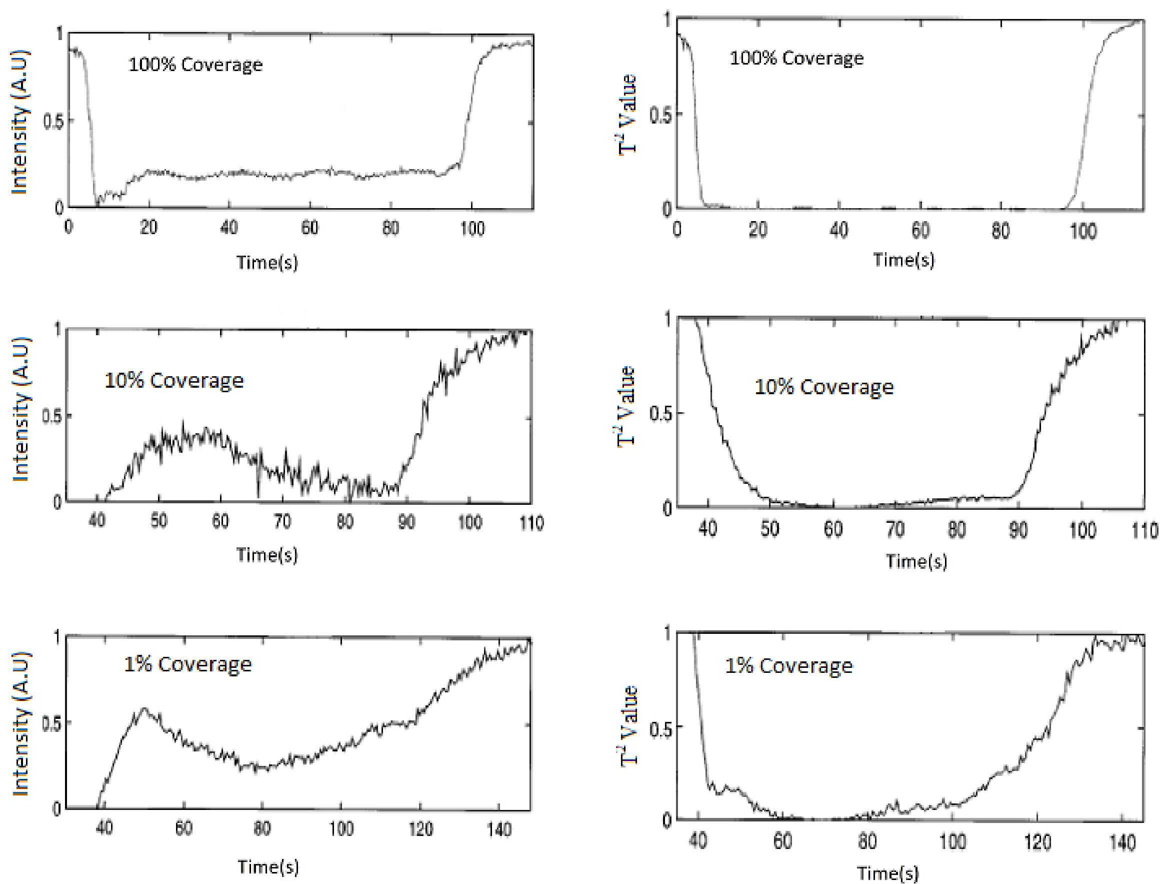

Figure 3.8.3 OES trace for decreasing open area etches. The left shows the untreated data. The right shows the treated system using T^2 analysis[47].

As can be seen from the images on the left the pure OES signal shows a clear end point for the blanket etch but as the open area decreases the noise increases and the end point is

more difficult to resolve. In the case where the T^2 treatment has been used the end point is made clearer and the noise is significantly reduced. The Q statistic was also investigated and although it was shown to cause an improvement it had inherent drawbacks due to the inability to differentiate between process drift and genuine end points.

PCA has been shown here to be extremely useful in the determination of end point for low open area etch processes. This has been further explored by Yue *et al.[38]* where end point signals have been detected for open areas of as low as 0.46%. This was achieved by applying the PCA technique to OES data containing an end point signal, this enables the separation of the endpoint signal from the noise and ‘‘background’’ signals due to photo-resist and chamber etching. The OES data is mean centred prior to the PCA treatment (scaled to have zero mean). The OES data had been separated into the principal components (shown below Figure 3.8.4).

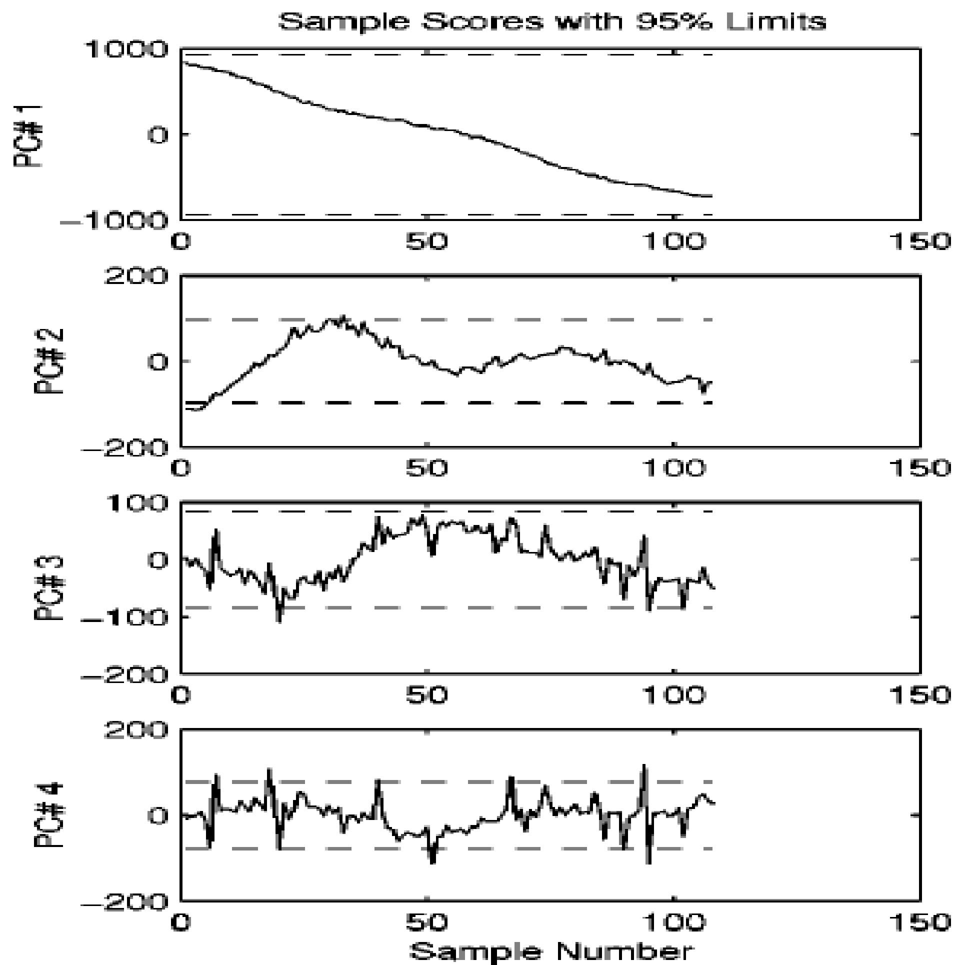

Figure 3.8.4 Principal components of Optical Emission Spectroscopy data[38]

The first principal component was shown to contain approximately 80% of the variance in the data set and exhibit a linear trend. This was shown to correspond to wavelengths which had a linear trend over the course of the entire etch with no significant variation which could be related to end point. Thus the first principal component was discounted. The second and third principal components both contain clear maximum or minimum which were shown to correspond to end point signals. This PCA was then applied to separate wavelength windows. By analysing which windows contained end point signals the majority of the wavelengths were discarded leaving only the ones that contain end point signals. The

next section of the work discusses the “sphere” criterion for discarding unwanted wavelengths. Each wavelength or group of wavelengths has a loading which is related to the transformation from the original data set to the lower dimensional one achieved through PCA. The wavelengths involved are placed onto a coordinate system as shown below (Figure 3.8.5). Any wavelengths that fall inside the sphere are discarded from the system. The radii in this case was set to 0.1 and as such thirty wavelengths are considered to contribute to the end point detection system. This system was shown to have been used successfully to determine end point for features in a silicon oxide etch with open area as small as 0.47%.

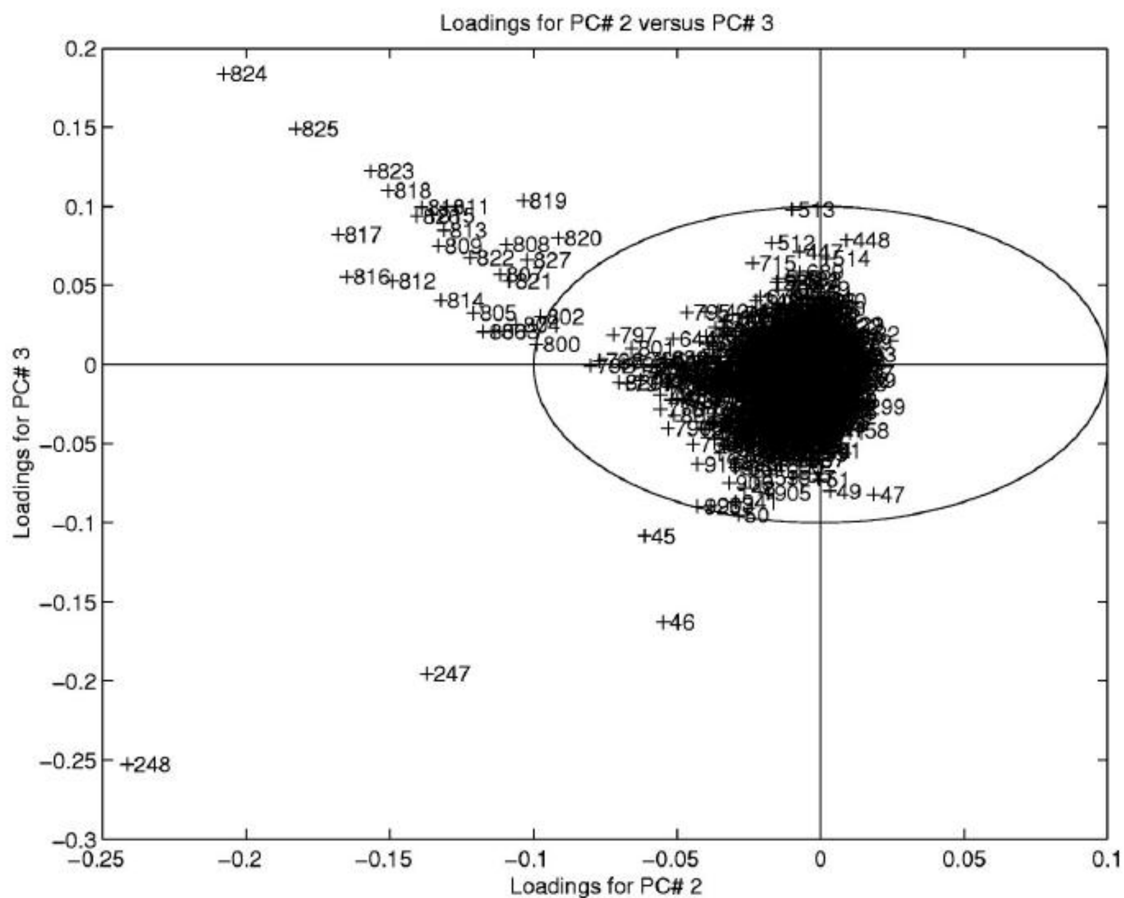

Figure 3.8.5 Loading plot of the second and third PCs. A circle criterion is used to select important wavelengths[38]

3.9. Laser Interferometry

Alongside OES Laser Interferometry (LIR) is one of the most commonly used techniques for determining end point in plasma etch processes. It is often used due to the limitations that are found in OES in certain circumstances. The unique ability of LIR is that it doesn't require a transition between separate materials. This is because it follows the etch process through the individual layers of material as described earlier. One of the earliest reported uses of LIR for end point detection was by Sternheim *et al.[49].* In this work is discussed two separate methods of LIR are discussed. The first method is shown below alongside results obtained using the method.

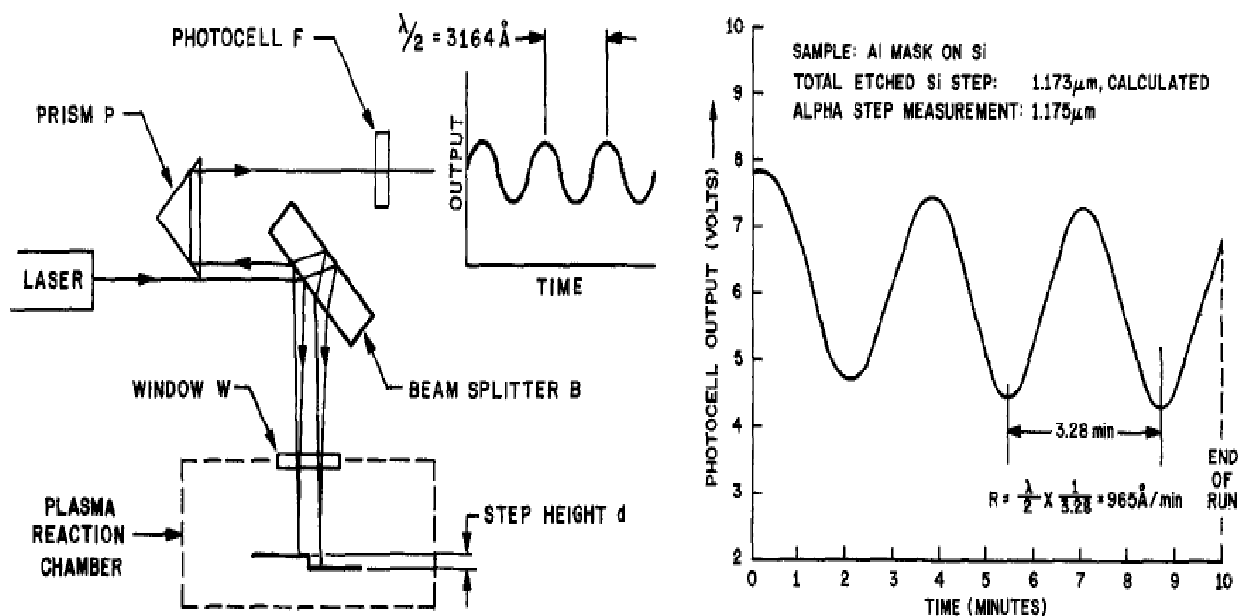

Figure 3.9.1 Double beam laser interferometer with typical response curve[49].

As can be seen in the diagram this method uses a double beam system. A laser beam is split into two these are then directed onto the surface of the wafer; either side of a growing feature edge in silicon. The beam is then reflected from the surface and directed onto the photocell. The resultant trace oscillates as the surface is etched and the depth of each cycle

can be found from the wavelength of the laser. The total etch depth is found from the sum of the fringes. The results in this case were found to be accurate to within 2% of measurements taken using a profilometer. The significant drawback of this method is that it uses two beams which have to be meticulously situated to fall on either side of the feature. In this case the diameter of the beam used was approximately 1mm, which is a significant area in terms of features in silicon etching.

The second method used is a single beam technique as shown below (Figure 3.9.2). In this case a single beam is directed onto the surface of silicon. Only the portion of the beam that is incident on the surface at 0° is reflected back to the photocell, the rest is scattered. The intensity of the measured signal corresponds to the depth of the trench as described in the theory section previously. As can be seen when the power is doubled (leading to increased etch rate) it is shown in the trace as an increased frequency.

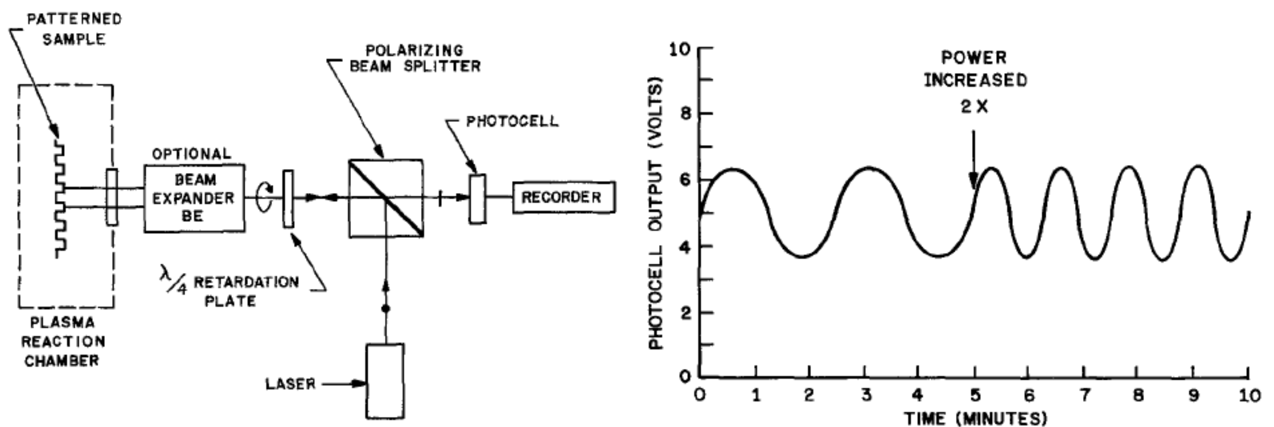

Figure 3.9.2 Single beam interferometer with typical response curve[49].

The accuracy of this method was measured as before and was shown to be better 6%. Both these methods are extremely useful as it is possible to follow the etch in real time and as such determine the effect of the plasma parameters on the etch rate. A limitation in this method is that in order to achieve accurate results the depth of the trench must be greater than half the wavelength of the laser.

Although the base technique for LIR is well understood there are many subtleties such as etching from a layer one material into a second material. By using the reflectance properties of the materials in question (with arbitrary etch rates) it is possible to calculate the interference patterns that will occur when etching certain materials in given configurations. This was investigated by Heimann *et al.*[50] and using the technique results were obtained which were able to correctly predict the reflectance observed when etching a layer of silicide over poly-silicon.

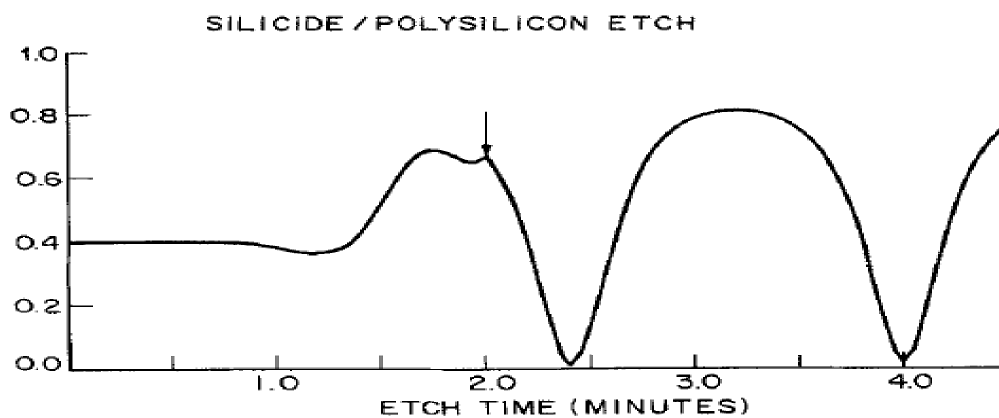

Figure 3.9.3 Calculated reflectance when etching a later of optically absorbent silicide over polysilicon[50]

As can be seen the interference pattern is flat until the plasma has removed the silicide and starts to etch the poly-silicon. This is one example of where modelling the reflectance is useful in predicting and explaining the more subtle aspects of LIR.

Optical emission interferometry has been proposed by Wong *et al.*[15] in this case rather than using an input laser as the source; the plasma itself acts as the light source. Light emitted from the plasma reflects from the surface of the wafer. As with laser interferometry a specific wavelength is chosen, in this case by capturing the light using a charge couple device such as those used in OES and analysing the phase of the light at the chosen wavelength. This phase changes as the depth of the trenches being etched varies. The phase change is oscillatory and as such the properties such as etch rate and end point can be determined. The results of this method when used to determine end point are shown below (Figure 3.9.4).

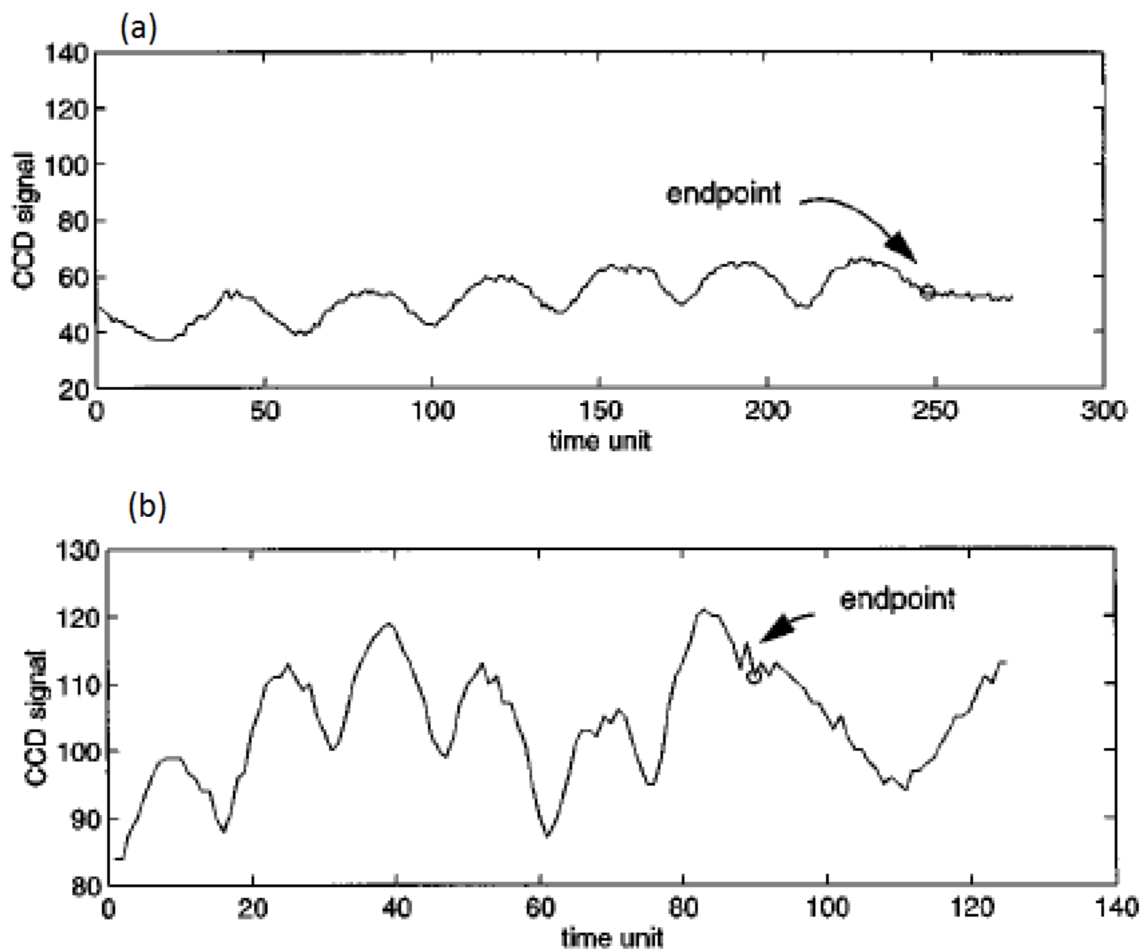

Figure 3.9.4 Optical emission interferometry to determine end point of a) bare poly-silicon and b) patterned silicon[15].

Although there is a clear point where the signal loses its oscillatory nature in both cases the oscillatory nature of the signal in the case of patterned silicon is less clear. The method has been shown to be able to deliver end point signals to enable process automation.

3.10. III/V Compounds

In addition to being able to monitor the etch rates involved with silicon and polysilicon it is also possible to monitor etch rates of many other materials such as III/V compounds. This was demonstrated by Hayes *et al.*[37] where InP/InGaAsP structures were etched and monitored using the technique. The separate quantum well are individually identified using the technique.

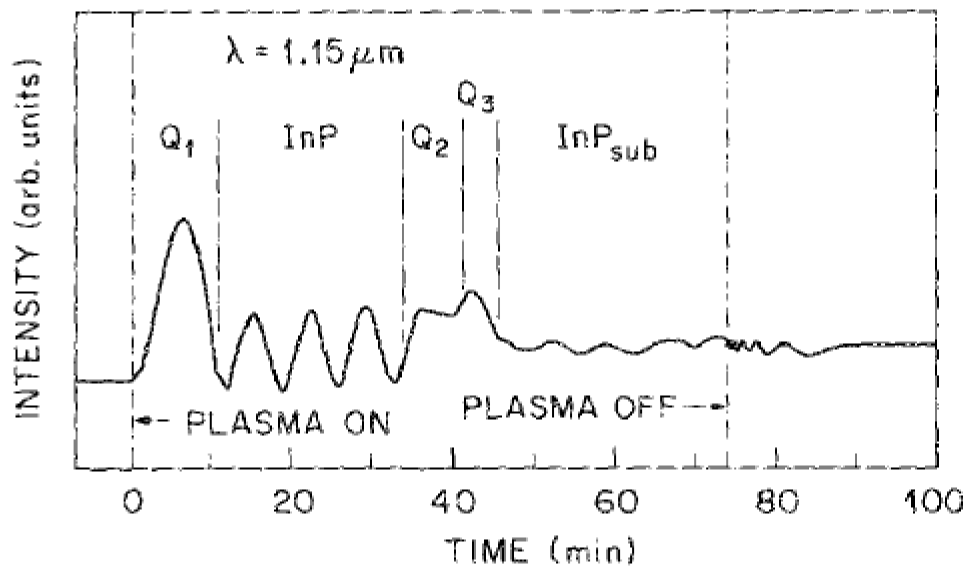

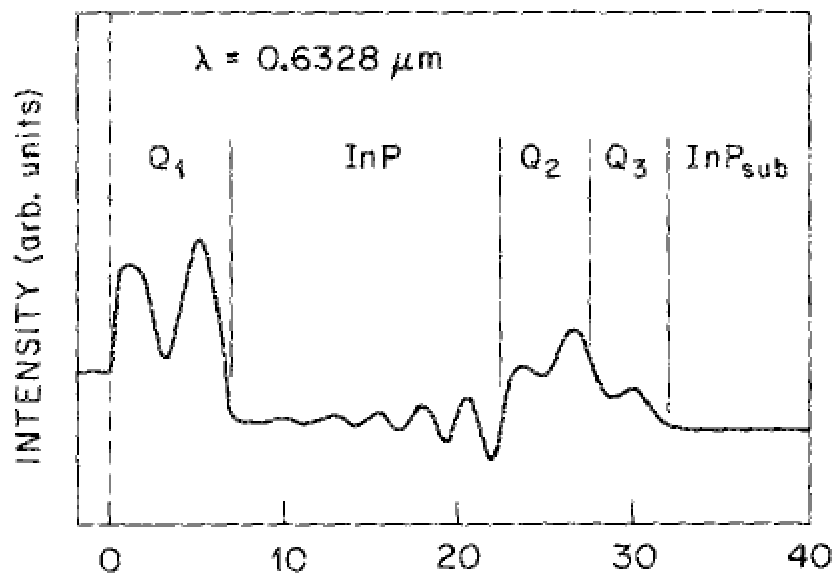

Figure 3.10.1 Etch rate monitoring using lasers with wavelengths of 1.15µm and 0.6328µm[37]. Here the quantum well structures are identified as Q1-Q3

As is shown here the technique can also be used using a smaller wavelength laser. This allows the method to be used to resolve smaller feature sizes. The requirement here is that the layers have to be thin. Where the larger wavelength resolves fringes for the entire layer, with the smaller wavelength the fringes are only resolved as the layer becomes

thinner. In addition to measuring the etch rates and end points in this instance it was shown that it is also possible to determine wafer temperature if the temperature dependence of the refractive index of the material in question is known. This is shown in the first trace where there are fringes evident after the plasma is deactivated. The fringes are a result of the wafer cooling leading to a change in the refractive properties.

LIR was also used by Aperathitis *et al.* [51] in the production of and assessment of laser mirrors in GaAs/$Al_xGa_{1-x}As$. The laser interferometry was used for real-time identification of heterointerfaces within the structure. The etch rate was also monitored and end point control was enabled using the technique.

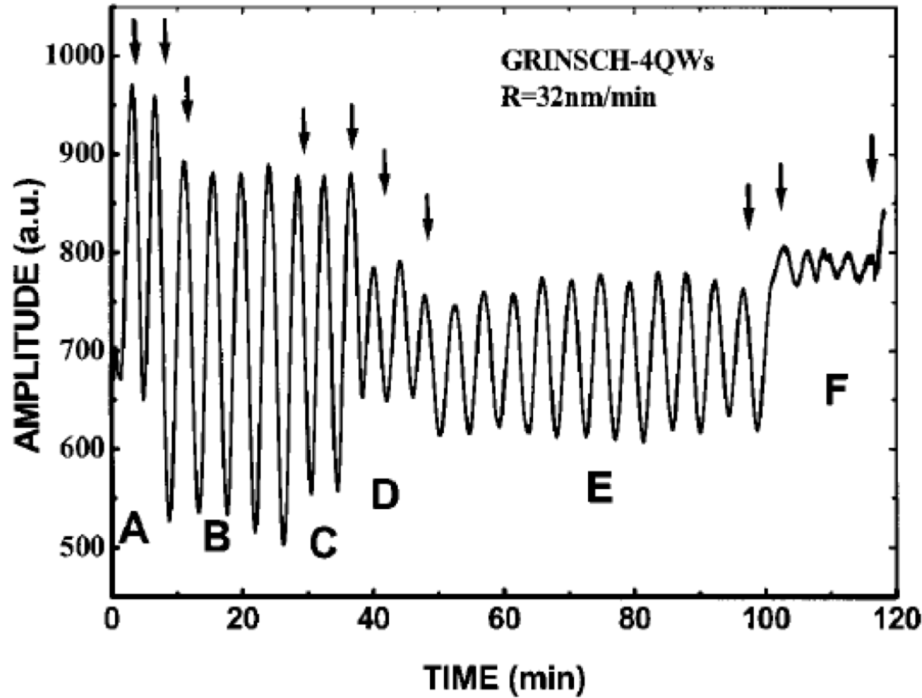

Layer	Al content x value	Thickness (μm)	Regions of laser structure
$p+$ GaAs	0.00	0.15	Region A
p $Al_xGa_{1-x}As$	0.00−>0.45	0.10	Region A
p $Al_xGa_{1-x}As$	0.45	0.60	Region B/cladding layer
p $Al_xGa_{1-x}As$	0.26	0.24	Region C/confinement layer
p $Al_xGa_{1-x}As$	0.26−>0.2	0.05	Spacer
$4\times(Al_xGa_{1-x}As/GaAs)$	0.20/0.00	0.0050/0.0080	QWs
n $Al_xGa_{1-x}As$	0.2−>0.26	0.05	Spacer
n $Al_xGa_{1-x}As$	0.26	0.24	Region D/confinement layer
n $Al_xGa_{1-x}As$	0.26−>0.45	0.10	Region E/cladding layer
n $Al_xGa_{1-x}As$	0.45	1.55	Region E/cladding layer
$n+$ $Al_xGa_{1-x}As$	0.45−>0.0	0.10	Region E/cladding layer
GaAs	0.00	0.10	Region F/buffer layer
GaAs substrate	0.00	400	Region F/substrate

Figure 3.10.2 Laser interferometry signal as a function of etching time, for a Graded Index Separate Confinement structure 4 quantum well (GIS-SC-4QWs) laser structure. The arrows denote heterointerfaces and A, B, C, D, E, and F are regions of the laser structure as described in the table alongside[51]

As can be seen from the above diagram (Figure 3.10.2 Laser interferometry signal as a function of etching time, for a Graded Index Separate Confinement structure 4 quantum well (GIS-SC-4QWs) laser structure. The arrows denote heterointerfaces and A, B, C, D, E, and F are regions of the laser structure as described in the table alongside[51]) the LIR was clearly able to follow the etch process and identify the changes in heterointerfaces. By looking at the variation in the oscillations the Aperathitis *et al.* were able to identify all of the changes in material as they were etched. Specifically the quantum wells were identified in real time as they were exposed and ethed. Under separate requirements any of these interface changes would be suitable to describe the end point of an etch. It is also clear that by counting the number of fringes it is possible to determine the depth of an etch in between heterointerfaces. In this work is also mentioned that the LIR was used as an *in situ* sensor to optimise the etch parameters.

From the work discussed so far it would appear that LIR has the potential to be the basis for end point detection system which could overcome the signal to noise ratios observed in OES end point detection. However there are several developing applications where LIR encounters serious obstacles. MicroElecroMechanical Systems (MEMS) often require the very deep etching of silicon (depths >10-15µm). Traditional LIR end pointing systems described thus far are unsuitable for this due to absorption of the monitoring wavelength, which is typically in the visible region of the spectrum. Heason *et al.*[21] show that through using a probing wavelength in the near infrared region the etch depth can be monitored through a wafer with no absorption affects. This offers new possibilities in end pointing and depth measurement in MEMS and optical devices. One of the processes often used for deep silicon etching is the Bosch process[52]. Alternate etch and passivation cycles of

several seconds each are used to achieve high aspect ratio features. A typical process run using the Bosch process is shown below (Figure 3.10.3)

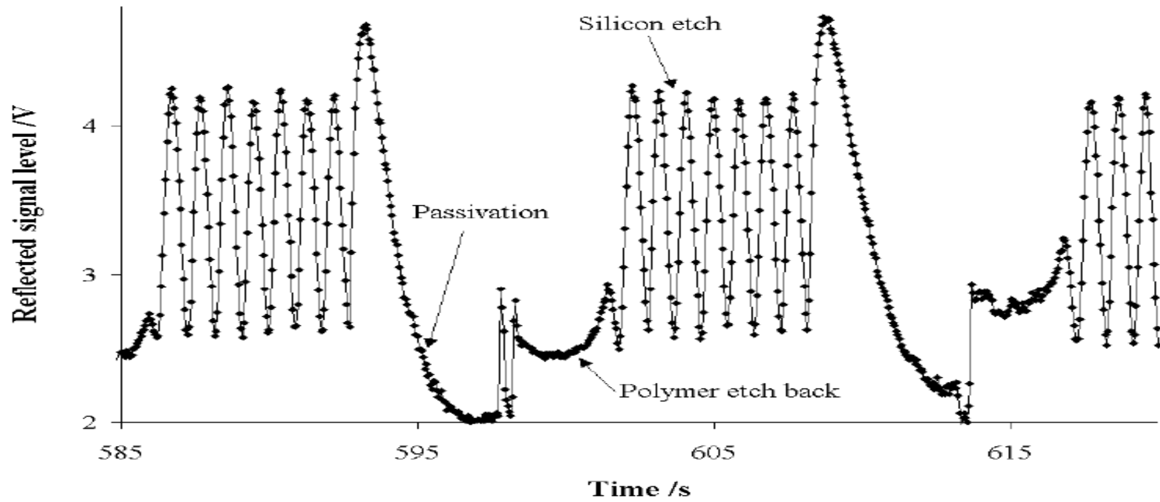

Figure 3.10.3 Part of an interference signal measured using near IR LIR to follow the process[21]

In this case recognition techniques were used to identify the regions where silicon was being etched and as such the determination of the etch depth and rate was possible. A further demonstration of the effectiveness of the technique was given by performing an etch through an entire wafer. The following trace (Figure 3.10.4) shows this. Although the individual fringes cannot be seen there is still an evident signal prior to the end of the etch.

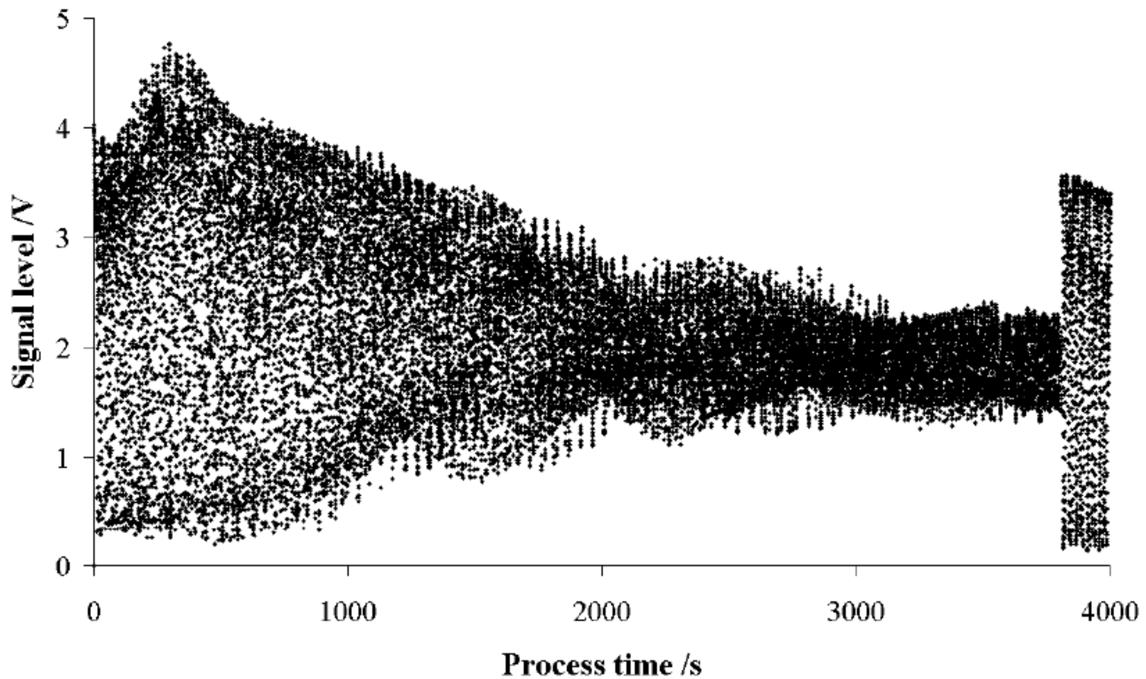

Figure 3.10.4 A trace for a complete etch through a 400µm silicon wafer[21].

Using an infrared laser source for end point detector shows a clear development for in-situ metrology for silicon etches applications. Although the use of infrared allows the resolution of larger feature it also prohibits the resolution of smaller features, which limits the ability as a universal end pointing technique.

3.11. Conclusion

Although there have been significant advances in the field of end point as described here the foundation of the end point detection systems are still essentially based upon the two systems described; laser interferometry and optical emission spectroscopy. Although these systems both have drawbacks there have been significant developments in the treatment of the raw data which has allowed improved results to be obtained. This is particularly evident

in the case of OES where principal component analysis and other techniques are required to deal with the sheer volume of data that is obtained. This is a particular area of interest as the introduction of algorithms can achieve an increase in the signal to noise ratio. This is a vital step in the development of end point control techniques as the open area associated with features continues to decrease the signal that is observed will also become smaller. Laser Interferometry is less susceptible to issues regarding noise but is approaching barriers due to the physical limitations of the technique. The wavelength of the laser that is used as the source of the interferometry ultimately determines the size of the feature for which the technique can be used to determine an accurate end point. The technique of matching wavelengths to the task is a viable option as demonstrated however there are further restraints with LIR in that the end point is only determined at one point on the wafer and inconsistencies in the etch rate due to plasma instabilities across the surface of the wafer are not accounted for. This issue is related to the placement of the focal point of the laser which itself is an issue which restricts the applications of LIR. In an industrial setting it is desirable to have a fully automated system; this is not feasible if the laser alignment is required with the introduction of each wafer.

Although there was a period of development where there were regular advances in the techniques applied this advance appears to have slowed in recent times. This is partly due to the capability of the current systems (largely based on the two techniques described here); however the current drive to develop the capability of mass production of MEMS systems presents a new challenge. One such example of an advance that has occurred as a direct result of this has been a development in the field of OES which is a time correlated system to allow the use of end point detection[53] in the Bosch process. Which has been

presented at conferences but the work is yet to be published in any journals. With this increased demand it is expected that the current techniques that have been discussed thus far will be further developed in order to overcome the non trivial obstacles evident in the field of end point detection.

3.12. References

1. Brattain, J.B., *The Transistor a Semiconductor Triode.* Physical Review, 1948. **74**: p. 230-231.
2. Brattain, J.B., *Nature of the Forward Current in Germanium Point Contacts. .* Physical Review, 1948. **74**: p. 231-232.
3. Moore, G.E. *Proc. Calcatech. Conf. on very Large Scale Integration*. in *California Institute of Technology*. 1979. pasadena California.
4. Jones, L.A., *et al.*, *Chemical Etching of Silicon: Smooth, Rough and Glowing Surfaces.* Progress in Surface Science, 1995. **50**(1-4): p. 283-293.
5. Irving, S.M., *A Plasma Oxidation Process for Removing Phortoresist Films* Solid State Technology, 1971. **16**(6): p. 47.
6. Vodjdani, N. and P. Parrens, *Reactive Ion Etching Of GaAs With High Aspect Ratio With Cl2-CH4-H2-Ar Mixtures.* Journal Vacuum Science and Technology B, 1987. **5**(6): p. 1591-1598.
7. Lee, J.W., *et al.*, *Development of advanced plasma process with an optical emission spectroscopy-based end-point technique for etching of AlGaAs over GaAs in manufacture of heterojunction bipolar transistors.* Solid State Electronics, 2001. **46**: p. 773-775.
8. R. J. Westerman, *et al*. *Endpoint detection method for time division multiplex etch processes*. in *Micromachining and Microfabrication Process Technology XI*. 2006.
9. Gormley, C., *et al*. *State of the Art Deep Silicon Anisotropic Etching on Silicon on Insulator Bonded Substrates for Dielectric Isolation and MEMS Applications*. in *Fifth International Symposium on Semiconductor Wafer Bonding, Technology and Applications*. 1999. The Fall Meeting of the Electrochemical Society, Hawaii, USA.
10. A. K. Paul, A.K. Dimri, and R.P. Bajpai, *Plasma etching processes for the realization of micromechanical structures for MEMS†.* Journal Indian Institute of Science, 2001. **81**: p. 669-674.
11. Dennis M. Manos and D.L. Flamm, *Plasma etching an introduction*. Plasma- Materials Interactions, ed. D.L.F. Orlando Auciello. 1989: Academic Press, Inc.
12. Hitchon, W.N.G., *Plasma Processes for Semiconductor Processing*. 1999, Cambridge: Cambridge University Press.
13. Roland, J.P., *Endpoint detection in plasma etching.* Jounal Vacuume Science Technology A - Vacuum, Surfaces and Films, 1985. **3**(3): p. 631.
14. Bose, F., *Characterization of plasma etch proceses using measurements of discharge impedence.* Jounal Vacuume Science Technology B: Microelectronics, 1994. **12**(4): p. 2805.
15. K. Wong, *et al.*, *Endpoint prediction for polysilicon plasma etch via optical emission interferometry.* Jounal Vacuum Science Technology A - Vacuum, Surfaces and Films, 1997. **15**(3): p. 1403-1408.
16. Haverlag, M., *In situ ellipsometry and reflectometry during etching of patterned surfaces: Experiments and simulations.* Jounal Vacuume Science Technology B - Microelectronics and Nanometer Structures, 1992. **10**(6): p. 2412.
17. Marcoux., P.J. and P D Foo, *Methods of End Point Detection for Plasma Etching.* Solid State Technology, 1981. **24**(4): p. 115-122.
18. Chambers, J.J., K. Min, and G.N. Parsons, *Endpoint uniformity sensing and analysis in silicon dioxide plasma etching using in situ mass spectrometry.* Jounal Vacuum Science Technology B - Microelectronics and Nanometer Structures, 1998. **16**(6): p. 2996-3002.
19. De Castro, R.M., *et al.*, *End-point detection of polymer etching using Langmuir probes.* IEEE Transactions on Plasma Science, 2000. **28**(3): p. 1043-1049.
20. Aperathitis, E., *et al.*, *Evaluation of reactive ion etching processes for fabrication of integrated GaAs/AlGaAs optoelectronic devices* Materials Science and Engineering B 2001. **80**(1-3): p. 77-80
21. D J Heason and A.G. Spencer, *Infrared interference patterns for new capabilities in laser end point detection.* Journal Physics D: Applied Physics, 2003. **36**: p. 1543-1549.

22. Donnelly, V.M. and T.R. Hayes, *Excimer laser induced etching of InP.* Applied Physics Letters, 1990. **57**(7): p. 701-703.
23. Rahman, M., *et al*., *Minimization of dry etch damage in III–V semiconductors.* Journal of Physics D: Applied Physics, 2001. **34**: p. 2792-2797.
24. Klick, M., *SEERs-based process control and plasma etching.* Solid State Technology, 1999.
25. Y. Ra and C.H. Chen, *Direct current bias as an ion current monitor in the transformer coupled plasma etcher.* Journal Vacuum Science and Technology A, 1993. **11**(6): p. 2911-2913.
26. Austin, D.J., Solid State Technology, 1997.
27. Klick, M. *Nonlinearity of the radio-frequency sheath*. in *Frontiers in Low Temperature Plasma Diagnostics II*. 1998. Bad Honnef, Germany.
28. Michael Klick, Wolfgang Rehak, and Marita Kammeyer, *Plasma Diagnostics in rf Discharges Using Nonlinear and Resonance Effects.* Japanese Journal Of Applied Physics, 1997. **36**: p. 4625-4631.
29. Benson, T.E., *et al*., *Sensor systems for real-time feedback control of reactive ion etching.* Jounal Vacuume Science Technology B, 1996. **14**(1): p. 483-488.
30. Yue, H.H., *et al*., *Fault Detection of Plasma Etchers Using Optical Emission Spectra.* IEEE Transactions on Semiconductor Manufacturing, 2000. **13**(3): p. 374-385.
31. Barry M. Wise, *et al*., *A COMPARISON OF PRINCIPAL COMPONENT ANALYSIS, MULTIWAY PRINCIPAL COMPONENT ANALYSIS, TRILINEAR DECOMPOSITION AND PARALLEL FACTOR ANALYSIS FOR FAULT DETECTION IN A SEMICONDUCTOR ETCH PROCESS.* Journal of Chemometrics, 1999. **13**: p. 379-396.
32. Dineen, D.M., *Plasma Etching - An Essential Tool for Fault Analysis*. 2004, Oxford Instruments: Oxford.
33. Sofge, D.A. *Virtual Sensor Based Fault Detection and Classification on a Plasma Etch Reactor*. in *The Second Joint Mexico International Workshop on Neural Networks and Neurocontrol*. 1997. Playa del Carmen Quintana Roo Mexico.
34. Barma, G.G., *Automatic problem detection and documentation in a plasma etch reactor.* IEEE Transactions on Semiconductor Manufacturing,, 1992. **5**(1): p. 56-59.
35. G A Vawter, J F Klem, and R.E. Leibenguth, *Improved epitaxial layer design for real time monitoring of dry etching in III-V compound heterostrucures with depth accuracy of ±8nm.* Journal Vacuum Science Technology A, 1994. **12**: p. 1973-7.
36. S E Hicks, *et al*., *Reflectance modelling for in situ dry etch modelling of bulk Si02 III-V multilayer. structures.* Journal Vacuum Science Technology B, 1994. **12**: p. 3306-10.
37. Todd R. Hayes, *et al*., *Maskless laser interfermonetric monitoring on InP/InGaAsP heterostructure reactive ion etching.* Applied Physics Letters, 1990. **57**(26): p. 2817-19.
38. H. Henry Yue, *et al*., *Plasma etching endpoint detection using multiple wavelengths for small open-area wafers.* Journal Vacuum Science and Technology A, 2001. **19**(1): p. 66-75.
39. Hirobe, K. and T. Tsuchimoto, *End Point Detection in Plasma Etching by Optical Emission Spectroscopy.* Journal Electrochemical Society: Solid-State Science and Technology, 1980. **127**(1): p. 234-235.
40. Litvak, H.E., *End point control via optical emission spectroscopy.* Journal vacuum Science and Technology B: Microelectronics and Nanometer Structures, 1995. **14**(1): p. 516-520.
41. Winzer, P.J., *Shot-noise formula for time-varying photon rates: a general derivation.* Journal Optical Society of America B, 1997. **14**: p. 2424-2429.
42. Richard, A.G. and M.D. Vincent, *Optical emission actinometry and spectral line shapes in rf glow discharges.* Journal Of Applied Physics, 1984. **56**(2): p. 245-250.
43. Joel O. Stevenson, *et al*., *A Plasma Process Monitor/Control System.* Surface and Interface Analysis, 1998. **26**: p. 124-133.

44. Lee, J.W., *et al.*, *Utilization of Optical Emission Spectroscopy for End-PointDetection during AlGaAs/GaAs and InGaP/GaAs Etching in BCl3/N2 Inductively Coupled Plasmas.* Journal of The Electrochemical Society,, 2001. **148**(9): p. 472-474.
45. Chen, R., H. Huang, and C.J. Spanosc, *Plasma etch modeling using optical emission spectroscopy.* Journal Vacuum Science and Technology A, 1996. **14**(3): p. 1901-1906.
46. Rangan, S., C. Spanos, and K. Poolla. *Modelling and Filtering of Optical Emission Spectroscopy Data for Plasma Etching Systems*. in *IEEE International Symposium on Semiconductor Manufacturing*. 1997. San Francisco, CA, USA.
47. David A. White, *et al.*, *Low Open-Area Endpoint Detection Using a PCA-Based T2 Statistic and Q Statistic on Optical Emission Spectroscopy Measurements.* IEEE Transactions on Semiconductor Manufacturing, 2000. **13**(2): p. 193-207.
48. Le, M., *Variation Reduction in Plasma Etching via Run-to-Run Process Control and Endpoint Detection*, in *Department of Electrical Engineering and Computer Science*. 1997, MIT: Massachusetts.
49. Sternheim, M., W.v. Gelder, and A.W. Hartman, *A Laser Interferometer System to Monitor Dry Etching of Patterned Silicon.* Journal Electrochemical Society: Solid-State Science and Technology, 1983. **130**(3).
50. Heimann, P.A. and R.J. Schutz, *Optical Etch-Rate Monitoring: Computer Simulation of Reflectance.* Journal Electrochemical Society: Solid-State Science and Technology, 1984. **131**(4): p. 881-885.
51. Aperathitis, E., *et al.*, *Laser interferometry as a diagnostic tool for the fabrication of reactive ionetching-edge-emitting lasers.* Jounal Vacuum Science Technology B - Microelectronics and Nanometer Structures, 2002. **20**(5): p. 1994-1999.
52. McAuley, S.A., *et al.*, *Silicon micromachining using a high-density plasma source.* Journal of Physics D: Applied Physics, 2001. **34**(18): p. 2769-2774.
53. R. J. Westerman, *et al*. *Endpoint detection method for time division multiplex etch processes*. in *MICROMACHINING AND MICROFABRICATION PROCESS TECHNOLOGY XI*. 2006. Unaxis USA Inc.

4. Chapter 4 – Optical Emission Spectroscopy

4.1. Optical Emission Spectroscopy (OES) - Theory

When an electron is subject to an electric field from a positively charged nucleus, for example in the hydrogen atom, solving the motion of the electron is a quantum mechanical problem. Solutions of this problem give rise to discrete, quantized levels of energy. This can be considered as a central field problem where these levels are quantized according to the spherical co-ordinates r, θ, and Φ.

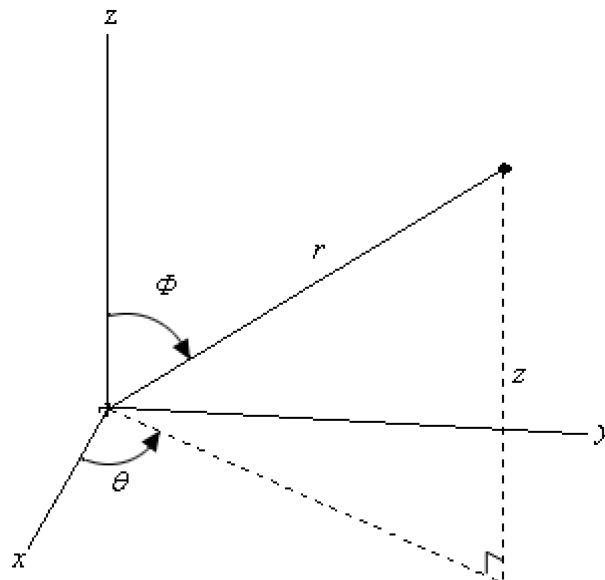

Figure 4.1.1 Spherical coordinate system[1]

These coordinates each have an associated quantum number n, l, m_l, respectively. In addition to these the electron has another degree of freedom, the spin or intrinsic angular momentum, which is related to a fourth quantum number, s. Of the four quantum numbers it is the radial factor (r) and its corresponding quantum number (principle quantum number) which is the most contributes the most significant part to the determination of the magnitude of the energy of the electronic state[1]. The other quantum numbers are associated with the angular momentum of the electron. Quantization means that the electron can only be found in certain states where the electron has values for these quantum numbers that are either integers or half integer in the case of the spin; n can be any integer from 1 to ∞, l can take from 0 to n-1, m can take the values from $-l$ to $+l$ and s can either be +1/2 or $-1/2$. Below is a diagram

showing the energy levels for Hydrogen. These energy levels are a result of the integral values allowed by the quantization. In addition to the energy states based on the *n* quantum number there are also deviations from these levels caused by the other quantum numbers, however the effect of these is too small to be resolved on this diagram. When an electron moves from an initial energy state to a final energy state the transition can be supplied through an optical event (also through other means but for the we are interested in the optical transitions This event can either be the absorption or emission of a photon, where absorption will cause the electron to gain energy and "jump" up a level and emission will cause the electron to lose energy and drop to a lower energy.

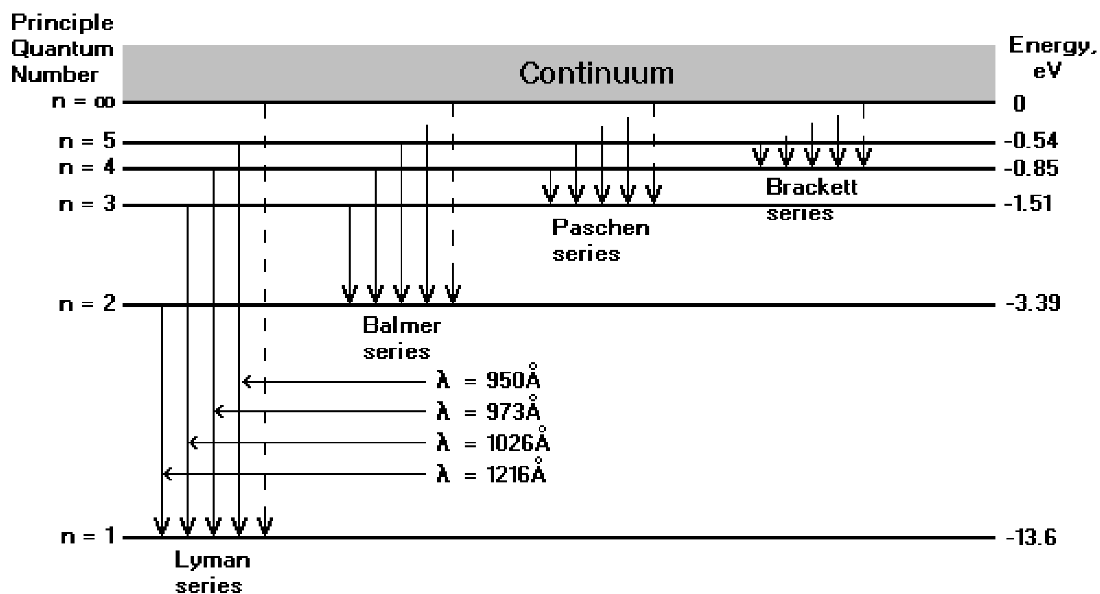

Figure 4.1.2 Energy levels and transitions of Hydrogen atom

If we know the energy of the two states involved in the transition it is possible to determine the frequency of the photon involved.

$$v = (1/hc)(E_f - E_i)$$

Where v is the frequency, h is Plancks constant, c is the speed of light, E_f and E_i are the the energy of the final and initial state respectively. From this the corresponding wavelength of a transition can be found from

$$\lambda = c / v.$$

For all atoms there are a significant number of known bound states which are available to be occupied by electrons. However there are selection rules associated with angular momentum and spin numbers, which only allow radiative transitions between certain energy levels. These selection rules are as follows:

$\Delta n = 0, 1, 2 \ldots$ (unrestricted)

$\Delta l = +$ or $- 1$ for one optical electron

$\Delta L = \Delta \, l \, \Sigma l_i = 0, \pm 1$ for all optical electrons

$\Delta S = 0$ and

$\Delta J = 0, \pm 1$ where $J = L + S$ is the total angular momentum.

As a result of these selection rules the numbers of electronic transitions that can occur radiatively are significantly reduced. Without this restriction, if each of the species within a plasma were to radiate there would be tens of thousands of spectral lines essentially resulting in a continuum, which would be of no use for characterization.

For molecules the physics becomes further complicated by the motion of the atomic nuclei relative to the centre of mass of the molecule. For example in the case of a diatomic molecule the two atomic nuclei can vibrate along the molecular axis and rotate around the centre of mass. The lowest order solution for the vibratory states can be approximated as a simple harmonic oscillator with the intra-nuclear axis represented as a mass-less spring and the nuclei as point masses. Rotation can be described as a rigid rotor with a mass-less rod with two point masses (nuclei) rotating around the centre of mass. When this approximation is made it is found that both the vibrational and rotational states are quantized with energies given by the following equations:

The vibrational states are given by:

$$E_v = kv_0(v + \frac{1}{2})$$

The rotational states given by:

$$E_R = B_0 N(N+1)$$

These vibrational and rotational motions are coupled and as such are modified by the addition of higher order corrections. This problem is simplified through the use of the Born-Oppenheimer approximation[2]; this enables us to consider the nuclei being fixed at their respective equilibrium points. Although this simplifies matters the molecular orbital case is still a more complicated one than the central field problem of the atom, in the case of the molecule there is a strong electric field between along the inter-nuclear axis. It is found that the simplest method of dealing with this problem is to consider the projections of the angular momentum along the inter-nuclear axis rather than the angular momenta themselves. These projections exhibit quantization and follow selection rules in an analogous manner to the angular momentum. This is described by replacing the quantum numbers for the angular momentum.

L is replaced by Λ, the spin quantum number S is replaced with its projection Σ and the total angular momentum J=L+S is replaced by Ω = Λ+ Σ. There are further shorthand techniques which were developed using these symbols and others to fully describe the relevant quantum numbers for a diatomic molecule and although they are beyond the scope of this review can be found in Herzberg[3]. The result of these transition selection rules is a set of molecular energy levels as shown in the figure below. Emissions occur as a result of electronic transitions between two energy levels. A transition between two vibrational levels will generally result in a photon in the infra red range whilst a transition between two electronic states will result in a photon in the ultra violet or visible region. Different gases will have energy levels at different energies. Therefore the magnitude of the energy released in a transition will vary according to the species within which the transition occurs. This in effect

means that each species has a specific spectral finger print which can be used to identify it. When a species is in a plasma, the electric (and sometimes magnetic) field will cause the species to dissociate, leading to ionised forms of the species. The field will also cause electronic transitions to occur within the species. This causes the species to emit photons.

These emissions lead to the characteristic glow observed when a plasma is active. Photons are emitted outside of the visible spectrum as well, depending on the energy of the transition and the species involved. A spectrum is taken and there are peaks in intensity at certain frequencies which are determined by the contents of the gas in the plasma. The main gases that are present are the input gases as required for the etch process. However there are also the by-products of the etch process as well. For example in the case of a silicon etch SF_6 is the reactant gas, there will be high concentrations of Fluorine in the plasma. There will be high intensity spectral lines for these Fluorine species (such as 704nm[4, 5]). One of the products of the etch process are species of the form SiF_x, these species decrease in concentration once the etch process is completed. SiF_x has a spectral line at 440nm[4, 5], which shows useful variation over the course of the etch. Details of the mechanism of silicon etch which gives rise to the production of these spectral lines is detailed in chapter 2. Using these characteristic spectral lines it is possible to determine when there is a change in material on the surface that is being etched. If the common situation of a silicon layer above a silicon oxide layer is considered. The end point required is the point at which the silicon is removed and the silicon oxide layer is exposed. As this occurs there will be an increase in intensity of spectral lines associated with Fluorine which is no longer being used to etch the silicon. There will also be a corresponding decrease in the by-product SiF_x which is no longer being produced. These intensity changes can be observed and an end point signal generated.

In the general case there are many wavelengths that can be observed whilst monitoring an etch process to determine an end point. Most end point detection systems will use one or two wavelengths to determine when an end point has occurred. The choice of these wavelengths is a significant challenge in the determination of end point from OES. These wavelengths correspond to transitions in the product and reactant species contained within the plasma as described previously. Different processes therefore will lead to significantly different intensities depending on the species involved. It is also likely that there will be variation in the intensities observed when different plasma etch tools are considered; this can be due to the tool condition or window position. Another factor that contributes to the complexity of end point detection is when masks are involved; the mask material may have similar

chemistry to the material being etched. This can lead to the formation of mask etch products which are similar to the products of the film being etched. All of these factors can make it difficult to anticipate the wavelengths which will exhibit the most significant change at end point.

4.2. Limitations of Optical Emission Spectroscopy as an End Point Detection System

In the case of OES the major limitation is that as the features being etched become smaller and smaller the change in the signals observed at end point also become smaller and smaller. In the case of low open area etches it is difficult to determine the end point as the signal is difficult to distinguish from the ambient noise exhibited in the spectral information due to the instability of the plasma. Secondly as the features are being etched one part may be finished before another and begin to exhibit the required signal for end point whereas another part of the wafer may be unfinished. This issue is made more significant as the diameter of the wafer that is involved is increasing as the industry standard increases. As a result of this the signal corresponding to the end point is a gradual change rather than an instantaneous one. This leads to issues about how to define the end point, whether it be at the start of the signal change or at the end. This is an important definition to make as choosing the end point at the wrong time could lead to over or under etch issues as discussed earlier. A further complication with the use of OES as the end-pointing system is that it requires a stop layer in the design of the feature that is being etched. This is the required as in order for a change to be clear in the trace of the signal; the intensity of the spectral lines associated with the etching process must change. This is caused by a change in the concentration of the plasma reactants or products. In some devices there is no stop layer as the feature is simply a trench such as with the etching of gratings for optical microelectromechanical systems[6]. For these cases there will clearly be no change in the optical properties when end point is achieved. In some instances a stop layer has been introduced in order to allow the use of OES for end point determination[7], however as devices become smaller this becomes unfeasible due to the extra size required with a stop layer.

4.3. Noise in Optical Emission Spectra

When a signal is obtained from OES for the determination of end point it has been related to an individual species such as SiF_x. In reality when a signal is taken that corresponds to a single species it is difficult to obtain a clean end point. This is partly due to the gradual nature of the change that occurs as the features are etched. However there is also a significant problem associated with the noise in the signal. There are several causes of noise in an OES system due to the detection method. The most obvious of these is known as "shot" noise and is due to the quantum detection of photons. Shot noise is proportional to the square root of the signal intensity. Another form of detector based noise is "dark" noise. This is when the detector picks up a signal even in the absence of light. A constant dark signal can be removed from the results by normalization but the random dark noise associated will continue to be present. Dark noise is temperature limited and as such can be neglected if a strong signal is considered as it will not increase proportionately with signal strength. In such cases it is shot noise which is the limiting factor in signal to noise ratio due to its relation to the signal intensity. Although the noise that occurs due to the detector can be significant it is often noise directly associated with the plasma itself which lead to the largest noise effects. One common problem associated with obtaining a clean end point signal is a drift in the signal. A major contribution to this the changing condition of the plasma chamber over time. One example of this is "window clouding", where deposition or sputtering of the inner surface of the window cause the intensity in the signal obtained at the OES detector to have a non constant mean. Another source of signal drift is that as an etch process is the effect of thermal transients in the plasma e.g. If the etch time of a process is long enough the walls of the plasma chamber may have sufficient time to exhibit a change in temperature which in turn will have an effect upon the overall plasma conditions. In addition to this there are other fluctuations that may be observed in the trace directly related to plasma instabilities, these in turn can be caused by variations in the input to the plasma (such as pressure, flow rate, power etc). All of these noise sources have an impact on the signal that is captured by the OES system. In the case of low open area etching where there is only a small area etched there is often only a slight change that occurs in the signal at end point. In extreme cases (open area <1%) it becomes difficult to distinguish between noise and a change due to end point. This is known as having a low signal to noise (S/N) ratio. In these situations the ratio can be improved by improving the signal quality or by reducing the noise. Signal strength can be improved through the use of improved methods of capturing the spectrum. For example

previous systems have used monochromatic methods to sample individual spectra relating to specific wavelengths. In current systems this method has often been replaced by using charge coupled devices (CCD) which can obtain signals for multiple wavelengths simultaneously. In addition to being able to obtain multiple wavelengths the use of CCDs means that as CCD technology develops (specifically the resolution capabilities) the electronics of an OES system can be improved and stronger signal to noise ratios can be obtained.

The second method for improving the S/N ratio is to reduce the noise present; this can be conducted as before by improving the quality of the detection system. However it can also be carried out analytically through the combination of multiple signals in order to eliminate uncorrelated noise which effect only individual channels or certain combinations of channels. By combining multiple signals the effective strength of the total signal can be improved, as before with the single wavelength case the problem of identifying which signals to incorporate into a multi-signal case is not arbitrary. One method is to carry out multivariate analysis of the signals obtained to determine which wavelengths change significantly as end point is reached and passed.

4.4. References

1. Rae, A.I.M., *Quantum Mechanics*. 3rd ed. 1996: Instiute of physics.
2. B. H. Bransden and C.J. Joachain, *Physics of atoms and molecules*. 2003: Prentice Hall.
3. Herzberg, G., *Molecular Spectra and Molecular structure: Spectra of Diatomic molecules*. Vol. 1. 1950, Princeton: Van Nostrand.
4. Herman, I., P. , *Optics Diagnostics for Thin Film Processing*. 1996: Academic Press.
5. Chen, R., H. Huang, and C.J. Spanosc, *Plasma etch modeling using optical emission spectroscopy.* Journal Vacuum Science and Technology A, 1996. **14**(3): p. 1901-1906.
6. E. Aperathitis, D.C., M. Kayambakia, M. Androulidakia, G. Deligeorgisa, K. Tsagarakia, Z. Hatzopoulosa, A. Georgakilasa, , *Evaluation of reactive ion etching processes for fabrication of integrated GaAs/AlGaAs optoelectronic devices* Materials Science and Engineering B 2001. **80**(1-3): p. 77-80
7. D J Heason and A.G. Spencer, *Infrared interference patterns for new capabilities in laser end point detection.* Journal Physics D: Applied Physics, 2003. **36**: p. 1543-1549.

5. Chapter 5 - Principal Component Analysis

5.1. Principal Component Analysis - Theory

The data acquired by an OES system can be thought of as a two dimensional matrix. Each value contained within the matrix corresponds to the intensity of signal for individual wavelengths at certain times in the etch process.

$$\boldsymbol{X} = \begin{bmatrix} x_{11} & x_{12} & \cdots & x_{1j} & \cdots & x_{1n} \\ x_{21} & x_{22} & \cdots & x_{2j} & \cdots & \cdots \\ \vdots & \vdots & \vdots & \vdots & \vdots & \vdots \\ x_{i1} & x_{i2} & \cdots & x_{ij} & \cdots & x_{in} \\ \vdots & \vdots & \vdots & \vdots & \vdots & \vdots \\ x_{m1} & x_{m2} & \cdots & x_{mj} & \cdots & x_{mn} \end{bmatrix}$$

$$X = \begin{bmatrix} x_{11} & x_{12} & \cdots & x_{1j} & \cdots & x_{1n} \\ x_{21} & x_{22} & \cdots & x_{2j} & \cdots & \cdots \\ \vdots & \vdots & \vdots & \vdots & \vdots & \vdots \\ x_{i1} & x_{i2} & \cdots & x_{ij} & \cdots & x_{in} \\ \vdots & \vdots & \vdots & \vdots & \vdots & \vdots \\ x_{m1} & x_{m2} & \cdots & x_{mj} & \cdots & x_{mn} \end{bmatrix}$$

As described above X is a matrix containing *m* time samples and *n* wavelength channels. Each sample x_{ij} corresponds to the signal intensity of the *i*-th time sample and the *j*-th wavelength channel. This matrix can easily be split into individual traces such that a column vector can be considered as a trace of one individual wavelength. Conversely a row of the matrix is a trace of a fixed time and the intensities of all of the wavelengths involved in the trace. In OES it is common to take for a range of intensities from 200 to 800nm to be taken with intensity measurements taken for every 0.5nm. This leads to a large matrix of results containing up to 1200 results for each time interval. With results often being taken every 0.1 seconds this leads to a significant data set for even short etch processes.

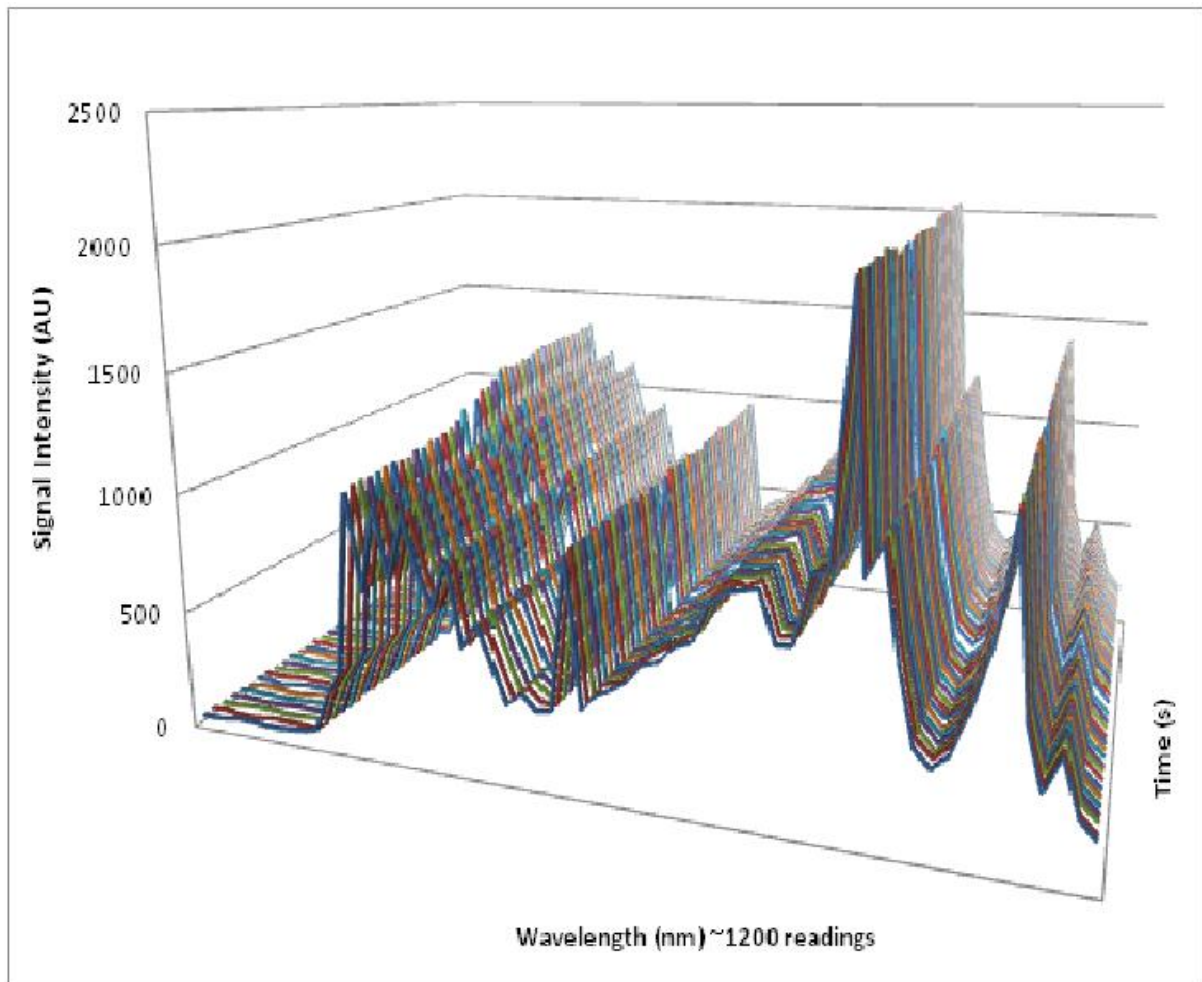

Figure 5.1.1 Multivariate optical emission data often contains vast numbers of readings. For the purpose of this report up to 1200 wavelengths are recorded in each time interval which is generally set to 0.1s. A 30 minute process would collect 21,600,000 individual measurements.

Many of the wavelength intensities will exhibit no change due to the change in plasma conditions at end point. As a result many of these signals contribute nothing to either the noise or signal and can be discarded. Principal Component Analysis (PCA) is a technique which identifies how much of a change is observed in the signals over the course of the etch. The level of change is determined on a relative scale whereby the signals exhibiting the greatest level of variation fall into the first principal component and the next most significant being in the second component and so on. Using this technique it is possible to

discard groups of signals depending on their potential contribution to an end point signal. Thus the vast amount of data can be reduced to only those wavelengths which make a significant contribution to the objective signal.

When a square matrix **X** is considered, an eigenvector of the matrix is a vector where multiplying the original matrix by the eigenvector is equivalent to multiplying the matrix by a scalar quantity. This is described mathematically below.

$$\boldsymbol{X}\boldsymbol{v}_i = \lambda_i \boldsymbol{v}_i$$

Here v_i are the eigenvectors and λ_i are the eigenvalues associated with the matrix **X**. By forming all the eigenvectors as columns of a matrix **S** and where **X** is square, **X** can be decomposed as shown below.

$$\boldsymbol{X} = \mathbf{S\Lambda S^{-1}} = [\mathbf{v_1} \cdots \mathbf{v_n}]\begin{bmatrix} \lambda_i & & \\ & \ddots & \\ & & \lambda_n \end{bmatrix}[\mathbf{v_1} \cdots \mathbf{v_n}]^{-1}$$

Λ is a diagonal matrix containing the eigenvalues of **X**. In the symmetric case a set of orthonormal eigenvectors can be chosen. This leads to the following decomposition on a symmetric matrix.

$$\boldsymbol{X} = \mathbf{Q\Lambda Q^t} = [\mathbf{v_1} \cdots \mathbf{v_n}]\begin{bmatrix} \lambda_i & & \\ & \ddots & \\ & & \lambda_n \end{bmatrix}\begin{bmatrix} \mathbf{v_1}^T \\ \vdots \\ \mathbf{v_n} \end{bmatrix}$$

This can be generalised for the non-square case, in this instance the technique is known as singular value decomposition (SVD) and is described below.

$$\boldsymbol{X} = \mathbf{U\Sigma V^t} = [\mathbf{u_1} \cdots \mathbf{u_m}]\begin{bmatrix} \sigma_i & & & \\ & \ddots & & \\ & & \sigma_r & \\ & & & 0 \end{bmatrix}\begin{bmatrix} \mathbf{v_1}^T \\ \vdots \\ \mathbf{v_n}^T \end{bmatrix}$$

Here, if **X** has dimension (m x n), **U** and **V** are orthogonal matrices of size (m x m) and (n x n) respectively. **Σ** is a diagonal matrix of singular values, $\sigma_{i,}$, in decreasing order; there are only r singular values that correspond to the rank of the matrix **X**.

In order to perform PCA on a data set the data must be mean centred, as an end point signal will then involve a clear shift away from the mean. In order to achieve this, the data is centred using the mean for the area of the etch known as the main etch. This section is when the plasma has stabilised and a consistent etch rate has been achieved. Clearly the mean has to be taken prior to an end point in the process.

The basis of principal component analysis is the deconstruction of the aforementioned **X** matrix as follows:

$$\mathbf{X} = \mathbf{T}\mathbf{V}^{\mathbf{T}} = (\mathbf{X}\mathbf{V})\mathbf{V}^{\mathbf{T}}$$

$$\mathbf{V} = [\mathbf{V}_1 \cdots \mathbf{V}_2]$$

$$\boldsymbol{T} = [\ \boldsymbol{t}_1 \cdots \ \boldsymbol{t}_n] = [\boldsymbol{X}_1 \ \cdots \ \boldsymbol{X}_n \boldsymbol{v}_n]$$

Here **V** is an orthonormal set of vectors and **T** is a projection of **X** onto **V**. The **X** data is mean-centred and the eigenvectors are calculated by taking the singular value decomposition of the covariance matrix as described above.

$$\boldsymbol{X} = [\mathbf{v}_1 \cdots \mathbf{v}_n] \begin{bmatrix} \sigma_{t_1}^2 & & \\ & \ddots & \\ & & \sigma_{t\ n}^2 \end{bmatrix} \begin{bmatrix} \mathbf{v}_1{}^{\mathbf{T}} \\ \vdots \\ \mathbf{v}_n{}^{\mathbf{T}} \end{bmatrix}$$

$$\boldsymbol{S} = \boldsymbol{V}\boldsymbol{\Lambda}\boldsymbol{V}^{\boldsymbol{T}}$$

Here the eigenvalues give the variance of the projected components **T**, in decreasing order of variance. The process of PCA can be thought of as a rotation of the data contained in **X** onto a statistically independent set of vectors **V**. These vectors are known as the principal components. The $\mathbf{t}_i$ values are the scores associated with the principal components and the $\mathbf{v}_i$ are the principal component loadings. The scores ($\mathbf{t}_i$) are related to the individual sample points so that $\mathbf{t}_i$ is a vector containing values for each sample point, this will give information about which of the principal components contains significant data regarding the end point. The loadings ($\mathbf{v}_i$) directly relate the variables to the principal components. By using a combination of these two vectors it will be possible to determine firstly which principal components exhibit a significant change at end point. Secondly it is possible to find which wavelengths contribute to the aforementioned significant principal components. When the principal components are considered against their scores, the results are that each principal component is a combination of wavelengths that exhibit a certain degree of variation. For example the first 90% of variation could be contained in the first principal component and the next 8% in the second. By viewing the principal components scores which change over time it is possible to view the variation associated with multiple wavelengths in one variable. This will allow the determination of end point with increased accuracy.

5.2. Experimental Method

OES results were obtained using two plasma etch systems. These are described below. Once the data was collected using these systems it was processed using MatLab to perform the matrix operations required to obtain the principal component data.

5.3. Surface Process Technology Systems (SPTS) Advanced Silicon Etch (ASE) - 100% Resist Coverage

This system was based at the London Centre for Nanotechnology. Six inch silicon wafers were used. The ASE machine is a fully automated plasma etcher, all of the controls including gas flow rates, chamber pressure, chamber temperature and the loading apparatus are operated using software attached to a separate control and electronics unit.

5.4. Surface Process Technology Systems (SPTS) Advanced Silicon Etch (ASE) Patterned Silicon - 15% Coverage

In this case the wafer was patterned with approximately 15% open area exposed to the plasma. The rest of the surface was coated in a masked resist with a depth of approximately 3µm. In order to obtain a change in plasma chemistry during the etch the wafer was initially exposed to a deposition plasma whereby a polymer layer was coated across the surface. The deposition plasma was set so that a layer of several hundred nanometres was applied to the surface. The significance being that the layer was thinner than that of the resist. Once the carbon surface layer was applied the plasma parameters were switched so that an etch plasma was present. This etched through the thin layer of deposited material and through to the exposed silicon.

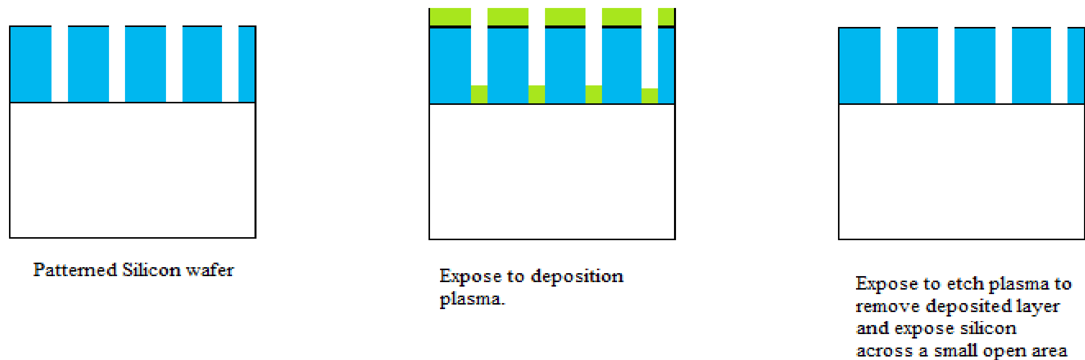

Figure 5.4.1 Process of deposition followed by etching to obtain an artificial end point signal

5.5. SPTS Pegasus Oxide Etch ~ 1% Open Area

The final system used was an SPTS Pegasus^{TM} system based at Surface Process Technology Systems, Newport Junction 28 site. In this case a 300mm wafer coated with a thick layer of resist was used as a carrier. Four sections of patterned silicon with an oxide layer were fixed to this carrier wafer. These were then exposed to a C_4F_8 plasma. In this case the C_4F_8 etches the oxide on the surface and exposes the silicon below, this leads to a change in the plasma chemistry. Due to the patterned nature of the oxide layer and the large open area of the carrier wafer the overall open area that can be assumed to exhibit a change in plasma chemistry in this case is in the region of 0.1 - 1%.

5.6. Results and Discussion - SPTS Advance Silicon Etch tool

The first set of tests conducted were on a silicon wafer with a blanket covering of resist. SF_6 was used as the etchant gas in an SPTS Advanced Silicon Etch (ASE) tool, based in the London Centre for Nanotechnology. The PCA loadings and scores are shown below (**Error! Reference source not found.**). The spetragraph was set to collect data in the range from 200nm to 800nm; however in this instance a standard glass viewing window was used, this

blocks the ultra violet (UV) part of the spectrum, therefore the first wavelengths to show any signals were from approximately 326nm.

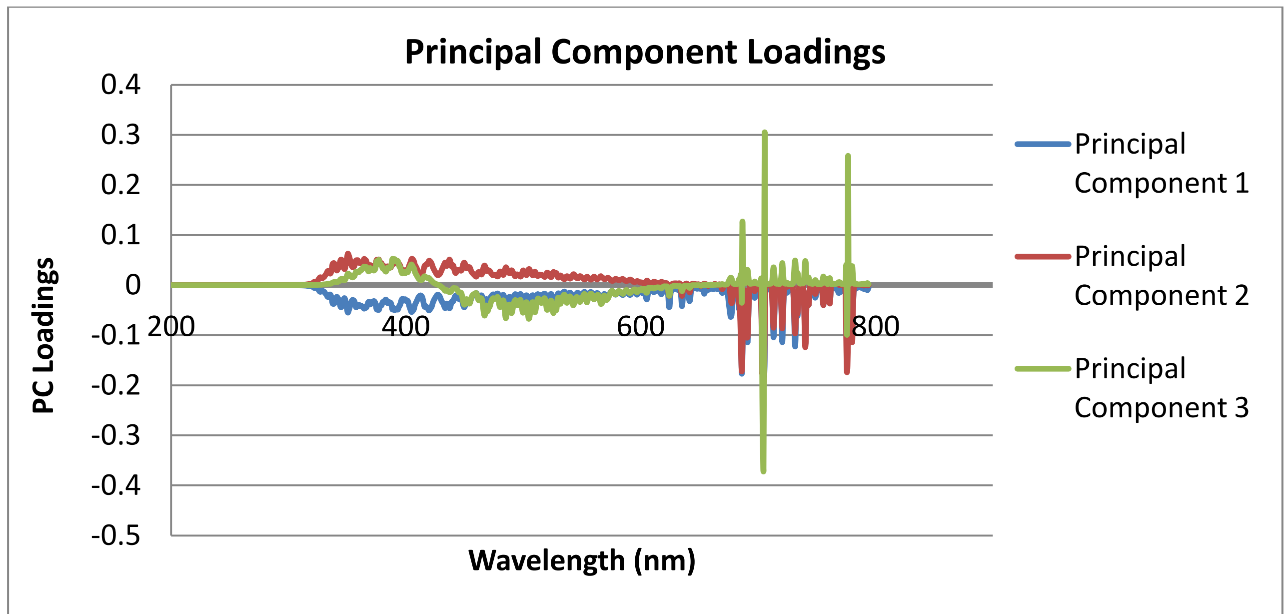

Figure 5.6.1 PCA loadings for blanket etch of resist

Whilst the resist was being etched the emission spectra showed a large degree of oscillation as the resist layer was removed (Figure 5.1.1). These oscillations represent a principle which has been used in a technique known as optical emission interferometry (O.E.I)[1, 2]. Unlike other types of interferometry this method utilises the glow discharge from the plasma as the source of light for interferometry.

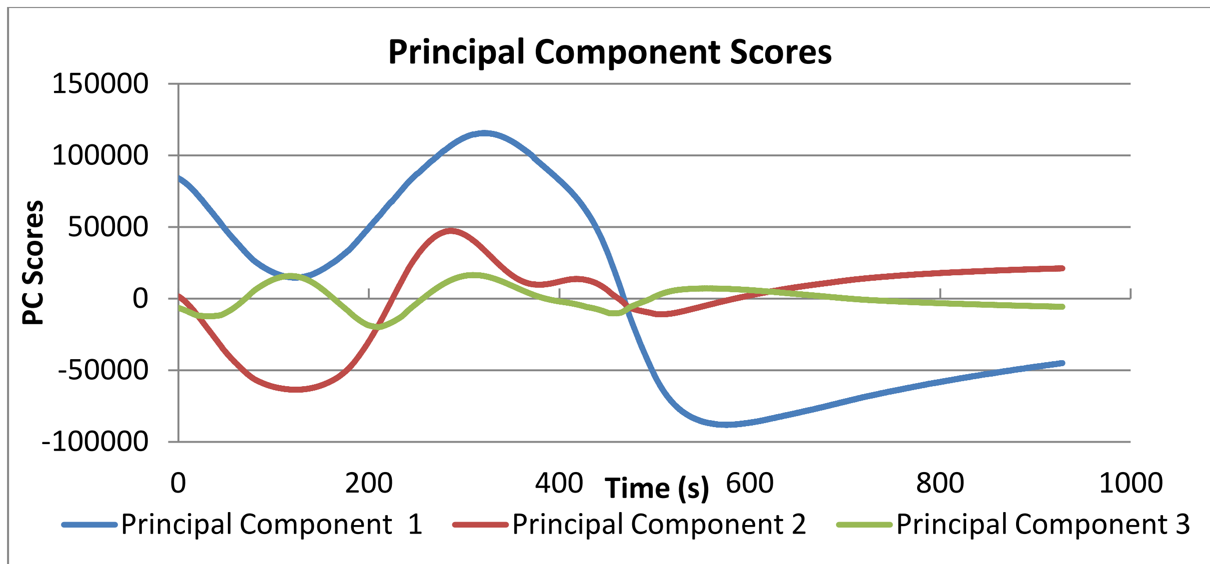

Figure 5.6.2 Principal Component Analysis Scores of blanket resist etch. An end point can be resolved between 600 and 750 seconds where the oscillatory nature is replaced by a linear pattern.

The interferometry pattern is shown in approximately the first 500 seconds of the etch process. Once the resist is stripped and the underlying silicon is exposed the oscillations disappear as the nature of the etch has changed. The resist is etched slowly due to the high selectivity of the etch process, by definition the resist is not etched favourably with the polymer of the resist chemically inert to the etch gas of Fluorine. The etch mechanism to remove the resist is more of a physical process rather than a chemical one. The slow etch rate of the resist results in the large period observed in the oscillation. Once the silicon is exposed the etch rate is significantly higher and period of the oscillations is much smaller. Therefore the oscillations associated with the etch are no longer resolvable using the optical emission spectroscopy equipment. In order to resolve the etch of the silicon using optical emission interferometry in this manner, the OES data capturing equipment would have to be able to record individual readings at a higher rate.

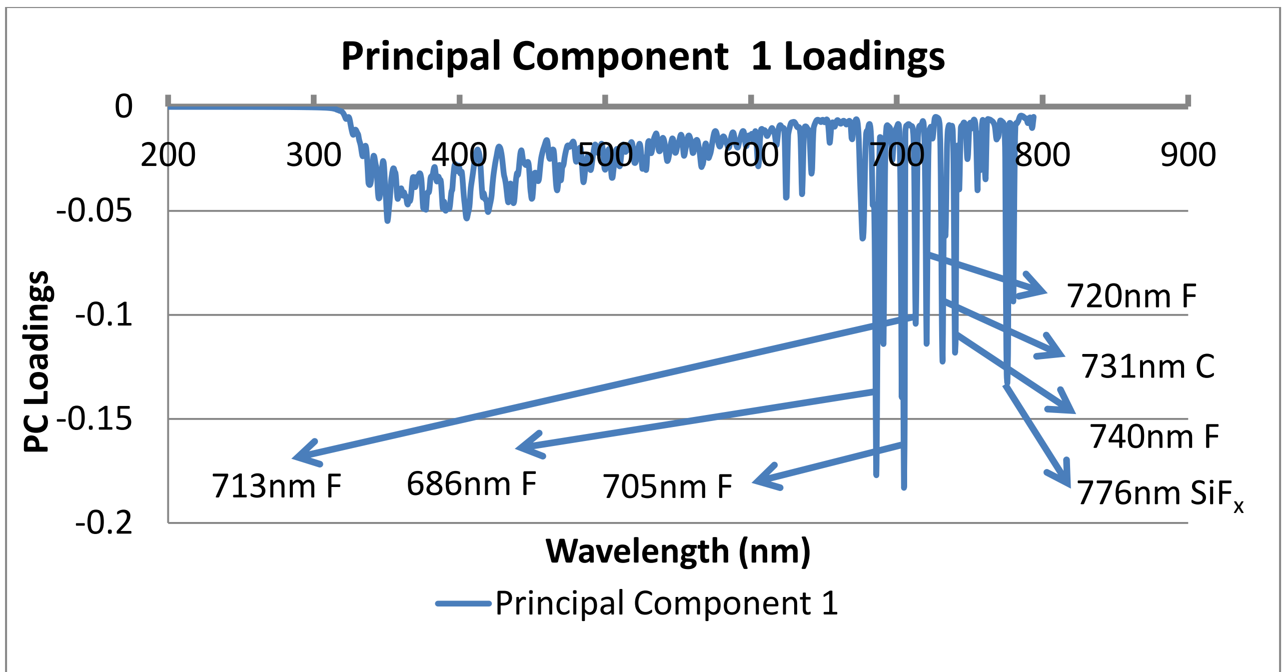

Figure 5.6.3 First Principal Component Loading

The first principal component shows significant contributions from wavelengths in the range of 680nm to 780nm (Figure 5.6.3). As shown in the graph the majority of these wavelengths are associated with Fluorine species[3], there are contributions from 776nm and 731nm which are associated with SiF_x and Carbon species respectively. The contributions from all of the wavelengths are negative; therefore the PC scores give an inverted representation of the process chemistry. As the photo resist is removed and the silicon begins to be etched the level of fluorine in the chamber drops. This is inverted by the PCA technique and as a result an increase is observed in the PC1 score as shown below (Figure 5.6.4). The increase is shown to begin at approximately 600 seconds.

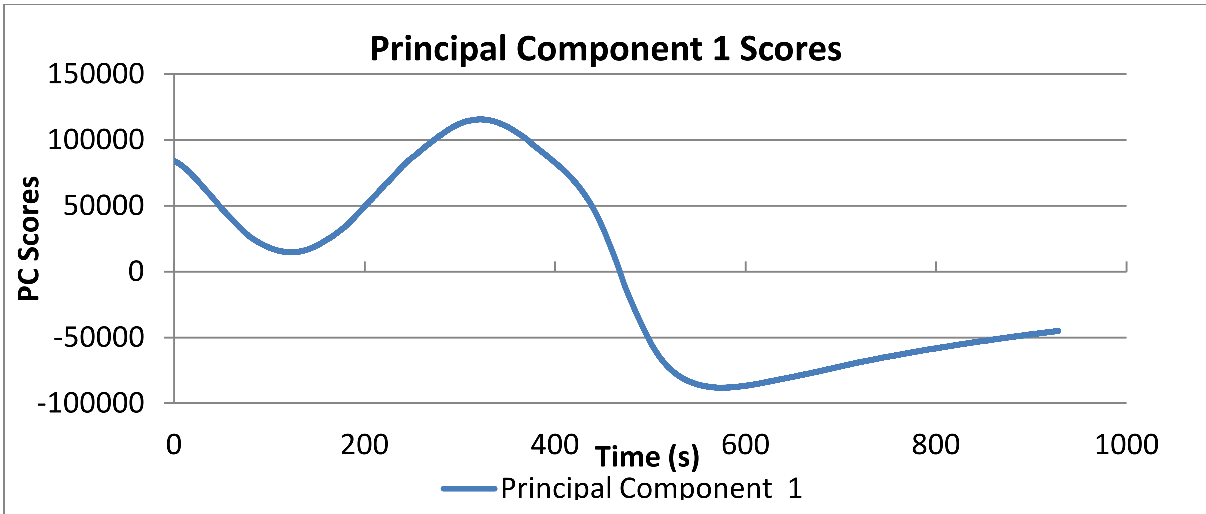

Figure 5.6.4 First Principal Component Scores

The second principal component loadings shown below (Figure 5.6.5) have the same trend in terms of the key wavelengths. However the wavelengths between 300nm and 650nm are inverted from the 1st to the 2nd component loading.

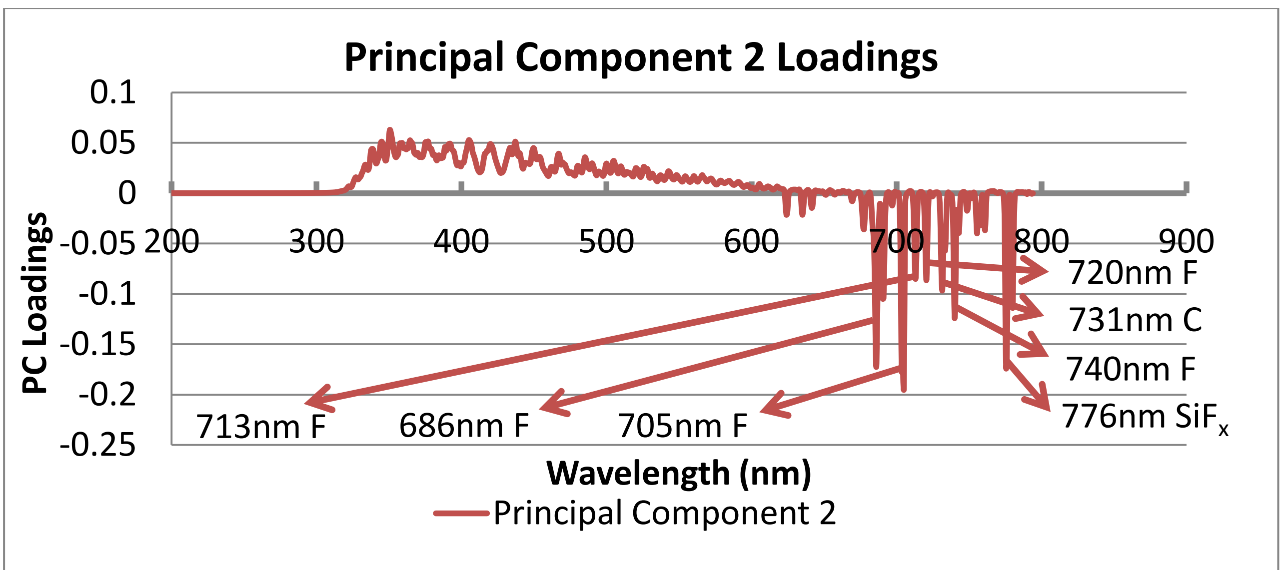

Figure 5.6.5 Second Principal Component 2 Loading

The magnitude of the oscillations in the 2nd component is less than that of the 1st (Figure 5.6.2). This suggests that the inversion of the contribution from wavelengths in the range of 326nm to 650nm has contributed to the reduction in magnitude of the oscillations seen in principal component 2

compared with principal component 1. The oscillations seen in the scores are contributed to by all the wavelengths. All light in the chamber will be reflecting from the surface of the substrate and causing interference patterns. The wavelengths with associations to specific chemistry happening with the chamber (such as 705nm with fluorine) contribute to oscillations, but their contribution is masked by the more significant contribution to the chemistry related variation (silicon etch) rather than the oscillations (resist stripping).

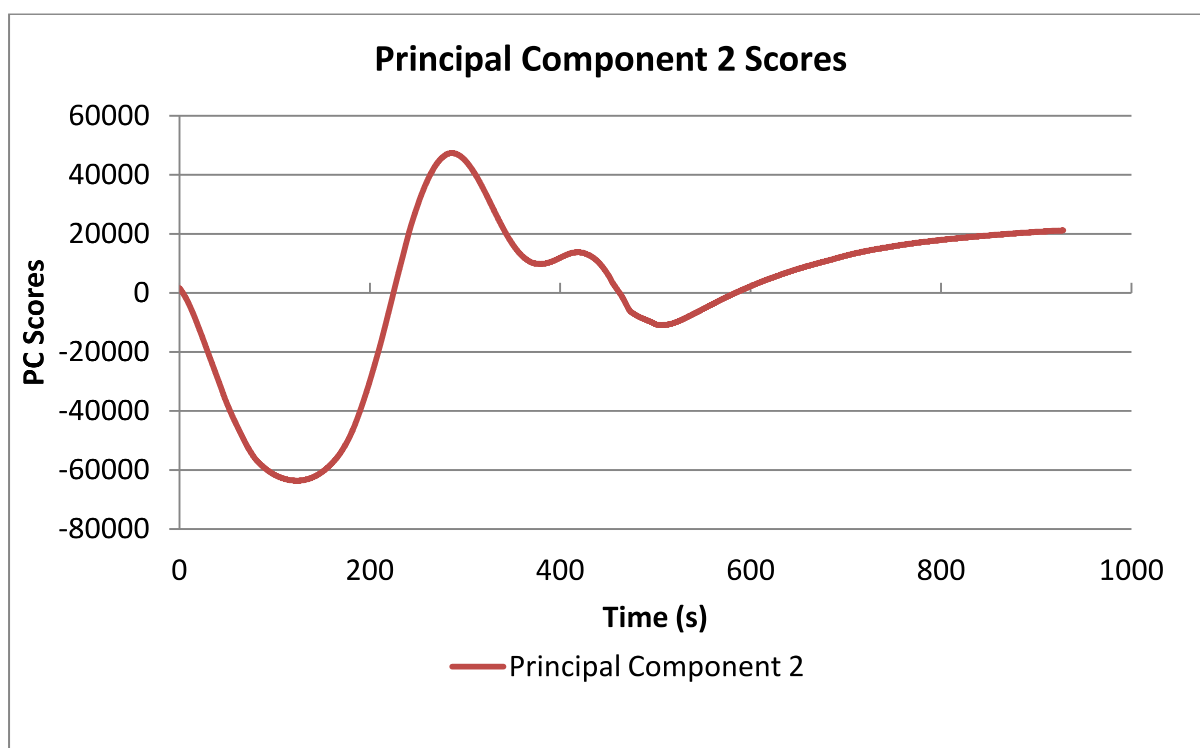

Figure 5.6.6 Second Principal Component Score

The 3rd principal component shows a less significant contribution from the wavelengths above 650nm (Figure 5.6.7). There are significant contributions from the lines associated with 686nm, 705nm and 776nm which are associated with fluorine, fluorine and SiF_x species respectively showing a positive contribution. However other than these specific lines there is not a significant contribution in this range of wavelengths whereas in PC1 and PC2 there was a larger contribution from wavelengths in this range. Interestingly, 705nm also shows a significant negative contribution and is associated with Fluorine. This suggests that fluorine exhibits both positive and negative

variation across the course of the etch process. The decrease in the concentration of fluorine is clearly associated with the commencement of the silicon etch once the resist has been removed. An increase in the signal associated with fluorine can be explained as being a result of the oscillations observed and is an artefact of the interferometry taking place rather than the process chemistry. This is reinforced by the fact that the other significant wavelengths (686nm and 776nm) both have positive and negative contributions, although these are significantly smaller than the contribution from the 704nm spectral line.

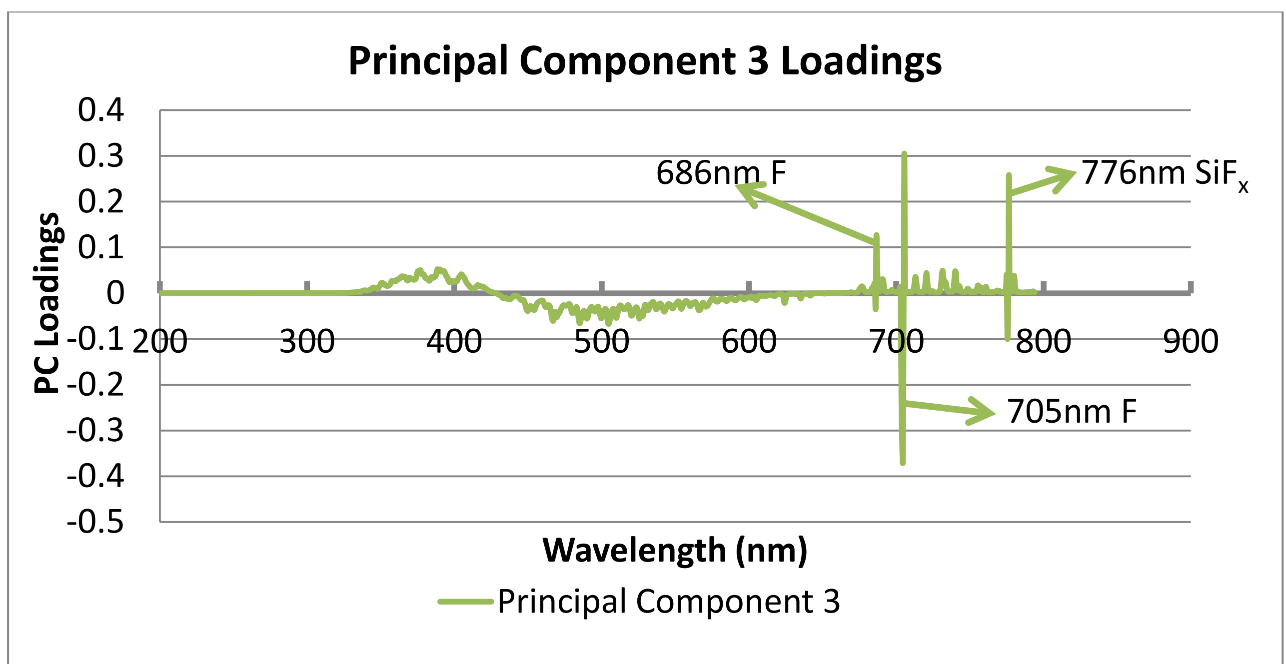

Figure 5.6.7 Third Principal Component 3 Loading

The 3rd principal component score does show oscillations at the start of the etch process (Figure 5.6.8) however these are in a different phase to those observed in the first two components (Figure 5.6.2), with a higher frequency observed in PC3. This is due to the difference in the wavelength of the light that is causing the interferometry fringes. Earlier in the report interferometry was discussed as an endpoint technique. The following equations were used to explain the theory behind the technique:

$$EtchRate = \frac{\Delta d_{\text{film}}}{\Delta \text{t}}$$

$$\Delta d_{film} = \frac{\lambda}{2n_2 cos\theta_2}$$

By merging the two we have:

$$EtchRate = \frac{\lambda}{\Delta \mathrm{t} 2n_2 cos\theta_2}$$

$$EtchRate = \frac{\lambda}{\Delta \mathrm{t} C}$$

Where C =$2n_2 cos\theta_2$

Therefore if the wavelength increases, the time period will also increase (assuming the etch rate remains the same). Given we have seen a decrease in the time period, the wavelength causing the fringes must also be reduced suggesting that the fringes are caused by wavelengths lower than observed in the first two components.

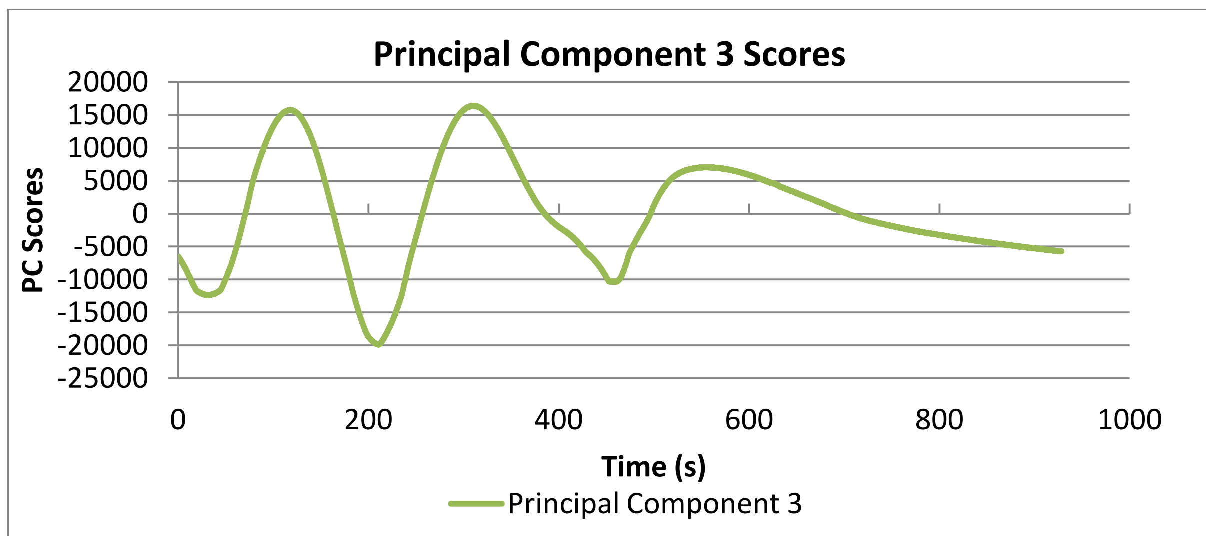

Figure 5.6.8 Third Principal Component Score

5.7. SPTS Patterned Silicon ~ 15% Open Area

The final etch process that PCA was applied for the purpose of this report was a switched process. A layer of passivation material was applied to the surface using a deposition plasma (C_4F_8). This layer was then removed using an SF_6 plasma as the layer is removed the underlying silicon is exposed which causes a change in the emission spectrum observed. For the purpose of this experiment a deposition cycle significantly longer (10x) than would usually be used was applied. This was done so that there would be a sizeable layer for the etch process to remove and provide an observable transition.

The following graph (Figure 5.7.1) shows all of the loadings for the polymer removal process. The loadings are the contributions from the wavelengths to the scores. The following section contains the separate loadings for all of the components alongside their corresponding scores.

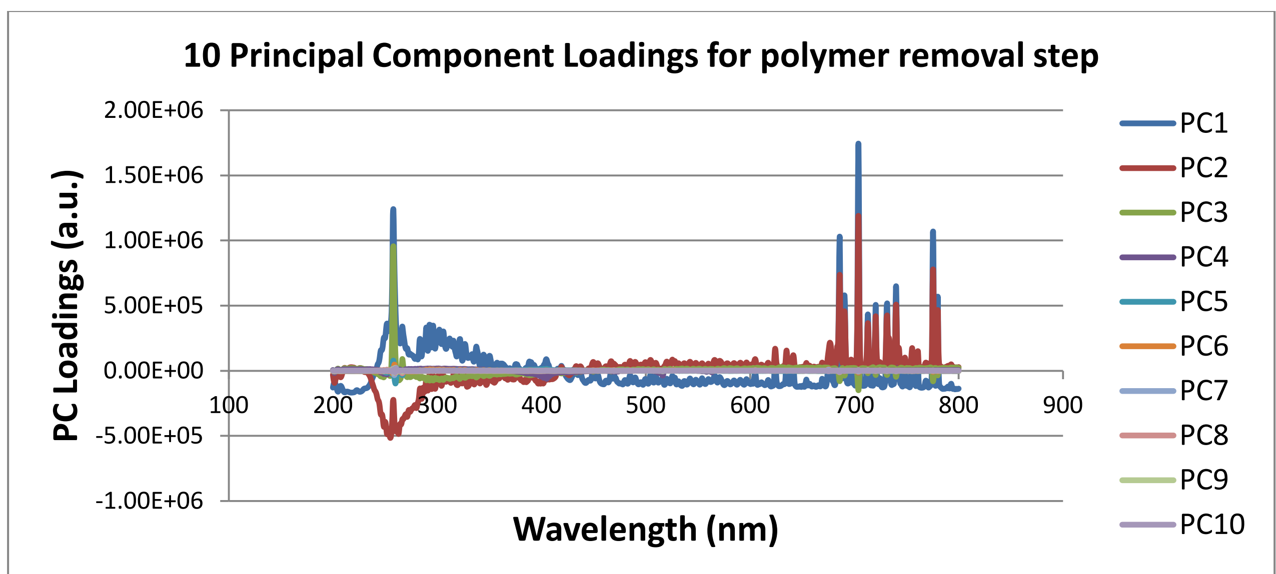

Figure 5.7.1 First 10 principal component loadings from polymer removal step

The following graph (Figure 5.7.2) shows the principal component scores for the first three components over the course of five cycles of the etch process described previously. The

two stages of the process which are clearly shown in the following graph, the first being the deposition stage and the second the etch. In the first stage the plasma chemistry remains stable, whereas in the second stage the chemistry changes as the deposited polymer layer is removed and the underlying silicon is etched. This chemistry change is apparent in the principal component scores shown.

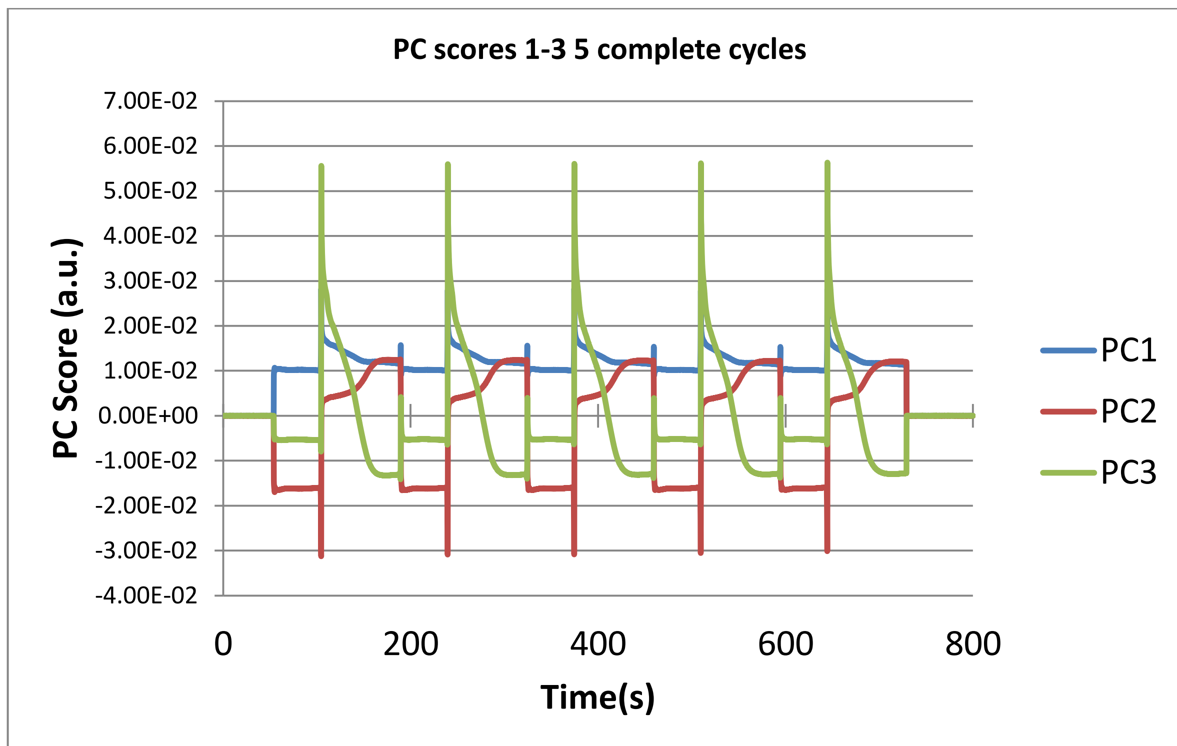

Figure 5.7.2 Principal Component scores for 5 process cycles

The next graph shows the ten principal component scores over the course of a single polymer removal step. Again this graph has been expanded in the following section to ensure its clarity.

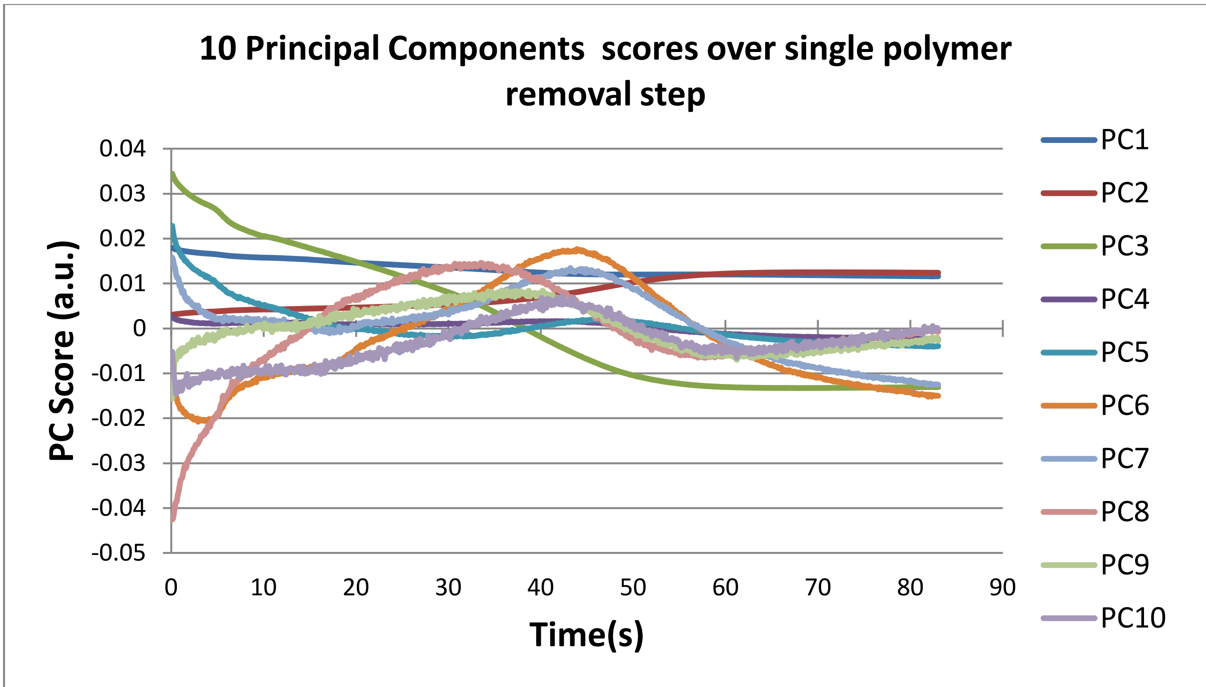

Figure 5.7.3 Principal Component scores over single polymer removal stepThe first principal component loadings (wavelength contributions) are shown below (Figure 5.7.4). The significant contributions are positive from wavelengths associated with fluorine and from a wavelength associated with CF_2.

The first of the principal component loadings is shown below (Figure 5.7.4)

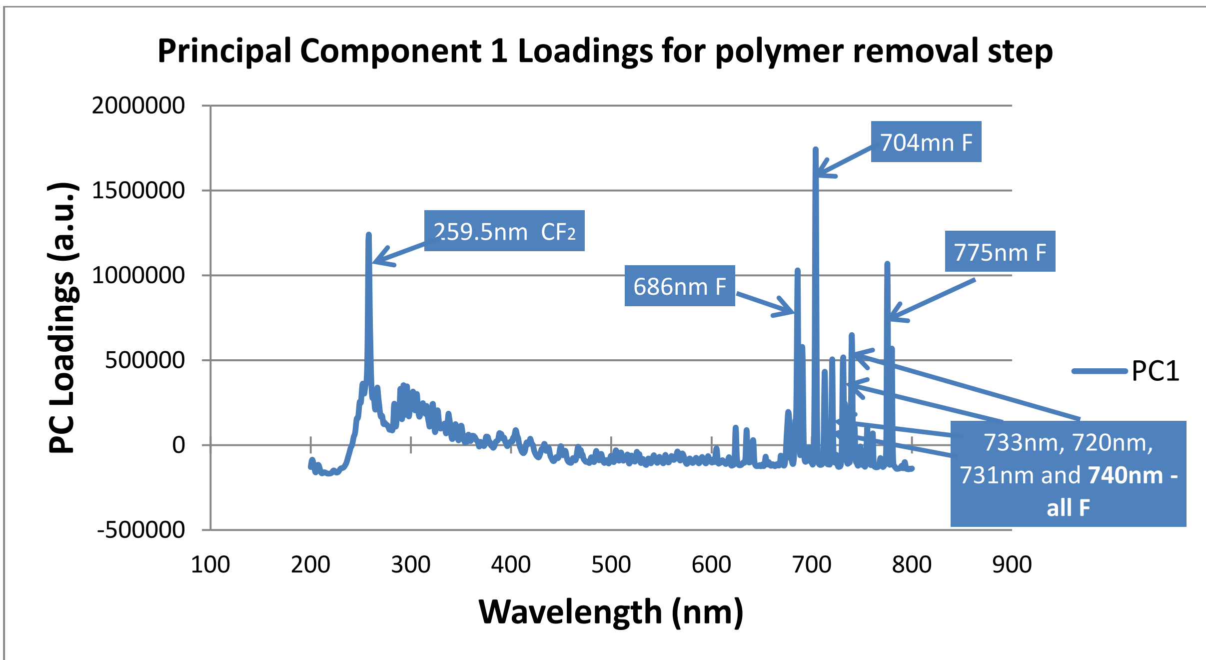

Figure 5.7.4 1st Principal Component Loading

The scores corresponding to the 1st PC loadings is shown below (Figure 5.7.5). The score stabilises after approximately 45 seconds. This corresponds to the expected chemistry, the positive contribution to the PC results in the PC score following the chemistry of the plasma. The fluorine in the chamber is reduced, the magnitude of the PC falls. The fluorine rich polymer is removed and the reactant fluorine from the SF_6 begins to be used up in etching the exposed silicon, thus the overall level of fluorine in the chamber is reduced. This is reflected in the fall in the PC score followed by its stabilisation.

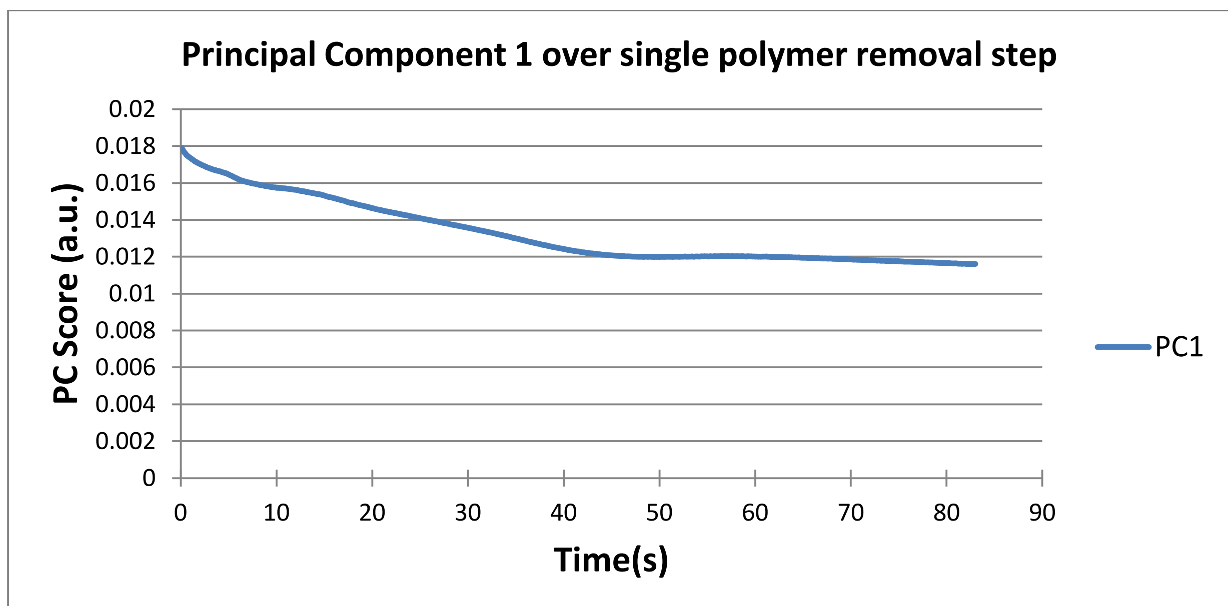

Figure 5.7.5 1st Principal Component score

The second component is again contributed to by the CF_2 chemistry (259.2nm) and a selection of Fluorine lines (Figure 5.7.6). In this case the contribution from the CF_2 is inverted.

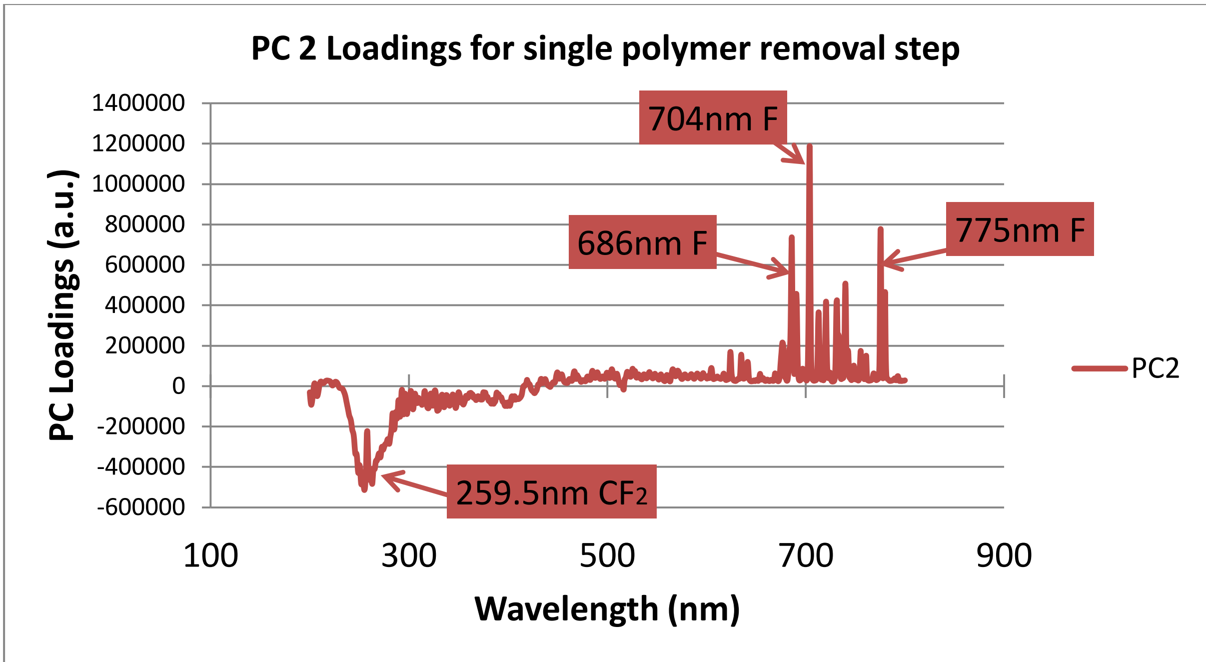

Figure 5.7.6 2nd Principal Component loading

The inversion of the CF_2 contribution results in the score for PC2 increasing once the polymer is removed and the underlying silicon begins to be etched.

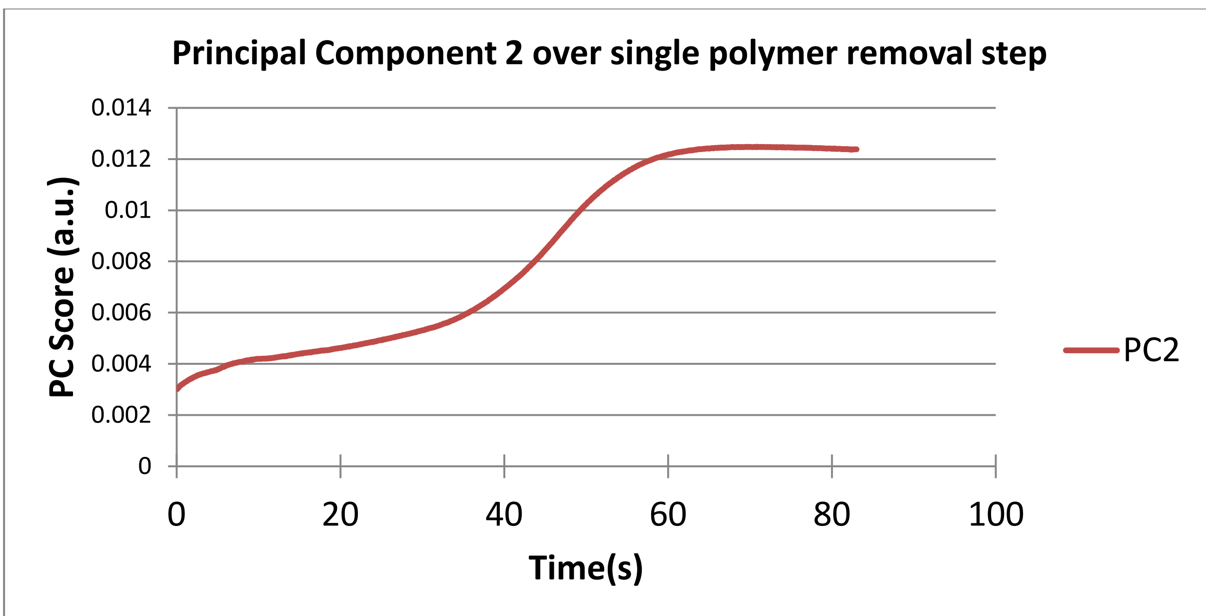

Figure 5.7.7 2nd Principal Component score

The third principal component loading (Figure 5.7.8) shows a predominant contribution from 259.5nm which is associated with CF_2. There are no significant contributions from other wavelengths.

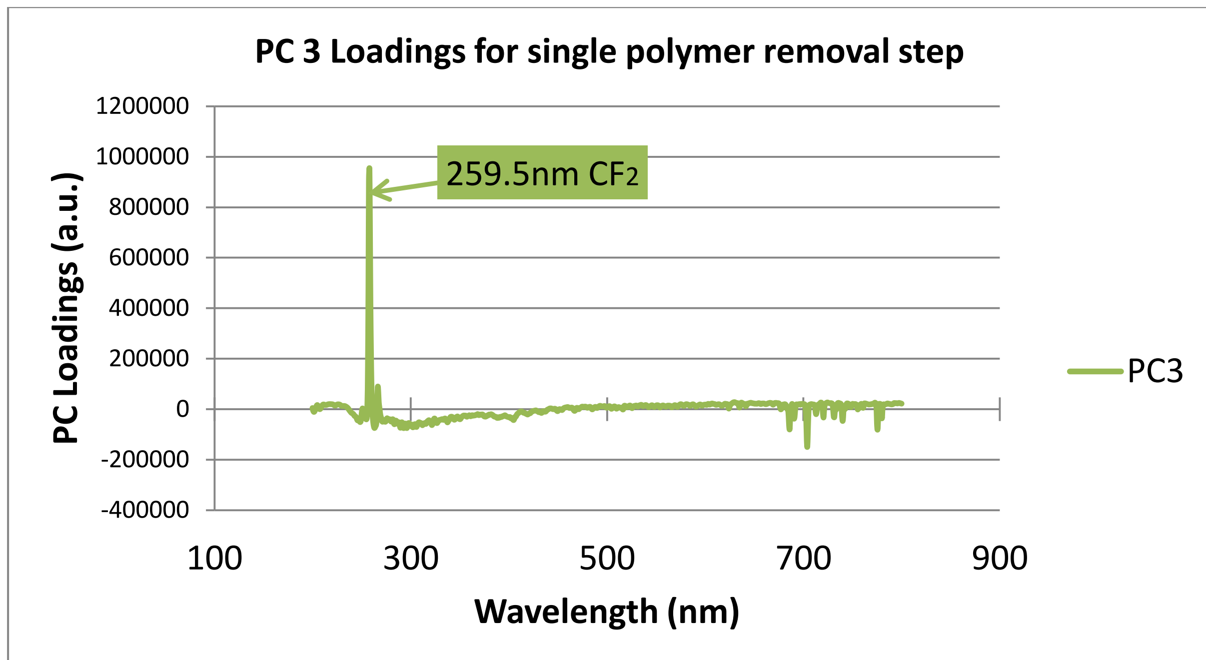

Figure 5.7.8 3rd principal component loading

The third PC score has only one significant contributor and as such the PC score directly follows the chemistry associated with the CF_2 species. It falls to a minimum once the polymer layer is removed (Figure 5.7.9).

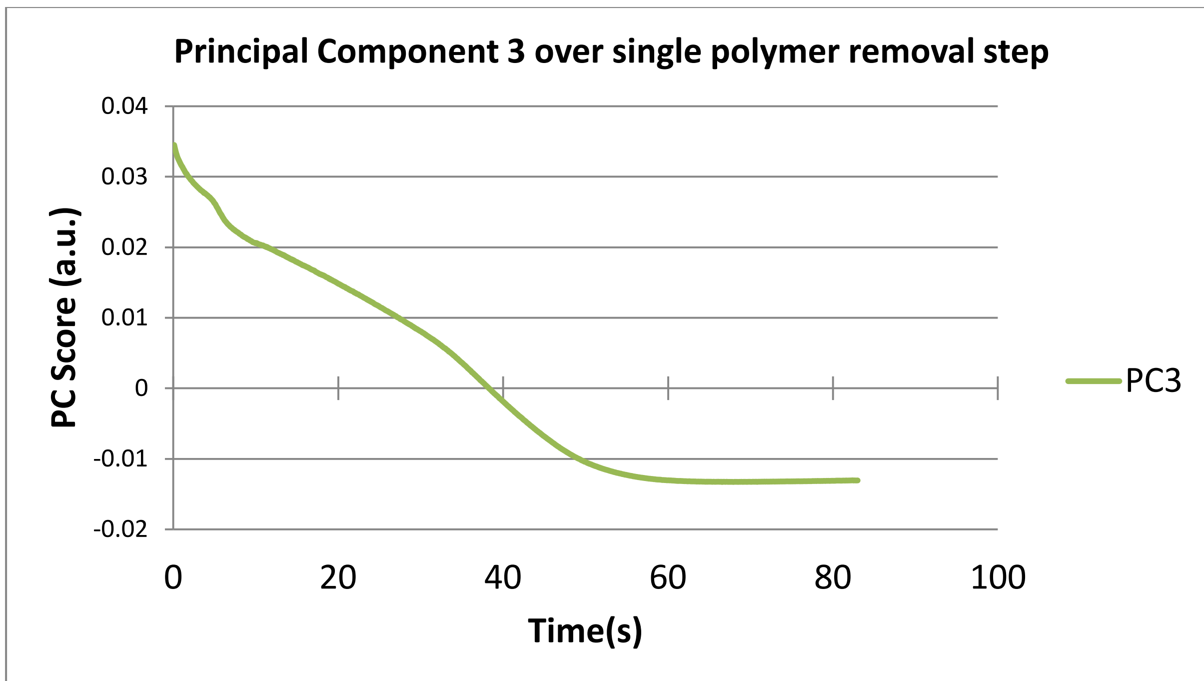

Figure 5.7.9 3rd principal component score

PC 4 presents an interesting case (Figure 5.7.10 4th principal component loading. Fluorine lines as seen previously are present, as is a previously unseen C_2 line at 516nm. However there appears to be a more significant contribution from 407.6nm. The literature associates this line with several materials one of which is Oxygen[3]. There has been no oxygen added to the system at this point from the process recipe. However the masking material for the patterning of the wafers (Poly (methyl meth acrylate)) contains oxygen in the form of a polymer. Although this material is designed to have a low etch rate (high selectivity) it is likely that small amounts are etched once the deposited polymer is removed and the mask is exposed. The contribution from the 'Oxygen' line is negative.

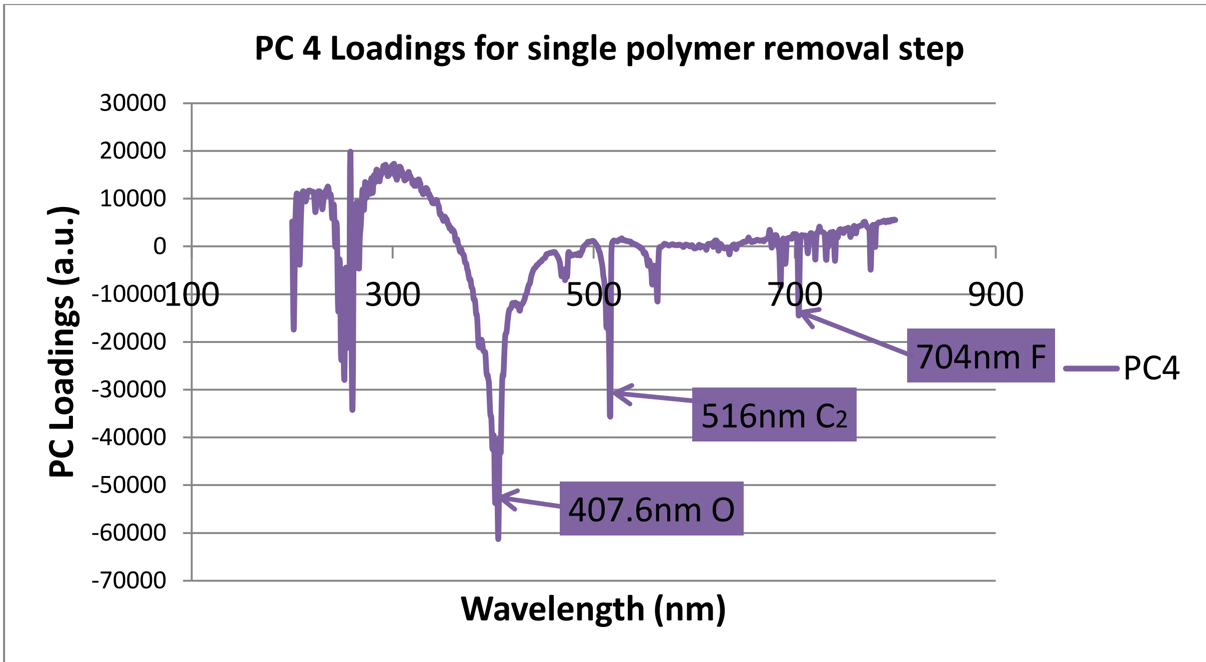

Figure 5.7.10 4th principal component loading

The negative contribution from the 'oxygen' spectral line is negative; so will be represented in the score inversely to the chemistry occurring in the chamber. As the resist is exposed the level of oxygen in the chamber is increased. This is inverted by the PCA process to deliver a score (Figure 5.7.11) which drops as the resist is exposed.

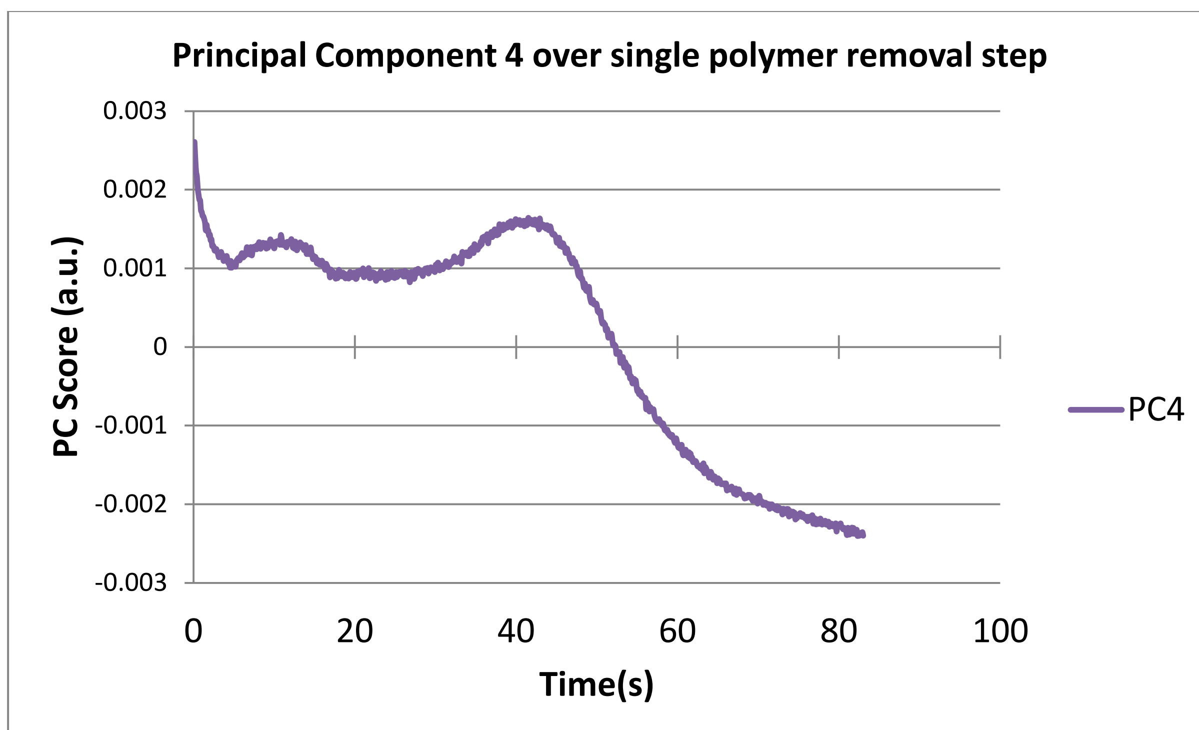

Figure 5.7.11 4th principal component score

PC 5 only shows significant contributions from the CF_2 line. It shows both positive and negative contributions. This is reflected in the corresponding scores showing a fall once the CF_2 is removed. The scores leading up to the removal of the CF_2 are erratic, although in general there is an increase in the score as the CF_2 is removed.

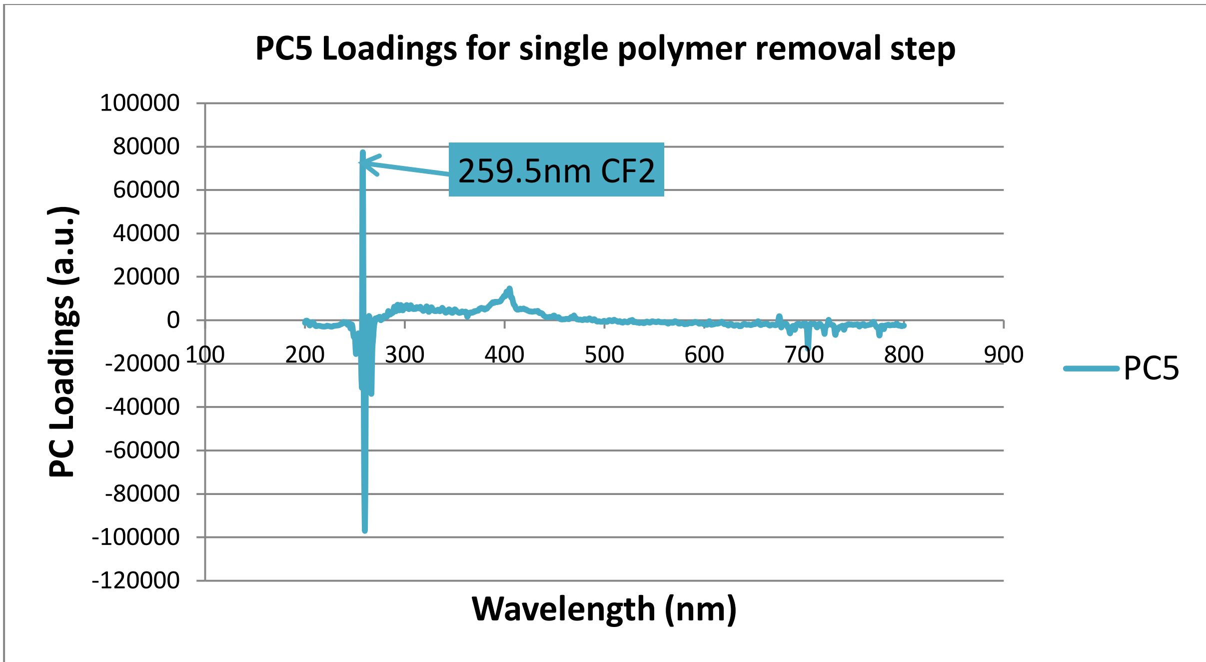

Figure 5.7.12 5th principal component loading

As described above PC 5 shows an initial fall, followed by a rise starting at approximately 30 seconds, lasting until approximately 45 seconds into the etch. This corresponds to the end points seen in the other principal components, with all showing end points between 40 seconds and 60 seconds.

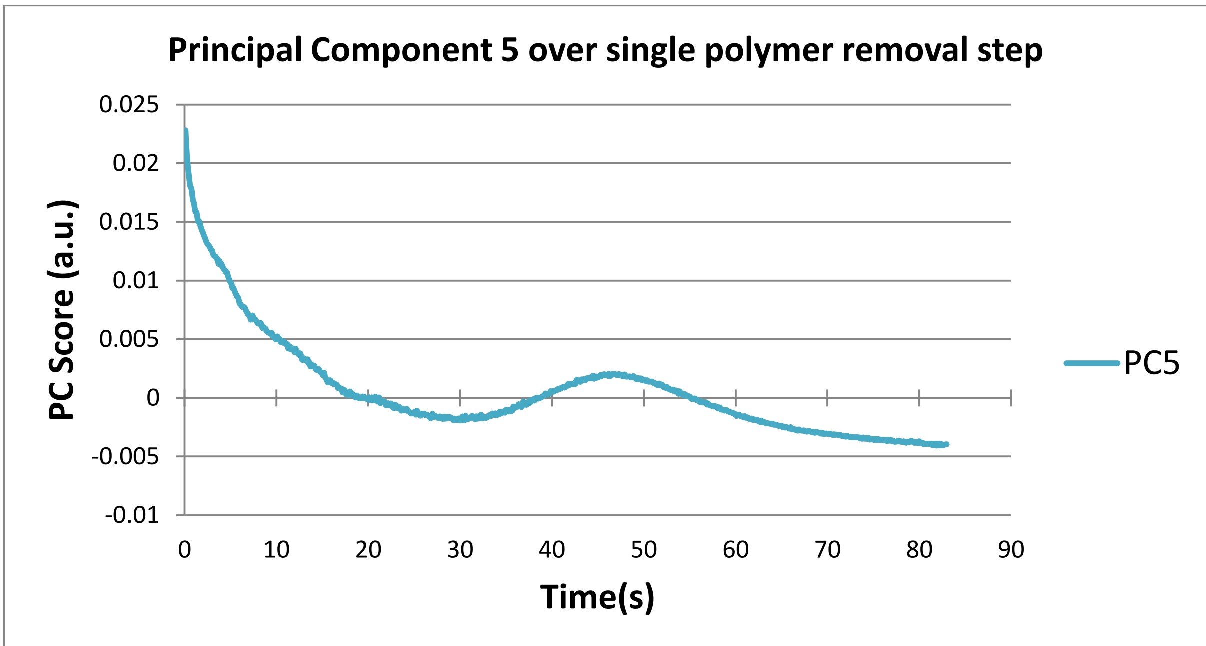

Figure 5.7.13 5th principal component score

The patterned wafer used to obtain the above spectral information was imaged using a scanning electron microscope, some of the images are shown below.

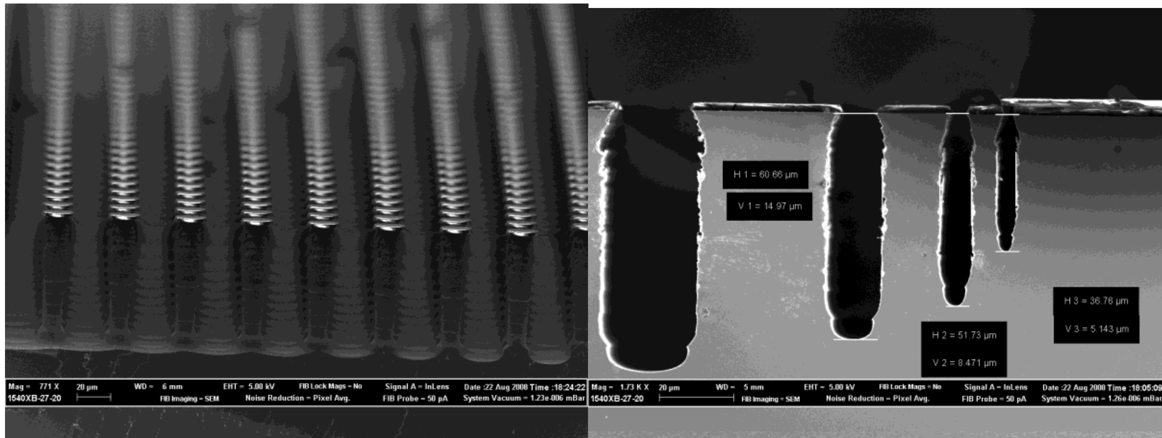

Figure 5.7.14 Scanning electron microscope images showing two separate areas on a patterned wafer after etching. The degradation caused by excessive cycle times during Bosch process is shown on both areas.

The image on the left shows pillars which were masked with circular disks of resist, at the base of the pillars it is possible to see the individual layers associated with each cycle of etch and passivation layer. At the top of the pillars is a more interesting pattern. There has been significant under etch beneath the mask. This is shown more clearly in the second image (different area on the wafer) in which the etch can clearly be seen to undercut the mask. This is likely to be an artefact of the increasing of the times of the two cycles, specifically the etch cycle. As discussed previously it is possible that this under-etch is occurring in the time indicated on the spectral graph where all of the passivation material appears to have been removed. By a slight adjustment of the proportion of etch time to deposition time it may be possible to reduce this under-etch and achieve more uniform side walls.

5.8. SPTS Silicon Oxide Etch Low Open Area ~1%

Four patterned sections of wafer were placed on a carrier wafer heavily coated with resist. The patterning of the silicon oxide coated wafer meant that there was a low open area on the original wafer, as low as 15%, including the large surface area of the carrier wafer the open area of the etch could be considered to be in the region of 0.1 to 1%. This results in a very low signal to noise ratio, which in turn means it will be difficult to resolve an end point. This is shown below where the untreated signal data for several wavelengths is presented. In this etch process a CF_4 was used as the reactant gas. The mechanism of etch by fluorocarbons in plasmas is a complex one with numerous pathways[4-11]. A full set of these reaction pathways is found in appendix 1 at the end of this report. One possible pathway for the etch of SiO_2 by fluorocarbon is described below:

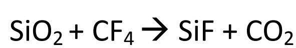

$$SiO_2 + CF_4 \rightarrow SiF + CO_2$$

SiF and CO_2 are both volatiles which can be removed from the process chamber; this is merely one option which can facilitate the etching of silicon oxide. In reality many combinations of the different pathways listed in appendix 1 would happen, with the rapid creation and destruction of many intermediary species during the process.

It would be expected that if wavelengths associated with CF species are monitored using OES there would be an increase in the intensity of these species at the end point, once C_xF_x species are no longer being used up to remove SiO_2. During the etch the C_xF_x species are reacted with the oxide resulting in low intensity signals for their associated wavelengths. Once the oxide is removed the abundance of the C_xF_x species increases and the associated intensity also increases.

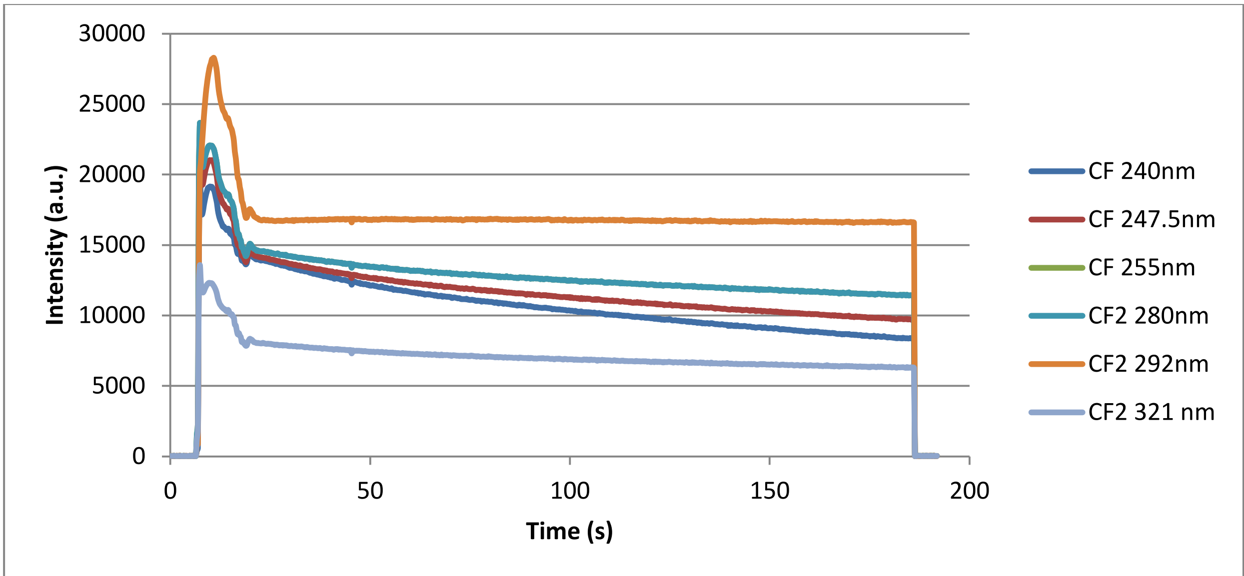

Figure 5.8.1 Untreated spectral data from patterned oxide etch

The etch process for this case was a straightforward etch, with no switching involved. Given the parameters and the thickness of the oxide layer the end point was expected to be approximately 2 minutes into the etch. There is no clear end point found using these wavelengths at this time.

PC 1	82.1014
PC 2	98.6247
PC 3	99.6380
PC 4	99.8015
PC 5	99.8792
PC 6	99.9177

Figure 5.8.2 Table detailing the percentage of variation contained in the first 6 principal components

From the above table 99.8% of the variation is included in the first 4 principal components. Although there is only a small percentage included in the 4th PC from the loadings graph shown below, the majority of that variation is related to two wavelengths: 440nm and 662nm, these are commonly associated with SiF_x[12] and CO[12] species respectively. These two wavelengths also feature heavily in the variation of the PC2 and PC3 as shown below (Figure 5.8.3 PC loadings from the treated data of patterned silicon on oxide wafer.

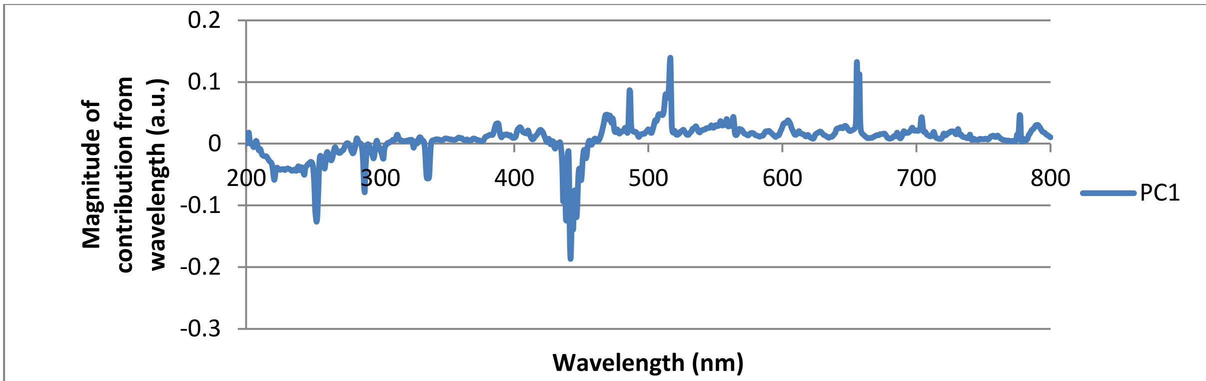

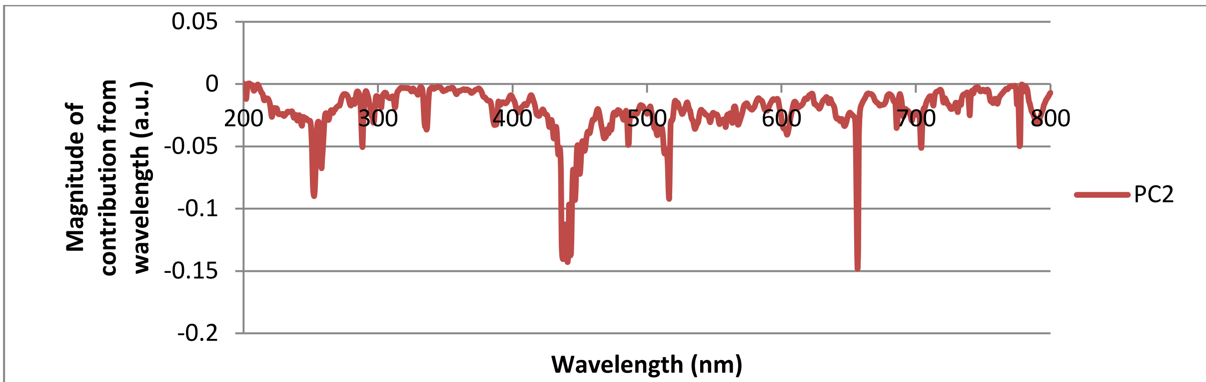

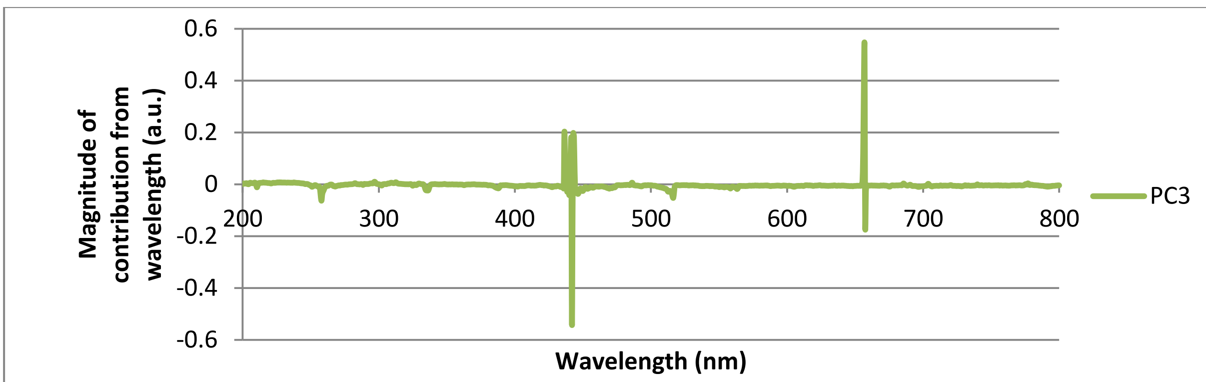

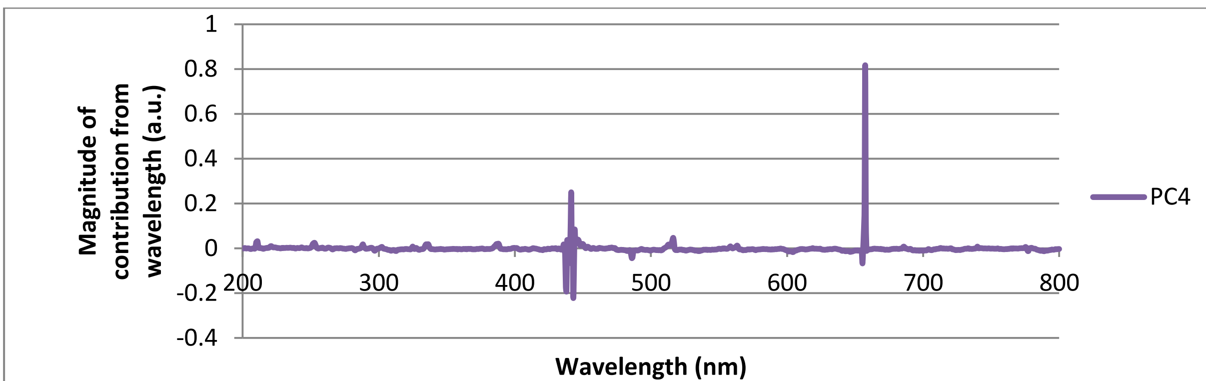

Figure 5.8.3 PC loadings from the treated data of patterned silicon on oxide wafer

The following graph (Figure 5.8.4 1st 4 Principal Component scores of treated oxide etch shows the principal component scores. The magnitude of the 1st PC is so large that it swamps the information provided by the later PCs. The 1st PC appears to offer very little in terms of end point information.

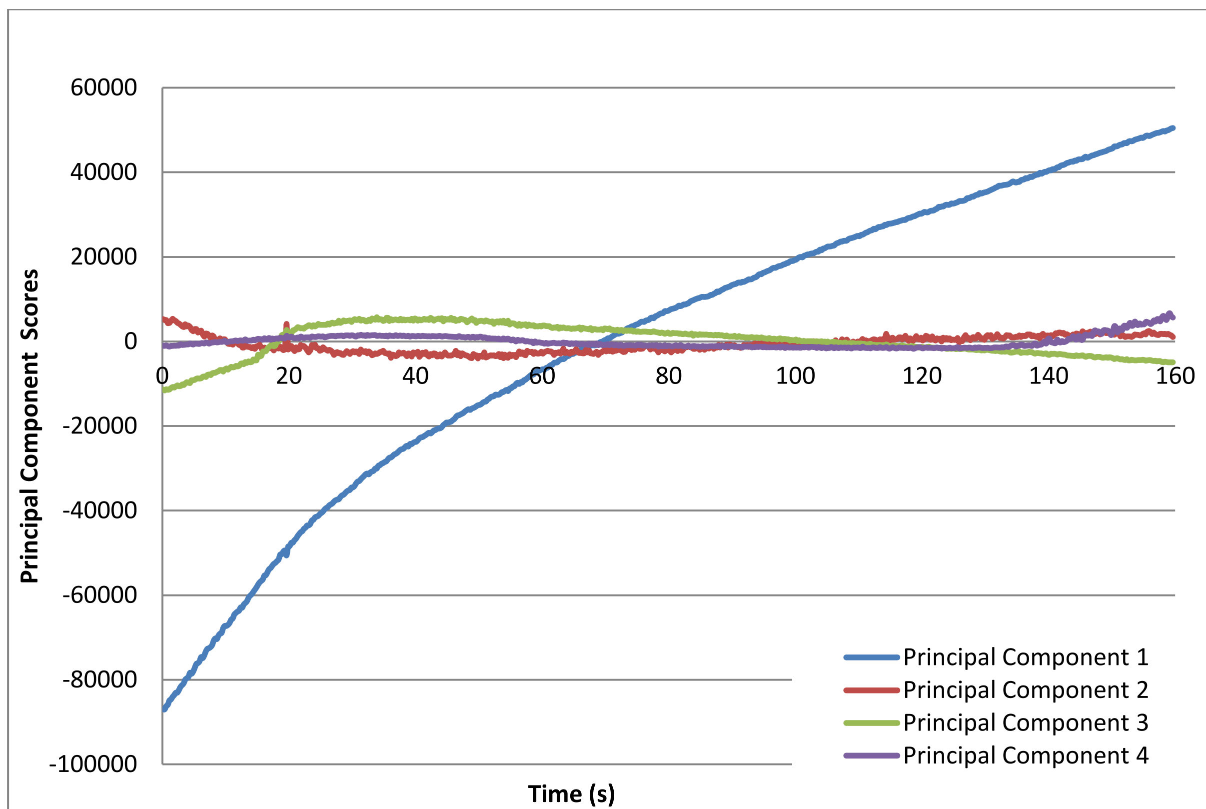

Figure 5.8.4 1st 4 Principal Component scores of treated oxide etch

The graph below (Figure 5.8.5) detailing the PC scores for the PC2, PC3 and PC4 shows these three PCs follow the etch with all three exhibiting a sign change towards the end of the etch. Although these sign changes occur at different points through the etch they are separated by approximately 15 seconds and as such represent a reasonable location for the end point of the etch.

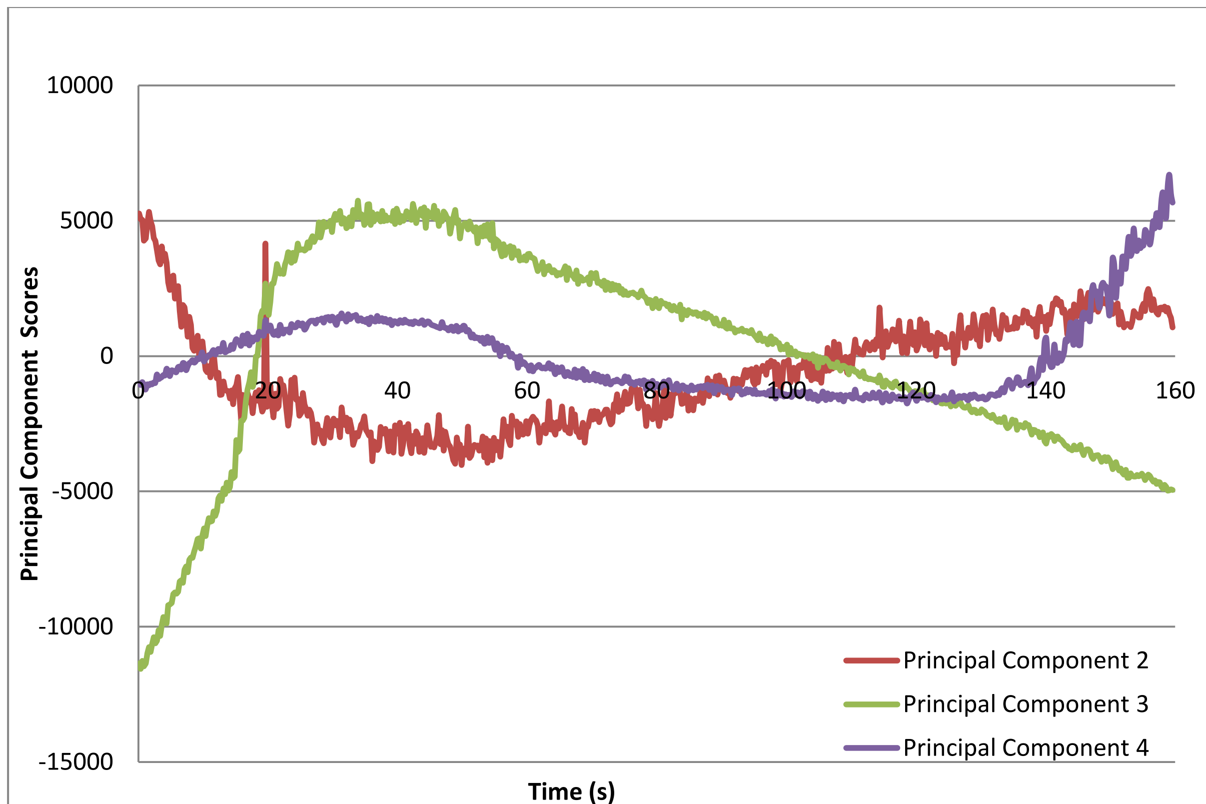

Figure 5.8.5 Principal Components 2-4 only

Although there is still a degree of ambiguity to the results and a clear end point cannot be identified it is clear that there has been a significant increase in the clarity of the results. This is a dramatic improvement on the untreated data. It is possible to resolve a clearer end point at approximately 140 seconds into the etch in PC4. The data contained in the 4th principal component, predominantly relates to two wavelengths: 440nm and 662nm which correspond to SiF_x and CO species[3] respectively, both these species would be expected to drop once the oxide layer has been removed. However PC4 rises, this is counter to expectations from the loading graph for PC4, which has positive contributions from both 440nm and 662nm. However there is a negative contribution from the 440nm spectral line which could potentially lead to an inversion of the score. The end point time agrees with the analysis of the film after the etch which showed that although the oxide layer had been

completely removed there was very little over-etch. The etch was halted shortly after this apparent end point.

5.9. Conclusion

Optical Emission Spectral data was obtained from several etch processes across a range of open areas. The data was collected using two OES systems supplied by Verity, these being the SD-1024D and the SD-1024FH. This data is often insufficient to supply a consistent end point for a variety of reasons. The two most significant of these are a low open area leading to a low signal to noise ratio and secondly thick or non uniform layers leading to gradual clearing of the layer and as a result an end point which spans a large period of time.

Principal Component Analysis was applied to each of the etch processes followed in order to determine whether the statistical technique would achieve an improvement in the ability to obtain a clear end point.

The first experiments involved 100% open area etches. The first experiment involved a 100% open area covering of resist, as such a major problem was the gradual clearing of the surface layer. This is reflected in the results as there is no single point which can be identified as an end point. However PCA is not suggested as a solution to this and as such would not be expected to make an improvement. Another problem with this experiment is that the nature of the resist by design is to be impervious to the plasma. Although the resist will be removed by a persistent etching plasma it will be a far from uniform film removal. This is fully reflected in the extended duration of the end point.

The next sets of results involve a change in the open area. The first experiment involved an open area of approximately 15% the second an open area of approximately 1%. In both

cases the PCA technique led to an improvement on the signals obtained. The first case is a more complicated one in which to determine the end point. This is due the method of application of the sacrificial layer. This was applied using a deposition plasma, which is an isotropic process. Therefore the passivation layer is applied to both the surface which will be etched by the anisotropic plasma but also the sidewalls, which will also be etched but at a slower rate. Thus what is seen in the results is the point at which the majority of the material is removed, followed by a point when the entirety of the layer has been removed. Distinguishing between these two points is a significant challenge. However that the PCA enables the user to be aware of the two stages suggests an improvement in the ability to interpret the data as a result. The second case clearly shows a large improvement in the obtained signal. In the pre-treatment case there is no identifiable end point, with only a general trend observable. Upon application of the PCA it becomes possible to identify a small range over which the end point has occurred. This end point corresponds to that which predicted by the plasma process recipe parameters and expected etch rate.

Overall the use of PCA appears to offer a significant improvement to the ability to be able to obtain information about the processes occurring throughout the course of the etch. A dramatic improvement to the signal strengths obtained is achieved through the use of PCA. This is a result of essentially combining the signals which are relevant to an end point whilst discarding those which are not. Through this method it is possible to resolve end points where previously, using the untreated data, end point was not apparent. One of the benefits of using PCA is that the loadings results can be used to identify the wavelengths that are directly related to the determination of end point i.e. those which exhibit the greatest change from before to after an end point. This is extremely useful as the significant

drawback with using PCA is that it requires the information from the entire etch, and as such it cannot be conducted in real time. This is something that is highly desirable in the field of end pointing. However being able to identify the key wavelengths involved means that in an industrial scenario it is possible to run what is essentially a training run in order to establish which wavelengths to observe during the process. This coupled with regression techniques to identify the patterns that are consistent with end point could lead to an automated system for recognizing end points.

In summary PCA was used to enable the improved analysis of end point signals in optical emission spectroscopy. However it is only part of the solution as it can only be used once the etch has been completed. The ideal situation is for a system which can identify in real time which signals will exhibit significant changes over the course of an etch. This could potentially be achieved with a library of etch processes and the changes that occur alongside them.

5.10. References

1. Timothy J. Dalton, William T. Conner, and Herbert H. Sawin, *Interferometric real-time measurement of uniformity for plasma etching.* Journal Electrochemical Society, 1994. **141**(7).
2. F. Heinrich, H.P. Stoll, and H.C. Scheer, *New and simple optical method for in situ etch rate determination and endpoint detection.* Applied Physics Letters, 1989. **55**(14).
3. Herman, I., P. , *Optics Diagnostics for Thin Film Processing*. 1996: Academic Press.
4. S. F. Wong, M. J. W. Boness, and G. J. Schulz, *Vibrational Excitation of O2 by Electron Impact above 4 eV.* Physical Review Letters, 1973. **31**.
5. I. C. Plumb and K. R. Ryan, *Gas-Phase Reactions of SF_5, SF_2, and SOF with O(3p): Their Significance in Plasma Processing*

Plasma Chemistry and Plasma Processing, 1986. **6**.

6. Toshio Goto and Masaru Hori, *Radical Behaviour in Fluorocarbon Plasma and Control of Silicon Oxide Etching by Injection of Radicals.* Japanese Journal Of Applied Physics, 1996. **35**.
7. T. Kimura and K. Ohe, *Probe measurements and global model of inductively coupled Ar/CF4 discharges.* Plasma Sources Science Technology, 1999. **8**(4).
8. E. Gogolides, et al., *Etching of SiO2 and Si in fluorocarbon plasmas: A detailed surface model accounting for etching and deposition.* Journal Of Applied Physics, 2000. **88**.
9. M. W. Kiehlbauch and D. B. Graves, *Temperature resolved modeling of plasma abatement of perfluorinated compounds.* Journal Of Applied Physics, 2001. **89**.
10. Kimura, T., A.J. Lichtenberg, and M.A. Lieberman, *Modelling finite cylinder electronegative discharges.* Plasma Sources Science Technology, 2001. **10**.
11. P. Ho, et al., *Modeling the plasma chemistry of C2F6 and CHF3 etching of silicon dioxide, with comparisons to etch rate and diagnostic data.* Journal Vacuum Science and Technology A 2001. **19**.
12. *Through Silicon Via and 3-D Wafer/ Chip Stacking Technology*. in *VLSI Circuits, 2006*. 2006: IEEE Conference Publications.

6. Chapter 6 - Independent Component Analysis

6.1. Introduction

Independent component analysis (ICA) is a statistical and computational technique for revealing hidden factors that underlie sets of random variables, measurements, or signals[1]. ICA belongs to class of blind source separation methods for separating data in underlying informational components. A key factor is that the method can be used without any prior information regarding the nature of the source signals, hence the term blind.

ICA delivers a set of loading factors, whereby maximizing the independence between them identifies these factors. ICA is a generative model for observed multivariate data given as a large set of samples. This set or database of samples are considered to be linear mixtures of unknown latent variables, the mixing parameters are also unknown. The latent variables are assumed non-gaussian, mutually independent and they are called the independent components of the observed data. These independent components, also called sources or factors, can be found by ICA.

Previous data reduction and feature extraction techniques such as factor analysis and principal component analysis are similar to ICA. Essentially these techniques analyze a large dataset and attempt to reduce it to a smaller dataset, by maintaining pertinent and relevant data whilst rejecting the static data[2]. The significant deviation of ICA from these techniques is that PCA and FA obtain signals based on a weaker property than independence. Specifically PCA and FA find signals that are uncorrelated to each other. For example if PCA were used to separate a selection of signals from mixtures of microphone outputs, the results would be a selection of new mixtures of voices. If ICA were applied to the same signals, each resultant signal would be independent from the others[3]. The signals obtained by ICA would be a set of independent voices.

6.2. Independent Component Analysis – An Overview

The simplest example of ICA is to imagine a situation where there are two people speaking at the same time in a room. The speech is recorded using two separate microphones. If the voice signals are analyzed on a fine timescale it becomes apparent that the amplitudes of the two signals at any one point in time are unrelated. This is the case because two individual physical processes, two separate people talking, generate the two signals. As we know that the two signals are unrelated we can potentially separate the mixture by looking for unrelated time varying signals within the combined mix of signals. By using this technique, we know that the two extracted signals are unrelated, we also know that the two voices are unrelated, thus we know that the two extracted signals are the two voices.

This is a fundamental characteristic of the technique of ICA, knowing that each voice is unrelated suggests a strategy for separating the individual signals from the mixture. Although this appears mundane, it is a vital prerequisite for ICA to effectively separate data into its original signals[4]. Here the mixing and separating of signals has been based on voices, however so long as the signals are unrelated, any signal type can be used. ICA has been used to disseminate such broad ranging signal mixtures as function magnetic resonance imaging (fMRI)[5], stock prices[6] through to analysing signals associated with the firing of neurons.[7].

In the example of mixed voice signals, the separation of the signals was based on the physically unrelated nature of the voices. For general use this approach is formalized by identifying the notion of the unrelated nature of the sources as *statistical independence*. If two or more signals are statistically independent, the value of one signal provides no information regarding the value of the other signals.

6.3. Independent Component Analysis – A Basis

The fundamental principal that Independent Component Analysis is based on is the physically realistic assumption that signals originating from different sources or physical processes will be statistically independent. If this assumption is accepted there is an implication that it can also be reversed. This leads to the novel assumption that if statistically independent signals can be extracted from a mixture of signals, then these extracted signals must be from separate physical sources (such as different people's voices). Although this assumption is not logically warranted, it is found to work in practice. ICA separates signal mixtures into statistically independent signals. If the assumption of statistical independence is valid, then the signals obtained through independent component analysis will be from a separate physical process and a desired signal. The above statement is a purely intuitive illustration of ICA; clearly there is a significant degree of fundamental mathematics involved in the use of ICA. In the following section the mathematical theory of the application of ICA will be explained.

6.4. ICA – Mathematical Theory

ICA is a multivariate, parallel version of projection pursuit. ICA will extract a series of signals simultaneously whereas projection pursuit will deliver the results one at a time.

The core theory of ICA is that of statistical independence, in order to follow ICA it is vital that independence is fully understood. If two signals y_1 and y_2 are completely independent of each other then the value of y_1 has no information about the value of y_2. Eg. A first coin toss, y_1, lands on heads, that result contains no information about the result of a second coin toss y_2. The results of the two coin tosses are said to be statistically independent.

6.5. Independence of Joint and Marginal Distributions

6.5.1. Independent Events: Coin Tossing

The above example of tossing a coin is a commonly used statistical example; it will be used here to aid the description of independent results using mathematical parlance and symbols.

If every coin toss has an outcome that is independent of every other coin toss and a probability of obtaining a head of $P_h = 0.5$ then the probability of obtaining two consecutive heads is

$$P_h \times P_h = \prod_{i=1}^{2} Ph \tag{6.1}$$

$$= 0.5^2 \tag{6.2}$$

$$= 0.25 \tag{6.3}$$

Here the symbol ∏ is the standard notation for representing products. If we take the expansion of this to the Nth case then the probability of obtaining exactly N heads from N coin tosses is

$$\prod_{i=1}^{N} P_h = P_h^N \tag{6.4}$$

Here the probability is assumed to be 0.5, as for a fairly weighted coin, however if the coin were biased so that the probability of obtaining a head is P_h=0.2, then the probability of obtaining N heads is P_h raised to the power N.

$$P_h^N = 0.2^N \tag{6.5}$$

So the probability of obtaining 4 heads with the weighted coin described above is 0.2^4 = 0.0016. It is important to note that the probability can only be calculated in this manner, as each toss of the coin is totally *independent* of the any others.

6.5.2. Independent Signals: Speech

The previous example considers only the simple case of coin tossing; the same approach can be extended to more interesting and useful examples, such as speech.

The probability that the amplitude of a voice signal s falls within an extremely small range around the value s^t is given by the value of the *probability distribution function* (pdf) $p_s(s^t)$ of that signal at s^t. From this we can now state that $p_s(s^t)$ is simply the probability that the variable s adopts the value s^t. Given that speech signals have near-zero amplitude for the majority of their time, the pdf of s=0, as shown in the following image (Figure 6.5.1).

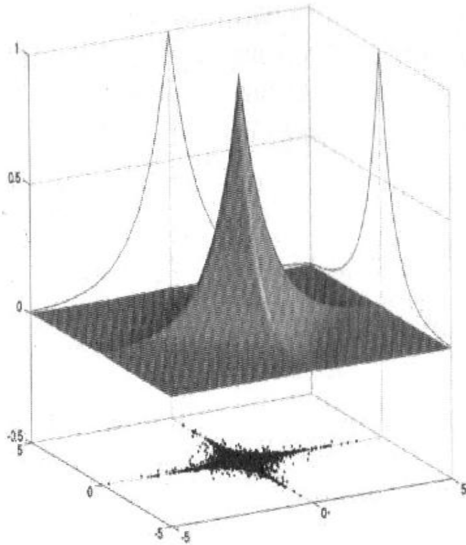

Figure 6.5.1 A Probability Distribution Function for two high-kurtosis variables such as speech. The joint probability is shown on the horizontal plane (image taken from [4]).

The contrasting image of of two typical *gaussian* pdfs associated with signal mixtures is also shown below (Figure 6.5.2).

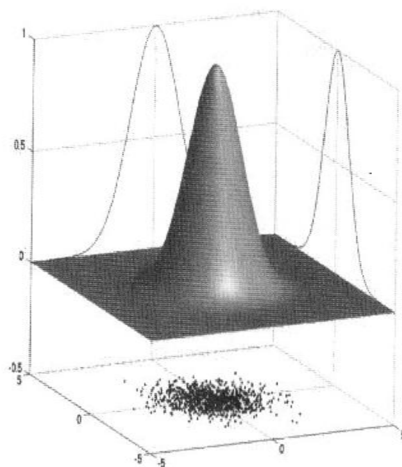

Figure 6.5.2 A Probability Distribution Function for two gaussian variables such as signal mixtures is shown in the solid surface. The joint probability is shown on the horizontal plane (image taken from [4]).

If we assume that two speech signals s_1 and s_2 from two separate people are independent, the implication is that the *joint probability* $p_s(s_1^t, s_2^t)$ that $s_1 = s_1^t$ when $s_2 = s_2^t$ is given by the probability $p_{s1}(s_1^t)$ that $s_1 = s_1^t$ times the probability $p_{s2}(s_2^t)$ that $s_2 = s_2^t$

$$p_s(s_1^t, s_2^t) = p_{s1}(s_1^t) \times p_{s2}(s_2^t). \tag{6.6}$$

The joint probability for all the values of **s** can be visualized for two variables as shown in the above diagram **(**Figure 6.5.1**)**, such that the probability that **s** = (s_1^t, s_2^t) is given by the height p_s(**s**) above the two horizontal axes representing values of s_1 and s_2. The pdfs p_{s1} and p_{s2} are known as the marginal pdfs of the joint pdf p_s. A significant aspect of this joint pdf is that it can be obtained through the product of its two marginal p_{s1} and p_{s2}. As in the previous example of the coin tossing, this is only the case where the variables s_1 and s_2 of the marginal pdfs p_{s1} and p_{s2} are independent.

From the equation (6.6) the vector valued variable $\mathbf{s}^t$ = (s_1^t, s_2^t) has a pdf which can be written as

$$p_s(\mathbf{s}^t) = p_{s1}(s_1^t) \times p_{s2}(s_2^t) \tag{6.7}$$

By assuming that all speech signals can be approximated by the same super-gaussian pdf p_s, so that $p_s = p_{s1} = p_{s2}$ we are able to write

$$p_s(\mathbf{s}^t) = p_s(s_1^t) \times (p_s(s_2^t) \tag{6.8}$$

$$= \prod_{i=1}^{2} p_s(s_1^t). \tag{6.9}$$

If it is also assumed that all values of each signal are independent, then the probability of obtaining the observed *N* values in each signal is

$$p_s(s_1) = \prod_{t=1}^{N} p_s(s_1^t) \tag{6.10}$$

$$p_s(s_2) = \prod_{t=1}^{N} p_s(s_2^t) \tag{6.11}$$

So that the probability of obtaining the *N* pairs of signal values is

$$p_s(\mathbf{s}) = \prod_{t=1}^{N} p_s(\mathbf{s}^t) \tag{6.12}$$

During this derivation we have made the assumption that all values of each speech signal are independent. This assumption leads to the fact that the ordering of the signals is ignored. Despite the fact that this is a grand assumption, it does allow the probability of any signal to be estimated (this estimation can be incorrect if consecutive values are close to each other). Furthermore the assumption enables the calculation of any set of *M* independent signals to be estimated over *N* time steps. If we substitute equation (6.9) into equation (6.12) then

$$p_s(\mathbf{s}) = \prod_{t=1}^{N}\prod_{i=1}^{M=2} p_s(s_i^t). \tag{6.13}$$

This is the probability of obtaining the observed values if the signals s_1 and s_2 are independent and if *all* values of $\mathbf{s}^t$ are independent. It is common practice to express products. If we take the logarithm of equation (6.13) then we have

$$\ln p_s(\mathbf{s}) = \ln \prod_{t=1}^{N}\prod_{i=1}^{M=2} \ln p_s(s_i^t) \tag{6.14}$$

$$= \sum_{t=1}^{N}\sum_{i=1}^{M=2} \ln p_s(s_i^t). \tag{6.15}$$

Although this example and derivation is based on separating speech, the same technique can be applied to any mixture of signals, such as optical spectral data. For optical spectral data it would be that the result would be the probability of two components containing resultant signals which were independent.

A mathematical description of the technique used in the fixed point algorithm, which is used in this project is given in appendix 2. This derivation is taken from the work of Hyvärinen *et al*.[5], the team credited with creating the Fast ICA fixed point algorithm.

6.6. Independent Component Analysis methodology - low open area tests

One of the key requirements of an end-point system - as has been discussed in detail throughout this report - is the ability to resolve end-points in difficult conditions such as when dealing with samples with low open area.

In order to obtain a dual result, a piece of work was devised to determine the extent to which ICA technique is capable of dealing with low open area.

SPTS supplied patterned silicon on oxide wafers. A full wafer of this patterning has an open area of approximately 25%. This is a reasonably standard value for open area (although there are many cases as discussed earlier, which require much smaller open areas). This open area is within the capability of a standard OES configuration.

Given that 25% open area does not represent a significant challenge, the open area being etched needs to be reduced. This is achieved by taking a coupon of the full patterned wafer and cleaving it to produce smaller dies. An example of a coupon fixed to a wafer is shown below (Figure 6.6.1).

Figure 6.6.1 Carrier wafer with patterned Silicon On Insulator (SOI) coupons fixed to it

These dies can then be placed onto a carrier wafer. The carrier wafer itself can be of any material, so long as it is coated with a material that will not be removed in the silicon etch process. The two most common carrier wafers used in this work were nitride coated wafers and oxide coated wafers. It is also possible and convenient to use photo-resist coated wafers, however the selectivity of these is not as high as with nitride or oxide and they are required to be replaced more often as a result.

Once cleaved the patterned wafer dies or 'coupons' are fixed onto the carrier wafer using crystal bond. Crystal bond is a wax, which when heated to 50-60C liquefies allowing its convenient use as an adhesive. It is important to use an adhesive such as this as it ensures a good thermal contact between the carrier wafer and the wafer coupon. Given that etch processes are often executed at low temperatures a variation in temperature can have extremely dramatic consequences for etch performance.

The size of the die is critical as it determines the open area of the sample. The wafer is cleaved into pieces of approximately 20mm^2. 20mm^2 size samples have an open area of approximately 1%.

A selection of carrier wafers had SOI coupons fixed to them in a range from 6% down to 0.1% open area. The silicon depth to be etched in these wafers is 20 microns. These were etched using the following process recipe (Table 6.6.1 Process recipe parameters for SOI etch. Number of loops is arbitrary as over etch was substantial to ensure end point was reached and substantially passed.:

Helium is included in the recipe, it is not a process gas, it refers to the backside of cooling of the wafer as applied through the electrostatic chuck of the process chamber.

	Strike	Deposition	Etch 1	Etch 2
Step Number	1	2	3	4
Time (s)	2	1.1	1.2	1.5
Loop destination	0	0	0	2
Loop number	0	0	0	500
Pressure (mTorr)	48	48	30	30
Platen Power (W)	0	0	300	300
Source Power (W)	2500	2500	2500	2500
Coil Current (A)	10	10	10	10
O_2 (scms)	0	0	0	0
Ar (scms)	200	0	0	0
SF_6 (scms)	1	1	455	455
C_4F_8 (scms)	100	240	0	0
He Pressure (mTorr)	8.5	8.5	8.5	8.5
Platen Temp (°C)	10	10	10	10

Table 6.6.1 Process recipe parameters for SOI etch. Number of loops is arbitrary as over etch was substantial to ensure end point was reached and substantially passed.

The OES data was collected with a Verity Spectrograph. The data was then extracted and the data for the single wavelength of 440nm was compared with the results obtained using the fast ICA statistical approach.

6.7. ICA Methodology – Repeatability Tests

In order to establish the validity of independent component analysis as a statistical technique it was necessary to run multiple repeats of similar process runs.

By repeating the process runs, the repeatability of ICA can be established. Patterned SOI wafers pieces (coupons) were processed using the SPTS Rapier DSi process tool. The recipe for the etch was given above (Table 6.6.1 Process recipe parameters for SOI etch. Number of loops is arbitrary as over etch was substantial to ensure end point was reached and substantially passed.

The OES data was collected using a Verity Spectrograph. This OES data was then treated using ICA as a statistical technique after the process run was complete. Matlab was used to treat the statistical data. Matlab is a numerical computing environment. This widely used software was developed by MathWorks and allows matrix manipulations and implementation of algorithms, alternative programming languages such as C, C++, Java and Fortran can also be interfaced using Matlab.

6.8. ICA Results

6.9. OES – No processing

Optical Emission Spectroscopy has been described both in this work and in many previous studies[8-15] as an excellent tool for the real time analysis of plasma performance. One of the key diagnostic capabilities afforded by OES is end point control as described in more

detail previously in this work. The figure below (Figure 6.9.1 Mid process optical emission spectrum) is an example of a complete spectrum snap shot. This example is taken at an instant in a silicon etch process prior to the exposure of the buried silicon oxide layer. A selection of the peaks are identified in the graph, with fluorine species showing the largest intensities. A peak associated with C_2 is also identified.

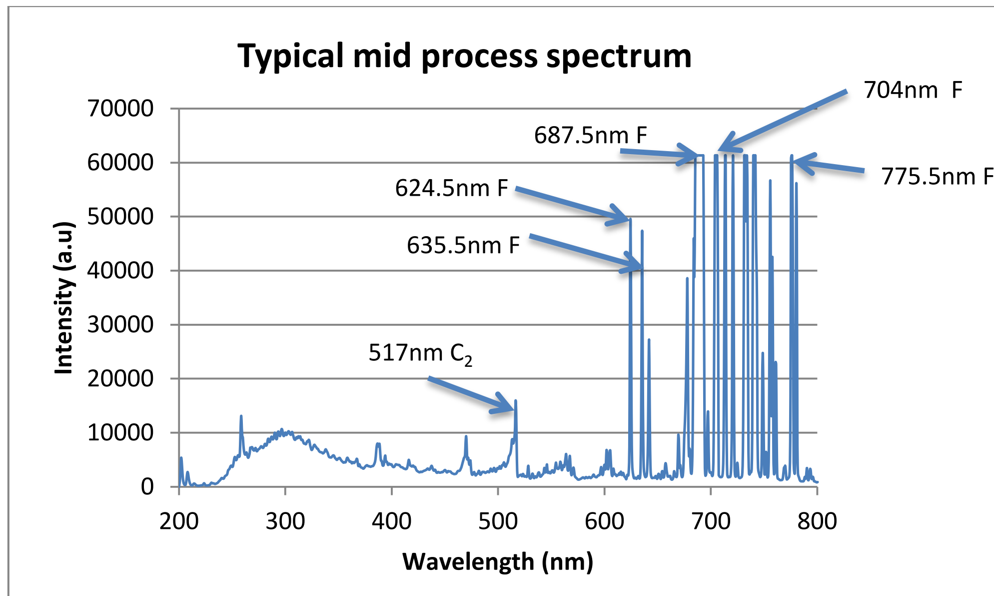

Figure 6.9.1 Mid process optical emission spectrum

The large amount of data detailed in this graph is for a single snap shot of the process. Typically a spectrograph will record this level of data every 0.5 seconds or more. It is not a trivial task to identify which is the key data required to provide the most useful information. The following graph (Figure 6.9.2) is a similar snapshot although this data point is taken significantly after the end point of the process. The buried oxide layer has been exposed at this point, and no silicon is being etched, but the plasma is still active. The two graphs are clearly similar, with slight variation between the two. Although it seems clear that there is a significant increase in two wavelengths at approximately 624.5nm and 635.nm upon closer inspection these wavelengths show little change which associated with a genuine end point. In fact with those examples it is most likely that this is a random fluctuation in the plasma.

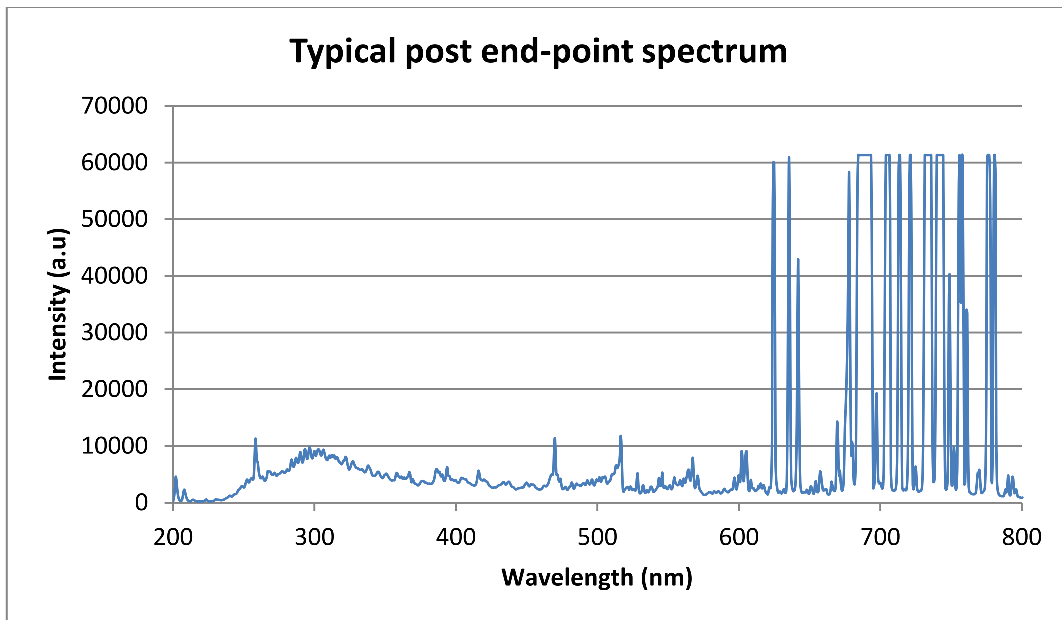

Figure 6.9.2 Post end-point spectrum

6.10. One wavelength – A selection of single wavelengths over the given time of the etch

The most commonly used technique for the determination of end-point is to monitor a specific wavelength. The below graph (Figure 6.10.1) shows the results of monitoring a single wavelength over the course of an etch process. This particular instance details the results of monitoring three separate wavelengths 273nm, 440nm and 706.5nm. 273nm is a spectral line which is not associated with any chemistry that is taking place over the course of this process. 440nm is widely associated with SiF_3 species and is often used in OES diagnostics of silicon etch processes. 706.5nm is a spectral line which is commonly associated with fluorine species[16]. The example data was taken from the process run carried out on wafer sample 56, with an open area of approximately 1%.

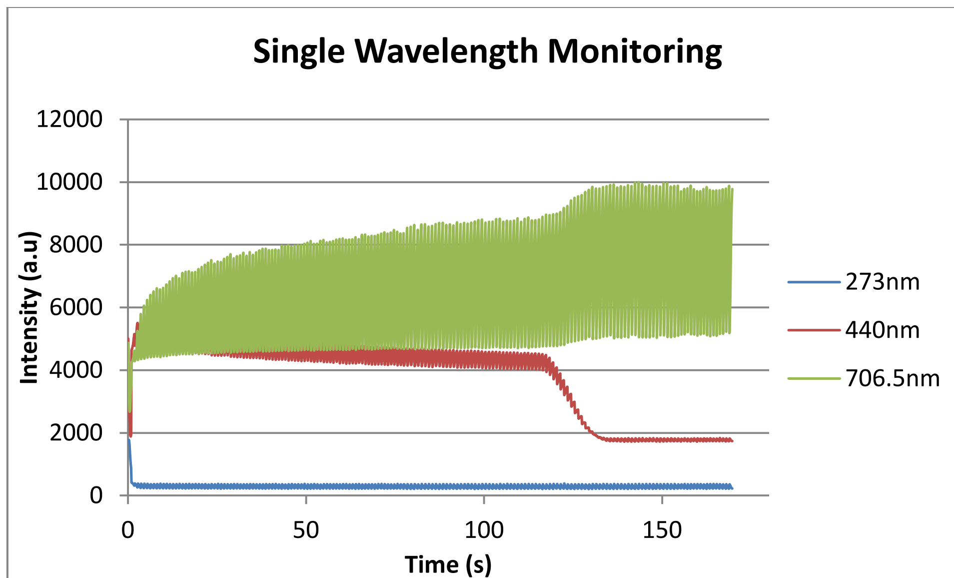

Figure 6.10.1 Single wavelength time series. Wavelengths of 273nm (Dummy), 440 nm (SiFx) and 706.5nm (F) shown.

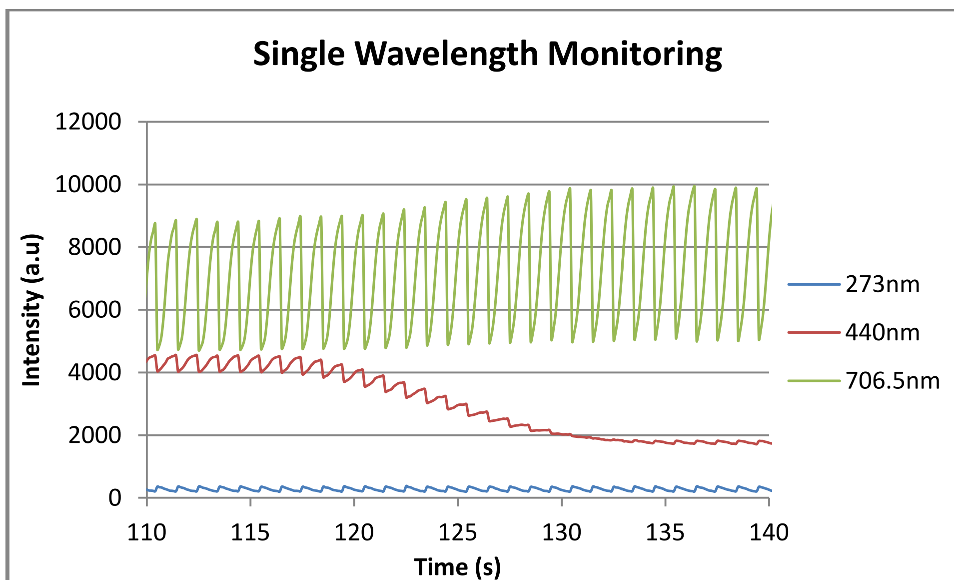

6.10.2 Single wavelengths showing cyclic nature of Bosch process used. Wavelengths of 273nm (Dummy), 440 nm (SiFx) and 706.5nm (F) shown.

The three examples shown describe several of the key issues with OES end point determination. The 440nm shows a clear drop in intensity at the end point (as silicon is no

longer being etched SiF_x is no longer formed), the 706.5nm shows a clear rise in intensity at the end point (as all silicon has been removed F is no longer consumed and is more abundant in the chamber) whereas the 273 shows no change (it is essentially a control wavelength, not expected to show any variation). This example is of a Bosch™ process Silicon etch and the variation between deposition and etch step is clearly recognizable in the OES data with the peaks and troughs associated with the different steps of the process. The deposition stage of the process runs at lower powers and the optical intensity or brightness of the plasma is reduced as a result. This illustrates the problem with OES which is the choice of which wavelength to monitor is key to the efficiency of OES as an end point system.

6.11. Independent Component Analysis

Independent Component Analysis (ICA) is a statistical technique superficially similar to principal component analysis and factor analysis, although much more powerful than these techniques.

ICA defines a generative model for the observed multivariate data, where the multivariate data is provided in the source of a large database of measurements. In the model, the data variables are assumed to be linear mixtures of some unknown latent variables, and the mixing system is also unknown. The latent variables are assumed non-gaussian and mutually independent and they are called the independent components of the observed data. These independent components, also called sources or factors, can be found by ICA. ICA is an offline statistical technique – it is applied to the spectroscopy data post process.

In order to evaluate ICA as a statistical technique to be used with end-point detection masked silicon on oxide wafers were etched in an SPTS rapier plasma etch tool. The silicon etched was a thickness of 20um, beneath the silicon is a buried oxide layer. When the silicon is exposed during the etch process, the characteristic change in plasma chemistry occurs which can be observed with OES equipment. The data obtained from the OES was then processed separately, offline using the ICA technique. The data was extracted from the spectroscope hard drive in the form of a '.dat' file. This is then opened in Matlab where the data is processed using the 'FastICA' algorithm. The fastICA algorithm is a freely available piece of Matlab coding copyright (c) of Hugo Gävert, Jarmo Hurri, Jaakko Särelä, and Aapo Hyvärinen.

The FastICA algorithm is a computationally highly efficient method for performing the estimation of ICA. It uses a fixed-point iteration scheme that has been found in independent experiments to be 10-100 times faster than conventional gradient descent methods for ICA. There are a number of parameters which can be adjusted in order to achieve the best results from ICA.

Firstly the 'approach' is chosen. There are two options for this parameter:

1. Symmetric 'symm' where all the independent components are estimated in parallel or

2. Deflation 'defl' where the independent components are estimated one-by-one in a similar manner to projection pursuit.

Secondly the number of Independent Components is assigned. In the typical case this will be equal to the number signals which are present in the original data. For

the case of spectroscopy – where there are large numbers of signals – it is advisable to use a dimension reduction technique such as principle component analysis to determine the number of final components. If the number of components is chosen simply using the number of independent components it is possible and likely that the results will not offer the full benefit of ICA.

The final significant parameter to be defined is the nonlinearity 'g', this can take four values:

1. 'pow3' $g(u)=u^3$

2. 'tanh' $g(u) = \tanh\,(a1 \times u)$

3. 'gauss' $g(u) = u \times \exp\,(\frac{-a2 \times u^2}{2})$

4. 'skew' $g(u)=u^2$

The combination of these parameters allow for eight possible iterations of the results to be achieved for a single set of data.

6.12. ICA results of wafer 59 - 10 components

The first processing carried out using ICA was for the data obtained from etching wafer 46. The spectroscopic data was taken using the Verity SD1024F. The full spectral data was treated using principal component analysis for dimension reduction. The majority of the variance was found to be well within the first 10 principal components. The data beyond these ten components was discarded and the data contained within the ten was treated using ICA. For the purposes of the initial trials the parameters were chosen as a symmetric

with a non-linearity of ‘pow3’. The results of this first process are shown below (Figure 6.12.1)

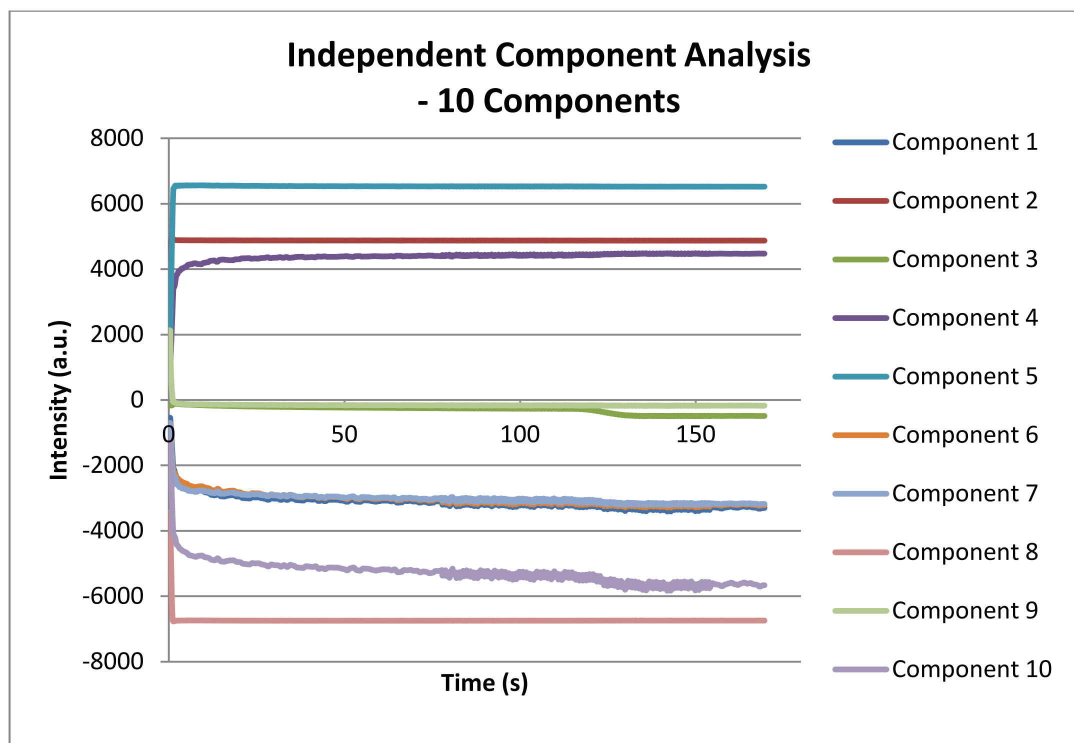

Figure 6.12.1 First Independent Component Analysis results - 10 components

These results show how the full spectroscopic data has been manipulated and reordered to deliver components that contain the full end-point data. The majority of the components show little variation, however component 3 (in this instance) shows the end-point of the process clearly (Figure 6.12.2). The nature of the independent component analysis technique results in a random ordering of the results. IC 1 is not necessarily more significant than IC 10. In the case of principal component analysis it is possible to assign physical significance of these components. In a similar manner the degree of contribution to these components is shown on the graph below (Figure 6.12.3 Graph showing ICA contributions from wavelengths.

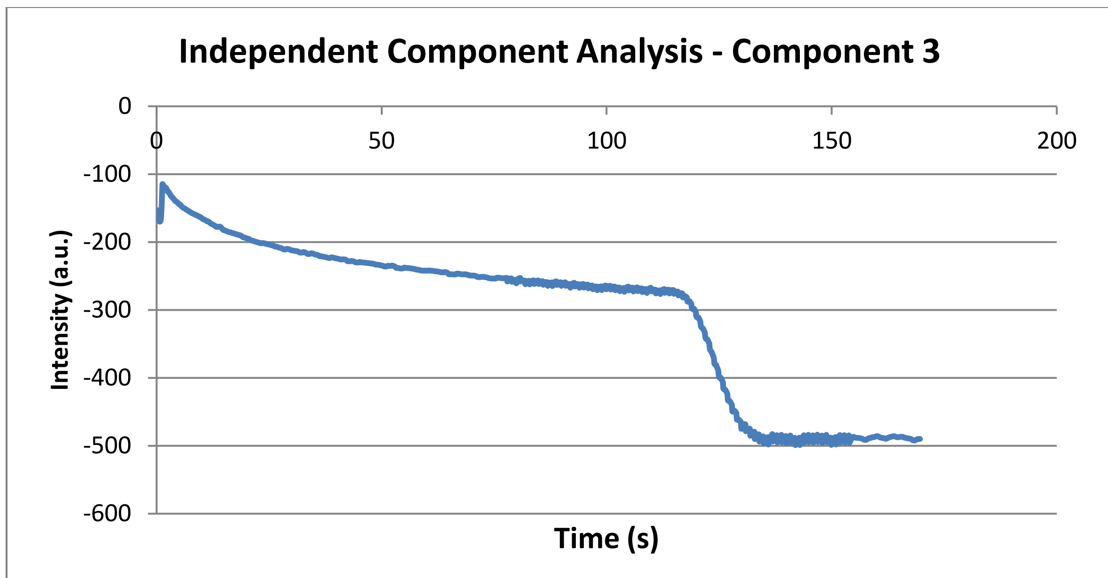

Figure 6.12.2 Single component from wafer 46 process run showing clear end point.

Whilst all the components are shown on a single graph it is difficult to see whether the process has worked. Simply by choosing a single component to investigate it is possible to clearly see that one of the components contains significant end-point data. This graph shows that ICA can be used as a viable tool for extracting an end-point from spectroscopic data.

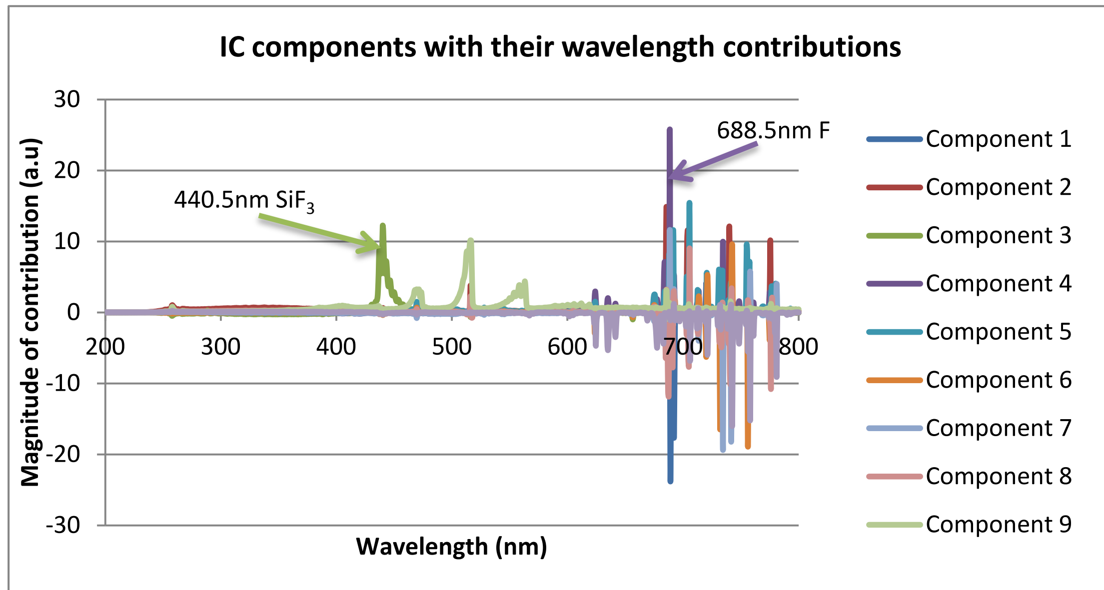

Figure 6.12.3 Graph showing ICA contributions from wavelengths.

The wavelength contributions vary significantly across the full range of components. The majority of the components exhibit a large degree of contribution from wavelengths in the 650nm to 800nm range. This range of wavelengths contains spectral lines which are often associated with the fluorine radicals. This is to be expected given that the etchant gas present in the plasma being observed is SF_6, which results in a high concentration of Fluorine and Fluorine radicals in the plasma. Despite the high level of contributions from these wavelengths the components involved actually contain very little variation across the course of the etch process. This is also a result of the high concentration of Fluorine; the intensities in spectral lines associated with Fluorine are relatively high. When these lines exhibit random fluctuations due to the unstable nature of plasma a small percentage change in a Fluorine line will swamp those changes associated with a genuine end point.

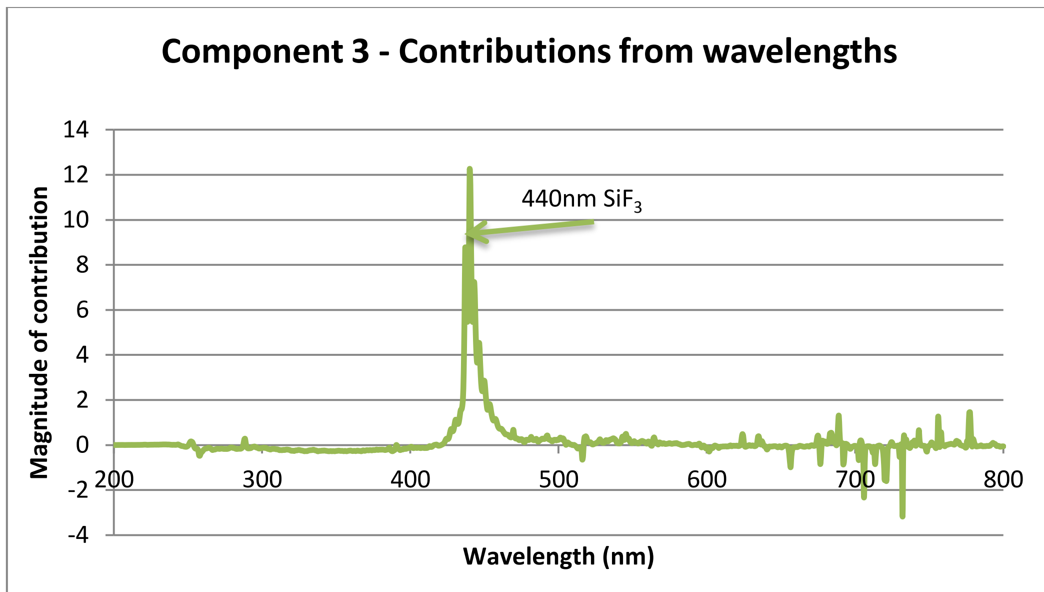

Figure 6.12.4 Wavelength contributions to ICA - component 3

If we look at the contributions to component (Figure 6.12.4), we can see that there are contributions from the range associated with Fluorine lines, however these contributions are dwarfed in comparison to those from the 440nm range. The 440nm spectral line is widely accepted as being attributable to the presence of the SiF_3 radical[17]. This in turn can be used as a measure of the concentration in of SiF_x[16] species in general. If we refer back to the details of the relative intensities of various wavelengths shown earlier in this work (Figure 6.9.1) we can see that relative to the Fluorine lines, SiF_x at 440nm has far lower intensity. However it is clearly SiF related spectral lines which contribute most successfully to valid end-point data. This is essentially where ICA exhibits its power as an end-point statistical tool.

6.13. A comparison of the effect of different parameters on Independent Component Analysis performance

As has been mentioned earlier, there are a number of parameters which can be chosen to improve the output of the ICA algorithm. The effects of changing these parameters for the ICA results on wafer 46 have been collated and are compared on the following graph (Figure 6.13.1).

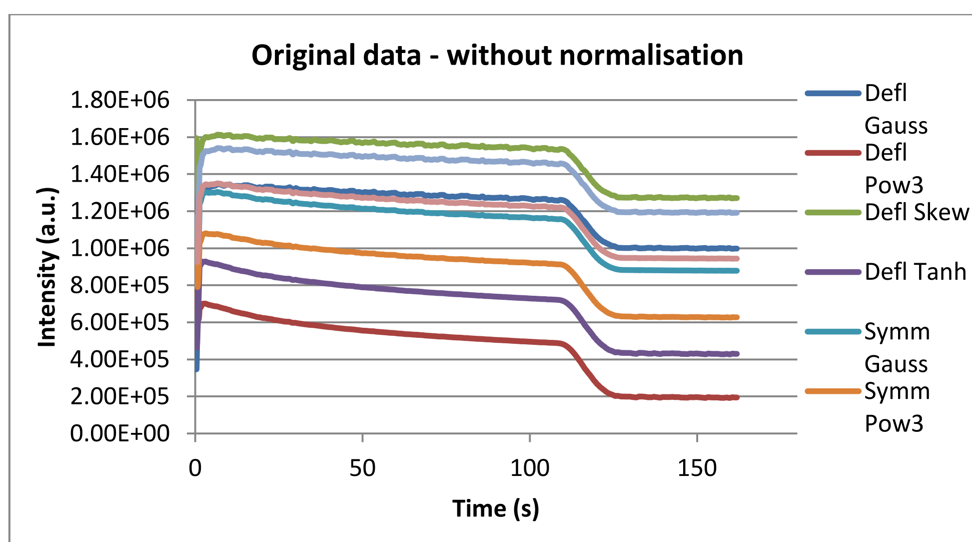

Figure 6.13.1 Independent Component Analysis results for different parameters.

The results have been normalized so as to allow a direct comparison which is shown in the following graph (Figure 6.13.2).   This normalization was conducted by using the signal intensity prior to the signal drop as a standard point; the ratio of the different techniques was then used as a scaling factor to facilitate the direct comparison. Essentially this delivers a scaling factor based on the signal drop as a percentage of the overall signal.

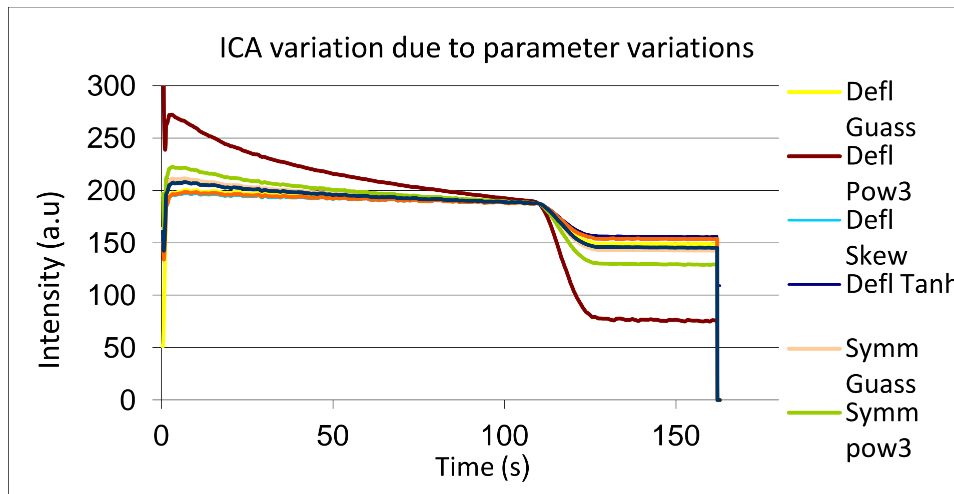

Figure 6.13.2 Comparison of different ICA parameters

In this case the deflation technique using the pow3 non-linearity has delivered the best result. Best here is defined as a measure of the signal drop as a percentage of the signal prior to that drop in signal. This method can be used to compare signals obtained from the same etch process as it merely provides an indicator of the relative success of the techniques. However it is not reliable in terms of analysing data from a wider selection of process runs. The issue is that there could be a significant drop in terms of the percentage of the intensity; however it is important to introduce a measure of the noise across the process run. For example a large signal drop could be seen, but if the noise before and after the signal drop was equivalent to the signal drop then the result is not useful in terms of supplying end point data.

6.14. Comparison of Independent Component Analysis and Principal Component Analysis methods for improving signal to noise ratio

In the previous section we began to discuss how to compare ICA results for more than a single etch process. The most significant measure of the success of OES end-point detection techniques is that of signal to noise ratio. Essentially the end point signal is compared with

the noise inherent in the signal. The following graph (Figure 6.14.1) shows the areas used to determine the two factors i.e. noise and signal drop.

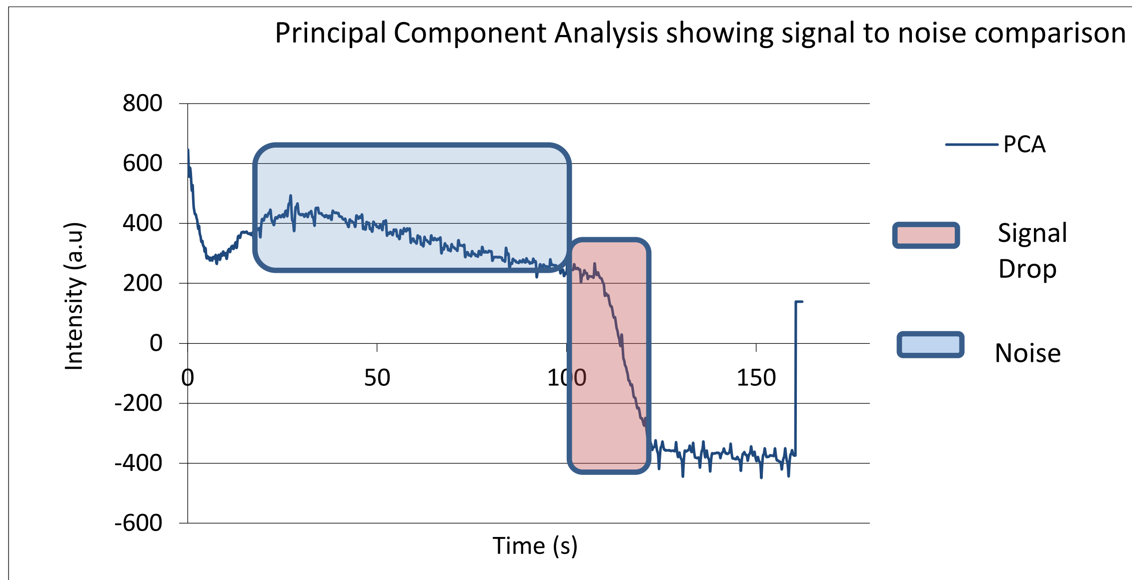

Figure 6.14.1 Graph showing example of signal drop and noise area.

Here principal component analysis was used as the statistical technique on the original data from wafer 46. Principal component analysis is an industry standard for multivariate analysis in end-point detection. For the purposes of this work, PCA has been used to make a direct comparison of the efficiency of ICA as a statistical tool. For each of the processed wafers the area representing the noise in the previous graph is used in conjunction with the area representing the signal drop to create a numerical value for the signal to noise ratio. This value allows for the quantitative comparison of the results of ICA across the full range of processed wafers. In addition it is also possible to use the value to compare the results of ICA to the results of other statistical techniques as applied to the OES data obtained from the etch processes.

In order to establish the validity of ICA as a statistical tool for end-point detection it is clear that the results of more than a single etch process are required. As detailed above we have

now established an operable method for the direct comparison of different statistical techniques

The following graph (Figure 6.14.2) shows the results of comparing multiple process runs. The two techniques of ICA and PCA were both applied to the same data sets for each wafer in turn.

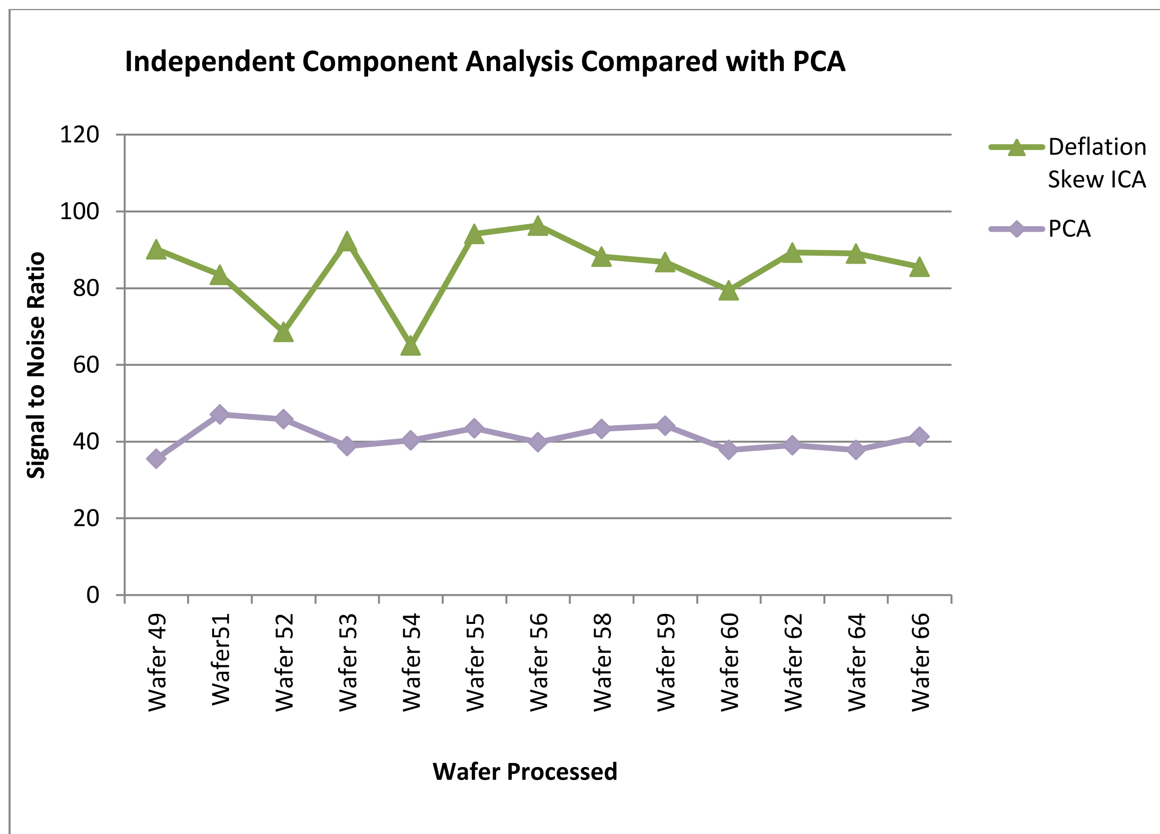

Figure 6.14.2 Comparison of Independent Component Analysis to Principal Component Analysis across full range of wavelengths

In this case only one parameter of ICA was chosen to more clearly illustrate the effectiveness of the technique. For each process etch, once the OES data was processed using ICA and PCA, ICA was found to deliver a better result in terms of signal to noise ratio.

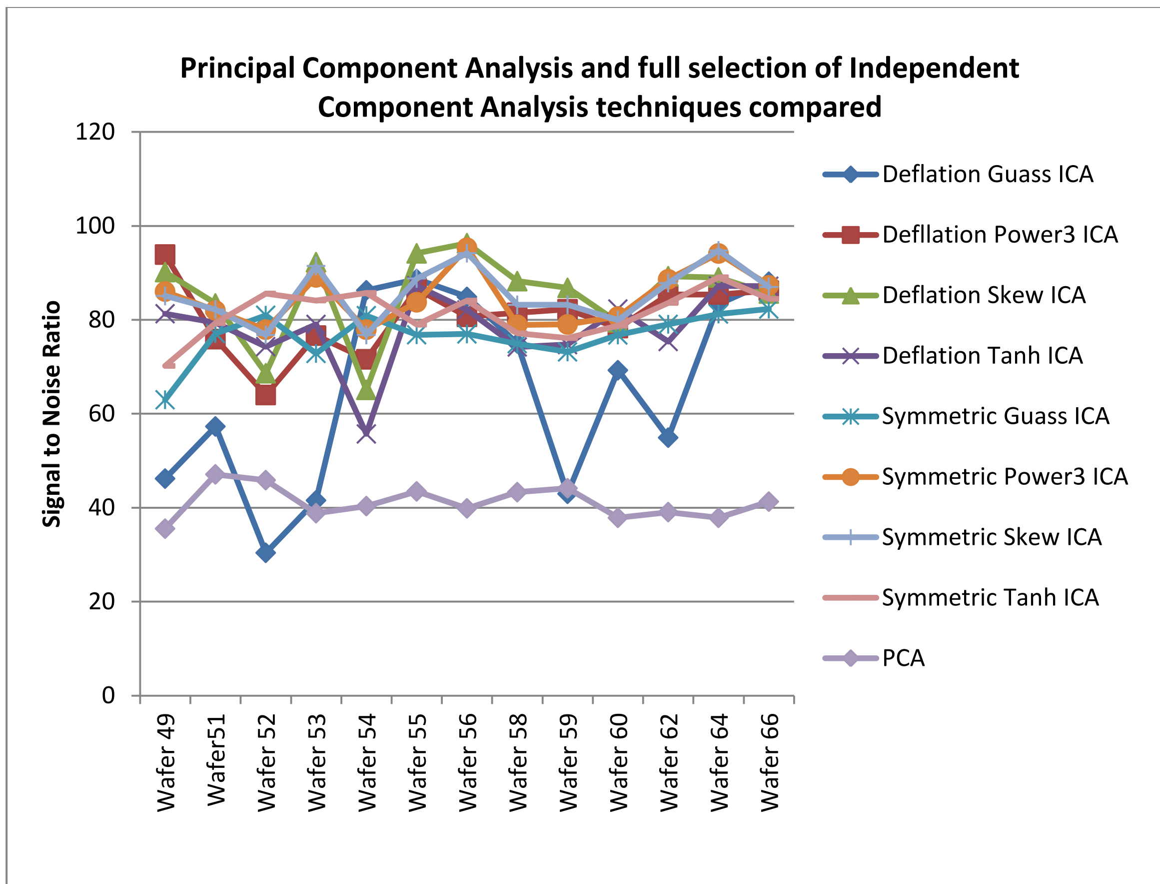

Figure 6.14.3 Comparison of all eight ICA parameter iterations and PCA technique

Previously the results demonstrated the improvement in signal to noise ratio offered by ICA compared to PCA using just one of the parameter combinations. The next work carried out was to establish the results across the full range of parameter combinations. The above graph (Figure 6.14.3) shows the details of all of the ICA parameter combinations across the full range of processed wafers.

ICA consistently delivers a superior signal to noise ratio compared to that found using PCA. The generative nature of ICA as a statistical technique means that there are clear anomalies where the results of the process deliver poor quality results such as wafers 59 or 60 where the deflation approach was used in conjunction with a Gaussian non-linearity. In these cases the alternative approaches delivered superior results. In the general case where ICA has

been successfully been applied there is an approximate doubling in signal to noise ratio over that of PCA.

6.15. Comparison of ICA results for reduced open area

The significance of open area and the challenge it represents in terms of end point detection in silicon etch has been discussed previously within the course of this work. As the exposed silicon being etched is reduced relative to the surface area of the entire sample, the change in plasma chemistry observed at end point becomes less marked. The relative strength of the signal change to the inherent noise in the system falls as a result of this reduced exposed area. For example where a sample is masked across the majority of its surface with only small trenches exposed to the plasma.

Industrial demands for low open areas are consistently pushing the capabilities of end-point equipment. The burgeoning market of Through Silicon Vias (T.S.V.) - where a vertical electrical connection (via) is created running through the entire wafer - often calls for open area etching of less than 1%.

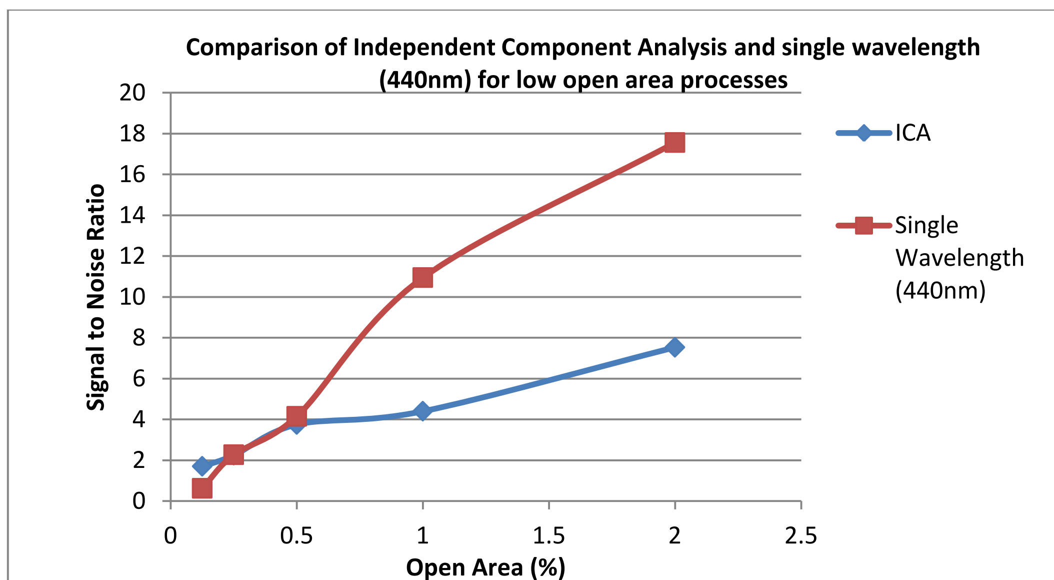

Figure 6.15.1 Low open area Optical Emission Spectroscopy data

For these results a wafer of masked Silicon on Oxide with an open area of approximately 25% was used as a source of low open area samples. The original wafer was cleaved into multiple smaller pieces; by cutting these to specific sizes it is possible to obtain controlled open area samples. The cut to size wafer pieces or 'coupons' were mounted onto oxide coated carrier wafers. By reducing the size of the coupon, extremely low open area samples were created. These samples were then etched and the corresponding OES data captured and processed to deliver results for both the single wavelength (440nm) and Independent Component Analysis.

At higher open areas the single wavelength case delivers good results with high signal to noise ratio. In these cases the results are better than those obtained through ICA. However as the open area is reduced to the limit, the single wavelength results begin to deteriorate. At extremely low open areas where a single wavelength doesn't deliver a valid end point signal change it is possible to obtain a result using ICA. The process of combining signal changes from a variety of wavelengths delivers an end point signal which has a useable signal to noise ratio.

6.16. ICA - Discussion

It has been shown through the course of this project that both Principal Component Analysis and Independent Component Analysis offer an advantage to the user in reactive ion etching. When applied to optical emission spectroscopy data from the plasma process there are clear benefits to using a statistical technique. Initially PCA has been successfully used; this has been established as an industry standard[18, 19]. ICA shows a consistent improvement over PCA in terms of the signal to noise ratio that the two techniques can deliver, although ICA requires PCA as an initial treatment in order to reduce the dimensions of the data involved.

The benefits offered by ICA as a statistical technique mirror that of PCA. The prime benefit is the merging of multiple wavelengths each containing key information to the state of the etch process. The gain that this offers the user is clear, the user is able to apply the statistical technique to the etch data and the algorithm will deliver a trace, which will contain all of the pertinent process information such as end-point. However there is a clear problem with this, in fact there are several.

The first issue is that the algorithm has to be set up correctly to deliver the key results. Throughout this report 10 components have been chosen to work with as the first 10 components contain the vast majority of the variation across the course of the etch. Beyond these 10 components the degree of variation is extremely low for each component. This degree of variation is not useful as it contains no pertinent information about the etch process. This is further complicated by the fact that for separate etch processes, the degree of variation contained within the later components can be larger. It is possible that a process could be developed whereby the number of components to deliver the best results is easily definable; however there has been a significant degree of work conducted outside of this report into the identification of the key number of components to achieve the best results from ICA[20].

The problem is best considered from the point of view of a process technician. When running plasma etch processes a technician will much prefer to follow OES data associated with one or possibly two (as a ratio) wavelengths. This will show clear results which can be shown to be directly associated with the plasma chemistry taking place within the chamber. However in order to make the most of ICA the technician would have to attempt to fine tune the statistical technique by selecting the correct number of components, identifying the key components and identifying the parameters required to fine tune the

algorithm. It is unlikely that the technician will be prepared to go to such lengths in order to attain a slight increase in the signal to noise ratio over that of viewing a single wavelength.

One of the key advantages that ICA could offer is the ability to reduce the in depth process knowledge required on the part of the user to be able to identify an end point, specifically ICA would have the potential to identify the key wavelengths without the input of the user. However if the user is required to have an equally in depth knowledge of the statistical technique the benefit is less clear. Having spent a significant section of my studies ensconced in an industrial work place it has become clear that the extra steps that would be added, in order to gain the modest benefit offered by ICA ensures that it is unlikely to be taken up as an industry standard. In fact the more widely available PCA is in fact often shunned by process technicians as it is not immediately clear how it relates to the actual process chemistry taking place within the chamber. Although the chemistry of the chamber is clearly what is being highlighted by the PCA or ICA techniques, the manner in which certain aspects of the chemistry are combined can be difficult to describe.

6.17. References

1. Lee, T.-W., *Independent Component Analysis - Theory and Applications*. 1998: Kluwer Academic Publishers.

2. Joliffe, *Principal Component Analysis (Springer Series in Statistics)* 2002: Springer. 502.

3. Hyvärinen, A., *Independent Component Analysis (Adaptive and Learning Systems for Signal Processing, Communications and Control Series)*. 2001: Wiley-Blackwell.

4. Stone, J.V., *Independent Component Analysis: A Tutorial Introduction*. 2004: MIT.

5. Hyvärinen, A.O., Erkki, *A Fast Fixed-Point Algorithm for Independent Component Analysis.* Neural Computation, 1997. **9**(7): p. 1483-1492.

6. Back, A.D.W., Andreas S., *A First Application of Independent Component Analysis to Extracting Structure for Stock Returns.* IOMS: Information Systems Working Paper 1997. **IS-97-22**.

7. Savin, C.J., Prashant; Triesch, Jochen, *Independent Component Analysis in Spiking Neurons.* PLoS Computational Biology, 2010. **6**(4).

8. Lee, J.W., *et al.*, *Utilization of Optical Emission Spectroscopy for End-Point*

   Detection during AlGaAs/GaAs and InGaP/GaAs Etchingin BCl3/N2 Inductively Coupled Plasmas. Journal of The Electrochemical Society,, 2001. **148**(9): p. 472-474.

9. Chen, R., H. Huang, and C.J. Spanosc, *Plasma etch modeling using optical emission spectroscopy.* Journal Vacuum Science and Technology A, 1996. **14**(3): p. 1901-1906.

10. Kim, B., J.K. Bae, and W.-S. Hong, *Plasma control using neural network and optical emission spectroscopy.* Jounal Vacuum Science Technology A - Vacuum, Surfaces and Films, 2005. **23**(2): p. 355-358.

11. Richard, A.G. and M.D. Vincent, *Optical emission actinometry and spectral line shapes in rf glow discharges.* Journal Of Applied Physics, 1984. **56**(2): p. 245-250.

12. Marcoux., P.J. and P D Foo, *Methods of End Point Detection for Plasma Etching.* Solid State Technology, 1981. **24**(4): p. 115-122.

13. Hirobe, K. and T. Tsuchimoto, *End Point Detection in Plasma Etching by Optical Emission Spectroscopy.* Journal Electrochemical Society: Solid-State Science and Technology, 1980. **127**(1): p. 234-235.

14. Litvak, H.E., *End point control via optical emission spectroscopy.* Journal vacuum Science and Technology B: Microelectronics and Nanometer Structures, 1995. **14**(1): p. 516-520.

15. Herbert, E.L. *End point control via optical emission spectroscopy*. 1996: AVS.

16. Herman, I., P. , *Optics Diagnostics for Thin Film Processing*. 1996: Academic Press.

17. Flamm, D.L., *Mechanisms of silicon etching in fluorine and chlorine containing plasmas.* Pure and Applied Chemistry, 1990. **6**(9): p. 1709.

18. White, D.A., *et al*., *Low Open-Area Endpoint Detection Using a PCA-Based T2 Statistic and Q Statistic on Optical Emission Spectroscopy Measurements.* IEEE Transactions on Semiconductor Manufacturing, 2000. **13**(2): p. 193-207.

19. WISE, B.M., *et al*., *A COMPARISON OF PRINCIPAL COMPONENT ANALYSIS, MULTIWAY PRINCIPAL COMPONENT ANALYSIS, TRILINEAR DECOMPOSITION AND PARALLEL FACTOR ANALYSIS FOR FAULT DETECTION IN A SEMICONDUCTOR ETCH PROCESS.* Journal of Chemometrics, 1999. **13**: p. 379-396.

20. Yang, Z.L., Stephen; Weng, Xuchu and Hu, Xiaoping, *Ranking and Averaging Independent Component Analysis by Reproducibility (RAICAR).* Human Brain Mapping, 2008. **29**: p. 711-725.

7. Chapter 9 – Nanorod Fabrication

7.1. Silicon Nanorod Methodology

Using a range of equipment based both at the London Centre for Nanotechnology in London and plasma etch equipment based at the junction 24 site of Surface Process Technology Systems in Newport silicon nanorods (pillars) were created from plain, boron doped p-type silicon. A range of different sized samples, primarily 500µm^2 were created as test samples to develop the plasma etch process recipe. 500um^2 was used as this creates a large enough sample to deliver results representative of the performance of the etch recipe. Smaller sample sizes take less time to pattern, but the etch performance may be significantly different due to different etch performance at the edge of the array. 2mm^2 samples were created to be made into full working device structures. 2mm^2 was chosen as the full size sample as this matches the physical mask sizes available for the later stages in device production (PECVD of amorphous silicon, sputtering of ITO and deposition of gold electronic contacts). A significant amount of work has been conducted by colleagues within the research group into planar amorphous silicon based solar cells[1]. This work was conducted using samples of this size (2mm^2), by maintaining the same size samples; a direct comparison is possible into the efficiencies of the planar devices compared with nanorod based devices. For each of the sample sizes there was a range of different diameter and pitch samples created. Initially diameters of 1µm with a pitch of 2µm in a hexagonal arrangement were patterned and etched. Once the recipe development for these pillars was complete both the size and pitch of the sample design was reduced with the diameters having a range down to 100nm diameter and

the pitch being reduced to 500nm. The hexagonal arrangement was maintained throughout all of the samples.

The entire development system is based on two process areas: Patterning and etching, these two processes are described in detail below.

7.2. Mask Patterning – London Centre for Nanotechnology (LCN).

The following is a full description of the methodology that was used to develop a hard mask suitable for dry etching.

7.3. Electron Beam Resist Spin-coating

A 100mm diameter silicon wafer is cleaned using an isopropyl alcohol; this removes any dust or particulate matter that may have contaminated the wafer. This size wafer is chosen to match the standard size used in the electron beam lithography equipment. The wafer is spin-coated with electron beam resist. The resist used in this work was PMMA (polymethyl methylacrylate) in Anisole 6% solids supplied by MicroChem. The resist is applied using a spin coater within the LCN clean room, with the solution being applied at room temperature. A two-stage process is used to ensure that a smooth coating is applied. A ramping speed is used initially, this allows the resist to spread evenly over the entire wafer; at this stage the majority of the resist solution is removed. The second stage is a faster spin setting, this spreads the solution on the wafer, and the speed chosen determines the final thickness of the layer that is applied. Once the spin recipe is complete, the wafer is placed on a hot plate for 75 seconds at 180°C. This cures the polymer and at which point the wafer is ready for patterning.

7.4. Electron Beam Lithography

When creating a patterned mask for etching there are two types of resist techniques that can be used, these are described below and in the following diagram (Figure 7.4.1).

1. Positive – the radiation used to expose the resist causes the exposed area to be rendered vulnerable to the developing fluid. In this case radiation breaks bonds in the polymer of the resist, when the masked sample is placed into developing fluid the weakened areas are removed.
2. Negative – the area that radiation falls upon is strengthened by the radiation. In this case bonds in the polymer are formed by imparting energy into the polymer. For example cross-links between polymer branches can be formed, strengthening the polymer. When the resist coated sample is placed into the developer liquid the areas not strengthened by the radiation are removed.

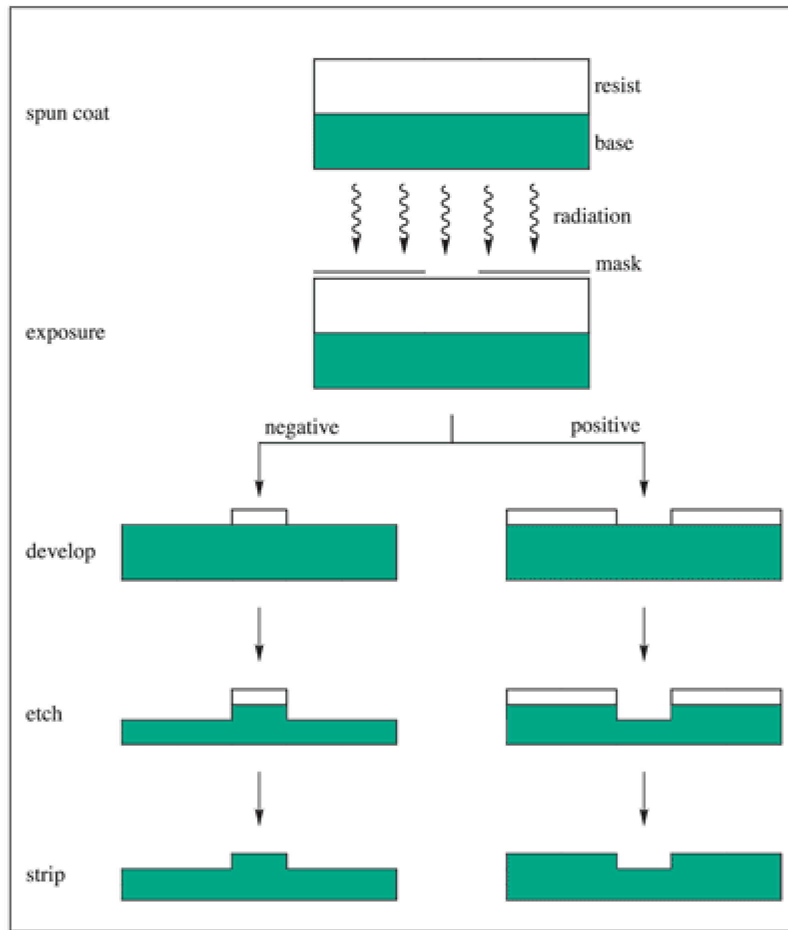

Figure 7.4.1 Positive and Negative Mask Application

For the work carried out in developing patterned samples for nanorod (pillar) etching a positive resist technique was used.

The wafer is placed into the Raith-2 150 direct write electron lithography tool; the appropriate pattern is either drawn up or loaded from a previously written pattern. For the purposes of the work test samples and full device patterns were used. The test samples were fixed at 500um^2, whilst the device patterns were set at 2mm^2 (for reasons described above). The patterning process takes a finite amount of time for each area of patterning, although this time is short, the full patterning requires many

complete areas to be patterned. Through the use of the test samples, many more samples can be created in the time taken to make one full device size sample.

The lithography tool is calibrated to the wafer whilst it is in place to ensure that the focus is sharp enough on the tool to attain high resolution patterning. If the focus is not sharp enough the patterning will be inaccurate and achieving the best resolution will not be possible. The tool is set up so that the exposure time of the focused e-beam is enough to expose the thickness of the resist layer. For the purposes of the work, the thickness was set at 300nm. This thickness will be enough to enable the liftoff process, whilst not requiring impractical levels of exposure time (thicker layers of resist require increased exposure times). Thinner layers of resist result in the layer of evaporated metal formed across the step features of the design, being too thick and causing the liftoff process to fail.

Once the tool is correctly focused with the pattern designs loaded, the arrangement of patterns is programmed into the tool so that the full selection of test samples and device samples will be exposed. For the more densely packed structures, it can take upwards of ten hours to fully expose a full size device structure. Thus in most cases the exposures are left running overnight or preferably over the course of a full weekend. Once the exposure pattern is complete, the wafer is removed from the e-beam chamber. The wafer patterning needs to be developed at this point, initially the wafer is placed into a solution of 1:3 Methyl Isobutyl Ketone : Isopropyl Alcohol (MIBK:IPA) for 1 minute, this removes the exposed resist. The wafer is then placed into a pure IPA solution to stop the development. The solutions for these stages

were supplied by MicroChem. Once development has been stopped and the sample dried, the e-beam exposure process is complete.

7.5. Ashing – Oxygen Plasma Etch

The development process is not a completely foolproof system, although in general it delivers acceptable results. On occasion it was found that thin layers of un-developed polymer resist remained between the patterned areas. As such it is often considered prudent to carry out a brief ashing process. This involves exposing the patterned sample to an oxygen plasma; the plasma removes any undeveloped polymer that is left between the patterned areas. However the plasma simultaneously strips the polymer that is left on the patterned areas, so only a short period of ashing is carried out. Depending on the thickness of the patterned layer ashing periods of 20 seconds to a minute can be used, anything beyond this begins to strip the polymer completely and destroy the patterning. Once the ashing is complete, the patterning is complete, however the mask that is in place, consisting of the unexposed polymer, is not resilient enough to act as a mask for deep reactive ion etching.

7.6. Electron Beam Evaporation

In order to etch silicon successfully a hard mask is required; for the purposes of this work a titanium mask was chosen. Work carried out by colleagues in the department had observed good results using Titanium in deep reactive ion etch processes. To apply the mask, the samples are placed into an Edwards A500 electron beam evaporator. The chamber is then pumped to vacuum (10^{-7} atmosphere) so as to remove any contaminants; an electron beam is then focused

onto a crucible containing titanium. The titanium is heated to its boiling point and evaporation occurs, the titanium evaporates to the wafer, situated above the crucible on a manifold. The manifold is set to rotate so that an even layer of material will be deposited. The thickness is monitored using a vibrating quartz crystal, as material is deposited onto the crystal, the vibrational frequency changes according to the mass of material deposited. From this it is possible to determine the thickness of the layer of material applied to the crystal and also to the wafer present in the chamber. The evaporated material (titanium) is applied uniformly across the entire wafer (or sample). Where the silicon is exposed, the titanium fixes to the silicon, where the titanium lands on polymer it is bonded to the polymer. A titanium layer of between 50-60nm was applied to the wafer during this work. This thickness was chosen as similar thicknesses had been used by colleagues for through wafer etch processes using deep reactive ion etching. Once the appropriate layer of material is applied the evaporation is halted. The tool is allowed to cool and upon reaching room temperature the wafer (or sample) is removed from the evaporation chamber.

7.7. Liftoff

In order to complete the patterning process, unwanted titanium needs to be removed from the wafer. A liftoff process is used to achieve this. The wafer or sample is placed into acetone, which dissolves the polymer bonded to the wafer. Once the acetone has soaked into the sample (the time for this depends on the size of the sample), the sample is then treated to ultrasonic stimulation; this agitates the deposited material and removes it from the surface of the wafer or sample. Where there is polymer attached to the wafer it is removed and any metal attached to the

polymer is also removed as a result. Where the metal is bonded to silicon the acetone has no effect and the titanium remains bonded to the wafer. At the boundary between polymer coated areas and non coated areas, there will be an overlap. However this overlap should only be very thin to the order of a tens of nanometers, this should simply be broken as the other areas of titanium are removed. The result is that only the areas exposed to the e-beam remain coated with titanium, thus a hard mask suitable for deep reactive ion etching is achieved.

7.8. Plasma Etching

Once the masking is complete, with the appropriate pattern chosen, the silicon is etched in order to create the pillar structures. This is achieved using the previously described Bosch™ process (see chapter 2). First a layer of Silicon is etched using an anisotropic SF_6 plasma with an applied wafer bias. This process will etch perpendicular to the surface of the wafer with the plasma drawn to the surface of the wafer because of the applied. At the surface of the wafer the Fluorine radicals bond with silicon to remove it. Next a layer of polymer is deposited using a C_4F_8 plasma; this is an isotropic process so the layer is applied to both vertical and horizontal surfaces equally. The third step is a second anisotropic SF_6 etch, this step removes the deposited polymer layer which is parallel to the surface of the wafer, however any polymer perpendicular to the wafer surface is relatively unaffected by the SF_6 plasma, hence the silicon that is covered by the polymer layer remains undamaged by the plasma. Once the polymer layer covering the surface parallel to the plane of the wafer is removed the SF_6 begins to act on the silicon beneath it. As underlying silicon is exposed it, is unprotected by the polymer layer. Although the etch stage is anisotropic, there is a degree of lateral etch which occurs

simultaneously at the base of the feature. In order to prevent significant lateral etching the etch stage of the process is kept limited in time. Once the etch phase is complete another isotropic polymer layer is applied and the entire process is repeated. Using this method it is possible to etch deep structures in silicon whilst maintaining high quality etch profiles. As mentioned above there is a degree of lateral etch in the etch phase. This results in what are known as scallops. This process has been described in more detail earlier in this report.

The parameters of the plasma during the different steps can be used to control the quality of the etch process. The gas pressures, the bias voltage, the relative times of the different steps and the power of the RF field used to create the plasma are manipulated to create the ideal plasma conditions for the etch profile required. The depth of the features is controlled by the length of time of the full etch. Depending on the mask used, the final pattern and structures required, the etch recipe is manipulated to deliver the ideal profile. In this case the spacing between the features leads to a significant change in the etch recipe required. Through the use of test samples, the correct etch recipe is devised so as to ensure that when applied to the full test sample, the features are etched correctly.

7.9. Pillar Etch Results

7.9.1. Run 1

In order to establish a satisfactory process recipe test samples of approximately 0.5mm^2 were fixed onto oxide coated carrier wafers using crystal bond. 200mm diameter silicon wafers coated with thermally grown oxide were used as the carriers.

A stock recipe for etching silicon VIAs of similar dimensions supplied by SPTS was used as a starting point in order to develop an effective recipe for the etching of silicon nanorods. The recipe used is as follows (Table 7.9.1.1 Run 1 Recipe Conditions:

Included within the etch recipe is ‘Helium Pressure’. The helium is a temperature control mechanism. The etch process is an exothermic one, therefore the temperature of the wafer is found to rise if left uncontrolled. The helium pressure refers to a backside pressure, where helium is applied to the backside of the wafer within the process chamber. This is facilitated by the design of the electrostatic chuck that the wafer sits on within the process chamber.

	Strike	Deposition	Etch
Step Number	1	2	3
Time (s)	2	1	1.2
Loop destination	0	0	2
Loop number	0	0	25
Pressure (mTorr)	40	40	23
Platen Power (W)	0	0	600
Source Power (W)	2500	2500	2500
Coil Current	15	10	10
O_2 (scms)	0	0	0
Ar (scms)	200	0	0
SF_6 (scms)	1	1	250
C_4F_8 (scms)	270	270	0
He Pressure (mTorr)	1	1	0
Platen Temp (°C)	10	10	10

Table 7.9.1.1 Run 1 Recipe Conditions

The original recipe contained a total of 500 loops for deep silicon etch. The etch rate for this recipe was quoted as being 3µm per minute. The above recipe was adjusted so as to consist of 25 loops, leading to an adjusted etch time of 57 seconds. Given the etch rate this should lead to a total etch depth of approximately 3µm.

The results obtained from this process are shown in scanning electron microscope images below. The pillars in these images show a high level of uniformity across the entire sample. However there are clearly problems with the etch recipe as there is a high level of re-entrance occurring through the course of the etch.

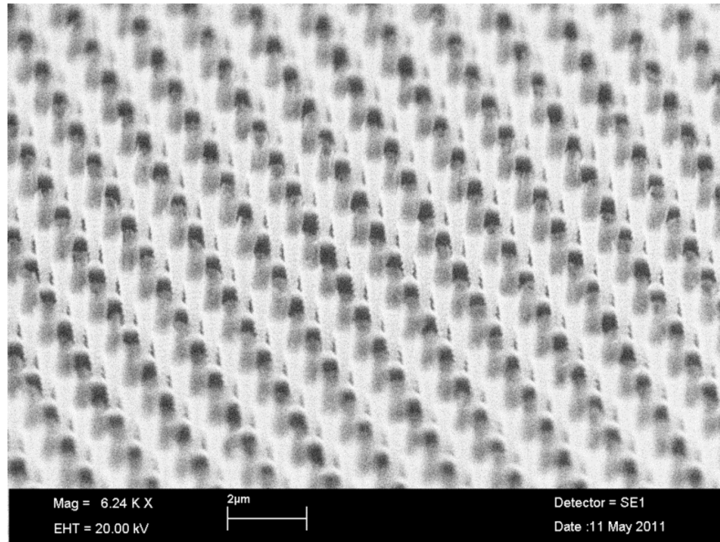

7.9.1.1 Run 1 - Pillars showing good uniformity across wide area

As described above this etch recipe has led to a high degree of re-entrance. This is more clearly seen in the following images. This is a result of the base of the pillars being over-etched at the base. Although pillars remain on this short etch, as the etch time is increased the base of the pillars will be thinned out to the point that the pillars will fail.

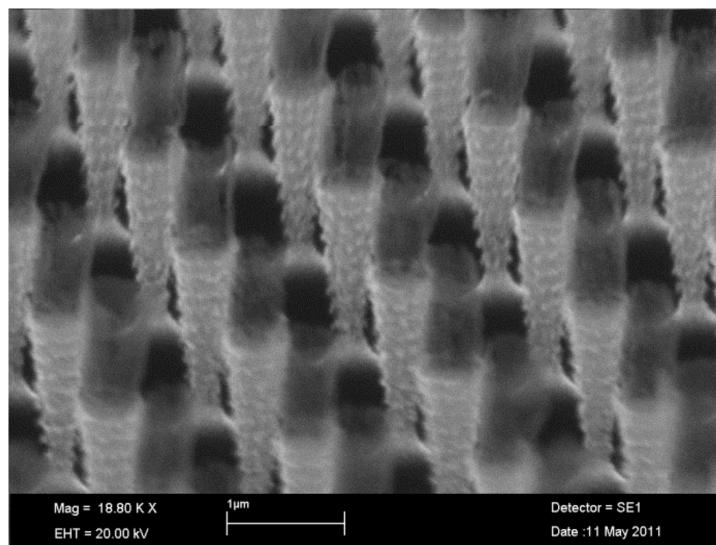

Figure 7.9.1.2 Run 1 - Pillars showing re-entrant features and mask etch.

In addition to the re-entrance problem described above there is the further problem of mask removal occurring. The mask has etched centrally, resulting in the centre of the pillar etching. The etch process is less efficient at surface edges. This results in a ring of silicon remaining around the edge of the pillar, creating a shell like structure at the top of the pillar.

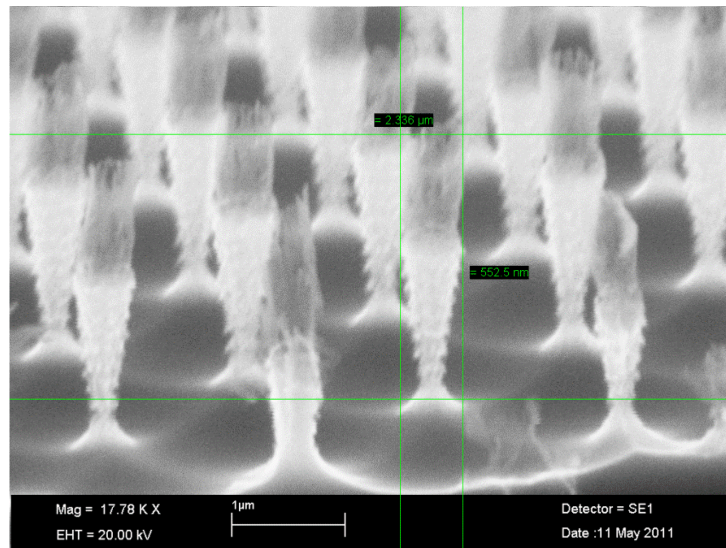

Figure 7.9.1.3 Run 1 - Pillars at edge of sample.

In the SEM image above the shell like structure at the top of the pillars is more clearly shown. In addition it is clear to see that the mask has been etched approximately half way through the etch process. The total etch depth is approximately 2.3µm.

7.9.2. Run 2

The process recipe for the second test run was altered to attempt to reduce the re-entrant nature of the etch results. The platen power of the etch was reduced by 200W to 400W.

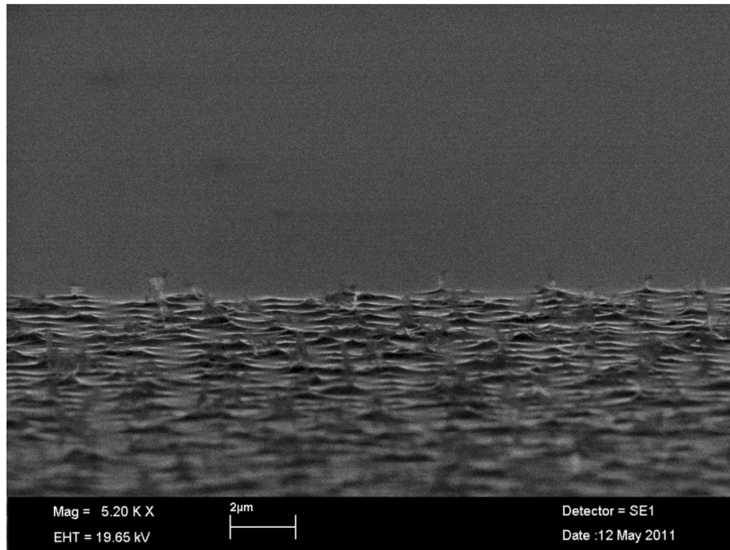

Figure 7.9.2.1 Run 2 - majority of pillars have been removed

The results of the change in platen power show that the problem has not been resolved. The majority of the pillars have been totally etched to leave only a very small number remaining.

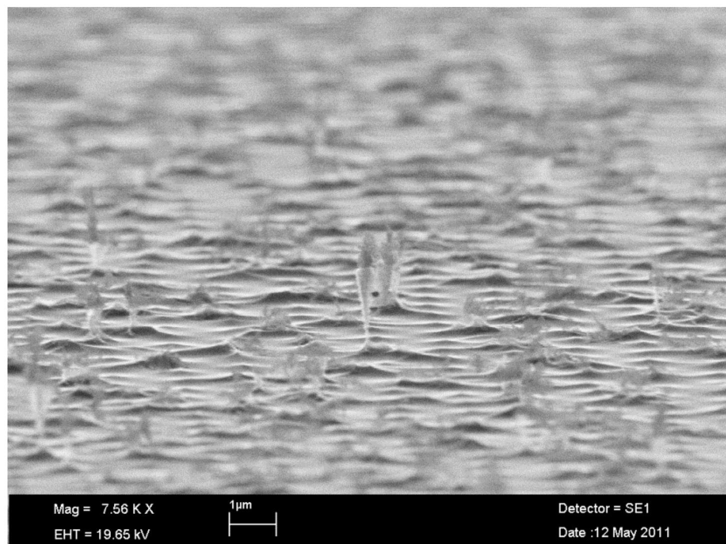

Figure 7.9.2.2 Run 2 some pillars remain but highly re-entrant

The individual pillars that remain are highly re-entrant. The base of the pillars remain are extremely thin. This suggests that the majority of the pillars have been etched through completely at the base, collapsed and been removed completely.

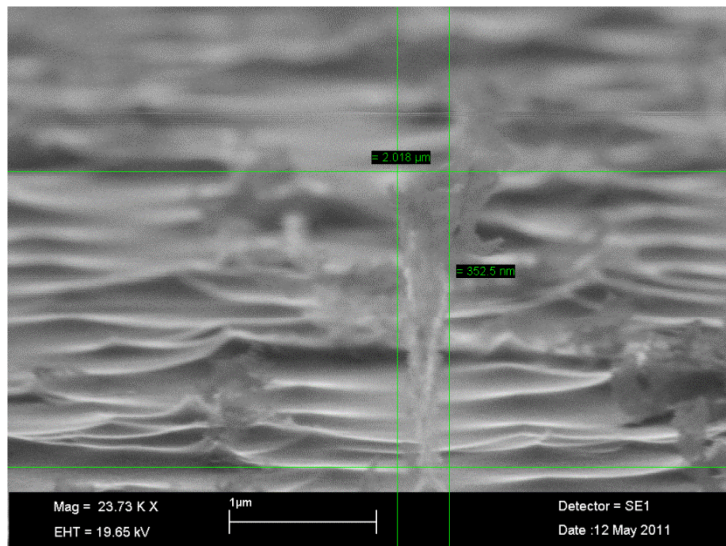

Figure 7.9.2.3 Run 2 - individual pillar shows extreme re-entrant

The total etch depth shown above is approximately 2µm, slightly less than observed in the previous run.

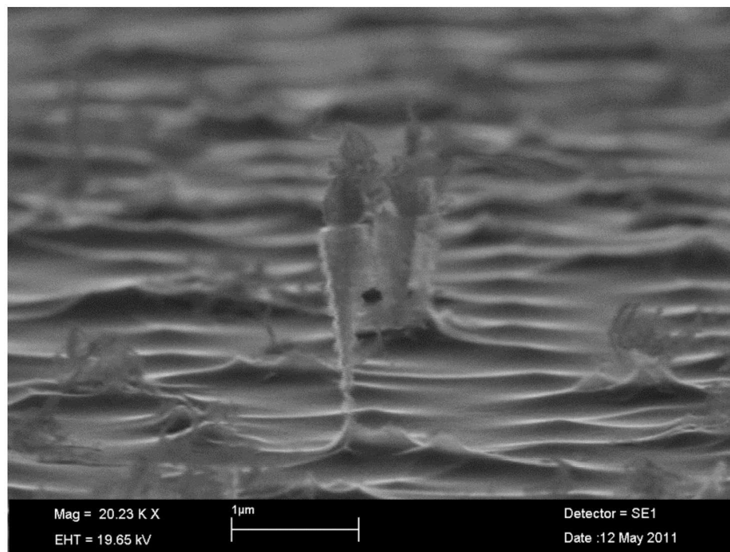

Figure 7.9.2.4 Run 2 pillars highly re-entrant with mask etching evident at pillar top

In addition it is clear from the above picture that there is still clearly etching of the mask occurring. The shell like structure above the pillar is still evident suggesting the mask has been etched again as described previously.

7.9.3. Run 3

The results seen up to this point had been far more highly re-entrant than had been expected. This was assumed to be due to the high power of the platen, however reducing the power did not have the desired effect of reducing the re-entrant. It was subsequently discovered that the modulation control of the power supply to the platen was not correctly configured. The result of which was that the modulation was not applied and as such the power was approximately 30% higher than the value quoted. For run 3 the modulation was reconfigured so that the true power values were used. An SEM image of the sample was also taken prior to the etch process, this is shown below.

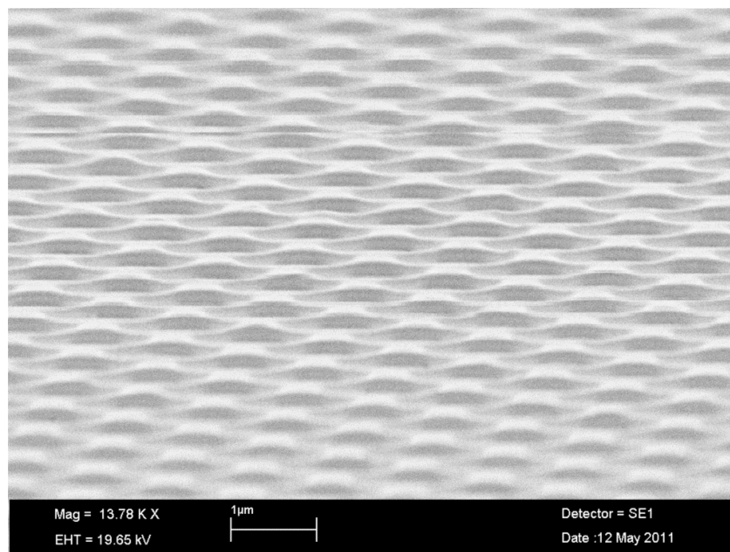

Figure 7.9.3.1 Run 3 - central area of Titanium mask prior to etching

The mask is shown in the image above, prior to any etching. In the central areas observed here it appears that although there is a regular patterning to the mask it is not as expected. An attempt to determine the problem with the masking an area of the sample was masked with tape so as to be able to observe an area of etched and un-etched silicon.

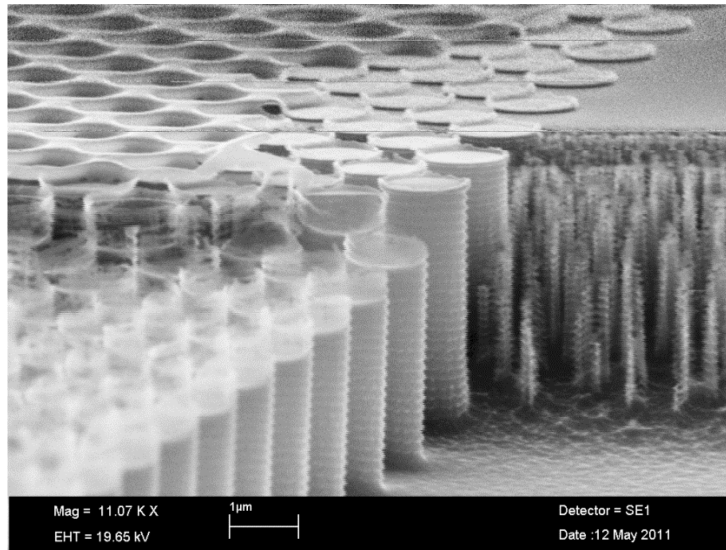

Figure 7.9.3.2 Run 3 - showing taped and un-taped at edge area of sample

The area in the above SEM image shows where tape was applied across the sample. The etched and un-etched areas can clearly be seen. In addition at the edge of the sample the mask can be observed with higher clarity. The edge areas of the mask appear as would be imagined, simple discs. Further into the sample area the mask appears notably different.

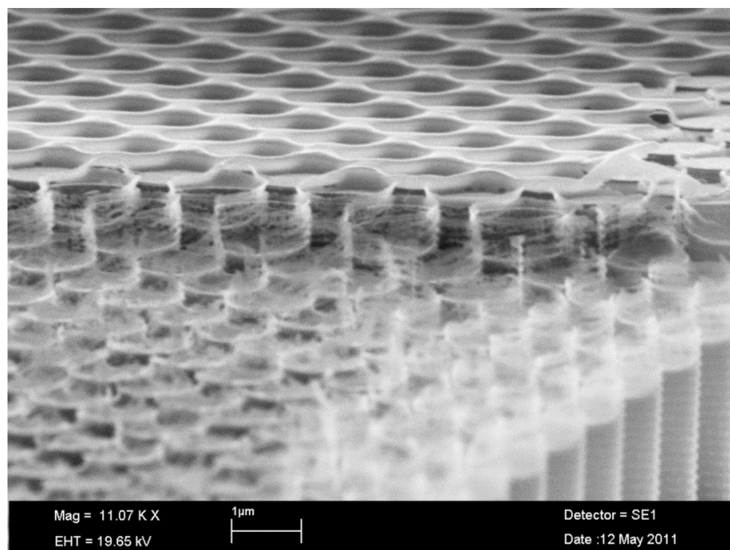

Figure 7.9.3.3 Run 3 - Shell like pillar etch structure

At the transition from the two distinguishing mask styles it appears that the mask has not correctly lifted off, there is a raised area of mask around the central disc. This raised area is Titanium affixed to the resist material. In correct mask fabrication the raised area should be completely removed leaving only the central disc.

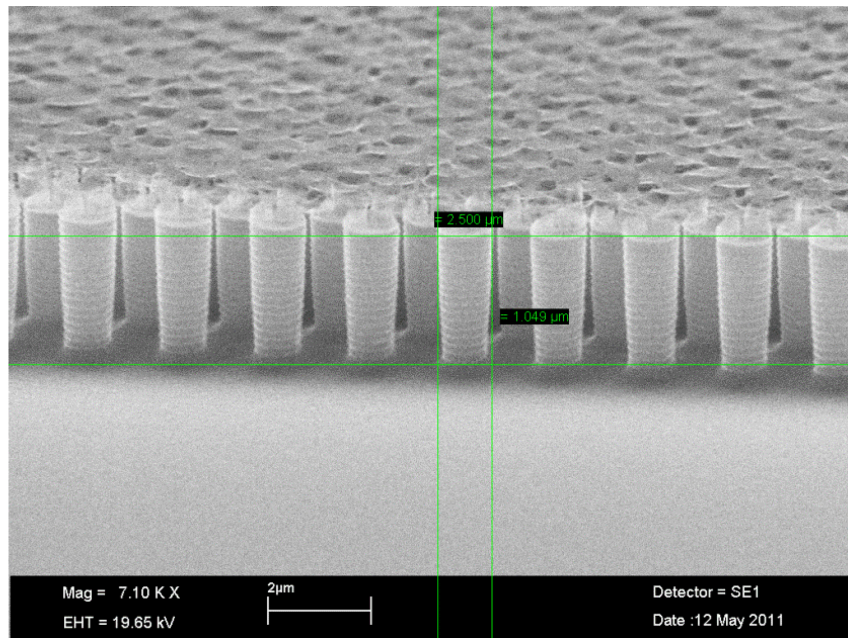

Figure 7.9.3.4 Run 3 - pillars at edge of mask area, not etched correctly further into masked area

At the edge of the sample where the mask has been fabricated correctly the pillars now shows significantly reduced re-entrance. The profile is still re-entrant but the profile of the features is closer to the target of 90°. The etch depth of 2.5µm is closer to the expected etch depth associated with this recipe.

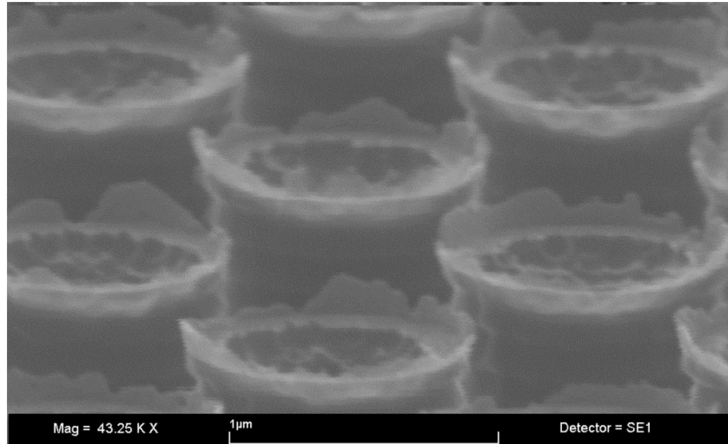

Figure 7.9.3.5 Run 3 - Pillar tops showing mask etching

The above high magnification image of the pillar tops shows a high degree of mask removal. It is possible to see etching of the central core of the pillars. These pillars were found at the edge of the masked area.

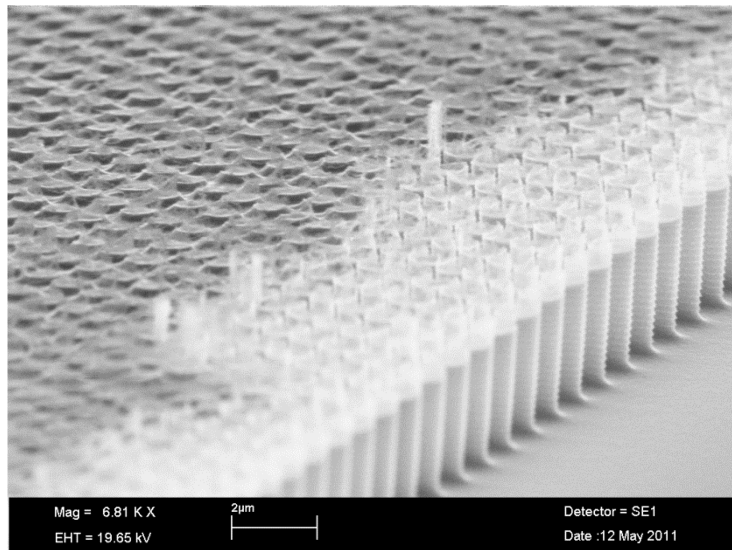

Figure 7.9.3.6 Run 3 - pillars at edge of mask clearly defined, further in the mask has issues

This SEM image clearly shows that although there is pillar etching occurring at the edge of the sample there is no such etching further into the sample area. Clearly there are significant issues with the fabrication of the Ti mask.

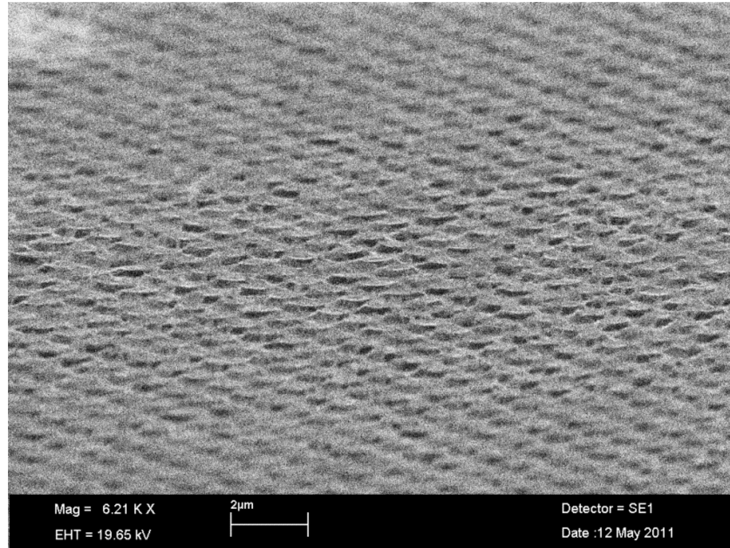

7.9.3.7 Run 3 - Central area of mask showing no etching having occurred.

The SEM image above shows the central area of the sample. It appears that little or no etching has occurred in this area, although the level of etching is not comprehensively clear it appears that there are is no clear pillar definition in the central areas. This suggests a problem with the mask fabrication technique.

7.9.4. Run 4

The results of Run 3 indicated that the reduction in platen power had yielded significant improvements in the etch performance with good pillar profile. The platen power was further reduced to 150W in order improve the profile further. The same sample from run 3 was reused here.

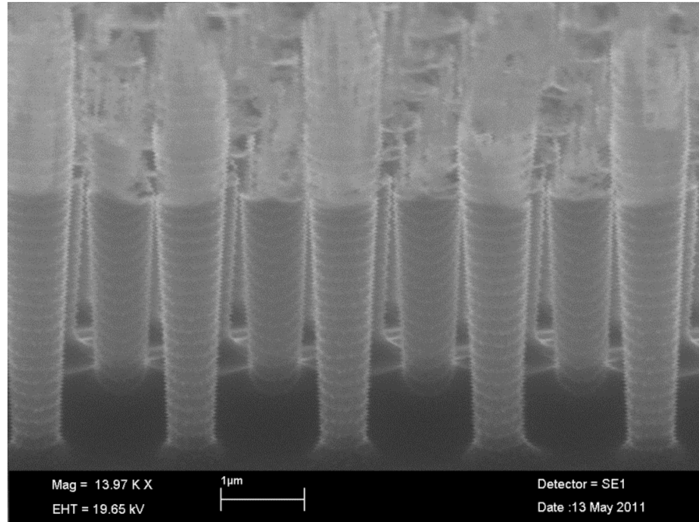

Figure 7.9.4.1 Run 4 - A shell like structure at top of pillars, pillars etched at edge of mask

The change in platen power has shown a further improvement in the re-entrant of the pillars with the profile being closer to the target of 90° angle.

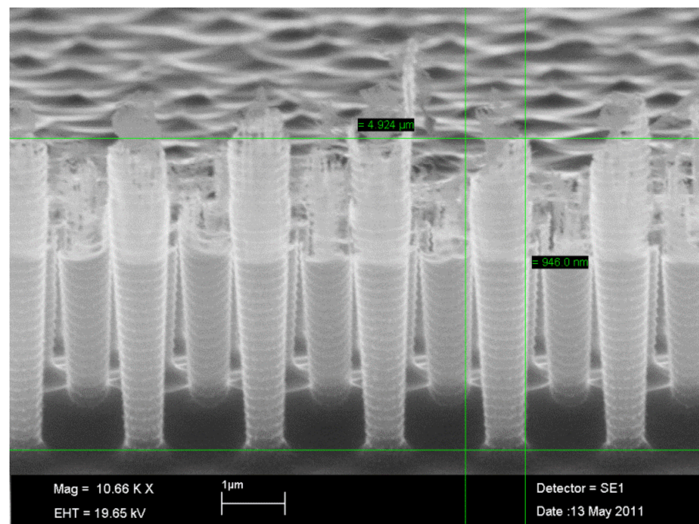

Figure 7.9.4.2 Run 4 - Pillars re-entrant with shell like structure at edge of wafer, mask problem still evident

The etch depth shown here is a result of a double etch. However the true depth of the etch is unclear as the top of the shell like structure at the top of the pillars has been etched completely.

7.9.5. Run 5

Having observed problems with the mask in the previous runs, the mask fabrication technique was adapted to include an increased soak time in acetone. This results in an improved liftoff stage and an improvement in the quality of the definition of the individual features of the mask as shown below (Figure 7.9.5.1).

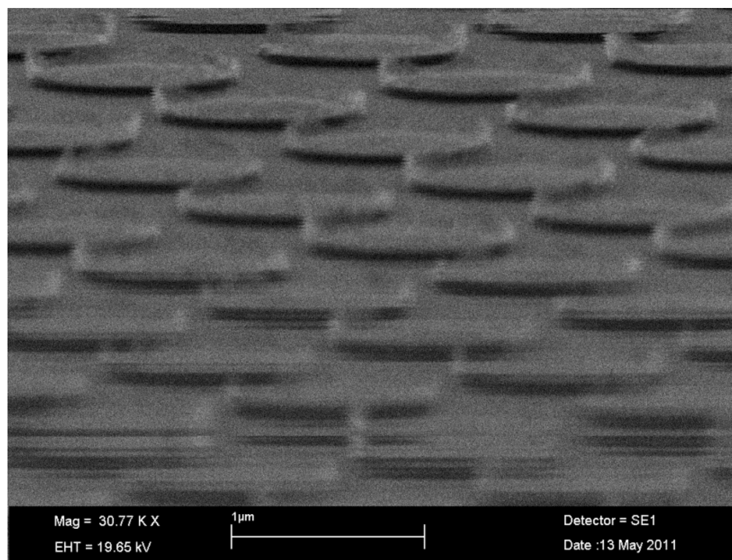

Figure 7.9.5.1 Run 5 - pre-etch mask clearly defined throughout

The above mask image shows the individual discs making up the mask. The fact that each disc is individually identifiable shows the improvement in the mask fabrication technique.

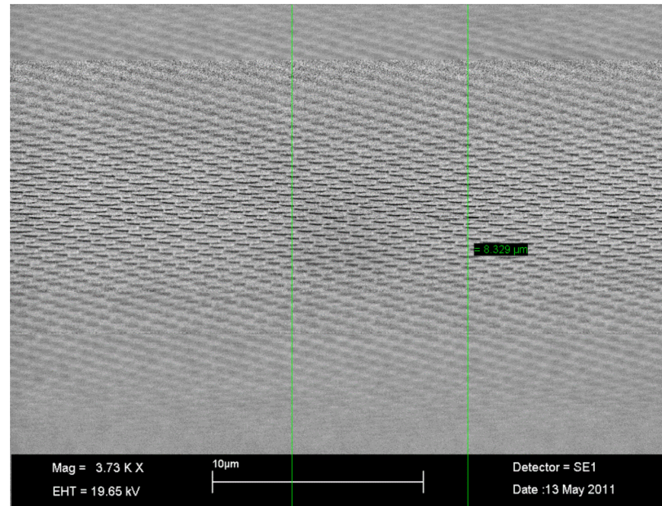

Figure 7.9.5.2 Run 5 - Low magnification mask showing clear definition throughout

On lower magnification it is clear that the quality of the mask extends across the entirety of the sample, rather than simply at the edge. The implication is that the longer acetone soak time has enabled the acetone to penetrate further into the sample to break down the resist that sits between the mask discs.

For the etch process the recipe was significantly changed. A secondary etch step was introduced as detailed below. In addition the number of loops of the recipe was increased to 50.

	Strike	Deposition	Etch 1	Etch 2
Step Number	1	2	3	3
Time (s)	2	1	0.6	0.6
Loop destination	0	0	2	2
Loop number	0	0	0	50
Pressure (mTorr)	40	40	23	23
Platen Power (W)	0	0	150	0
Source Power (W)	2500	2500	2500	2500
Coil Current (A)	15	10	10	10
O_2 (scms)	0	0	0	0
Ar (scms)	200	0	0	0
SF_6 (scms)	1	1	0	250
C_4F_8 (scms)	270	270	0	0
He Pressure (mTorr)	1	1	0	0
Platen Temp (°C)	10	10	10	10

Table 7.9.5.1 Run 5 detailing recipe adjustments

The etch step has been split into two sections, the first with a platen power of 150W the second with no platen power applied. The first step has the platen power in an anisotropic etch stage. This first step removes the polymer passivation layer parallel to the surface of the sample. The passivation layer affixed to the sidewalls is not removed due to the anisotropic nature of the first step. The second etch step is isotropic due to the lack of platen power. This step will etch both the passivation layer and the silicon surface, however due to the selectivity of the etch chemistry it will preferentially etch the Silicon. The removal of the platen power reduces the physical aspect of the etch (due to ion bombardment/sputtering). This in turn should reduce the damage caused to the titanium mask.

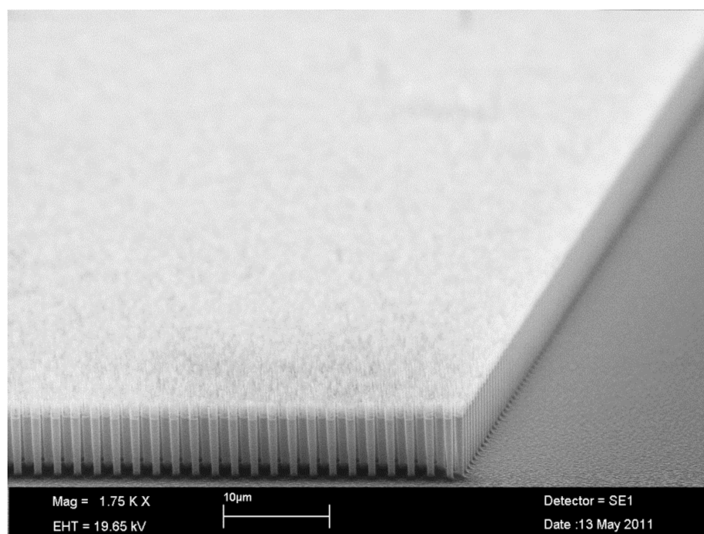

Figure 7.9.5.3 Run 5 - Pillar etching throughout sample area

The image above shows that it is clear that the etching has been uniform across the entire sample. The shell like structure is still evident across all of the pillars however it is a smaller percentage of the overall etch depth. The reduction of the overall time

for which platen power is in place has been effective at reducing the damage to the mask.

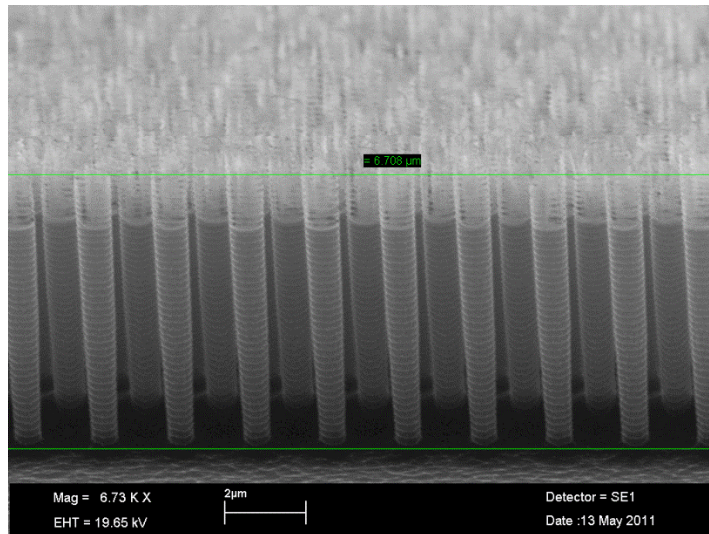

Figure 7.9.5.4 Run 5 - Pillars less re-entrant, however shell like structure is still evident. Pillars evident throughout masked area

The above image shows in detail that the shell like structure has been reduced in size relative to the entire depth of the etch. Re-entrance is low with good quality profile evident.

7.9.6. Run 6

For run 6 the number of loops used in the process recipe was reduced to 25 in order to investigate the etching of the mask.

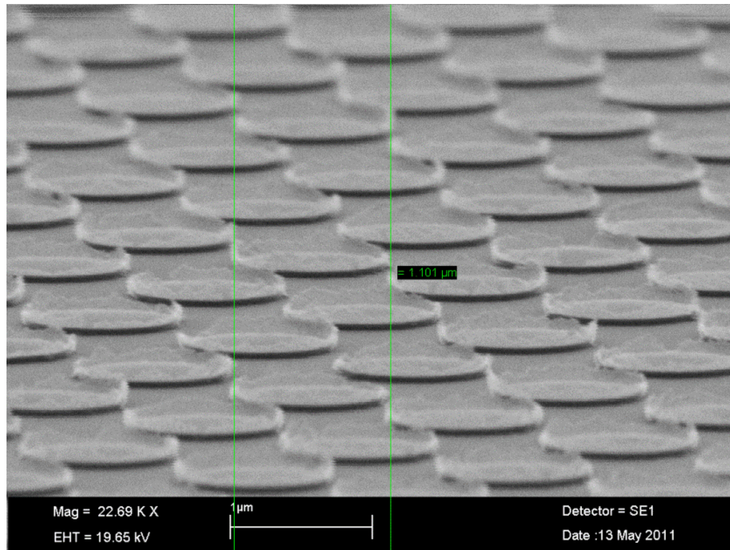

Figure 7.9.6.1 Run 6 - Pre etch mask

The Run 6 sample has well defined discs in the pre-etch SEM image. It is possible to see where the titanium at the edge of the mask disks has torn, when the surrounding titanium was removed in the lift off process.

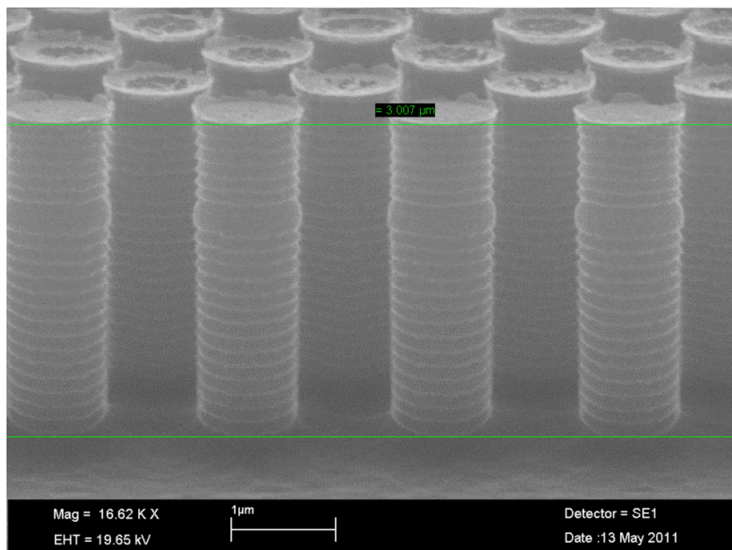

Figure 7.9.6.2 Run 6 - Pillars showing beginning of mask removal, evidence of double etch step

There is clear evidence of the start of the mask removal. This allows the visualisation of the mask etch process. As a result in the reduction in the number of loops a reduced etch of 3.007µm was observed.

7.9.7. Run 7

Run 7 was a continuation of Run 6 in essence it is the second set of 25 loops. The same sample was used to further investigate the formation of the shell like structure. A change in the recipe was also incorporated. The initial etch step was significantly altered so that the etchant gas used was oxygen rather than SF_6 as shown in the recipe table below.

	Strike	Deposition	Etch 1	Etch 2
Step Number	1	2	3	3
Time (s)	2	1	0.6	0.6
Loop destination	0	0	2	2
Loop number	0	0	0	25
Pressure (mTorr)	40	40	23	23
Platen Power (W)	0	0	0	70
Source Power (W)	2500	2500	2500	2500
Coil Current (A)	15	10	10	10
O_2 (scms)	0	0	200	0
Ar (scms)	200	0	0	0
SF_6 (scms)	1	1	0	250
C_4F_8 (scms)	270	270	0	0
He Pressure (mTorr)	1	1	0	0
Platen Temp (°C)	10	10	10	10

Table 7.9.7.1 Run 7 Etchant gas for Etch 1 changed to O2

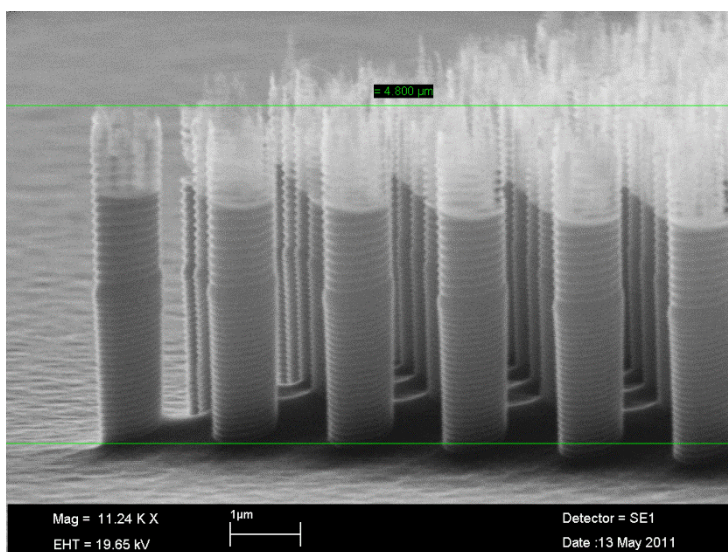

Figure 7.9.7.1 Run 7 - Continuation of run 6 showing further result of mask etching

The notch that can be seen approximately half way up the pillars is an artefact of the break in the etch process.

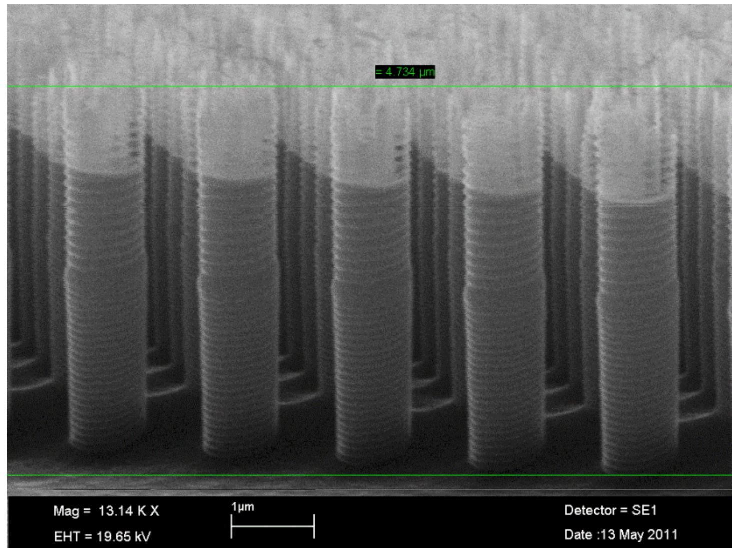

Figure 7.9.7.2 Run 7 - Pillars etched with shell like structure shown

Although there is still mask removal, it is entirely possible that this is down to the fact that the majority of the mask was removed in the previous part of the etch (run 6). The true evaluation of the success of the oxygen etch step will be shown in the following run (run 8).

7.9.8. Run 8

From Run 7 it was clear that the silicon was still etched when the oxygen step was introduced, however due to the dual nature of the recipes used it was difficult to say whether the mask erosion would continue to take place.

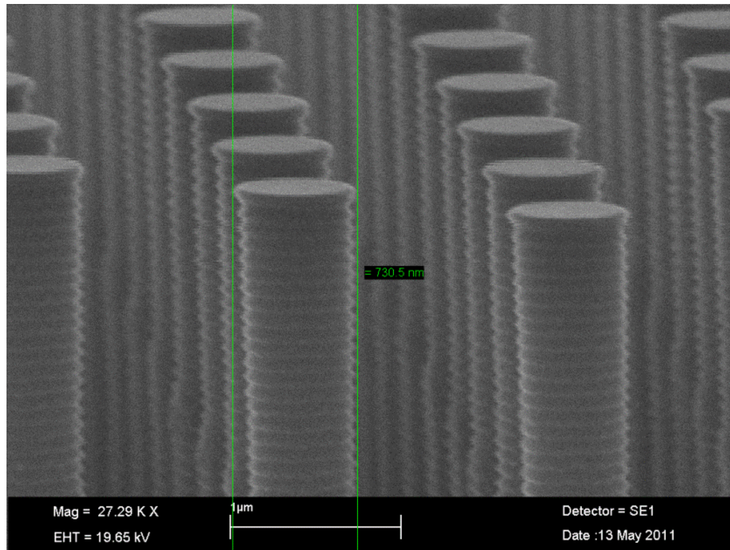

Figure 7.9.8.1 Run 8 - Well defined pillars, no mask removal, low re-entrant

From the above SEM image it is clear that the mask has not been removed. There is no sign of the shell like structure that has been seen in previous process runs. The profile of the pillars appears to be well defined with an angle approaching 90°.

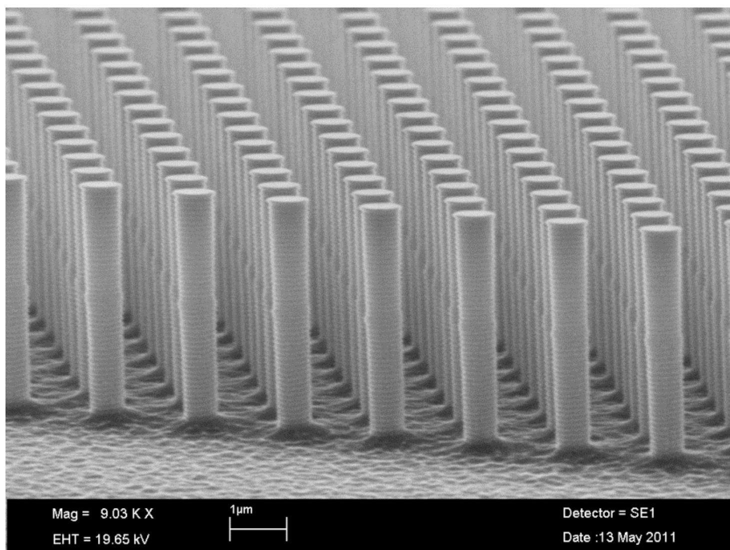

Figure 7.9.8.2 Run 8 - Clear pillars, clean etch no mask erosion

From the lower magnification SEM image above it is clear that the pillar etch has been uniform. There is no sign of mask removal and the profile of the pillars is extremely good with no signs of re-entrance. This process was run with a total of 50

loops, etching to approximately 4µm. The recipe used here is an acceptable recipe for etching pillars with this mask, however as the pitch and the diameter of the pillars is altered it is likely that there will be a change in the results obtained.

7.9.9. Run 9

The sample used for process run 9 was different from the previous runs. The pitch remained the same at 2µm but the pillar diameter was changed to 700nm. The process recipe was extended to be a total of 100 (loops from 25) in order to etch deeper into the Silicon and create taller pillars.

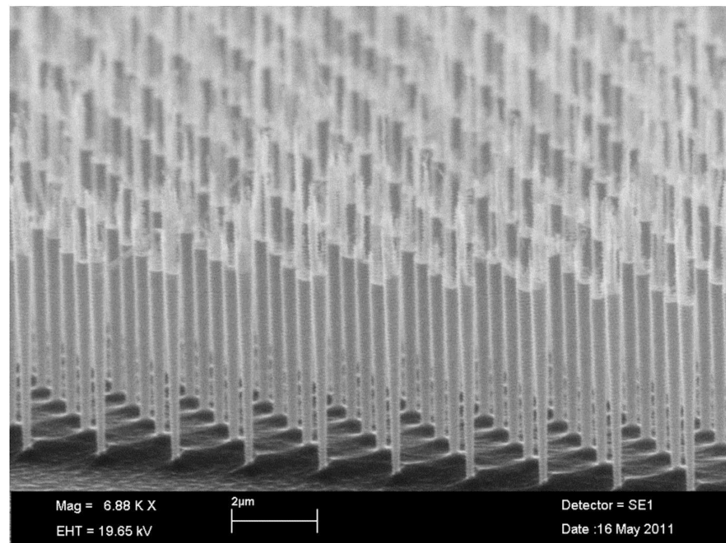

Figure 7.9.9.1 Run 9 - low diameter pillars showing re-entrant with shell like structure

From the SEM image above it is clear that there is an issue with the recipe as there is clear mask removal. In addition there is a definite degree of re-entrance. The increase in etch time to 100 loops has been shown to be excessive in this instance.

7.9.10. Run 10

The recipe for process run 10 was altered to have a shorter etch time of 75 loops. In addition the delay of the activation of the platen power was reduced to 0.1seconds. This should have the effect of reducing the re-entrance seen in the pillars.

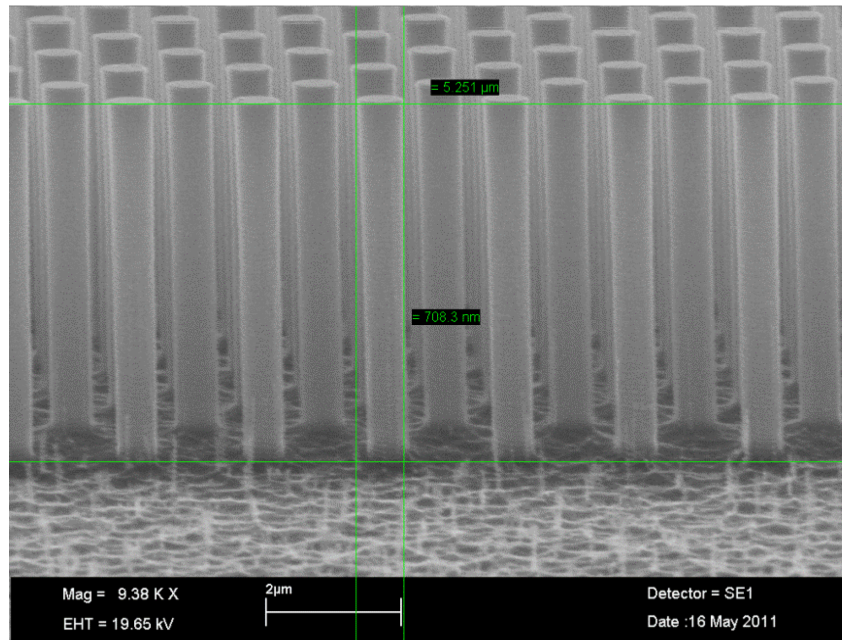

Figure 7.9.10.1 Run 10 - Pillars etched cleanly, no re-entrant. Some grass evident at base of pillars.

The pillars of process run 10 show very low signs of re-entrance. There is no sign of mask removal taking place. There is a degree of grassing evident outside of the sample area. In between the pillars there is little grassing.

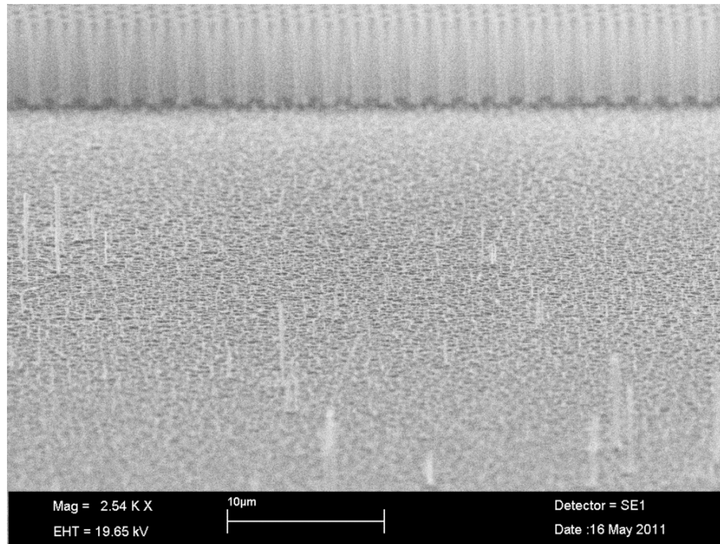

Figure 7.9.10.2 Run 10 - Grass shown with pillars for comparison

The grass is clearly evident outside the sample area.

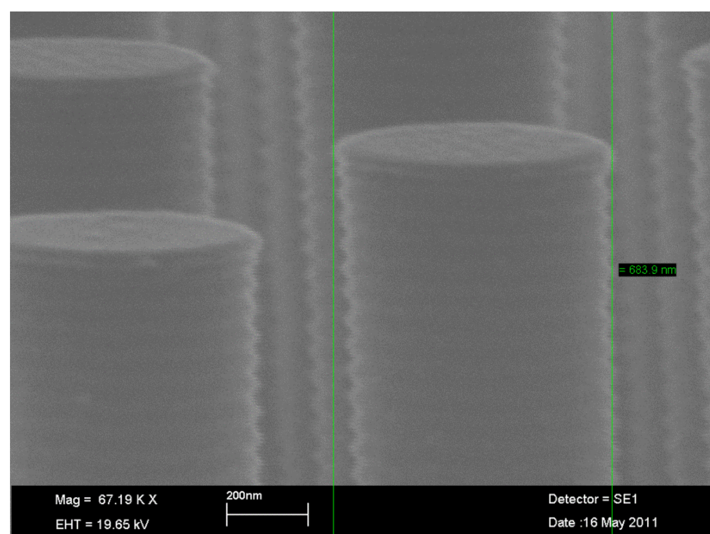

Figure 7.9.10.3 Run 10 - Pillar tops high magnification, scallops shown.

The pillar tops of the sample are clearly defined with little or no signs of mask removal. Although there are scallops in the sidewalls of the pillars they are not encroaching significantly into the core of the pillar.

7.9.11. Run 11

The process recipe for run 11 was changed so that the second etch step was changed to 0.8 seconds in an attempt to increase the overall etch rate.

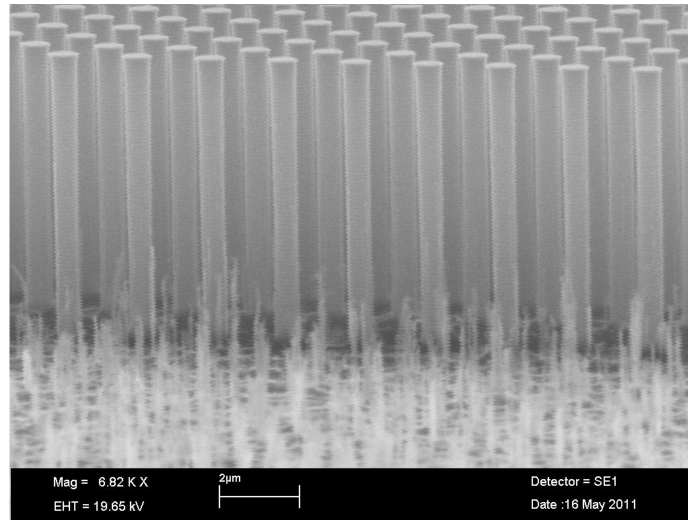

Figure 7.9.11.1 Run 11 - Post etch shows cleanly etched pillars with low re-entrant; grass like structures are highly evident at base of pillars

The result of changing the etch recipe appears to have been an increase in the degree of grassing seen outside the sample area.

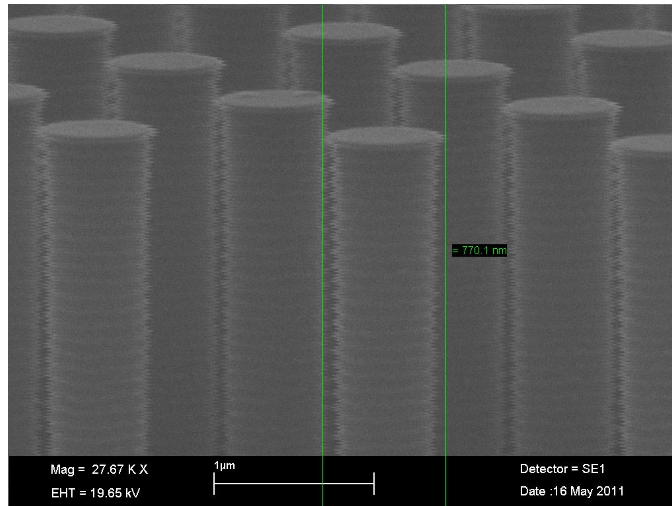

Figure 7.9.11.2 Run 11 - Pillar tops showing scallop result of Bosch process. Mask diameter shown.

The pillars shown in Run 11 have low levels of re-entrant and low levels of mask removal. Pillar diameters of 770nm are shown. This recipe is acceptable for pillar diameters of 700nm, although there is grassing outside of the sample. This would not have an impact on device performance and given the thin nature of the grass it is likely that it would be removed in the HF step which is used to remove the Titanium mask.

7.9.12. Run 12

The recipe for process run 12 was maintained from the previous run. However a wider diameter sample of 1um was used.

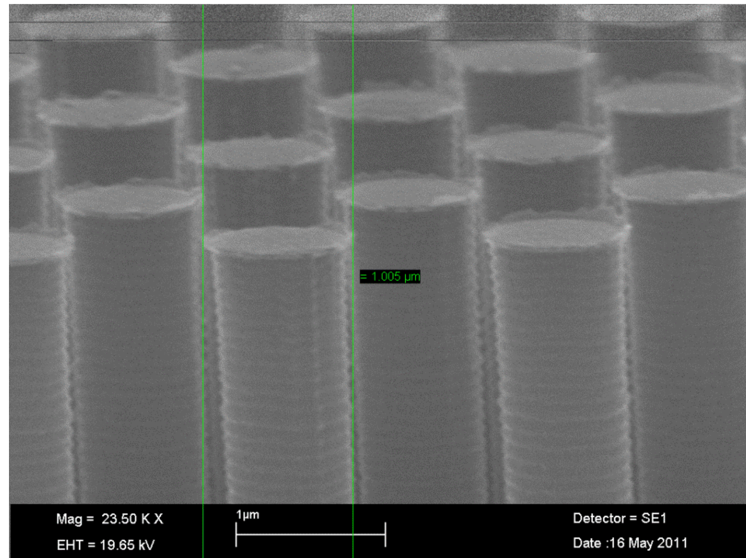

Figure 7.9.12.1 Run 12 - Pillar tops clearly defined

The pillars in run 12 are clearly defined with no mask removal and no significant degree of re-entrant. The diameter of 1µm is as expected from the mask. There is a slight degree of undercut although not significant.

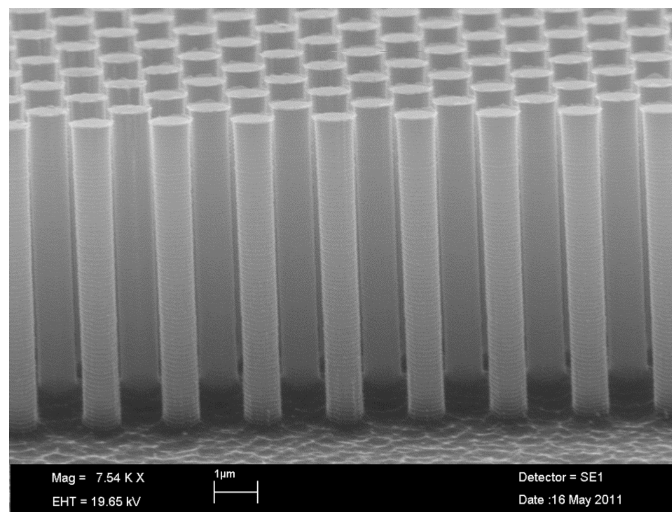

Figure 7.9.12.2 Run 12 - Pillars etched cleanly with very low re-entrant and low grass

It is clear from the above SEM image that there is no grassing, no mask removal and no sign of re-entrant.

7.9.13. Run 13

Run 13 is a duplicate of run 12 with a duplicate sample and duplicate process conditions.

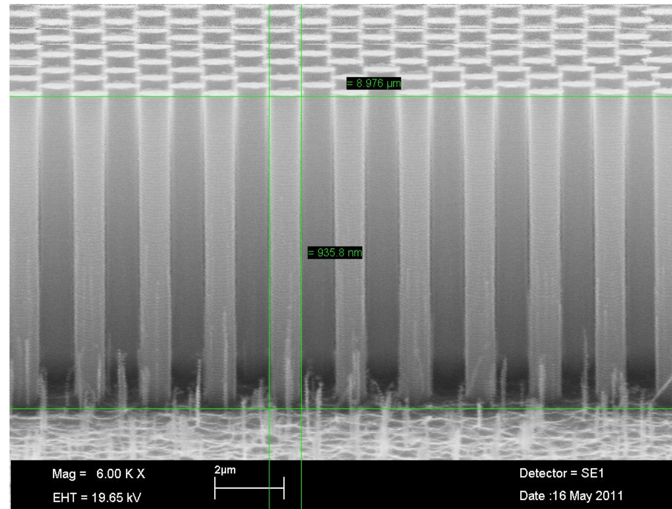

Figure 7.9.13.1 Run 13 - shows some grass evident at base of pillars, re-entrant is low

There is some grassing shown outside of the sample, however inside the sample the surface looks clean.

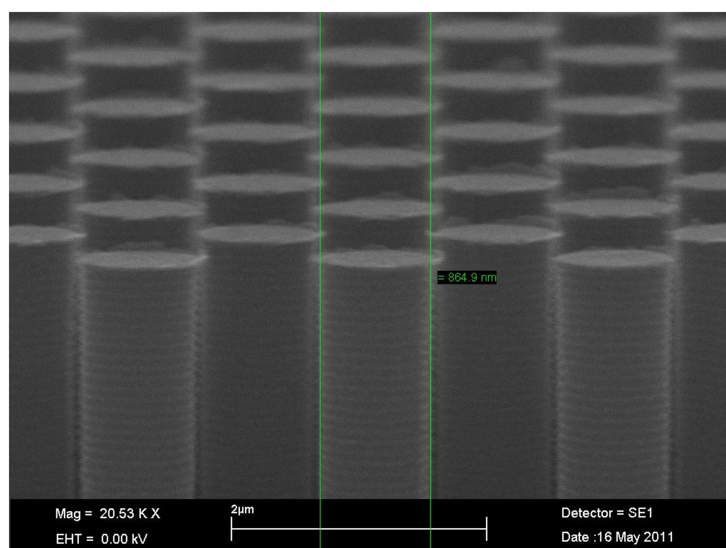

Figure 7.9.13.2 Run 13 - Pillar tops are clean and well defined

As can be seen from the pillar tops compared to the pillars themselves, there is a degree of undercut. This is caused as a result of the nature of the Bosch process. It is exacerbated by the increased length of the secondary etch step (etch 2 increased to 0.8seconds)

7.9.14. Run 14

Having achieved a satisfactory process recipe for relatively large pillar diameters (1µm), the next stage is the development of recipes for smaller diameter pillars which are more closely packed (lower pitch). In order to assess the recipe the same was used as in the previous run but the number of loops (etch time was cut to 25).

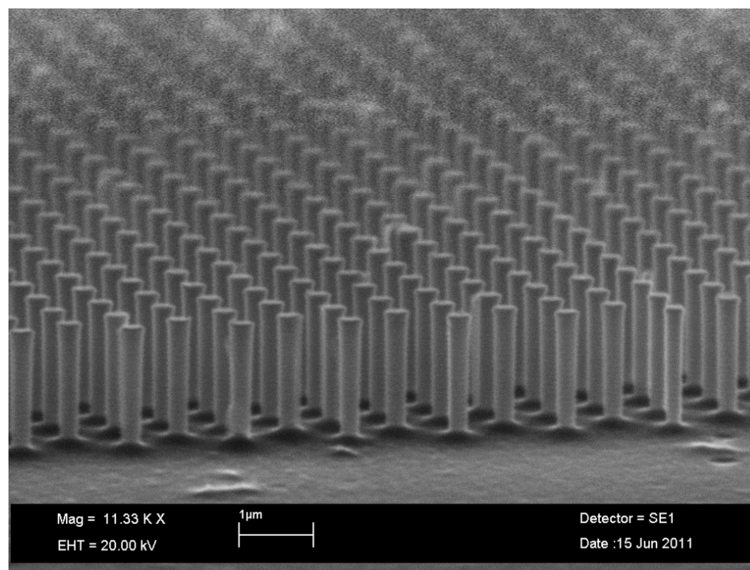

Figure 7.9.14.1 Run 14 - pillars etched cleanly with good definition. Re-entrant is low but evident.

The above SEM image shows that the pillars have been cleanly etched with high uniformity and no sign of mask removal. However there is a slight degree of re-entrance suggesting that there would be a problem with the etch recipe if the full number of loops were used.

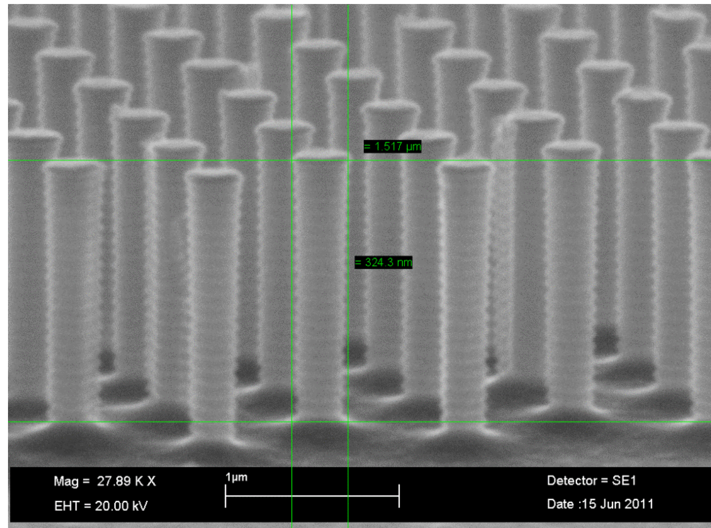

Figure 7.9.14.2 Run 14 - Pillars show good definition with low grass.

The SEM image above (Figure 7.9.14.3) clearly shows the re-entrance with the pillar tops significantly wider than their corresponding bases. The lack of grass is also clearly evident.

7.9.15. Run 15

Process run 15 was a continuation of run 14 using the same sample with a further 50 loops of the process.

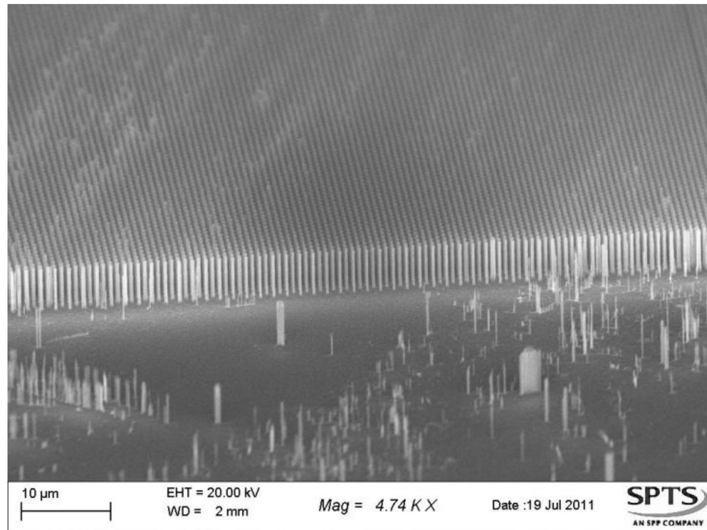

Figure 7.9.15.1 Run 15 - Pillars cleanly etched throughout sample area. There are some un-etched areas outside of sample.

The SEM image above shows clear uniformity through the entirety of the sample. There are significant areas outside of the sample which are un-etched. These areas are likely due to the contaminants added during the transfer of the sample after the first etch process. They are not consistent across the whole sample area as is found with grassing.

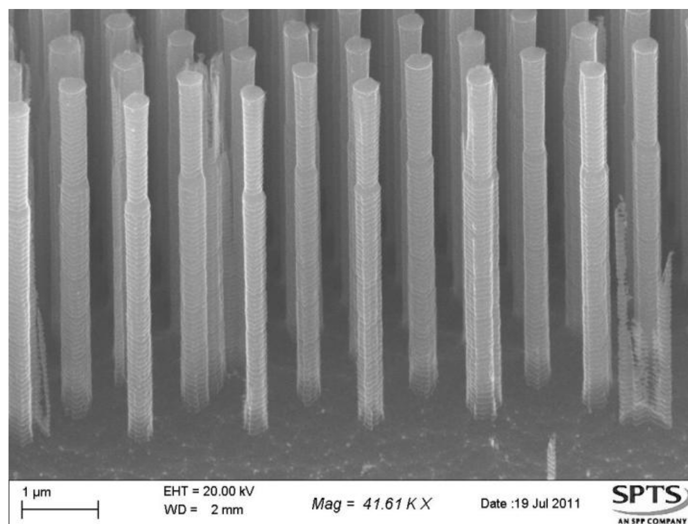

Figure 7.9.15.2 Run 15 - Majority of pillars etched cleanly some mask removal on individual pillars evident.

The notch seen at two thirds of the height of the pillars shows where the second stage of the etch process began (run 15). Below that point the etch shows a reduced degree of re-entrance with the angle of the pillars close to 90°.

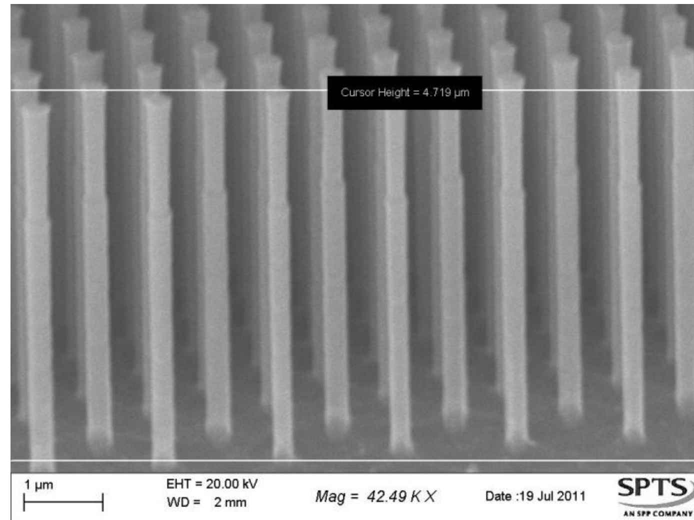

Figure 7.9.15.3 Run 15 Pillar height reduced to 4.7um

The total etch depth is shown in the above SEM image, this is less than might be expected for a full 75 loops when compared with previous runs. However the more closely packed nature of the pillars (lower pitch) makes the area between the pillars less accessible to the plasma and as such the etch rate is reduced.

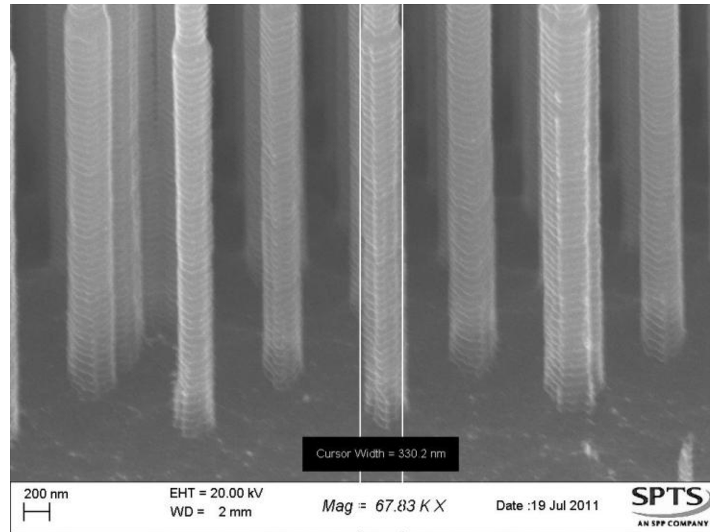

Figure 7.9.15.4 Run 15 - Pillar diameters reduced to 330nm

As discussed above the re-entrance is low, it appears as if there is a possible amount of tapering occurring at the base of the pillars.

7.9.16. Run 16

The success of run 15 lead to an increase in the number of loops from 50 (run 15) to 150. In addition a sample with pillars of 200nm diameter were used.

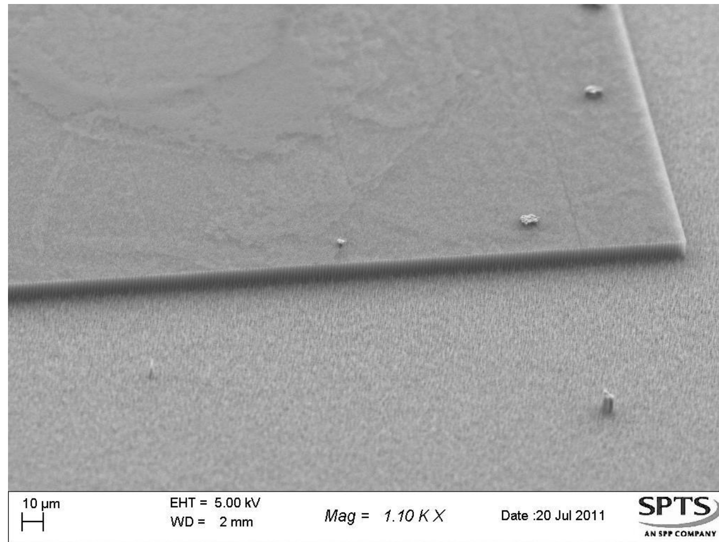

Figure 7.9.16.1 Run 16 - Sample area clearly defined but significant grassing is evident

The above SEM image clearly shows that the pillars have been etched neatly, however there is a large degree of grassing outside the sample.

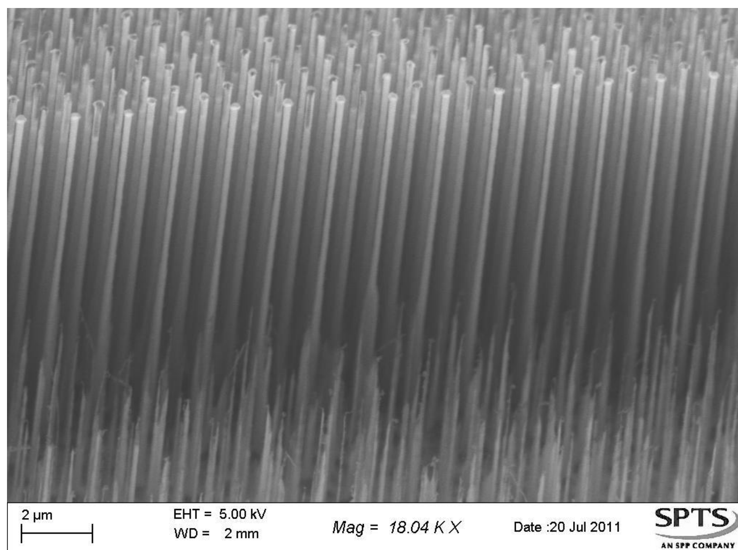

Figure 7.9.16.2 Run 16 - Pillars show clean etch profile, thickening at base. Grassing is highly evident.

The above SEM image shows that the pillars have etched with low re-entrance. However there is mask removal beginning to take place at the tops of the pillars. There is also a large degree of grass outside the sample.

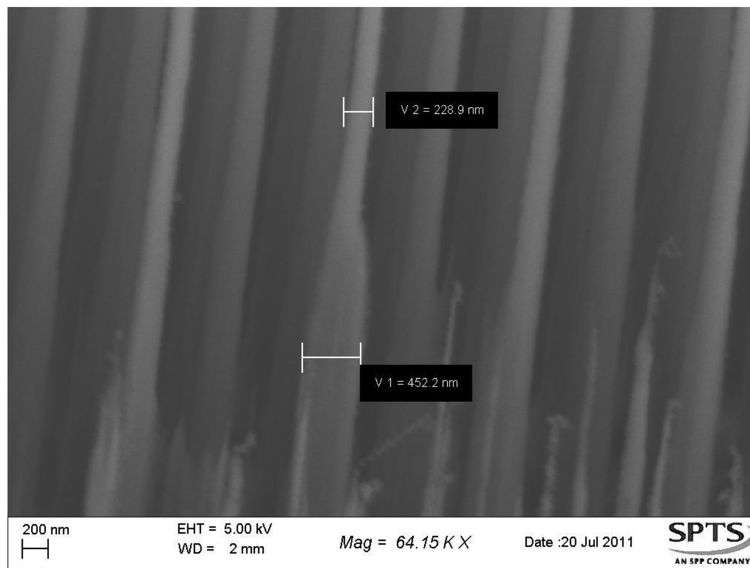

Figure 7.9.16.3 Run 16 - Pillars thicker at base. Approximately double the diameter as at the top.

Run 16 also shows significant tapering at the base of the sample. This tapering coincides with the formation of grass outside the sample.

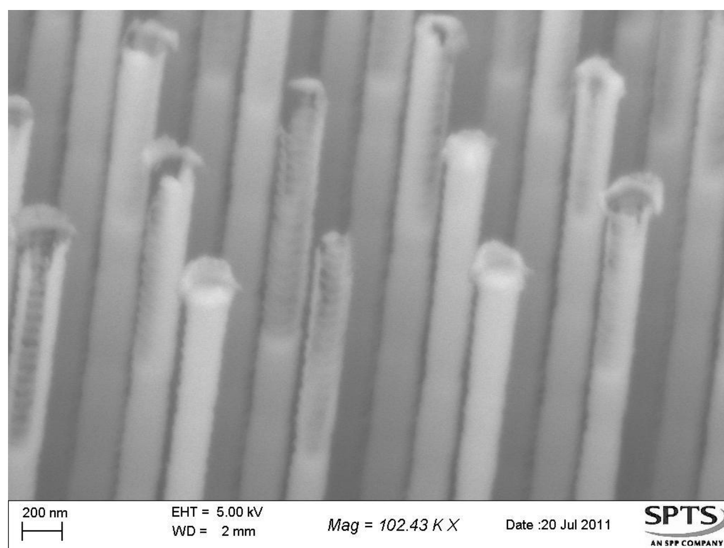

Figure 7.9.16.4 Run 16 - Mask has been removed leading to pillar cores being etched leaving shell structure.

As described above there has also been mask removal with shell like structures evident at the tops of the pillars.

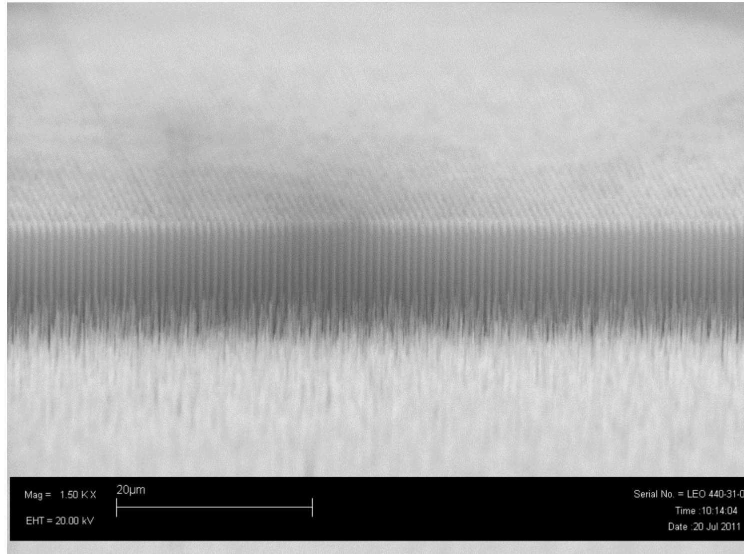

Figure 7.9.16.5 Run 16 - Significant grassing observed outside of sample area.

Although there is clear uniformity in the etching of the pillars it is clear from the above image that the mask has failed towards the end of the etch process. In addition the significant degree of grassing would not be suitable for device performance.

7.9.17. Run 17

In order to combat the grassing of run 16 a reduction was made to the platen power, from 70W to 65W. In addition a total of 100 loops were used to reduce the mask removal also seen in run 16. A 300nm diameter sample was used for this process run.

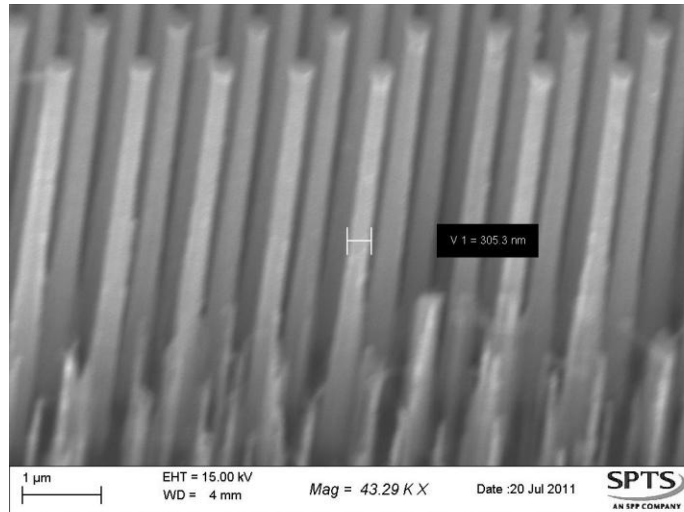

Figure 7.9.17.1 Run 17 - Pillars etched at 300nm diameter, grass evident outside of sample.

Although initially the profile of the pillars is good, there is clear tapering at the base of the pillars. It is thought that this is a result of the closely spaced nature of the pillars inhibiting the access of the plasma to areas between the pillars.

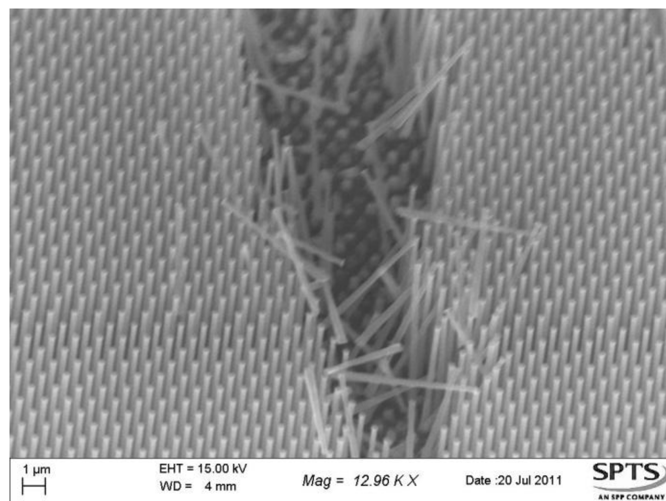

Figure 7.9.17.2 Run 17 - Pillars knocked over reveal sample area not suffering from grassing.

The above SEM image shows knocked over pillars within the sample area. This allows the visualisation of the space between the pillars. In terms of process control this is extremely useful as it shows that the area has not suffered from grassing.

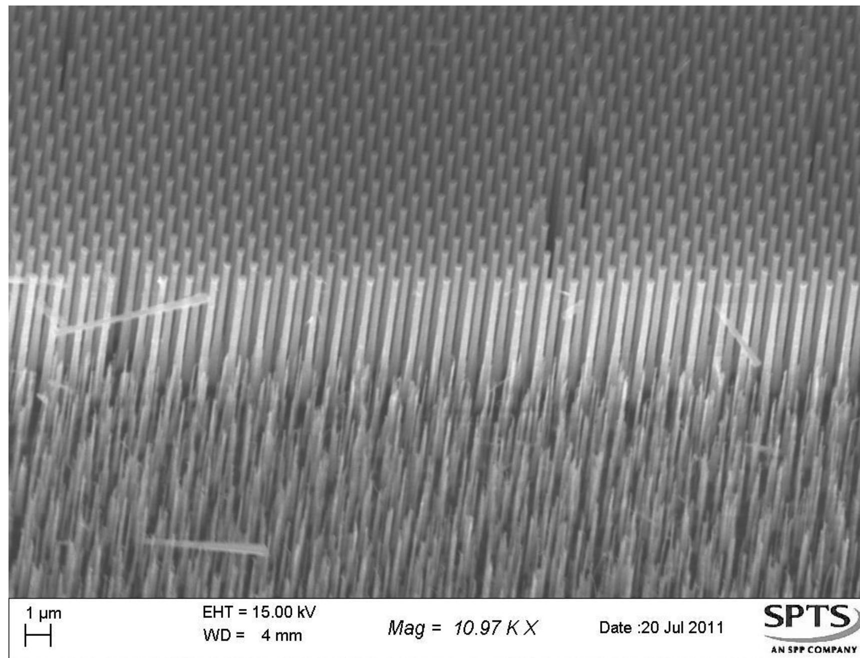

Figure 7.9.17.3 Run 17 - Outside of sample area grass is highly evident.

The grassing seen in run 16 is still highly evident outside of the sample area.

7.9.18. Run 18

For process run 18 a sample with 150nm mask diameter has been used a pith of 500nm was used. The process recipe from run 17 was maintained.

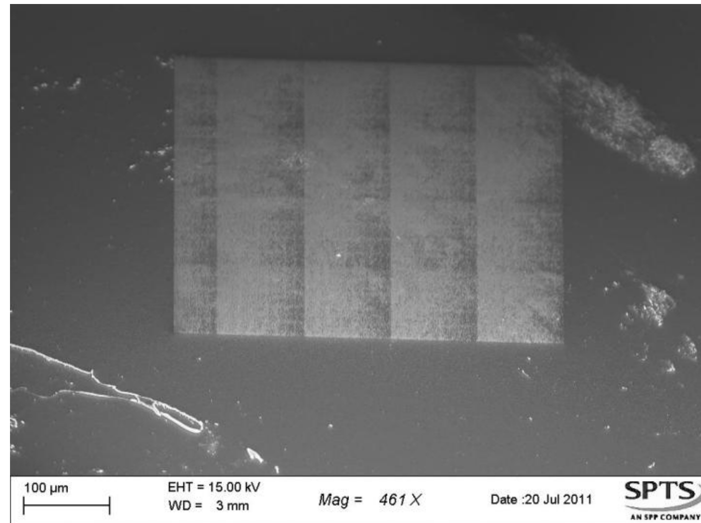

Figure 7.9.18.1 Run 18 - Mask is patchy in regular areas, potentially due to low diameter of mask

The above SEM image shows a problem with the mask fabrication technique. The liftoff technique appears to have struggled with the large area of Titanium being removed whilst attempting to leave only a small disc of 150nm diameter. The pitch of these samples is quite large relative to the diameter of the discs.

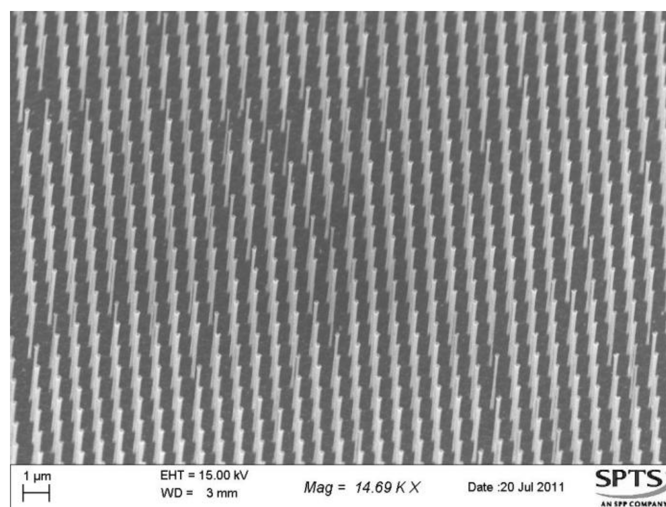

Figure 7.9.18.2 Run 18 -Pillars regular and cleanly etched

Where the mask fabrication has delivered acceptable masking the plasma etch is able to cleanly etch the pillars with decent profile, low grassing and no mask removal.

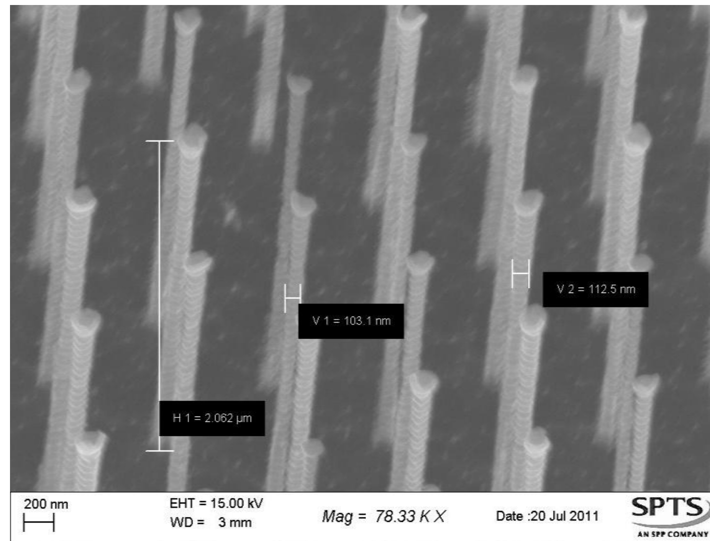

Figure 7.9.18.3 Run 18 - Low grassing found between pillars

The above SEM image shows that between the pillars there is a low degree of grassing. The value assigned to the height of the pillars of 2.062 is circumspect due to the angle of viewing of the pillars; given the angle of viewing it can be assumed that the height of the pillars could be as much as 50% more than the quoted value. The undercut that has been mentioned previously has become more of a significant issue with the pillars measured at between 112.5nm and 103.1nm compared to the mask size of 150nm.

7.9.19. Run 19

The sample mask for process run 19 was 200nm diameter discs. The same recipe from run 18 was repeated.

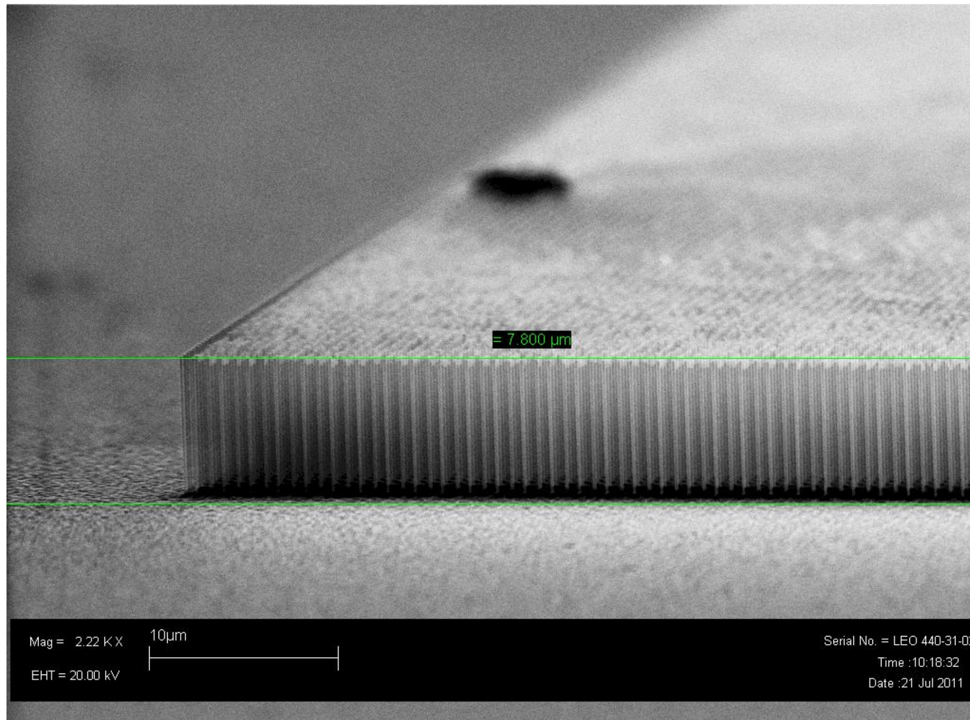

Figure 7.9.19.1 Run 19 - Pillars well populated, cleanly etched zero grass evident.

From the above SEM image it is clear that there has been a uniform etch of the pillars. There is little or no grassing evident inside or outside the pillars. There is however a small degree of mask removal observed at the top of the pillars.

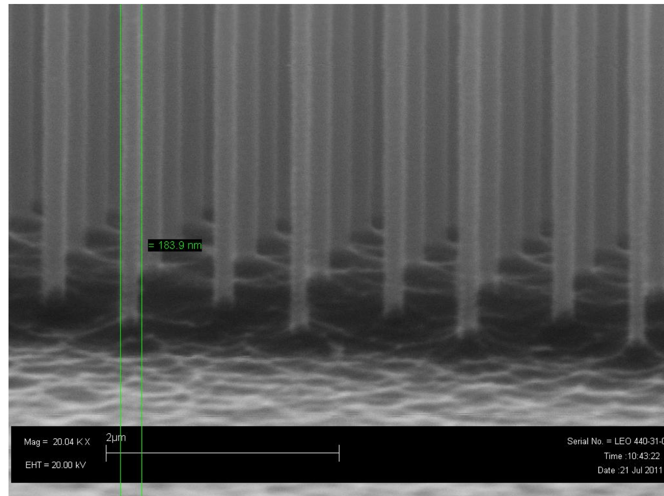

Figure 7.9.19.2 Run 19 - Zero evidence of grass between pillars or outside sample area. Pillars cleanly etched with low re-entrance.

The base of the pillars as shown in the above SEM image shows that the pillars have etched cleanly with no grassing and little or no re-entrance. The disparity between the pillar diameter and the mask diameter is due to the inherent undercut nature of the Bosch process.

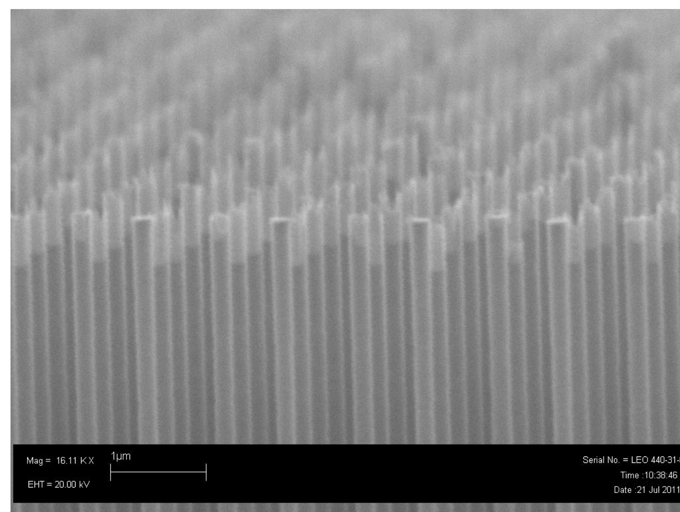

Figure 7.9.19.3 Run 19 - Pillar tops show signs of mask removal.

As described above there has been a small degree of mask removal and formation of the shell like structure observed in previous etches processes.

7.9.20. Run 20

The mask design for this sample was 100nm diameter with a 500nm pitch. The recipe was reduced to 50 loops.

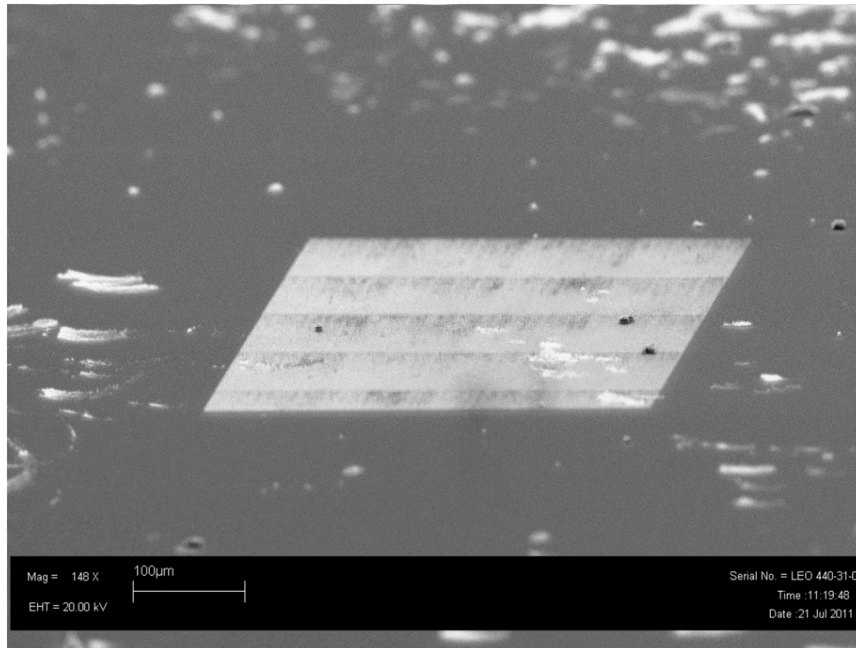

Figure 7.9.20.1 Run 20 - Mask has areas where mask has been removed.

From the above SEM image it is clear that there have been problems with the mask fabrication technique for creating 100nm diameter pillars. Some areas of the mask have been less fully populated with pillars.

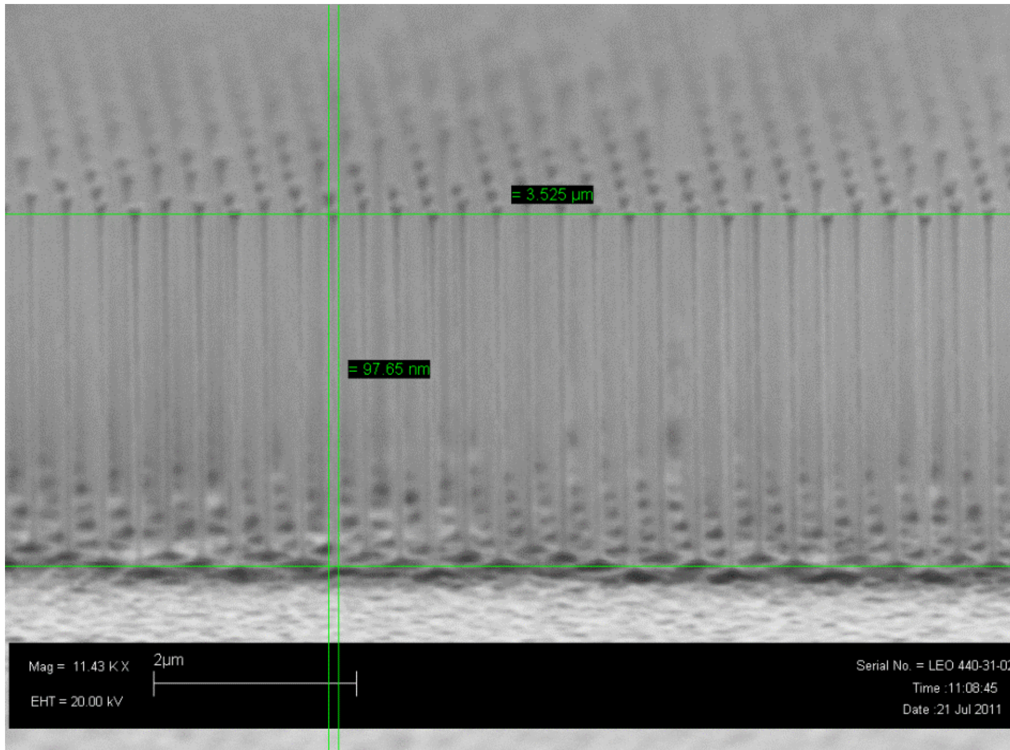

Figure 7.9.20.2 Run 20 - Low diameter pillars <100nm with aspect ratio of >30:1.

Where the masking has been uniform the pillars were etched cleanly with low levels of grass. The pillars have high aspect ratio of greater than 30:1. The profile etch of the pillars is approaching the target of close to 90° with neither tapering nor re-entrance.

7.9.21. Run 21

The sample for run 21 was a 150nm diameter mask design with 500nm pitch. The number of loops was reduced to 75 in order to reduce the mask removal.

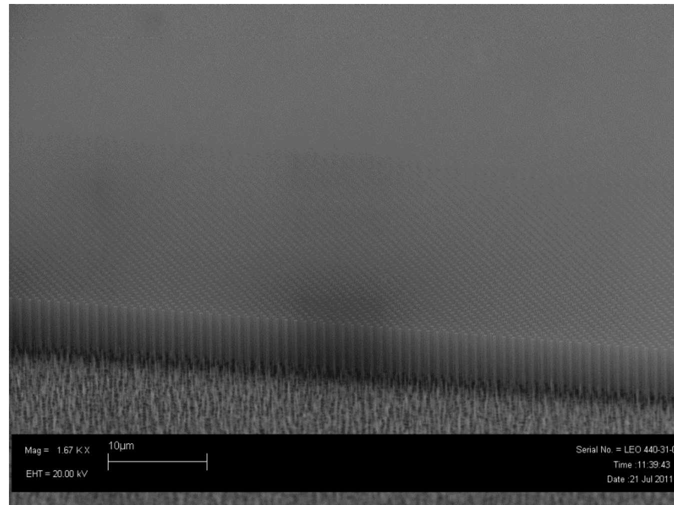

Figure 7.9.21.1 Run 21 - Highly regular pillars grassing outside sample area

The above SEM image clearly shows a high degree of uniformity in the etch profile, in addition the mask definition appears to have been consistent across the entire sample.

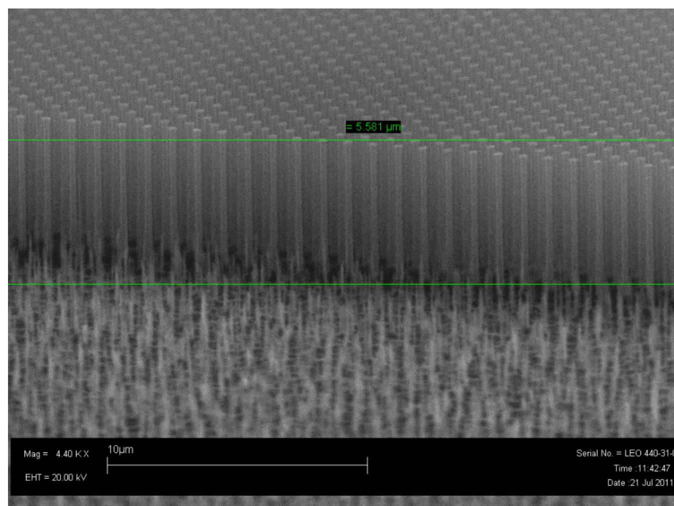

Figure 7.9.21.2 High quality pillar population slight grassing evident

Although there is a slight degree of grassing evident outside the sample, within the sample the grassing is minimal. There has been no mask removal across the sample.

7.10. Silicon Nanorod Fabrication – Discussion and Further Work

The full fabrication cycle for silicon nanorods (or pillars) has been described in detail over the course of this report. The development of the various recipes clearly involved a significant degree of trial and error with fine tuning required at practically every stage of the process. The results show that nanorods have been fabricated and reliable recipes for a variety of nanorod dimensions have been proven. Although the recipes have been developed to an acceptable level there is still the scope for developing these recipes further for deeper (taller) nanorods and also for a wider variety of pitch.

The aim from the outset of this part of the project was the fabrication of nanorods in bulk silicon. These nanorods would then be coated in a layer of amorphous silicon using plasma enhanced chemical vapour deposition (PECVD). The interface between the amorphous silicon and the p-type silicon forms the active region of the device. The final layer to be applied to the structure is Indium Tin Oxide (ITO). This layer acts as the transparent, conducting surface layer and is applied by sputtering. The final solar cell device structure is shown in the diagram below (Figure 7.10.1). The original plan for these samples was to develop photovoltaic devices using a number of different device structures which have been commonly used with planar devices.

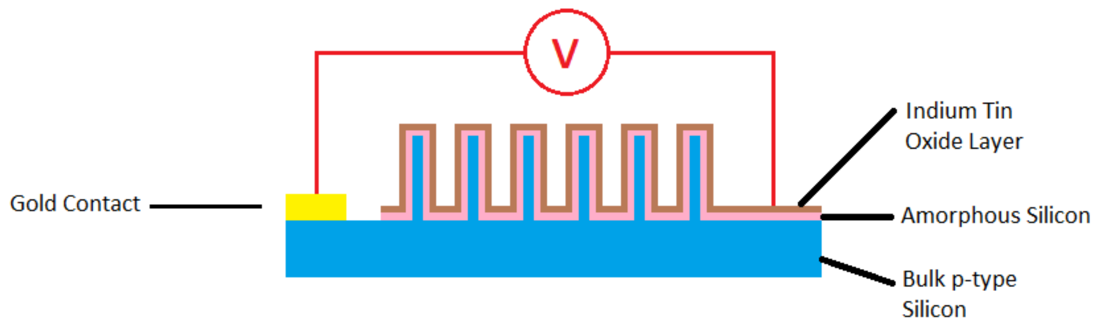

Figure 7.10.1 Silicon Nanorod photovoltaic device

Due to time constraints within the scope of the project only a single sample of silicon nanorods was physically processed to the point where a full device structure was created, unfortunately in the testing phase this device failed to function as a solar cell showing only resistive qualities when tested, rather than the generative qualities which would be found with a working device. This suggests a short circuit in the device structure between the metallic contacts and the ITO surface. It was suggested at the time that this could have been due to a lack of metallic contacts on the ITO surface. The probe used to measure the photovoltaic properties of the device is thought to have pierced the ITO layer creating the short circuit.

There was a plan in place for the production of many more samples to be tested using a gold contact on the ITO layer so as to ensure the continuity of the circuit. The gold layer in this case would offer the excellent electrical properties of gold[2] alongside its more mechanically durable properties. However the sputtering tool used to apply the ITO layer suffered a severe malfunction which went unrepaired for several months. Unfortunately the result of this was that the silicon nanorod samples which were created, including a range of pitch and diameters were left un-developed into full working devices. It was hoped that a colleague would be able to

process the samples and develop them into devices whilst still able to access the tools at the university; however this work was not completed.

This is an obvious area which could be further developed in terms of taking the project onwards. Given that the process recipes are fully developed for the production of the silicon nanorods the development of samples from the nanorod stage to full working devices would be entirely feasible as a continuation of the work carried out for the course of this project. The key results of this potential work would be regarding the comparison between efficiency of photovoltaic cells based on planar structures and those based on nanorods. The increase in surface area offered by the nanorod structures should lead to a significant increase in the efficiency of a device of a similar scale.

Once established as a working technique it would be possible to tune the device structure in terms of pillar diameters and pitch so that even higher efficiencies are achieved. Although the largest increase in surface area would be achieved by making the thinnest pillars possible with the highest density, it is likely not to be the case in practice. Computational modelling has been shown in the literature that there would be a point at which the efficiency would theoretically drop with extremely thin nanorods due to a lack of charge carriers available[3]. In the work mentioned here it has been suggested through modelling that the ideal nanorod would be highly doped in both p and n regions, have a narrow emitter width, have a radius approximately equally to the diffusion length of electrons in the p-type core and have a length approximately equal to the optical thickness of the material. In

addition the cell should be designed in such a way that leaves a low trap density near the p-n junction[3].

A further direction for the continuation of the work would be to design the pitch and size of the nanorods to act as an efficient light trapping system. Work has been conducted outside of this project into the effectiveness of light trapping[4]. This is the principle whereby the surface of a material is textured in such a way as to encourage the 'folding' of light back into the structure, thus increasing the likelihood of total internal reflection. This has been conducted using a variety of techniques including random texturing (black silicon) and periodic structures[5].

Although the aim of this work was to create nanorods for solar cell devices, there has been alternative work shown with nanorods being used for DNA mass sensors at the femto-molar level concentration[6]. This recent work shows the potential variation in applications for silicon nano-machining of this type and scale.

7.11. References

1. Ahnood, A., *Silicon thin films for mobile energy electronics*. 2011,Doctoral Thesis University College London: London.
2. Antler, M., *Gold in Electronic Components.* Gold Bulletin, 1983. **16**(1): p. 2-7.
3. Kayes, B.M.A., A and Lewis, Nathan S., *Comparison of the device physics principles of planar and radial p- n junction nanorod solar cells.* Journal Of Applied Physics, 2005. **97**.
4. Mokkapati, S. and K.R. Catchpole, *Nanophotonic light trapping in solar cells.* Journal Of Applied Physics, 2012. **112**(10): p. 1101.
5. Gjessing, J., A.S. Sudbo, and E.S. Marstein, *Comparison of periodic light-trapping structures in thin crystalline silicon solar cells.* Journal Of Applied Physics, 2011. **110**(3): p. 3104.
6. Lu, Y., *et al*., *Femtomolar Sensitivity DNA Photonic Crustal Nanowire Array Ultrasonic Mass Sensor*, in *MEMS 2012*. 2012, IEEE: Paris France.

8. Conclusion

Over the course of this project there have been three main avenues of research. The work has been carried out at a number of locations both at University College London and over the course of a two year placement with the sponsoring company Surface Process Technology Systems (SPTS).

The first was a study into principal component analysis (PCA) which was investigated as a technique in order to provide a basis and an introduction to the use of statistics to simplify the data obtained from OES. This initial investigation was carried out using patterned silicon wafers. Due to the lack of Silicon On Insulator wafers (required for typical OES end pointing) a system was developed using a modified version of the Bosch process. The deposition step of the Bosch process was extended resulting in a thick deposited polymer layer. This polymer layer being removed and exposing the underlying silicon is an artificial end point, allowing the evaluation of PCA as a statistical technique for end point detection. PCA was shown to be offer the key benefit of taking the full spectrum of optical data and reducing the dimensions to a user defined number (or component), with the end point of the process being contained within the component. Once the component containing the end-point is identified PCA also provides information regarding the contributions made to the component by the wavelengths analysed.

The second stage of the investigation involved the assessment of independent component analysis (ICA) as a statistical technique to improve the signal to noise ratio obtained from optical emission spectroscopy. ICA is a statistical technique and is considered to be an extension to PCA and a more powerful tool. It is widely used in facial recognition and signal

processing. The investigation into ICA showed that the technique is a valid option as a statistical treatment for OES data. ICA shows a marked improvement over the industry standard of principal component analysis, with both techniques applied to the same data sets and ICA delivering superior results.

The core of the investigation into ICA was carried out at the company headquarters of SPTS. Optical emission Spectroscopy data was collected whilst etching multiple patterned silicon-on-insulator (SOI) wafers. These wafers were etched in SPTS plasma process chambers of varying configurations. The OES was treated in the numerical computation program Matlab using a fast ICA algorithm technique. The ICA processed data was analysed by developing a technique where the magnitude of the signal drop -caused by the change in chemistry within the plasma - is compared to the noise in the signal. Essentially the signal to noise ratio of the contrasting techniques has been established as a method of quantifying the quality of the signal obtained. Using this technique ICA was evaluated and compared to PCA across the full selection of processed wafer. ICA was shown to deliver an approximate doubling of the signal to noise ratio compared to PCA.

A second aspect of ICA work was carried out with an investigation into its use in etching low open area. ICA was found to offer a slight improvement over the case of using a single wavelength.

The third and final section of this research was the development of a full fabrication sequence for the creation of silicon nanorods. The sequence incorporated a patterning and an etch step, both of which required a lengthy development process. The patterning used a positive resist based process to create hard titanium mask. The two key tools in the development of this patterning technique were an electron beam lithographer and an

electron beam evaporator. The EBL was used to pattern a silicon wafer with a range of discs in a hexagonal arrangement. The discs had diameters ranging from 1µm to 100nm and pitch from 2µm to 500nm. The electron beam evaporator was used to deposit Titanium into the patterned areas onto the wafer to create a fully patterned wafer. Once patterning was complete the patterned samples were used to develop an etch process capable of etching nanorods in Silicon. Successful process recipes were developed allowing the successful etch of the full range of sizes and pitches designed.   The intended culmination of this work was to develop the fabricated nanorod structure into a functioning photo cell device. This work was ongoing at the end of the project and is a clear direction for its continuation. The structures created in this piece of work - or replacements created using the processes developed over the course of this project - could be developed into functioning photovoltaic cell prototypes.

A further aspect of continued work would be a combination of the several dimensions of this project: to create a test of the limits of the ICA end pointing system using the fabrication of nanorods on SOI wafers to provide the low open area samples.

9. Appendix 1 - Reaction Mechanisms

9.1.1. Reaction Mechanisms of fluorocarbons within a plasma chamber.

Gas-phase reactions considered in the simulation, where p is the gas pressure in mTorr and T_e is the electron temperature in eV.

No.	Reaction j [a,b]	Rate coefficient k_j (m^3s^{-1})	ΔH_{ej} (eV)	References
	Reactions for fluorocarbons			
G1	$CF_4 + e \rightarrow CF_3 + F + e$	$2 \times 10^{-15} \exp(-13/T_e)$	12.5	[1,2]
G2	$CF_4 + e \rightarrow CF_2 + 2F + e$	$5 \times 10^{-15} \exp(-13/T_e)$	15.0	[1,3]
G3	$CF_4 + e \rightarrow CF + 3F + e$	$4.8 \times 10^{-17} T_e^{0.5} \exp(-20/T_e)$	20.0	[1,3]
G4	$CF_3 + e \rightarrow CF_2 + F + e$	3.3×10^{-16}	3.0	[1,3]
G5	$CF_2 + e \rightarrow CF + F + e$	3.3×10^{-16}	4.55	[1,3]
G6	$CF_3 + F \rightarrow CF_4$	$2.3 \times 10^{-19} \times p$		[1]
G7	$CF_2 + F \rightarrow CF_3$	$9 \times 10^{-22} \times p$		[1]
G8	$CF + F \rightarrow CF_2$	$9.6 \times 10^{-24} \times p$		[1]
G9	$CF_4 + e \rightarrow CF_3^+ + F + 2e$	$7 \times 10^{-14} \exp(-17.4/T_e)$	15.9	[1,2]
G10	$CF_4 + e \rightarrow CF_2^+ + 2F + 2e$	$7 \times 10^{-15} \exp(-24.7/T_e)$	22.0	[1,2]
G11	$CF_4 + e \rightarrow CF^+ + 3F + 2e$	$9 \times 10^{-15} \exp(-30/T_e)$	27.0	[1,3]
G12	$CF_3 + e \rightarrow CF_3^+ + 2e$	$8 \times 10^{-15} \exp(-12.2/T_e)$	8.5	[1,3]
G13	$CF_2 + e \rightarrow CF_2^+ + 2e$	$2.5 \times 10^{-14} \exp(-12.2/T_e)$	11.4	[1,3]
G14	$CF + e \rightarrow CF^+ + 2e$	$2.5 \times 10^{-14} \exp(-15.3/T_e)$	9.1	[1,3]
G15	$CF_4 + e \rightarrow F^- + CF_3$	$4.6 \times 10^{-15} T_e^{-1.5} \exp(-7/T_e)$	4.8	[1,3]
G16	$CF_3^+ + e \rightarrow CF_3$	4×10^{-14}	−8.5	[1,3]
G17	$X^+ + F^- \rightarrow X + F$	4×10^{-13}		[1]
G18	$CF_3^+ + F^- \rightarrow CF_4$	5×10^{-14}		[1]
G19	$CF_3 + F^- \rightarrow CF_4 + e$	5×10^{-16}	−4.8	[1,3]
	Reactions for oxygen-containing species			
G20	$O + e \rightarrow O^+ + 2e$	$9.0 \times 10^{-15} T_e^{0.7} \exp(-13.6/T_e)$	13.6	[3,4]
G21	$O_2 + e \rightarrow O_2^+ + 2e$	$2.13 \times 10^{-14} \exp(-14.5/T_e)$	12.1	[4,5]
G22	$O_2 + e \rightarrow O^- + O$	$8.8 \times 10^{-17} \exp(-4.4/T_e)$	3.64	[4]
G23	$O^- + O^+ \rightarrow O + O$	2.7×10^{-13}		[4]
G24	$O^- + O_2^+ \rightarrow O + O_2$	1.5×10^{-13}		[4]

G25 $O^- + e \rightarrow O + 2e$	$2.0 \times 10^{-13} \exp(-5.5/T_e)$	1.53	[4]
G26 $O_2 + e \rightarrow 2O + e$	$4.2 \times 10^{-15} \exp(-5.6/T_e)$	5.17	[4]
G27 $O_2 + e \rightarrow O + O(^1D) + e$	$5.0 \times 10^{-14} \exp(-8.4/T_e)$	7.13	[4]
G28 $O_2 + e \rightarrow O^+ + O^- + e$	$7.1 \times 10^{-17} T_e^{0.5} \exp(-17/T_e)$	17.32	[4]
G29 $O_2 + e \rightarrow O^+ + O + 2e$	$5.3 \times 10^{-16} T_e^{0.9} \exp(-20/T_e)$	18.84	[4]
G30 $O_2^+ + e \rightarrow O + O$	$5.2 \times 10^{-15}/T_e$	-6.97	[4]
G31 $O^- + O \rightarrow O_2 + e$	3×10^{-16}	−3.64	[4]
G32 $O_2 + e \rightarrow O_2(a^1\Delta_g) + e$	$1.7 \times 10^{-15} \exp(-3.1/T_e)$	0.977	[4,6]
G33 $O_2(a^1\Delta_g) + e \rightarrow O_2^+ + 2e$	$9.0 \times 10^{-16} T_e^{2.0} \exp(-11.6/T_e)$	11.16	[4,6]
G34 $O_2(a^1\Delta_g) + e \rightarrow O^- + O$	$2.28 \times 10^{-16} \exp(-2.29/T_e)$	2.66	[4,6]
G35 $O_2(a^1\Delta_g) + e \rightarrow O_2 + e$	$5.6 \times 10^{-15} \exp(-2.2/T_e)$	−0.977	[4,6]
G36 $O_2(a^1\Delta_g) + e \rightarrow O + O + e$	$4.2 \times 10^{-15} T_e^{2.0} \exp(-4.6/T_e)$	4.19	[4,6]
G37 $CF_3 + O \rightarrow COF_2 + F$	3.1×10^{-17}		[7]
G38 $CF_2 + O \rightarrow COF + F$	1.4×10^{-17}		[7]
G39 $CF_2 + O \rightarrow CO + 2F$	4×10^{-18}		[7]
G40 $COF + O \rightarrow CO_2 + F$	9.3×10^{-17}		[7]
G41 $COF + F \rightarrow COF_2$	8×10^{-19}		[7]
G42 $COF + CF_2 \rightarrow CF_3 + CO$	3×10^{-19}		[7]
G43 $COF + CF_2 \rightarrow COF_2 + CF$	3×10^{-19}		[7]
G44 $COF + CF_3 \rightarrow CF_4 + CO$	1×10^{-17}		[7]
G45 $COF + CF_3 \rightarrow COF_2 + CF_2$	1×10^{-17}		[7]
G46 $COF + COF \rightarrow COF_2 + CO$	1×10^{-17}		[7]
G47 $CF + O \rightarrow CO + F$	2×10^{-17}		[7]
G48 $CO_2 + e \rightarrow CO + O + e$	$4.47 \times 10^{-15} T_e^{-0.201} \exp(-4.53/T_e)$	6.1	[3,5]
G49 $COF_2 + e \rightarrow COF + F + e$	$1.13 \times 10^{-14} T_e^{-0.399} \exp(-13.10/T_e)$	6.0	[3,5]
G50 $CO + e \rightarrow CO^+ + 2e$	$3.47 \times 10^{-13} T_e^{-0.0487} \exp(-23.8/T_e)$	14.0	[7]

Reactions for silicon fluorides			
G51 $SiF_4 + e \rightarrow SiF_3 + F + e$	$4.80 \times 10^{-15} T_e^{0.8282} \exp(-11.22/T_e)$	7.25	[5]
G52 $SiF_4 + e \rightarrow SiF_2 + 2F + e$	$1.45 \times 10^{-14} T_e^{0.01834} \exp(-16.03/T_e)$	11.9	[5]
G53 $SiF_4 + e \rightarrow SiF + 3F + e$	$6.94 \times 10^{-18} T_e^{1.187} \exp(-18.98/T_e)$	18.6	[5]
G54 $SiF_3 + F \rightarrow SiF_4$	1.0×10^{-16}		[8]
G55 $SiF_2 + F \rightarrow SiF_3$	1.0×10^{-16}		[8]
G56 $SiF + F \rightarrow SiF_2$	1.0×10^{-16}		[8]
G57 $Si + F \rightarrow SiF$	1.0×10^{-16}		Assumed
G58 $SiF_4 + e \rightarrow SiF_3^+ + F + 2e$	$1.15 \times 10^{-14} T_e^{0.6641} \exp(-17.42/T_e)$	16.0	[5]
G59 $SiF_4 + e \rightarrow SiF_2^+ + 2F + 2e$	$3.44 \times 10^{-15} T_e^{0.5108} \exp(-22.83/T_e)$	23.4	[5]
G60 $SiF_4 + e \rightarrow SiF^+ + 3F + 2e$	$6.19 \times 10^{-16} T_e^{1.090} \exp(-26.99/T_e)$	25.1	[5]
G61 $SiF_3 + e \rightarrow SiF_3^+ + 2e$	$9.79 \times 10^{-15} T_e^{0.3633} \exp(-10.21/T_e)$	9.60	[5]
G62 $SiF_2 + e \rightarrow SiF_2^+ + 2e$	$2.80 \times 10^{-14} T_e^{0.2530} \exp(-11.62/T_e)$	10.80	[5]
G63 $SiF + e \rightarrow SiF^+ + 2e$	$6.25 \times 10^{-14} T_e^{0.3258} \exp(-7.80/T_e)$	7.26	[5]
G64 $SiF_4 + e \rightarrow F^- + SiF_3$	$3.18 \times 10^{-16} T_e^{-0.3792} \exp(-9.82/T_e)$	3.8	[5]
G65 $SiF_3^+ + e \rightarrow SiF_3$	4×10^{-14}		Assumed
G66 $SiF_3^+ + F^- \rightarrow SiF_4$	5×10^{-14}		Assumed

[a] $X = CF_x$ (x = 1–3).

[b] $O(^1D)$, $O_2(a^1\Delta_g)$ are metastables.

[c] ΔH_{ej} is calculated from the Fourth Edition of NIST-JANAF Thermochemical Tables.

Surface reactions considered on SiO_2 surfaces (dielectric window as well as substrate surfaces) during etching in the simulation, where T_s is the surface temperature of 300 K.

No.	Reaction [a,b]	Flux	Surface coverage	Rate coefficient [c,d]	Ref.
	Physical sputtering				
S1	$SiO_2^* \rightarrow Si(g) + 2O(g)$	Γ_{ion}	$1-\theta_{tot}$	$y_{sp,i} = A_i(\sqrt{E_i} - \sqrt{E_{th}})^e$	[9]
	Reactions with F atoms				
S2	$SiO_2^* \rightarrow SiO_2F_2(s)$	Γ_F	$1-\theta_{tot}$	$s_F = 0.02$	[9]
	$+ 2F(g)$				
S3	$SiO_2F_2(s) \rightarrow SiF_4(g) + O_2(g)$	Γ_{ion}	θ_F	$\beta_F = 0.0454(\sqrt{E_i} - \sqrt{E_{th}})^f$	[9]
	$+ 2F(g)$				
S4	$SiO_2F_2(s) \rightarrow SiF_2(g) + O_2(g)$	Γ_{ion}	θ_F	$\beta_F b = 0.0454b(\sqrt{E_i} - \sqrt{E_{th}})^i$	[9]
S5	$SiO_2F_2(s) \rightarrow SiF_4(g) + O_2(s)$	Γ_F	θ_F	$K(T_s) = \frac{K_0 \rho N_A}{M_w} \exp\left(-\frac{E_a}{kT_s}\right)$	[9]
	$+ 2F(g)$				
	Reactions with fluorocarbon radicals				
S6	$SiO_2^* \rightarrow SiO_2CF_x(s)$	Γ_{CF_x}	$1-\theta_{tot}$	$s_{CF_x} = 0.1$	Assumed
	$+ CF_x(g)$				
S7	$SiO_2CF_x(s) \rightarrow SiF_x(g) + 2CO(g)$	Γ_{ion}	θ_{CF_x}	$\beta_{CF_x} = 0.361(\sqrt{E_i} - \sqrt{E_{th}})^f$	[9]
S8	$SiO_2CF_x(s) \rightarrow Si(s) + 2COF_x(g)$	Γ_{ion}	θ_{CF_x}	$y_C = 0.0361$	[9]
S9	$SiO_2CF_x(s) \rightarrow SiO_2^* + CF_{x+1}(g)$	Γ_F	θ_{CF_x}	$k_{rec} = 0.60$	[9]
	$+ F(g)$				
	Reactions of polymer creation or loss				
S10	$CF_x^+(g) \rightarrow P$	Γ_{ion}	1	$y_{d,i} = -A_{d,i}\sqrt{E_i}^g$	[9]
				$(0 < E_i \leq \frac{1}{2}E_{th})$	[9]
				$y_{d,i} = A_i(\sqrt{E_i} - \sqrt{E_{th}})^h$	[9]
				$(\frac{1}{2}E_{th} < E_i < E_{th})$	[9]
S11	$SiO_2CF_x(s) \rightarrow P$	Γ_{ion}	θ_{CF_x}	$\beta_s = 0.0361$	[9]

The above tables were adapted from doctoral thesis on ‘Model Analysis of Plasma-Surface Interactions during Silicon Oxide Etching in Fluorocarbon Plasmas’ By Hiroshi Fukomoto of Kyoto University 2012

9.1.2. References

1. T. Kimura and K. Ohe, *Probe measurements and global model of inductively coupled Ar/CF4 discharges.* Plasma Sources Science Technologyhttp://iopscience.iop.org/0963-0252/8/4/305, 1993. **8**.
2. Ho, E.M.a.P., ed. *Handbook of Advaned Plasma Processing Techniques*. ed. R.J.S.a.S.J. Pearton. 2000, Springer: New York. 99.
3. Graves, M.W.K.a.D.B., *Temperature resolved modeling of plasma abatement of perfluorinated compounds.* Journal Of Applied Physics, 2001. **89**.
4. Kimura, T., A.J. Lichtenberg, and M.A. Lieberman, *Modelling finite cylinder electronegative discharges.* Plasma Sources Science Technology, 2001. **10**.
5. P. Ho, et al., *Modeling the plasma chemistry of C2F6 and CHF3 etching of silicon dioxide, with comparisons to etch rate and diagnostic data.* Journal Vacuum Science and Technology A 2001. **19**.
6. S. F. Wong, M. J. W. Boness, and G. J. Schulz, *Vibrational Excitation of O2 by Electron Impact above 4 eV.* Physical Review Letters, 1973. **31**.
7. I. C. Plumb and K. R. Ryan, *Gas-Phase Reactions of SF_5, SF_2, and SOF with O(3p): Their Significance in Plasma Processing*Plasma Chemistry and Plasma Processing, 1986. **6**.
8. I. C. Plumb and K. R. Ryan, . Plasma Chemistry and Plasma Processing, 1986. **6**.
9. E. Gogolides, et al., *Etching of SiO2 and Si in fluorocarbon plasmas: A detailed surface model accounting for etching and deposition.* Journal Of Applied Physics, 2000. **88**.

10. Appendix 2 - ICA Theory of operation

The following is a derivation of the principles of operation of the fixed point algorithm used in the independent component analysis section of the project. The work is originally conducted by Hyvärinen et al[1].

Fixed Point Algorithm ICA

The fixed point algorithm used in the work here relies on the data being a sphered or pre-whitened random vector **x**. In the case of blind source separation is a collection of linear mixtures of independent source signals.

1. Take a random initial vector **w**(0) of normalisation 1. Let k=1.
2. Let **w**(k) = $E\{x(w(k-1)^T x)^3\} - 3\mathbf{w}(k-1)$. The expectation can be estimated using a sample of **x** vectors (1000 for example).
3. Divide **w**(k) by its norm.
4. If $|\mathbf{w}(k)^T\mathbf{w}(-1)|$ is not close enough to 1, let $k = k + 1$ and return to step 2. Otherwise output the vector **w** (k).

The resultant vector **w**(k) is one of the columns of the (orthogonal) mixing matrix **B**. In blind source separation this means that **w**(k) separates *one* of the non-Gaussian source signals from the original data set or alternatively $\mathbf{w}(k)^T\mathbf{x}(t)$, t = 1,2, … is equal to one of the source signals.

Estimating Several Independent Components

In order to estimate several (n) independent components, the algorithm is run n times. An *orthogonalising projection* is added inside the loop allow the estimation of different components in each iteration.

The columns of the mixing matrix **B** are orthornormal due to the whitened nature of the data. Thus we can estimate the components one by one by projecting the current solution **w**(k) on the space orthogonal to the columns of the mixing matrix **B** previously found. Define $\overline{\mathbf{B}}$ as a matrix whose columns are the previously found columns of **B.** Then add the projection operation in the beginning of step 3

3. Let $\boldsymbol{w}\,(k) = \boldsymbol{w}\,(k) - \overline{\mathbf{B}}\overline{\mathbf{B}}^{\boldsymbol{T}}\,\boldsymbol{w}\,(k)$. Divide **w**($k$) by its norm.

The initial random vector should be projected this way before starting the iteration before starting the iterations. To prevent estimation errors in $\overline{\mathbf{B}}$ from deteriorating the estimate **w**(k), this projection step can be omitted after the first few iterations: once the solution **w**(k) has entered the basin of attraction of one of the fixed points, it will stay there and converge to that fixed point.

In addition to the hierarchical (or sequential) orthogonalization described above, any other method of orthogonalizing the weight vectords could also be used. In some applications, a symmetric orthogonalization might be useful. This means that the fixed-point step is first

performed for all the n weight vectors, and then the matrix $\mathbf{W}(k) = (\mathbf{w}_1(k),\ldots \mathbf{w}_n(k))$ of the weight vectors is orthogonalized, eg using the well known formula:

$$\text{Let } \mathbf{W}(k) = \mathbf{W}(k)\, \mathbf{W}(k)^T\, \mathbf{W}(k)^{-1/2}$$

Where $(\mathbf{W}(k)^T\, \mathbf{W}(k)^{-1/2})$ is obtained from the eigenvalue decomposition of $\mathbf{W}(k)^T\, \mathbf{W}(k) = \mathbf{EDE}^T$ as $(\mathbf{W}(k)^T\, \mathbf{W}(k)^{-1/2}) = \mathbf{ED}^{-1/2}\mathbf{E}^{\mathrm{T}}$.

1. Hyvärinen, A.O., Erkki, ***A Fast Fixed-Point Algorithm for Independent Component Analysis.*** **Neural Computation, 1997. 9: p. 1483-1492.**